Gran Sasso Science Institute

PHD PROGRAMME IN MATHEMATICS IN NATURAL, SOCIAL AND LIFE SCIENCES

Cycle XII - 2016/2019

Models for coupled active–passive population dynamics: mathematical analysis and simulation

PHD CANDIDATE

Thi Kim Thoa Thieu

ADVISORS:

Prof. Dr. habil. Adrian Muntean

Karlstad University, Sweden

Assoc. Prof. Dr. Matteo Colangeli

University of L'Aquila, Italy

GRAN SASSO SCIENCE INSTITUTE

SCHOOL OF ADVANCED STUDIES

Scuola Universitaria Superiore

Gran Sasso Science Institute

PHD PROGRAMME IN MATHEMATICS IN NATURAL, SOCIAL AND LIFE SCIENCES

Cycle XII - 2016/2019

Models for coupled active–passive population dynamics: mathematical analysis and simulation

PHD CANDIDATE

Thi Kim Thoa Thieu

ADVISORS:

Prof. Dr. habil. Adrian Muntean

Karlstad University, Sweden

Assoc. Prof. Dr. Matteo Colangeli

University of L'Aquila, Italy

Thesis Jury Members

Prof. Azmy S. Ackleh (University of Louisiana at Lafayette, USA)
Prof. Grigorios A. Pavliotis (Imperial College London, UK)
Prof. Emilio N. M. Cirillo (Sapienza University of Rome, Italy)
Prof. Corrado Lattanzio (University of L'Aquila, Italy)
Dr. Paolo Antonelli (GSSI, Italy)

Thesis Referees

Prof. Azmy S. Ackleh (University of Louisiana at Lafayette, USA)
Prof. Grigorios A. Pavliotis (Imperial College London, UK)

Contents

Abstract

In this dissertation, we study models for coupled active–passive pedestrian dynamics from mathematical analysis and simulation perspectives. The general aim is to contribute to a better understanding of complex pedestrian flows. This work comes in three main parts, in which we adopt distinct perspectives and conceptually different tools from lattice gas models, partial differential equations, and stochastic differential equations, respectively.

In part one, we introduce two lattice models for active–passive pedestrian dynamics. In a first model, using descriptions based on the simple exclusion process, we study the dynamics of pedestrian escape from an obscure room in a lattice domain with two species of particles (pedestrians). The main observable is the evacuation time as a function of the parameters caracterizing the motion of the active pedestrians. Our Monte Carlo simulation results show that the presence of the active pedestrians can favor the evacuation of the passive ones. We interpret this phenomenon as a discrete space counterpart of the so-called drafting effect. In a second model, we consider again a microscopic approach based on a modification of the simple exclusion process formulated for active–passive populations of interacting pedestrians. The model describes a scenario where pedestrians are walking in a built environment and enter a room from two opposite sides. For such counterflow situation, we have found out that the motion of active particles improves the outgoing current of the passive particles.

In part two, we study a fluid-like driven system modeling active–passive pedestrian dynamics in a heterogenous domain. We prove the well-posedness of a nonlinear coupled parabolic system that models the evolution of the complex pedestrian flow by using special energy estimates, a Schauder's fixed point argument and the properties of the nonlinearity's structure.

In the third part, we describe via a coupled nonlinear system of Skorohod-like stochastic differential equations the dynamics of active–passive pedestrians dynamics through a heterogenous domain in the presence of fire and smoke. We prove the existence and uniqueness of strong solutions to our model when reflecting boundary conditions are imposed on the boundaries. To achieve this we used compactness methods and the Skorohod's representation of solutions to SDEs posed in bounded domains. Furthermore, we study an homogenization setting for a toy model (a semi-linear elliptic equation) where later on our pedestrian models can be studied.

MSC 2020: 35Q35, 35K55, 76S05, 60H10, 60H30, 82C20, 82C80

PACS: 05.10Ln, 05.90.+m, 63.90+t

Key words: pedestrian dynamics, simple exclusion process, Forchheimer flows, Skorohod equations, nonlinear coupling, heterogenous domain, homogenization, drafting, evacuation

Chapter 1

Introduction

1.1 Background

In the literature, many models have been proposed to describe pedestrian dynamics in different scenarios. Some researchers consider macroscopic models, where the density and speed of the flow are accounted for, while others study microscopic models in which each individual is represented separately as a moving particle, hence, systems of interacting particles are considered. Pedestrians have a complex psychologic and sociologic behavior which is often only considered in simplified ways in the various approaches. This dissertation focuses on studying three different pedestrian models from three different perspectives: lattice gas models, a fluid-like driven system and stochastic differential equations. Here, we account for the same sociologic feature in which our crowd is assumed to be a mix of informed pedestrians (active) and uninformed pedestrians (passive). This type of mixed pedestrian dynamics is originally proposed in [RJM19] by considering the crowd motion in a complex geometry in the presence of a fire as well as of a slowly spreading smoke curtain.

We start off with microscopic crowd models of lattice types. One of our models describes the evacuation of pedestrian populations from an obscure room, while another model presents a scenario of pedestrians walking in a building environment and entering from opposite sides. Such a lattice-based approach is a modeling tool from statistical physics which was able to reproduce realistic phenomena for pedestrian flows (see e.g. [CFL09, KLSD08]). Our evacuation models always refer to a geometry (in which the dynamics takes place) that is partly unknown and possibly also with limited visibility. For more information on the topic, we refer the reader, for instance, to [ABCK16, FRNF13, MWS14, WS14, XJJS16, CCCM18, ZLX11] and references cited therein.

From a macroscopic perspective, by employing the idea of percolating fluids through a structured porous media, we are interested in a fluid-like driven system for active–passive pedestrian dynamics. We consider a system of parabolic equations consisting of a double nonlinear parabolic equation of Forchheimer type coupled with a semilinear parabolic equation. Some of the mathematical properties related to this type of equations have been already investigated for

scalar equations modeling Forchheimer flows in porous media; see for instance, in [HI11, ABHI09, CHK16, BZK60].

From the stochastic differential equations point of view, we are interested in a system of Skorohod-like stochastic differential equations modeling our active–passive pedestrians dynamics through a heterogenous domain this time in the presence of fire and smoke. In particular, the active–passive pedestrian dynamics is posed in a two dimensional bounded perforated domain, i.e. obstacles are part of the geometry. Therefore, boundary conditions must be specified for this particular class of stochastic differential equations. We decided to work with the classical Skorohod's formulation of SDEs with reflecting boundary conditions to obtain a correct dynamics of such pedestrians close to the boundary of the interior obstacles. We refer the reader, for instance, to [Lio84, Sai87, Sko61, Ö09] for related problems. In addition, we also prepare an homogenization playground where later on our microscopic pedestrian dynamics can be studied.

The main questions we are addressing in this dissertation are:

Q1: How to describe the evolution of a crowd, where different sub-populations (e.g. passive and active) interact and move differently?

Q2: Can we induce modifications of the dynamics of the active population to improve the outgoing current of the passive population?

Q3: What would be a possible way to describe macroscopically the motion of active and passive populations in an heterogeneous domain?

Q4: How to model in a well-posed manner the microscopic interactions with the interior boundaries (of a built environment) of the pedestrians stochastically interacting with each other?

1.2 Outline of the dissertation

- In Chapter 2, we provide the background and the settings of three models that we develop throughout this dissertation.

- In Chapter 3, we study the evacuation dynamics from an obscured room using a lattice gas model with two species of particles. Specifically, active species performs a symmetric random walk on the lattice, while the passive species is subject to a drift guiding the particles towards the exit. The numerical results show that the presence of the active pedestrians favors the evacuation of the passive ones. We interpret this phenomenon as a discrete space counterpart of the drafting effect typically observed in a continuum set-up as the aerodynamic drag experienced by pelotons of competing cyclists.

- In Chapter 4, based on the simple exclusion process, we study the dynamics of two populations of particles, mimicking pedestrians walking in a built environment entering a room from two opposite sides. In particular, passive particles belong to a group performing a symmetric random walk, while active particles have information on the local geometry in the sense that

as soon as particles enter a visibility zone, a drift activates them. The numerical results show that the dynamics of the active particles can improve the outgoing current of the passive particles.

- In Chapter 5, we consider a fluid-like driven system modeling active–passive pedestrian dynamics posed in a hetetogenous environment. We study the question of well-posedness of parabolic equations consisting of a double nonlinear parabolic equation of Forchheimer type coupled with a semilinear parabolic equation.

- In Chapter 6, we study the solvability of a coupled nonlinear system of Skorohod-like stochastic differential equations with reflecting boundary conditions modeling active–passive pedestrian dynamics through a heterogenous domain in the presence of fire. We use compactness methods together with the Skorohod's representation of solutions to SDEs.

- In Chapter 7, we consider a semilinear elliptic equation posed in periodically perforated domains and associated with a Fourier-type condition on internal interfaces. We provide a linearization scheme that allows us to prove the weak solvability of the microscopic model. Based on classical results for homogenization of multiscale elliptic problems with periodic coefficients, we design a modified two-scale asymptotic expansion to derive the corresponding macroscopic equation, when the scaling choices are compatible. Also, we prove high-order corrector estimates for the homogenization limit.

- In Chapter 8, we present briefly the results which obtained in this dissertation (in relation to questions Q1-Q4 from Section 1.1). We also provide a list of open issues for forthcoming considerations.

The notation used in each chapter is consistent within the respective chapter. The notation slightly changes from chapter to chapter.

Chapter 2

Modeling

In this chapter, we introduce three models that we use throughout this dissertation. In particular, one of the models is a lattice-gas-type approach based on Monte Carlo stochastic dynamics, another model employs a fluid-like driven system, while a third model is a system of stochastic differential equations of a Skohorod type. This part is based on [CCMT19, TCM19, TCM20, CCMT20, TM20].

The approaches chosen in this dissertation are in line with and extend [Cor15, Eve15].

2.1 Background

The modeling of pedestrian flows offers many challenging questions to science and technology in general. It would be of great practical relevance for instance to know how fast human crowds evacuate complex urban buildings. Unlike fluid flows, pedestrian flows are rarely uniform. Hence, their motion is difficult to predict accurately. In this work, we aim at presenting active–passive pedestrian dynamics models from different perspectives: lattice gas models, fluid-like driven system and SDEs. This is our attempt towards understanding how complex crowds move within complex environments.

2.1.1 Lattice gas models

Pedestrian dynamics and social human behavior are closely connected. The detailed behavior of human is already complicated, being caused by many physiological and psychological processes, still largely unknown. The statistical physics approach for social dynamics is offering a possible route for investigations. From the modeling point of view, the investigation of models of social dynamics involves two levels of difficulty. The first challenge is defining good microscopic models. The second challenge is the usual issue of inferring the macroscopic phenomenology out of the microscopic dynamics of such models. We are observing the microscopic dynamics of active–passive pedestrian populations by considering lattice gas models. In particular, for the first model, using the descriptions based

on the simple exclusion process, we study the pedestrian escape from an obscure room using a lattice gas model with two species of particles[1]. One species, called passive, performs a symmetric random walk on the lattice, whereas the second species, called active, is subject to a drift guiding the particles towards the exit. The drift mimics the awareness of some pedestrians of the geometry of the room and of the location of the exit. In the second model, we consider again a microscopic approach based on a modification of the classical simple exclusion process formulated for two different active–passive populations of interacting pedestrians (particles). Unlike the first model, two populations of particles, mimicking pedestrians walking in a built environment, enter now the room from two opposite sides with the intention to cross the room and then exit from the door on the opposite side.

Furthermore, these models belong to a recent research direction handling the evacuation behavior of crowds of pedestrians where the geometry in which the dynamics takes place is partly unknown and possibly also with limited or no visibility. Such crowd scenarios can be considered when catastrophic situations occur in urban environments, such as tunnels, underground spaces or in forests in fire. For more information, we refer the reader, for instance, to [ABCK16, FRNF13, MWS14, WS14, XJJS16, CCCM18] and references cited therein. In this context, the experimental information is provided, for instance, in [vKS17] and [OP17], which are also connected to the so-called "faster-is-slower" effect.

2.1.2 A fluid-like driven system

Looking at a heterogenous environment (e.g. a complex office building), we exploit the idea of percolating fluids through a structured porous media to tackle our pedestrian dynamics. See also Figure 2.5, where we make the analogy with flow in a structured porous media, inspired by an idea by Barenblatt and co-authors cf. [BZK60]. Like in Section 2.1.1, the standing assumption is that the crowd of pedestrian is composed of two distinct populations: active agents that follow a predetermined velocity field and passive agents that have no preferred direction of motion. In particular, we imagine that the active population of pedestrians have velocities similar to a non-Darcy flow, namely, to a generalized Forchheimer flow as formulated for slightly compressible fluids (see e.g. [ABHI09, HI11, CHK16]). On the other hand, we consider the flow of the passive population as a diffusion process, hence no predetermined flow directions are prefered. Mathematically, this is an about evolution system where a Forchheimer-like equation is nonlinearly-coupled to a diffusion-like equation. For more details on the modeling of the situation, we refer the reader to Section 2.3 and references mentioned there.

[1]The pedestrian is perceived in this context as a moving particle on a lattice, interacting with the other neighboring particles.

2.1.3 A system of stochastic differential equations

In crowd dynamics studies, the movements of pedestrians must directly be related to their decision making processes. Hence, the characteristics of pedestrian flows are apparently affected by decisions of pedestrians. This influence is necessary in order to model the processes properly. Stochastic tools become important to capture the essence of the interactions among the pedestrians, specially when a consensus is not available. It is clear that the dynamics of pedestrians can either be deterministic or stochastic. In the deterministic case, the behavior of pedestrians at a certain time is completely determined by the present state and can be predicted accordingly, while in the stochastic case the pedestrian behavior is governed by certain probabilities such that the pedestrians can react differently in the same situation. We turn our attention to consider a coupled nonlinear system of Skohorod-like stochastic differential equations modeling the dynamics of pedestrians through heterogenous domain in the presence of fire. In particular, our interest in this context is to study the role the internal geometry plays for mixed pedestrian flows where the dynamics of interacting particles stems from two distinct populations: an active population – these pedestrians are aware of the details of the environment and move towards the exit door, and a passive population – these pedestrians are not aware of the details of the geometry and move randomly to explore the environment and eventually to find the exit. Both populations wish to escape the geometry because they sense a smoke density which indicates the presence of a fire in the building. We use a suitable over-damped Langevin model for the movement of all pedestrians, which will be described in Section 2.4. Hence, our model belongs to the class of social-velocity models for crowd dynamics (see e.g. in [CPT14]). This pedestrian dynamics model is posed in a two dimensional multiple connected region D, containing obstacles with a fixed location together with the presence of a fire. Moreover, we assume that this fire is stationary placed within the geometry. Then, the pedestrians can choose a proper own velocity such that they evacuate and avoid the smoke caused by the fire.

On the other hand, in order to have a more realistic model, the overall dynamics is restricted to a bounded "perforated" domain, i.e. the obstacles are seen as impenetrable regions. The geometry is described in Subsection 2.4.1; see Figure 2.6 to fix ideas. Note that our interacting particles system is posed in a continouous two dimensional multiple connected region D, containing obstacles with a fixed location, a fire that produces smoke which is also seen as an obstacle. Hence, the stochastic differential equation system is restricted to a fixed bounded domain. For this particular class of stochastic differential equations, boundary conditions must be specified. We consider the case of reflecting boundary conditions. In order to achieve a correct description of the dynamics of the pedestrians close to the boundary of the interior obstacles, we refer to works on the classical Skorohod's formulation of SDEs (see e.g. in [Sko61, Lio84, Sai87]). In addition, we describe the movement behavior active pedestrians who are able to avoid collisions with the obstacles by using a motion planning map (*a priori* given paths

– solution to a suitable Eikonal-like equation; cf. Appendix A.2).

In the sequel, we provide more details about the setting model equations for each model.

2.2 Lattice gas dynamics

We start off with the lattice gas models for active–passive pedestrian dynamics. We provide the following two different pedestrian dynamics models that describe the joint evolution of such active and passive populations. One of the model is a lattice model for searching the drafting/aerodynamic drag effects, while an other model employs a simple exclusion process for bi–directional pedestrian flows.

2.2.1 Lattice gas

A lattice gas are particles jumping at random on a lattice (see in e.g. [Spo91]). We assume that the position of particles are restricted to a discrete subset of $\mathbb{R}^d (d \in \mathbb{N}^*)$. In general, this subset is taken to be the d-dimensional cubic lattice

$$\mathbb{Z}^d := \left\{ i = (i_1, \ldots, i_d) \in \mathbb{R}^d : i_k \in \mathbb{Z} \text{ for each } k \in \{1, \ldots, d\} \right\}. \tag{2.1}$$

We call a lattice $\Lambda = \mathbb{Z}^d$ and a state space for the lattice gas is a configuration $\eta \in \Omega = \{0, 1\}^\Lambda$. Since the dynamics of the lattice gas consists of a sequence of jumps. In order to keep track the number of particles, we introduce the so-called occupation number η_i of particles at lattice site i. In addition, η_i taking values in $\{0, 1\}$ such that

$$\eta_i = \begin{cases} 0 & \text{if the site } i \text{ is vacant,} \\ 1 & \text{if the site } i \text{ is occupied.} \end{cases} \tag{2.2}$$

For given the rates we construct the dynamics of lattice gas in the standard fashion. We consider a finite volume Λ, with $|\Lambda| < \infty$, where $|\Lambda|$ represents the number of points in the lattice Λ. Hence, the state space consists of a finite number of configurations. Therefore, the generator of Markov jump process acts on a function $f : \Omega \longrightarrow \mathbb{R}$ is given by

$$\mathcal{L}(\eta) = \sum_{\eta' \in \Omega} c(\eta, \eta')[f(\eta') - f(\eta)],$$

where $c(\eta, \eta')$ are the rate of exchange of the occupancies from the configuration η to η'.

2.2.2 A lattice model for active–passive pedestrian dynamics

In this subsection, we introduce a lattice gas model model for active–passive pedestrian dynamics. The *room* is the square lattice

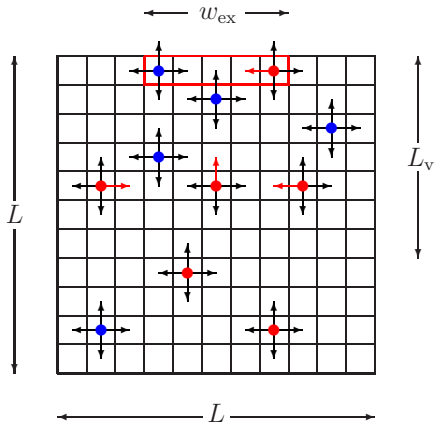

Figure 2.1: Schematic representation of our lattice model. Blue and red disks denote passive and active particles, respectively. The rectangle of sites delimited by the red contour denotes the exit. Black and red arrows (color online) denote transitions performed with rates 1 and $1+\varepsilon$, respectively.

$\Lambda = \{1,\dots,L\}\times\{1,\dots,L\} \subset \mathbb{Z}^2$ of side length L, with L an odd positive integer number, see Figure 2.1. An element $x = (x_1, x_2)$ of the room Λ is called *site* or *cell*. Two sites $x, y \in \Lambda$ are said *nearest neighbor* if and only if $|x - y| = 1$. We conventionally call *horizontal* the first coordinate axis and *vertical* the second one. The words *left*, *right*, *up*, *down*, *top*, *bottom*, *above*, *below*, *row*, and *column* will be used accordingly. We call *exit* a set of w_{ex} pairwise adjacent sites, with w_{ex} an odd positive integer smaller than L, of the top row of the room Λ symmetric with respect to its median column. In other words, the exit is a centered slice of the top row of the room mimicking the presence of an exit door. The number w_{ex} will be called *width* of the exit. Inside the top part of the room we define a rectangular interaction zone, namely, the *visibility region* V, made of the first L_{v} top rows of Λ, with the positive integer $L_{\mathrm{v}} \leq L$ called *depth* of the visibility region. By writing $L_{\mathrm{v}} = 0$, we refer to the case in which no visibility region is considered.

We consider two different species of particles, i.e., *active* and *passive*, moving inside Λ (we shall sometimes use in the notation the symbols A and P to respectively refer to them). Note that the sites of the external boundary of the room, that is to say the sites $x \in \mathbb{Z}^2 \setminus \Lambda$ such that there exists $y \in \Lambda$ nearest neighbor of x, cannot be accessed by the particles. The state of the system will be a *configuration* $\eta \in \mathcal{C} = \{-1, 0, 1\}^{\Lambda}$ and we shall say that the site x is *empty* if $\eta_x = 0$, *occupied by an active particle* if $\eta_x = 1$, and *occupied by a passive particle* if $\eta_x = -1$. The number of active (respectively, passive) particles in the configuration η is given by $n_{\mathrm{A}}(\eta) = \sum_{x\in\Lambda} \delta_{1,\eta_x}$ (resp. $n_{\mathrm{P}}(\eta) = \sum_{x\in\Lambda} \delta_{-1,\eta_x}$), where $\delta_{\cdot,\cdot}$ is Kronecker's symbol. Their sum is the total number of particles in the configuration η.

The dynamics in the room is modeled via a simple exclusion random walk with the two species of particles undergoing two different microscopic dynamics:

the passive particles perform a symmetric simple exclusion dynamics on the whole lattice, while the active particles, on the other hand, perform a symmetric simple exclusion walk outside the visibility region, whereas inside such a region they experience a drift pushing them towards the exit. In other words, the whole room is obscure for the passive particles, while, for the active ones, only the region outside the visibility region is obscure.

What concerns this precise setup, the dynamics is incorporated in the continuous time Markov chain $\eta(t)$ on $\mathcal{C}$ with rates $c(\eta, \eta')$ defined as follows: Let $\varepsilon \geq 0$ be the *drift*; for any pair $x = (x_1, x_2), y = (y_1, y_2)$ of nearest neighbor sites in Λ we set $\epsilon(x, y) = 0$, excepting the following cases in which we set $\epsilon(x, y) = \varepsilon$:

- $x, y \in V$ and $y_2 = x_2 + 1$, namely, x and y belong to the visibility region and x is below y;
- $x, y \in V$ and $y_1 = x_1 + 1 < (L + 1)/2$, namely, x and y belong to the left part of the visibility region and x is to the left with respect to y;
- $x, y \in V$ and $y_1 = x_1 - 1 > (L + 1)/2$, namely, x and y belong to the right part of the visibility region and x is to the right with respect to y.

Next, we let the rate $c(\eta, \eta')$ be equal

- to 1 if η' can be obtained by η by replacing with 0 a -1 or a 1 at the exit (particles leave the room);
- to 1 if η' can be obtained by η by exchanging a -1 with a 0 between two neighboring sites of Λ (motion of passive particles inside Λ);
- to $1 + \epsilon(x, y)$ if η' can be obtained by η by exchanging a $+1$ at site x with a 0 at site y, with x and y nearest neighbor sites of Λ (motion of active particles inside Λ);
- to 0 in all the other cases.

The *infinitesimal generator* $\mathcal{L}$ acts on continuous bounded functions $f : \Omega \to \mathbb{R}$ as

$$\mathcal{L}(\eta) = \sum_{\eta' \in \Omega} c(\eta, \eta')[f(\eta') - f(\eta)]. \tag{2.3}$$

The probability measure induced by the Markov chain started at η is denoted by P_η and the related expectation is denoted by E_η. We refer to [Pav14,Spo91] where similarly–in–spirit models are described mathematically in a rigorous fashion.

The initial number of active (respectively, passive) particles is denoted by $N_{\mathrm{A}} = n_{\mathrm{A}}(\eta_x(0))$ (respectively, $N_{\mathrm{P}} = n_{\mathrm{P}}(\eta_x(0))$). We also let $N = N_{\mathrm{A}} + N_{\mathrm{P}}$ be the initial total number of particles.

For any choice of the initial configuration $\eta(0)$ in Ω, the process will eventually reach the *empty configuration* $\underline{0}$ corresponding to zero particles in the room which is an absorbing point of the chain.

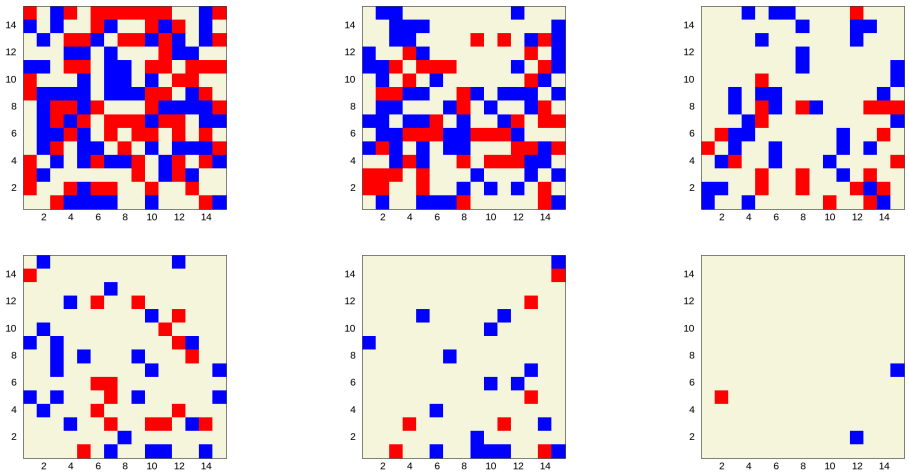

Figure 2.2: Configurations of the model sampled at different times (increasing in lexicographic order). Parameters: $L = 15$, $w_{\mathrm{ex}} = 7$, $L_{\mathrm{v}} = 5$, and $\varepsilon = 0.3$. Red pixels represent active particles, blue pixels denote passive particles, and gray sites are empty. In the initial configuration (top left panel) there are 70 active and 70 passive particles.

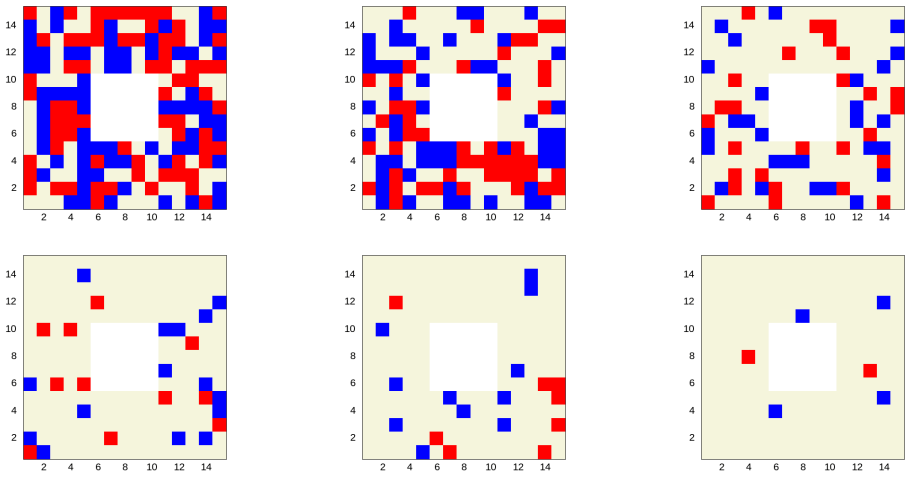

Figure 2.3: As in Figure 2.2, the obstacle is a centered 5×5 square. This fixed obstacle is depicted with white pixels.

As alternative working scenario, we will study the dynamics described above also in the presence of a solid obstacle hindering the pedestrian flow in the room. The *obstacle* is made of an array of sites permanently occupied by fictitious particles. In such a way these sites are never accessible to the actual interacting particles within our system.

The dynamics in both the presence and in the absence of the obstacle is the same and all the parameters have the same meaning and take similar values. In other words, we are implicitly assuming that the presence of the obstacle does not affect the pedestrian behavior: the obstacle is simply a barrier that must be avoided by the walking pedestrian.

Although, in principle, there is no restriction on the choice of the obstacle geometry, in this framework we always consider centered squared obstacles. A thorough investigation of the effect of the choice of obstacle geometry on the evacuation time for mixed pedestrian populations moving thorough partially obscure rooms deserves special attention and will be done in a forthcoming work.

The main goal of the work is to detect drafting in pedestrian flows, namely, identify situations when the evacuation of passive particles is favored by the presence of the active ones, even if no leadership or other kind of information exchange is allowed. We expect that this phenomenon will be effective, provided the active particles will spend a sufficiently long time in the room. This seems to help efficiently passive particles to escape. This effect is illustrated in the Figures 2.2 and 2.3, where we show the configuration of the system at different times both in the absence, and respectively, in the presence of an obstacle. Indeed, the sequences of configurations show that, though the evacuation of active particles is faster than that of the passive ones, even at late times the fraction of active particles is still reasonably high.

2.2.3 A simple exclusion process for bi–directional pedestrian flows

In this subsection, we consider a square lattice $\Lambda = \{1, \dots, L\} \times \{1, \dots, L\}$ with L a positive odd integer. The set Λ is referred in this context as *room* and its points $x = (x_1, x_2)$ as *sites*. Two sites at Euclidean distance one are called *nearest neighbors*. We call *horizontal* and *vertical* the first and the second coordinate axes, respectively. The horizontal and the veritical axes are, respectively, right and up oriented.

The *doors* are the sets made of w_{L} and w_{R} neighboring sites in the left–most and right–most columns of the room, respectively, and symmetric with respect to its median row. This mimics the presence of two distinct doors on the left and right boundary of the room. The odd positive integers $w_{\mathrm{L}}, w_{\mathrm{R}}$ smaller than L will be called *width* of the doors. Inside the room we define a rectangular driven zone, namely, the *visibility region* V, made of the first L_{v} left columns of Λ, with the positive integer $L_{\mathrm{v}} \leq L$ called *depth* of the visibility region. By writing $L_{\mathrm{v}} = 0$, we refer to the case in which no visibility region is considered.

The dynamics will be defined so that particles will be able to exit the room only from sites belonging to the doors: jumps from other sites to the exterior of Λ will be forbidden.

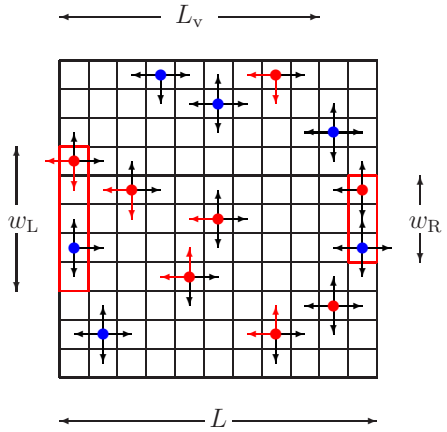

Figure 2.4: Schematic representation of our lattice model. Blue and red disks denote passive and active particles, respectively. The rectangles of sites delimited by the red contour denote the exit doors. Black and red arrows (color online) denote transitions performed with rates 1 and $1+\varepsilon_1$ or $1+\varepsilon_2$, respectively.

We consider two different species of particles, i.e., *active* and *passive* (we shall sometimes use in the notation the symbols A and P to refer to them), moving inside Λ with different dynamics. The interaction of particles inside the room is modelled via a simple exclusion random walk.

The passive particles enter through the left door and exit through the right door. They perform a symmetric simple exclusion dynamics on the whole lattice. Simultaneously, the active particles enter through the right door and exit through the left door. They perform a symmetric simple exclusion walk outside the visibility region, whereas inside such a region they experience also a drift pushing them towards the left door. In other words, the whole room is *obscure*[2] for the passive particles, while, for the active ones, only the region outside the visibility region[3] is obscure. The model also includes two external particle waiting lists, each of which is designed to collect particles of a given species when these move out from the lattice Λ through their exit door and to reinsert them back on the lattice through their entrance door.

More precisely, we consider $N_{\rm A}$ active particles and $N_{\rm P}$ passive ones randomly distributed in the room at time zero, one per site. The motion of the particles is described by a continuous time Markov chain that is rigorously defined in the Appendix. In more simple words, the dynamics is defined as follows: we first pick two non–negative numbers $\varepsilon_1, \varepsilon_2 \geq 0$ called the *horizontal* and the *vertical drift*

[2]We refer the reader to [CKMvS16b], where the authors discuss the gregarious behavior of crowds moving in the dark.

[3]The concept of visibility region was introduced by the authors in [CCMT19].

and, for any pair $x = (x_1, x_2), y = (y_1, y_2)$ of nearest neighbor sites in Λ we set $\epsilon(x, y) = 0$, excepting for the following cases:

- $\epsilon(x, y) = \varepsilon_1$ if $x, y \in V$ and $y_1 = x_1 - 1$, namely, x and y belong to the visibility region and x is to the right with respect to y;
- $\epsilon(x, y) = \varepsilon_2$ if $x, y \in V$ and $y_2 = x_2 + 1 \leq (L + 1)/2$, namely, x belongs to the bottom part of the visibility region and x is below y;
- $\epsilon(x, y) = \varepsilon_2$ if $x, y \in V$ and $y_2 = x_2 - 1 \geq (L + 1)/2$, namely, x belongs to the top part of the visibility region and x is above y.

Next, we assume that particles move with the following rates:

- a passive particle leave the room from a site in the right door with rate 1;
- an active particle leave the room from a site in the left door with rate $1+\epsilon_1$;
- if the number n_{A} of active particles in the room is smaller than N_{A} and the number of empty sites m_{R} in the right door is not zero then an active particle is added to a randomly chosen empty site of the right door with rate $[N_{\mathrm{A}} - n_{\mathrm{A}}]/m_{\mathrm{R}}$;
- if the number n_{P} of passive particles in the room is smaller than N_{P} and the number of empty sites m_{L} in the left door is not zero then a passive particle is added to a randomly chosen empty site of the left door with rate $[N_{\mathrm{P}} - n_{\mathrm{P}}]/m_{\mathrm{L}}$;
- a passive particle moves inside Λ from a site to one of its empty nearest neighbors with rate 1;
- an active particle moves from the site x inside Λ to its empty nearest neighbor y inside Λ with rate $1 + \epsilon(x, y)$.

We note that the quantities $N_{\mathrm{A}} - n_{\mathrm{A}}$ and $N_{\mathrm{P}} - n_{\mathrm{P}}$ represent the number of active, and, respectively, passive particles that exited the room and entered their own waiting list at the considered time, whereas $m_{\mathrm{L}} > 0$ and $m_{\mathrm{R}} > 0$ are the number of empty sites of the left and right doors at the same time.

The system will reach a stationary state, since passive particles exiting the domain via the right door are introduced back in one site randomly chosen among possible empty sites of the left door, while active particles leaving the system through the left door are introduced back also at one random site chosen among possible empty sites of the right door. The total number of active and passive particles in the room Λ is only approximatively constant during the evolution. It slightly fluctuates due to the fact that particles may enter waiting lists. On the other hand, the total number of particles N in the system (considering both the room and the waiting lists) is conserved.

In the study of this dynamics, the main quantity of interest are the stationary *outgoing fluxes* or *currents of active and passive particles* which are the values

approached in the infinite time limit by the ratio between the total number of active and passive particles, respectively, that in the interval $(0, t)$ exited through the left and the right door and entered the waiting lists and the time t. In order to discuss and to understand the behavior of currents with respect to the model parameters, we shall also look at the active and passive particles *occupation number profiles* of active and passive particles, namely, we evaluate the stationary mean value of the occupation numbers of active and passive particles which is equal to one if a site is occupied by a particle of the considered species or zero otherwise.

2.3 A fluid-like driven system

In this section, we introduce a fluid-like driven system for active–passive pedestrian dynamics. In this model, the active population of pedestrians have velocities similar to a non-Darcy flow, namely, a generalized Forchheimer flow as for slightly compressible fluids. Let a bounded set $\Omega \neq \emptyset$, $\Omega \subseteq \mathbb{R}^2$ a domain such that $\partial\Omega = \Gamma^N \cup \Gamma^R$, $\Gamma^N \cap \Gamma^R = \emptyset$ with $\mathcal{H}(\Gamma^N) \neq \emptyset$ and $\mathcal{H}(\Gamma^R) \neq \emptyset$, where $\mathcal{H}$ denotes the surface measure on Γ^N, Γ^R and take $S = (0, T)$. Find the pair (u, v), where $u : S \times \Omega \longrightarrow \mathbb{R}^2$ and $v : S \times \Omega \longrightarrow \mathbb{R}^2$, satisfying the following model equations

$$\begin{cases} \partial_t(u^\lambda) + \operatorname{div}(-K_1(|\nabla u|)\nabla u) = -b(u - v) \ \text{ in } S \times \Omega, \\ \partial_t v - K_2 \Delta v = b(u - v) \ \text{ in } S \times \Omega, \\ -K_1(|\nabla u|)\nabla u \cdot \mathbf{n} = \varphi u^\lambda \ \text{ at } S \times \Gamma^R, \\ -K_1(|\nabla u|)\nabla u \cdot \mathbf{n} = 0 \ \text{ at } S \times \Gamma^N, \\ -K_2 \nabla v \cdot \mathbf{n} = 0 \ \text{ at } S \times \partial\Omega, \\ u(t = 0, x) = u_0(x), \ x \in \bar{\Omega}, \\ v(t = 0, x) = v_0(x), \ x \in \bar{\Omega}. \end{cases} \tag{2.4}$$

Here $K_2 > 0$, while the function K_1 is linked to the derivation of a nonlinear version of Darcy's law involving a polynomial with non-negative coefficients in velocities. This choice is rather non-standard, see e.g. the works [HI11], [ABHI09], [CHK16] and references cited therein for more details in this sense. In addition, $\lambda \in (0, 1]$ is a fixed number and $b(\cdot)$ is a sink/source term. The nonlinear structure of K_1 is described in Section 5.3 together with the remaining model parameters entering (2.4) which are not explained here, as well as with the assumptions needed to ensure the existence of solutions to our problem.

2.4 A system of stochastic differential equations

In this section, we introduce a coupled nonlinear system of Skohorod-like stochastic differential equations modeling the dynamics of pedestrians through a heterogenous domain in the presence of fire. We provide the detail geometry as well as the setting of model equations.

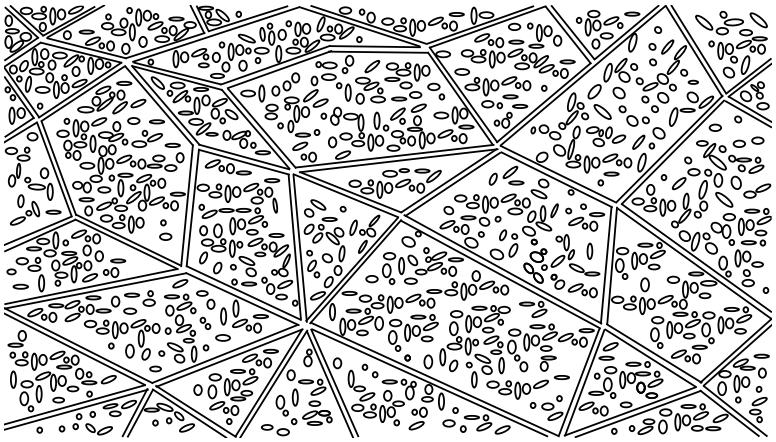

Figure 2.5: Sketch of a distributed flow through a fissured rock, scenario mimicking Fig.1 from [BZK60]. The fissured rock consists of pores and permeable blocks, generally speaking blocks are separated from each other by a system of fissures. Through the fissures, the flow is faster compared to the rest of the media.

2.4.1 Geometry

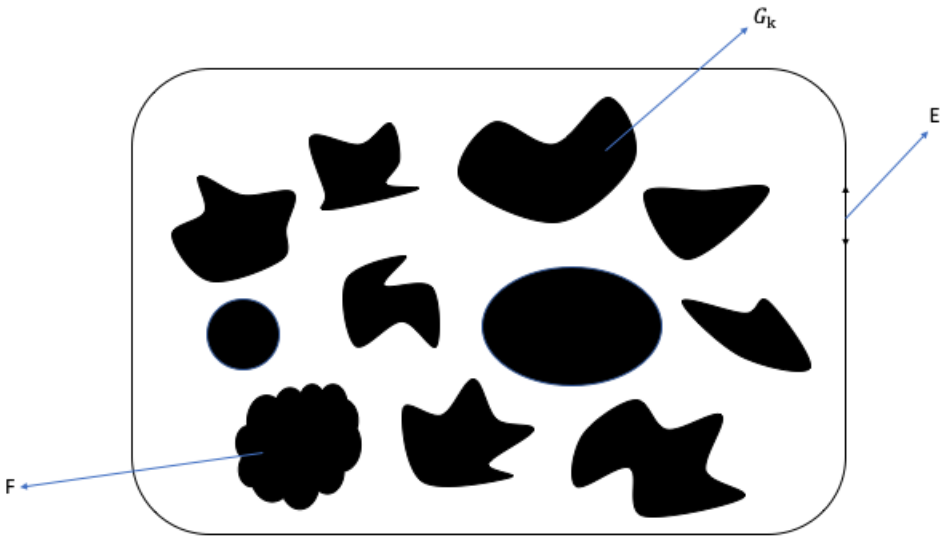

Figure 2.6: Basic geometry for our active-passive pedestrian model. Initially, pedestrians occupy some random position within a geometry with obstacles G_k. Because of the presence of the fire F, and presumably also of smoke, they wish to evacuate via the exit door E while avoiding the obstacles G_k and the fire F.

We consider a two dimensional domain, which we refer to as $\mathbb{O}$. As a building geometry, parts of the domain are filled with obstacles. Their collection is denoted by $G = \bigcup_{k=1}^{N_{\text{obs}}} G_k$, for all $k \in \{1, \ldots, N_{\text{obs}} \in \mathbb{N}\}$. A fire F is introduced somewhere

in this domain and is treated in this context as an obstacle for the motion of the crowd. Moreover, the domain has the exit denoted by E. Our domain represents the environment where the crowd of pedestrians is located. The crowd tries to find the fastest way to the exit, avoiding the obstacles and the fire. Let $D := \mathbb{O}\backslash(G \cup E \cup F) \subset \mathbb{R}^2$ with the boundary ∂D such that $\partial\mathbb{O} \cap \partial G_k = \emptyset$, $\partial\mathbb{O} \cap \partial G_k = \emptyset$ and $F \cap G_k = \emptyset$, we also denote $S = (0, T)$ for some $T \in \mathbb{R}_+$. Furthermore, N_A is the total number of active agents, N_P is the total number of passive particles with $N := N_A + N_P$ and $N_A, N_P, N \in \mathbb{N}$.

2.4.2 Active population

For $i \in \{1, \ldots, N_A\}$ and $t \in S$, let $\mathbf{x}_{a_i}$ denote the position of the pedestrian i belonging to the active population at time t. We assume that the dynamics of active pedestrians is governed by

$$\begin{cases} \frac{d\mathbf{x}_{a_i}(t)}{dt} = -\Upsilon(s(\mathbf{x}_{a_i}(t)) \frac{\nabla\phi(\mathbf{x}_{a_i}(t))}{|\nabla\phi(\mathbf{x}_{a_i}(t))|} \left(p_{\max} - p(\mathbf{x}_{a_i}(t), t)\right) + \Phi_1, \\ \mathbf{x}_{a_i}(0) = \mathbf{x}_{a_{i0}}, \end{cases} \tag{2.5}$$

where $\mathbf{x}_{a_{i0}}$ represents the initial configuration of active pedestrians inside D. In (2.5), $\nabla\phi$ is the minimal motion path of the distance between particle positions $\mathbf{x}_{a_i}$ and the exit location E (it solves the Eikonal-like equation). The function $\phi(\cdot)$ encodes the familiarity with the geometry; see also [YJQH16] for a related setting. We refer to it as the motion planning map. In this context, $p(\mathbf{x}, t)$ is the local discomfort (a realization of the social pressure) so that

$$p(\mathbf{x}, t) = \mu(t) \int_{D \cap B(\mathbf{x}, \tilde{\delta})} \sum_{j=1}^{N} \delta(y - \mathbf{x}_{c_j}(t)) dy, \tag{2.6}$$

for $\{\mathbf{x}_{c_j}\} := \{\mathbf{x}_{a_i}\} \cup \{\mathbf{x}_{b_k}\}$ for $i \in \{1, \ldots, N_A\}, k \in \{1, \ldots, N_P\}, j \in \{1, \ldots, N_A + N_P\}$. In (2.6), δ is the Dirac (point) measure and $B(\mathbf{x}, \tilde{\delta})$ is a ball center $\mathbf{x}$ with small enough radius $\tilde{\delta}$ such that $\tilde{\delta} > 0$. Hence, the discomfort $p(\mathbf{x}, t)$ represents a finite measure on the bounded set $D \cap B(\mathbf{x}, \tilde{\delta})$. In addition, we assume the following structural relation between the smoke extinction and the walking speed (see in [Jin97], [RN19]) as a function $\Upsilon : \mathbb{R}^2_+ \longrightarrow \mathbb{R}^2$ such that

$$\Upsilon(x) = -\zeta x + \eta, \tag{2.7}$$

where ζ, η are given real positive numbers. The dependence of the model coefficients on the local smoke density is marked via a smooth relationship with respect to an a priori given function $s(x, t)$ describing the distribution of smoke inside the geometry at position x and time t. Moreover, Φ_1 entering (2.5) is a associated process to ensures the reflecting process.

2.4.3 Passive population

For $k \in \{1, \ldots, N_P\}$ and $t \in S$, let $\mathbf{x}_{p_k}$ denote the position of the pedestrian k belonging at time t to the passive population. The dynamics of the passive

pedestrians is described here as a system of stochastic differential equations as follows:

$$\begin{cases} d\mathbf{x}_{p_k}(t) = \sum_{j=1}^{N} \frac{\mathbf{x}_{c_j} - \mathbf{x}_{p_k}}{\epsilon + |\mathbf{x}_{c_j} - \mathbf{x}_{p_k}|} \omega(|\mathbf{x}_{c_j} - \mathbf{x}_{p_k}|, s(\mathbf{x}_{p_k}, t))dt + \beta(s(\mathbf{x}_{p_k}, t))dB(t) + \Phi_2, \\ \mathbf{x}_{p_k}(0) = \mathbf{x}_{p_{k0}}, \end{cases} \tag{2.8}$$

where $\mathbf{x}_{p_{k0}}$ represents the initial configuration of passive pedestrians inside D and $\epsilon > 0$. In (2.8), ω is a Morse-like potential function (see e.g. Ref. [CMP13] for a setting where a similar potential has been used).We take $\omega : \mathbb{R} \times \mathbb{R}^2 \longrightarrow \mathbb{R}^2$ to be

$$\omega(x, y) = -\beta(y) \left(C_A e^{-\frac{x}{\ell_A}} + C_R e^{-\frac{x}{\ell_R}} \right), \text{ for } x, y \in \mathbb{R} \times \mathbb{R}^2 \tag{2.9}$$

while $C_A > 0, C_R > 0$ are the attractive and repulsive strengths and $\ell_A > 0, \ell_R > 0$ are the respective length scales for attraction and repulsion. Moreover, the coefficient β is the Heaviside step function. As in Subsection 2.4.2, the dependence of the model coefficients on the smoke is marked via a smooth relationship with respect to an a priori given function $s(x, t)$ (the smoke concerntration, cf. Appendix A.4) describing the distribution of smoke inside the geometry at position x and time t. In additions, Φ_2 is a associated process to ensure the reflecting process. Note that the passive pedestrians do not posses any knowledge on the geometry of the walking space. In particular, the location of the exit is unknown; see [CP19] for a somewhat related context.

2.5 Discussion

We presented three conceptually different crowd dynamics models that describe the joint evolution of active–passive populations.

In Section 2.2, we introduced two different lattice models for the active–passive pedestrian dynamics: one of the models describes the evacuation of pedestrian populations from an obscure room, while another model employs the scenario of pedestrians walking in a built environment and entering a room from two opposite sides. The descriptions are based on a simple exclusion process. From the statistical physics perspective, there are potential open directions that would need further discovery. A large scale model with a more complexity geometry (e.g. stadium, airport, ...) can be studied. The idea of mixed pedestrian flows brings in a lot interesting questions in the field of pedestrian evacuation studies, one of them is the topic of "exit choices". Also, it would be interesting to build a more realistic crowd model where the active pedestrians can transmit the information of the geometry to the passive pedestrians. Within this framework, one can consider an intelligent design of building interiors to provide a basis for smart evacuation signaling systems.

In Section 2.3, we presented a fluid-like driven system modeling the active–passive pedestrian dynamics in a heterogenous domain. It would be interesting

if we can extend the current model for a more complex geometry involving the presence of fire, smoke, obstacles as well as exit doors. From a micro-to-macro perspective, it is worth studying whether a generalized Forchheimer flow model (i.e. the first partial differential equation in (2.4)) can be obtained in principle via homogenization techniques (like in [LLPW11], e.g.), but it is not clear at this stage how a suitable microscopic model defined at the level of the geometry depicted in Figure 2.5 would look like.

In Section 2.4, we decided to consider a system of stochastic differential equations of Skohorod type modeling again the dynamics of active–passive pedestrian dynamics in a heterogenous domain. In order to have a more realistic model, it would be interesting to extend the scenario with including exit doors, where absorbing boundary conditions are defined. This brings in the question how to define mixed reflecting and absorbing boundary conditions in the Skorohod setup.

In order to connect microscopic and macroscopic time and length scales, it would be instructive to formulate hybrid pedestrian dynamics in complex geometries where there is a feedback mechanism between population dynamics at micro and macro scales and their surrounding environment. A multiscale setting where deterministic partial differential equation would need to be coupled with SDEs.

Chapter 3

A lattice model for active–passive pedestrian dynamics

In this chapter, we study the pedestrian escape from an obscure room using a lattice gas model with two species of particles. One species, called passive, performs a symmetric random walk on the lattice, whereas the second species, called active, is subject to a drift guiding the particles towards the exit. The drift mimics the awareness of some pedestrians of the geometry of the room and of the location of the exit. We provide numerical evidence that, in spite of the hard core interaction between particles – namely, there can be at most one particle of any species per site – adding a fraction of active particles in the system enhances the evacuation rate of all particles from the room. A similar effect is also observed when looking at the outgoing particle flux, when the system is in contact with an external particle reservoir that induces the onset of a steady state. We interpret this phenomenon as a discrete space counterpart of the drafting effect typically observed in a continuum set–up as the aerodynamic drag experienced by pelotons of competing cyclists. This is based on [CCMT19].

3.1 Introduction

This work is part of a larger recent research initiative oriented towards investigating the evacuation behavior of crowds of pedestrians where the geometry in which the dynamics takes place is partly unknown and possibly also with limited visibility. Such scenarios are encountered for instance when catastrophic situations occur in urban environments (e.g., in large office spaces), in tunnels, within underground spaces and/or in forests in fire. We refer the reader, for instance, to [ABCK16, FRNF13, MWS14, WS14, XJJS16] and references cited therein, as well as to our previous results; see e.g. [CCCM18]. Experimental information in this context is provided, for instance, in [vKS17] and [OP17] (also in connection with what is usually referred to as "faster-is-slower" effect). In the current framework, our hypothesis is that the crowd under consideration is always heterogeneous in the sense that some part of the population is well informed about

the details of the geometry of the location and corresponding exits as well as of the optimal escape routes and consequently adapts its motion strategy, while the rest of the population has a passive attitude and move without following a precise strategy. This is exactly the standing assumption we have investigated in [CMRT19, RJM19] for a dynamics in smoke scenario.

It turns out that in situations where the information can only difficultly be transmitted from pedestrian to pedestrian (like when large crowds are present and/or if the geometry of the evacuation is largely unknown or invisible and/or groups are not able to act rationally), the use of leaders to guide crowds towards the exists might not always be possible, or it works inefficiently. In such cases, leadership is not essential to speed up evacuation[1]. So, what can then be still done to improve evacuations for such unfavorable conditions, i.e. to decrease the evacuation time of the overall crowd? One of the main points we want to make here is the following: Even if information cannot be transmitted within the crowd, simply having a suitable fraction of informed pedestrians speeds up the overall evacuation time.

We study the typical time needed by a heterogeneous crowd of pedestrians to escape a dark room. The heterogeneity of the crowd is incorporated in the fact that we consider two pedestrian species, the *active* and the *passive* one, i.e., those who know the location of the exit and those who do not. Using a lattice–type model, we show that the presence of pedestrians aware of the location of the exit helps the unaware companions to find the exit of the room even in absence of any information exchange among them. This effect will be called *drafting* and it has a twofold interpretation: i) active particles, quickly moving towards the exit, will leave a wake of empty sites in which the unaware particles can jump in, so that they are guided to the exit; ii) active pedestrians, in their rational motion towards the exit, push their passive companions to the exit as well. People belonging to the same group do not necessarily have to move together or coherently, for they only share the same dynamical rules. In other words, the motion of one pedestrian is not directly affected by the motion of the pedestrians belonging to the same group. The sole interaction we consider here is the hard–core repulsion between any pair of pedestrians, regardless of their group. In this sense the situation we

[1]This is contrary to situations like those described on [IDCL05], where leadership is an efficient crowd management mechanism. Yet, often in pedestrian crowds there are no obvious leaders, such as those present, for instance, in political demonstrations. There is contrary evidence concerning the efficiency of the leadership in managing crowds. For instance, sometimes artists (who could be seen as leaders of crowds) have wrongly been accused of working against safety personnel or police. A famous example is that of the band Pearl Jam at the Roskilde Festival in 2001. A number of people died and responsibility was placed on the band and their actions. The inquiry that came later then altered this view. See some information on this matter can be found via https://uproxx.com/music/pearl-jam-roskilde/. Another example dates back to the 1989 Hillsborough Disaster. Using Hillsborough literature, police accused the crowds in the wake of the tragic event but, almost 30 years later, all accusations were dropped and blame was heavily placed on police and organisation. This article seems to cover it: https://www.tandfonline.com/doi/full/10.1080/14660970420002352O9?casa_token=O7xM8m5HQScAAAAA:AU8DNl8LPnuSv5a01w0iw3WXEXA2AHDE95M7szy6WAkzoql4v0c2Niv44wQK5WC1eDg_qYbNFJPLLA.

have in mind is different from the one considered in some experiments, where people in the same social group move coherently and not independently [vKS17].

We refer the reader to for instance to [ACK15, BCG$^+$16, CPT14] for some level of details on crowd dynamics modelling and to [CC18, CKMvS16b, CP17] for relevant works regarding the handling of the presence of the obstacles and the way they affect the pedestrian motion. Mind also that similar situations appear frequently also in soft matter physics cf. e.g. [DAM11].

The reminder of the chapter is organized as follows. In Section 3.2 we define the model. Section 3.3 is devoted to the study of the evacuation time. In Section 3.4 a slightly modified version of the model is considered, so that a not trivial stationary state is reached. For such a model the stationary exit flux is thus studied. In Section 3.5, we summarize our conclusions and give a glimpse of possible further research.

3.2 The model

The *room* is the square lattice $\Lambda = \{1, \dots, L\} \times \{1, \dots, L\} \subset \mathbb{Z}^2$ of side length L, with L an odd positive integer number, see Figure 3.1. An element $x = (x_1, x_2)$ of the room Λ is called *site* or *cell*. Two sites $x, y \in \Lambda$ are said *nearest neighbor* if and only if $|x-y| = 1$. We conventionally call *horizontal* the first coordinate axis and *vertical* the second one. The words *left*, *right*, *up*, *down*, *top*, *bottom*, *above*, *below*, *row*, and *column* will be used accordingly. We call *exit* a set of w_{ex} pairwise adjacent sites, with w_{ex} an odd positive integer smaller than L, of the top row of the room Λ symmetric with respect to its median column. In other words, the exit is a centered slice of the top row of the room mimicking the presence of an exit door. The number w_{ex} will be called *width* of the exit. Inside the top part of the room we define a rectangular interaction zone, namely, the *visibility region* V, made of the first L_{v} top rows of Λ, with the positive integer $L_{\text{v}} \leq L$ called *depth* of the visibility region. By writing $L_{\text{v}} = 0$, we refer to the case in which no visibility region is considered.

We consider two different species of particles, i.e., *active* and *passive*, moving inside Λ (we shall sometimes use in the notation the symbols A and P to respectively refer to them). Note that the sites of the external boundary of the room, that is to say the sites $x \in \mathbb{Z}^2 \setminus \Lambda$ such that there exists $y \in \Lambda$ nearest neighbor of x, cannot be accessed by the particles. The state of the system will be a *configuration* $\eta \in \Omega = \{-1, 0, 1\}^\Lambda$ and we shall say that the site x is *empty* if $\eta_x = 0$, *occupied by an active particle* if $\eta_x = 1$, and *occupied by a passive particle* if $\eta_x = -1$. The number of active (respectively, passive) particles in the configuration η is given by $n_{\text{A}}(\eta) = \sum_{x\in\Lambda} \delta_{1,\eta_x}$ (resp. $n_{\text{P}}(\eta) = \sum_{x\in\Lambda} \delta_{-1,\eta_x}$), where $\delta_{\cdot,\cdot}$ is Kronecker's symbol. Their sum is the total number of particles in the configuration η.

The dynamics in the room is modeled via a simple exclusion random walk with the two species of particles undergoing two different microscopic dynamics: the passive particles perform a symmetric simple exclusion dynamics on the whole

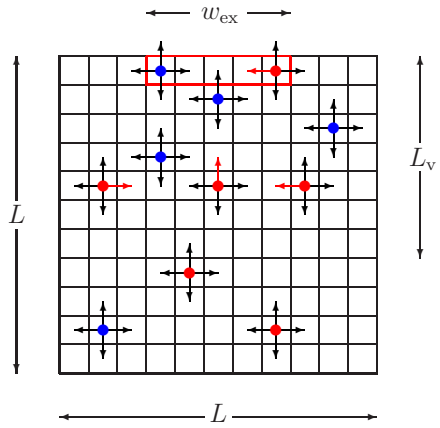

Figure 3.1: Schematic representation of our lattice model. Blue and red disks denote passive and active particles, respectively. The rectangle of sites delimited by the red contour denotes the exit. Black and red arrows (color online) denote transitions performed with rates 1 and $1+\varepsilon$, respectively.

lattice, while the active particles, on the other hand, perform a symmetric simple exclusion walk outside the visibility region, whereas inside such a region they experience a drift pushing them towards the exit. In other words, the whole room is obscure for the passive particles, while, for the active ones, only the region outside the visibility region is obscure.

What concerns this precise setup, the dynamics is incorporated in the continuous time Markov chain $\eta(t)$ on Ω with rates $c(\eta,\eta')$ defined as follows: Let $\varepsilon \geq 0$ be the *drift*; for any pair $x=(x_1,x_2), y=(y_1,y_2)$ of nearest neighbor sites in Λ we set $\epsilon(x,y)=0$, excepting the following cases in which we set $\epsilon(x,y)=\varepsilon$:

- $x,y \in V$ and $y_2 = x_2+1$, namely, x and y belong to the visibility region and x is below y;
- $x,y \in V$ and $y_1 = x_1+1 < (L+1)/2$, namely, x and y belong to the left part of the visibility region and x is to the left with respect to y;
- $x,y \in V$ and $y_1 = x_1-1 > (L+1)/2$, namely, x and y belong to the right part of the visibility region and x is to the right with respect to y.

Next, we let the rate $c(\eta,\eta')$ be equal

- to 1 if η' can be obtained by η by replacing with 0 a -1 or a 1 at the exit (particles leave the room);
- to 1 if η' can be obtained by η by exchanging a -1 with a 0 between two neighboring sites of Λ (motion of passive particles inside Λ);
- to $1+\epsilon(x,y)$ if η' can be obtained by η by exchanging a $+1$ at site x with a 0 at site y, with x and y nearest neighbor sites of Λ (motion of active particles inside Λ);

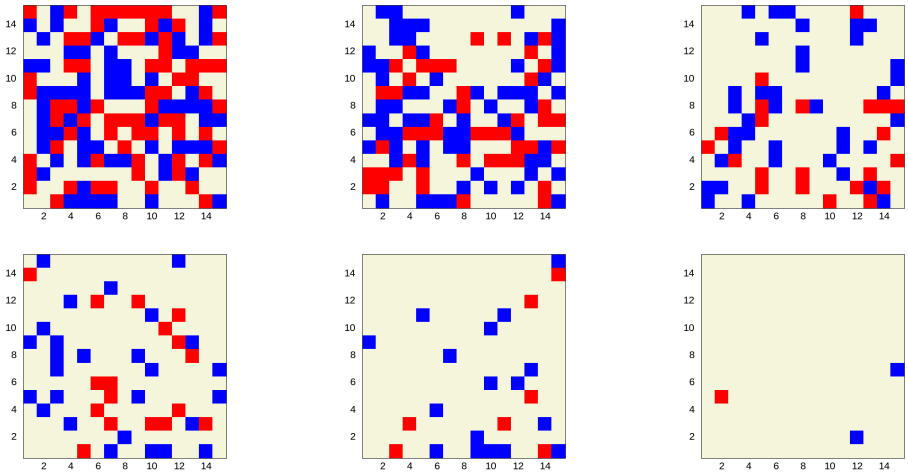

Figure 3.2: Configurations of the model sampled at different times (increasing in lexicographic order). Parameters: $L = 15$, $w_{\text{ex}} = 7$, $L_{\text{v}} = 5$, and $\varepsilon = 0.3$. Red pixels represent active particles, blue pixels denote passive particles, and gray sites are empty. In the initial configuration (top left panel) there are 70 active and 70 passive particles.

– to 0 in all the other cases.

The *infinitesimal generator* $\mathcal{L}$ acts on continuous bounded functions $f : \Omega \to \mathbb{R}$ as

$$\mathcal{L}(\eta) = \sum_{\eta' \in \Omega} c(\eta, \eta')[f(\eta') - f(\eta)]. \tag{3.1}$$

The probability measure induced by the Markov chain started at η is denoted by P_η and the related expectation is denoted by E_η. We refer to [Pav14,Spo91] where similarly–in–spirit models are described mathematically in a rigorous fashion.

The initial number of active (respectively, passive) particles is denoted by $N_{\text{A}} = n_{\text{A}}(\eta_x(0))$ (respectively, $N_{\text{P}} = n_{\text{P}}(\eta_x(0))$). We also let $N = N_{\text{A}} + N_{\text{P}}$ be the initial total number of particles.

For any choice of the initial configuration $\eta(0)$ in Ω, the process will eventually reach the *empty configuration* $\underline{0}$ corresponding to zero particles in the room which is an absorbing point of the chain.

As alternative working scenario, we will study the dynamics described above also in the presence of a solid obstacle hindering the pedestrian flow in the room. The *obstacle* is made of an array of sites permanently occupied by fictitious particles. In such a way these sites are never accessible to the actual interacting particles within our system.

The dynamics in both the presence and in the absence of the obstacle is the same and all the parameters have the same meaning and take similar values. In other words, we are implicitly assuming that the presence of the obstacle does not affect the pedestrian behavior: the obstacle is simply a barrier that must be avoided by the walking pedestrian.

Although, in principle, there is no restriction on the choice of the obstacle geometry, in this framework we always consider centered squared obstacles. A

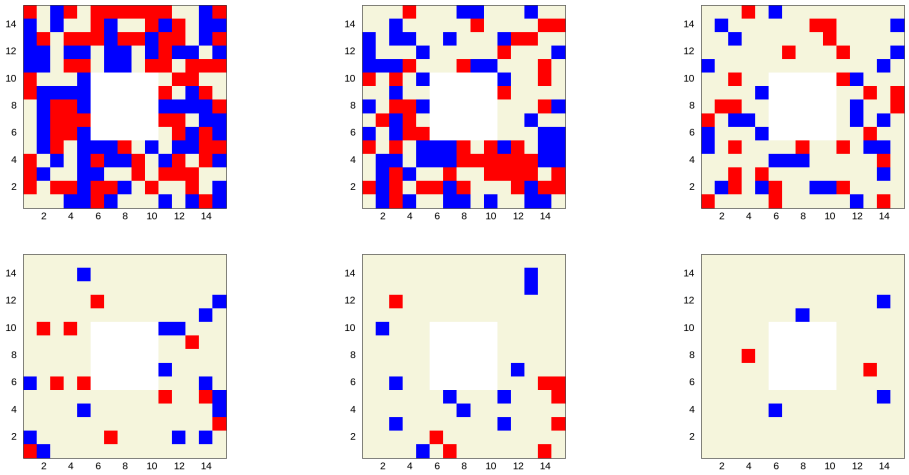

Figure 3.3: As in Figure 3.2, the obstacle is a centered 5×5 square. This fixed obstacle is depicted with white pixels.

thorough investigation of the effect of the choice of obstacle geometry on the evacuation time for mixed pedestrian populations moving thorough partially obscure rooms deserves special attention and will be done in a forthcoming work.

We simulate this process using the following scheme: at time t we extract an exponential random time τ with parameter the total rate $\sum_{\zeta \in \Omega} c(\eta(t), \zeta)$ and set the time equal to $t + \tau$. We then select a configuration using the probability distribution $c(\eta(t), \eta) / \sum_{\zeta \in \Omega} c(\eta(t), \zeta)$ and set $\eta(t + \tau) = \eta$.

As we have already pointed out in Section 3.1, the main goal of the paper is to detect drafting in pedestrian flows, namely, identify situations when the evacuation of passive particles is favored by the presence of the active ones, even if no leadership or other kind of information exchange is allowed. We expect that this phenomenon will be effective, provided the active particles will spend a sufficiently long time in the room. This seems to help efficiently passive particles to escape. This effect is illustrated in the Figures 3.2 and 3.3, where we show the configuration of the system at different times both in the absence, and respectively, in the presence of an obstacle. Indeed, the sequences of configurations show that, though the evacuation of active particles is faster than that of the passive ones, even at late times the fraction of active particles is still reasonably high.

3.3 The evacuation time

Consider the dynamics defined in Section 3.2, given a configuration $\eta \in \mathcal{C}$. We let τ_η be the first hitting time to the empty configuration, i.e.

$$\tau_\eta = \inf\{t > 0 : \eta(t) = \underline{0}\}, \tag{3.2}$$

for the chain started at η. Given a configuration $\eta \in \mathcal{C}$, we define the *evacuation time* starting from η as

$$T_\eta = \mathbb{E}_\eta[\tau_\eta] \, . \tag{3.3}$$

We have defined the evacuation time as the time needed to evacuate all the particles initially in the system, that is to say the evacuation time is the time at which the last particle leaves the room. In this section as well as in the next one, we study numerically the evacuation time for a fixed initial random condition and then produce various realizations of the process for specific values of the initial drift ε and of the visibility depth $L_{\rm v}$. To this end, we consider two geometrically different situations: (i) the empty roomand (ii) the room with a squared obstacle positioned at the center.

3.3.1 The empty room case

We consider the system defined in Section 3.2 for $L = 15$ (side length of the room), $w_{\rm ex} = 7$ (exit width), $N_{\rm P} = 70$ (initial number of passive particles) $N_{\rm A} = 0, 70$ (initial number of active particles) $L_{\rm v} = 2, 5, 7, 15$ (visibility depth), and $\varepsilon = 0.1, 0.3, 0.5$ (drift). More details are provided in the figure captions.

All the simulations are done starting the system from the same initial configuration chosen once for all by distributing the particle at random with uniform probability. More precisely, two initial configurations are considered, one for the case $N_{\rm P} = 70$ and $N_{\rm A} = 0$ and one for the case $N_{\rm P} = 70$ and $N_{\rm A} = 70$, chosen in such a way that in the two cases the initial positions of the passive particle is the same, see Figure 3.4 for a schematic illustration.

We then compute the time needed to evacuate all the particles initially in the systems and, by averaging over 10^5 different realizations of the process, we compute a numerical estimate of the evacuation time (3.3) for the chosen initial condition. Results are reported in Figure 3.5.

The main result of our investigation is the following: the evacuation time T_η corresponding to the initial configuration with active particles (see the illustration (b) in Figure 3.4) is *less* than that corresponding to the initial configuration with sole passive particles (see the illustration (a) in Figure 3.4). This result is non–trivial since our lattice dynamics is based on a hard core exclusion principle [Spo91] – the motion of particles towards the exit is hindered by the presence of nearby particles. In the context of this work, we refer to this phenomenon as drafting, marking this way the analogy with the drafting or aerodynamic drag effect encountered by pelotons of cyclists racing towards the goal; we refer the reader, for instance, to [BvDT$^+$18, BTvDA18] and references cited therein, for wind tunnel and computational evidence on drafting. It is crucial to note that the presence of active particles is essential for the onset of this phenomenon: if all active particles in the configuration (b) in Figure 3.4 (represented by the red pixels) were replaced by passive ones (blue pixels), the evacuation time would clearly become larger than with the configuration (a). This is essentially due to the exclusion constraint of the lattice gas dynamics.

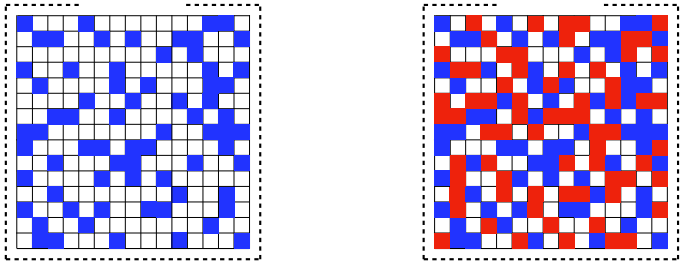

(a) (b)

Figure 3.4: Two initial configurations for the lattice gas dynamics. Blue and red pixels represent, respectively, passive and active particles. The thick dashed line surrounding a large fraction of the grid denotes the presence of reflecting boundary conditions. The exit door is located in presence of the missing segment of dashed line. In (a) only N_{P} passive particles are present. In (b), the passive particles occupy the same initial positions as in (a), and N_{A} active particles are also included (we fix $N_{\mathrm{A}} = N_{\mathrm{P}}$). We shall compare the evacuation time relative to the two configurations in (a) and (b).

In the left panel in Figure 3.5, the dependence of the evacuation time on the drift ε is shown. Open symbols refer to the evacuation time for $N_{\mathrm{P}} = 70$ and $N_{\mathrm{A}} = 70$; for each value of ϵ we repeat the measure of the evacuation time also for a system in which only passive particles are present. We then obtain the sequence of solid disks reported in the figure which is approximatively constant, since the dynamics of the passive particles does not depend on ε. We observe that the small fluctuations visible in the data represented by solid disks Figure 3.5 come from considering averages over a finite number of different realizations of the process (all starting from the given initial configuration).

Since the number particles in the initial configuration in the experiments with the presence of active particles is double with respect to that considered in the case of only passive particles, one would expect a larger evacuation time. This is indeed the case for a small visibility depth, i.e. for $L_{\mathrm{v}} = 2$. In such a case, it is worth noting that the evacuation time decreases when the drift is increased as it is in fact reasonable since a larger drift favors the fast evacuation of active particles, but it remains larger than the evacuation time in absence of active particles for all the values of ε that we considered. On the other hand, for larger values of the visibility depth, as long as the drift is large enough, the evacuation time in the presence of active particles becomes smaller than the one measured in the presence of only passive particles.

This effect is rather surprising. It can interpreted by saying that the presence of active particles, which have some information about the location of the exit,

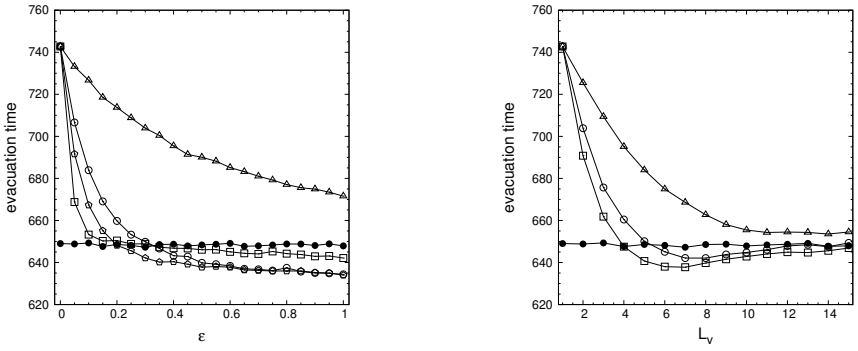

Figure 3.5: Evacuation time in an empty room for $L = 15$, $w_{\rm ex} = 7$, $N_{\rm A} = 0$ and $N_{\rm P} = 70$ (solid disks) and $N_{\rm A} = N_{\rm P} = 70$ (open symbols). Left panel: $L_{\rm v} = 2$ (open triangles), $L_{\rm v} = 5$ (open circles), $L_{\rm v} = 7$ (open pentagons), $L_{\rm v} = 15$ (open squares). Right panel: $\varepsilon = 0.1$ (open triangles), $\varepsilon = 0.3$ (open circles), $\varepsilon = 0.5$ (open squares).

helps passive particles to evacuate the room even if no information exchange is allowed, and, mostly, even in presence of the exclusion constraint of the lattice gas dynamics. Indeed, passive particles continue their blind symmetric dynamics, nevertheless their evacuation time is reduced. The sole interaction among passive and active particles is the exclusion rules, hence one possible interpretation of this effect is that active particles, while walking toward the exit, leave behind a sort of empty sites wake. Passive particles, on the other hand, can benefit of such an empty path and be thus blindly driven towards the exit. A different interpretation is that passive particles, due to the exclusion rule, are pushed by active particles towards the exit.

In the right panel of Figure 3.5, for the same choices of parameters and initial conditions, we show the evacuation time as a function of the visibility depth $L_{\rm v}$ for several values of the drift ε. Data can be discussed similarly as we did for those plotted in the left panel of the same figure: for small drift, and for any choice of the visibility length, the evacuation time in presence of active particles is larger than the one measured with sole passive particles. But, if the drift is increased, for a sufficiently large visibility depth, the evacuation time in presence of active particles becomes smaller than the one for sole passive particles though the total number of particles to be evacuated is doubled. As before we interpret these data as an evidence of the presence of the drafting effect.

Remarkably, for sufficiently large drift ε, the evacuation time is not monotonic with respect to the visibility depth. In other words, there is an optimal value of $L_{\rm v}$ which minimizes the evacuation time. The fact that for $L_{\rm v}$ too large, i.e., comparable with the side length of the room, the evacuation time increases with $L_{\rm v}$ can be explained remarking that if active particles exit the system too quickly then passive particles, left alone in the room, evacuate it with their standard time. Hence, the drafting effect is visible as long as the parameters ε and $L_{\rm v}$ make the motion of the active particles towards the exit enough faster than that of passive

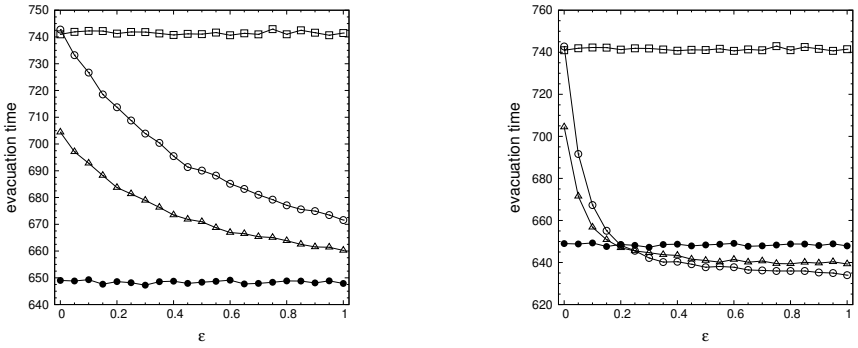

Figure 3.6: Evacuation time in an empty room for $L = 15$, $w_{\rm ex} = 7$, $N_{\rm A} = 0$ and $N_{\rm P} = 70$ (solid disks), $N_{\rm A} = 35$ and $N_{\rm P} = 70$ (open triangles), $N_{\rm A} = 70$ and $N_{\rm P} = 70$ (open circles) and $N_{\rm A} = 0$ and $N_{\rm P} = 140$ (open squares). Left panel: $L_{\rm v} = 2$. Right panel: $L_{\rm v} = 7$.

particles, but not too fast. Indeed, if the active particles move too slowly, they behave as passive ones: this would make the evacuation time larger, due to the standard exclusion constraint of our lattice gas dynamics. On the other hand, if the active particles move too fast, passive particles remain soon alone on the lattice, therefore the evacuation time relative to the configuration of type (b) in Figure 3.4 reduces to that relative to the configuration of type (a).

Before concluding this Section, we shall also highlight the effect of varying the relative amount of active and passive particles in the initial configuration. In Figure 3.6 we also present the average evacuation times for the cases with $N_{\rm P} = 70$, $N_{\rm A} = 35$ and $N_{\rm P} = 140$, $N_{\rm A} = 0$, for two different values of $L_{\rm v}$. One readily notices that when the number of passive particles is doubled (case $N_{\rm P} = 140$ and $N_{\rm A} = 0$) the evacuation time increases and it obviously results to be independent of ε and $L_{\rm v}$. For small visibility depth ($L_{\rm v} = 2$ in the left panel in Figure 3.6) the evacuation time for the case $N_{\rm A} = 35$ and $N_{\rm P} = 70$ is smaller than the one mesured in the case $N_{\rm A} = 70$ and $N_{\rm P} = 70$ for any ε and shows a monotonic decrease. The results are more interesting for larger visibility depth ($L_{\rm v} = 7$ in the right panel in Figure 3.6): if the drift ε is large enough, namely, larger than about 0.2, the total evacuation time in presence of active particles becomes smaller than the one measured for sole passive particles both for the case $N_{\rm A} = 35$ and $N_{\rm P} = 70$ and $N_{\rm A} = 70$ and $N_{\rm P} = 70$, that is to say, in both cases the drafting effect shows up. More interestingly, the evacuation time is smaller in the case in which more active particles are present (open circles in the picture): this is a sort of signature of the drafting effect.

3.3.2 The room with an obstacle

Simulations similar with those described in Section 3.3.1 have been run in presence of a centered square obstacle made of 5×5 sites of the room not accessible by both active and passive particles. As before, we have computed the evacuation time in such a case and results are reported in Figure 3.7.

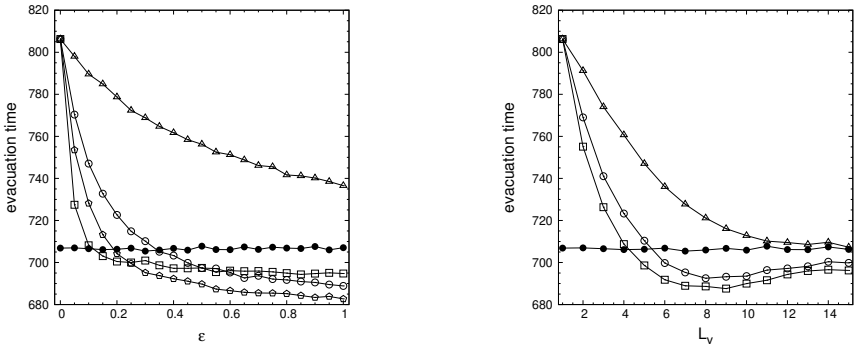

Figure 3.7: Evacuation time in a room with a 5×5 squared centered obstacle for $L = 15$, $w_{\rm ex} = 7$, $N_{\rm A} = 0$ and $N_{\rm P} = 70$ (solid disks) and $N_{\rm A} = N_{\rm P} = 70$ (open symbols). Left panel: $L_{\rm v} = 2$ (open triangles), $L_{\rm v} = 5$ (open circles), $L_{\rm v} = 7$ (open pentagons), $L_{\rm v} = 15$ (open squares). Right panel: $\varepsilon = 0.1$ (open triangles), $\varepsilon = 0.3$ (open circles), $\varepsilon = 0.5$ (open squares).

It is immediate to remark that plots in Figure 3.7 are very similar to those shown in Figure 3.5. Our interpretation of the results is then the same. We just mention that the vertical scale is slightly different and we notice that, in presence of an obstacle, the drafting effect is slightly increased. The fact that the presence of an obstacle with suitable geometry can favor the evacuation of a room is a fact already established in the literature, see, e.g., [CCCM18,CC18,CKMvS16b,CP17] and references therein.

3.4 The stationary flux

To detect non–trivial behaviors as time elapses beyond a characteristic walking timescale, we consider now a modified version of the model proposed in Section 2.2.2. Essentially, the current situation is as follows: Particles exiting the system are introduced back in one site, randomly chosen among the empty sites of the room so that the total number of active and passive particles is approximatively kept constant during the evolution. This way, the system reaches a final stationary state and in such a state we shall measure the flux of exiting active and passive particles.

The main idea is to add a *reservoir* in which particles exiting the room are collected. Particles in the reservoir are then introduced inside Λ with rates depending on the number of particles in such a reservoir and on the number of empty sites in the room.

More precisely, recall the definition of the number of active and passive particles $n_A(\eta)$ and $n_P(\eta)$ in the configuration η and fix two non–negative integer numbers $N_{\rm A}$ and $N_{\rm P}$. Consider the Markov process defined in Section 2.2.2 with an initial configuration with total number of active and passive particles respectively equal to $N_{\rm A}$ and $N_{\rm P}$ and rates $c(\eta, \eta')$, for $\eta, \eta' \in \mathcal{C}$, defined as in Section 2.2.2 with the following modification:

– if η' can be obtained by η by adding a $+1$ at an empty site x then $c(\eta, \eta') = [N_{\mathrm{A}} - n_{\mathrm{A}}(\eta)]/(L^2 - n_{\mathrm{A}}(\eta) - n_{\mathrm{P}}(\eta))$ (moving an active particle from the reservoir to an empty site in the room);

– if η' can be obtained by η by adding a -1 at an empty site x then $c(\eta, \eta') = [N_{\mathrm{P}} - n_{\mathrm{P}}(\eta)]/(L^2 - n_{\mathrm{A}}(\eta) - n_{\mathrm{P}}(\eta))$ (moving a passive particle from the reservoir to an empty site in the room).

At time t, the quantities $N_{\mathrm{A}} - n_{\mathrm{A}}(\eta(t))$ and $N_{\mathrm{P}} - n_{\mathrm{P}}(\eta(t))$ represent the number of active, and respectively, passive particles in the reservoir at time t, whereas $L^2 - n_{\mathrm{A}}(\eta(t)) - n_{\mathrm{P}}(\eta(t))$ is the number of empty sites of the room at time t.

With these changes in the definition of the rate, the total number of particles in the system (considering the room and the reservoir) is conserved. The number of particles in the room, on the other hand, will fluctuate due to the fact that particles can accumulate in the reservoir.

In the study of this dynamics, the main quantity of interest is the stationary *outgoing flux* or *current* which is the value approached in the infinite time limit by the ratio between the total number of particle that in the interval $(0, t)$ jumped from the exit to the reservoir and the time t.

3.4.1 The empty room case

We consider the system defined in Section 3.4 for $L = 15$ (side length of the room), $w_{\mathrm{ex}} = 7$ (exit width), $N_{\mathrm{P}} = 70$ (number of passive particles) $N_{\mathrm{A}} = 0, 70$ (number of active particles) $L_{\mathrm{v}} = 2, 5, 7, 15$ (visibility depth), and $\varepsilon = 0.1, 0.3, 0.5$ (drift). More details on the selected parameters regimes are provided in the figure captions.

As in Section 3.3.1, all the simulations share the same initial configuration obtained by distributing the particle at random with a uniform probability. More precisely, two initial configurations are considered, one for the case $N_{\mathrm{P}} = 70$ and $N_{\mathrm{A}} = 0$ and one for the case $N_{\mathrm{P}} = 70$ and $N_{\mathrm{A}} = 70$, chosen in such a way that in the two cases the initial positions of the passive particle is the same, see Figure 3.4.

We then let the system evolve and compute the ratio of the number of particles jumping from the exit to the reservoir to time. We consider, in particular, the flux of passive particles, in *absence* and in *presence* of the active ones. This observable fluctuates until it approaches a roughly constant value after about $k = 6.36 \times 10^7$ MC steps (corresponding, approximately, to time 328342) is reached. Our results are reported in Figure 3.8.

We show the dependence of the stationary flux of passive particles on the drift ε in the left panel of Figure 3.8. Open symbols refer to the flux for $N_{\mathrm{P}} = 70$ and $N_{\mathrm{A}} = 70$; for each value of ϵ we repeat the measure of the flux time also for a system in which only passive particles are present. We then obtain the sequence of solid disks reported in the figure which is approximatively constant, since the dynamics of the passive particles does not depend on ε.

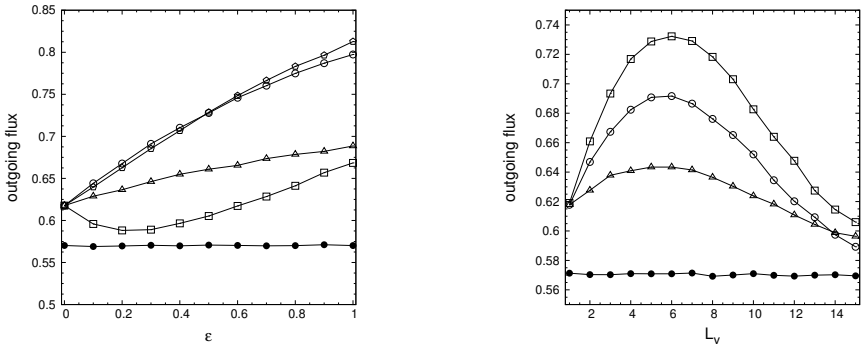

Figure 3.8: Stationary flux of passive particles in an empty room for $L = 15$, $w_{\rm ex} = 7$, $N_{\rm A} = 0$ and $N_{\rm P} = 70$ (solid disks) and $N_{\rm A} = N_{\rm P} = 70$ (open symbols). Left panel: $L_{\rm v} = 2$ (open triangles), $L_{\rm v} = 5$ (open circles), $L_{\rm v} = 7$ (open pentagons), $L_{\rm v} = 15$ (open squares). Right panel: $\varepsilon = 0.1$ (open triangles), $\varepsilon = 0.3$ (open circles), $\varepsilon = 0.5$ (open squares).

In the right panel of Figure 3.8, for the same choices of parameters and initial conditions, we show the stationary flux as a function of the visibility depth $L_{\rm v}$ for several values of the drift ε.

Both figures exhibit firstly an increase of the flux in presence of active particles at zero drift or zero visibility depth with respect to the case in which only passive particles are present (filled disks in Figure 3.8. This situation can be understood by considering that, despite the exclusion constraint of the lattice gas dynamics, doubling the number of particles can justify the increase of the flux at zero drift, if no complete clogging is reached. It is instructive to follow the sequence of empty symbols in Figure 3.8 for increasing values of ε or $L_{\rm v}$. Note that an increase of the drift yields a monotonic increase of the stationary flux as long as the visibility depth is not too large. In fact, the monotonic increase of the flux is not observed with $L_{\rm v} = 15$ (see the open squares in the left panel). This means that in the presence of such a large visibility depth the evacuation of the passive particles can be hindered by the presence of active particles if the drift is not large enough.

A quite interesting and a priori unexpected fact is the non–monotonicity of the stationary flux with respect to the visibility depth: this can be seen by looking at the different curves in the left panel and it is also put in evidence in the plots of the right panel.

It is also worth looking at the behavior of the transient fluxes as functions of time in the same evacuation set-up discussed earlier in Sec. 3.3, in which no external particle reservoir is included. To this aim, for a given initial condition, we averaged the flux of passive particles over 10^3 different realizations of the process. Coherently with the behavior observed for the stationary fluxes in Fig. 3.8, we notice once more that the presence of active particle enhances the outgoing flux of passive particles, for all the considered values of ε and L_v, this being again a trace of the underlying drafting phenomenon.

To get a deeper insight in this interesting effect, we show in Figure 3.10 the

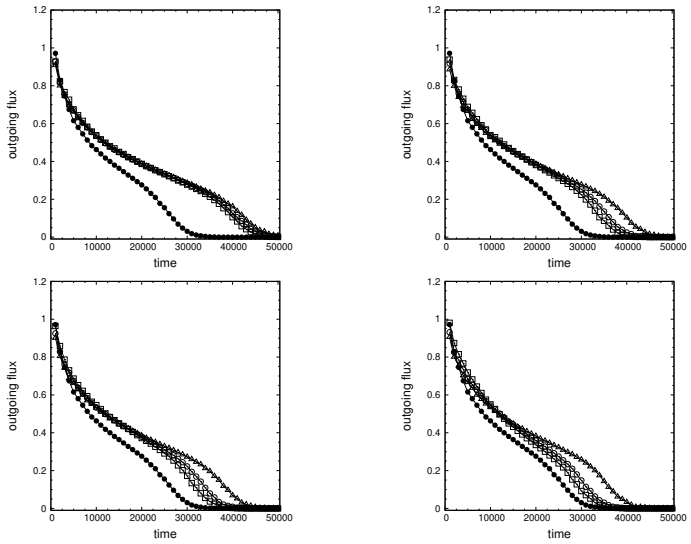

Figure 3.9: Transient flux of passive particles in an empty room for $L = 15$, $w_{\rm ex} = 7$, $N_{\rm A} = 0$ and $N_{\rm P} = 70$ (solid disks) and $N_{\rm A} = N_{\rm P} = 70$ (open symbols). In the various panels, shown are the cases with $\varepsilon = 0.1$ (empty triangles), $\varepsilon = 0.3$ (empty circles) and $\varepsilon = 0.5$ (empty squares). Different values of L_v are considered: $L_v = 2$ (top left panel), $L_v = 5$ (top right panel), $L_v = 7$ (bottom left panel), and $L_v = 15$ (bottom right panel).

stationary occupation number profile. To obtain these results, we have run the dynamics for a sufficiently long time (order of 6.36×10^7 MC steps) so that the system reaches the stationary state. Starting off from that time, we have averaged the occupation number $|\eta_x(t)|$ over time at each site of the room. The resulting function takes values between zero and one; see Figure 3.10 for an illustration.

The plots indicate that for large drift and large visibility depth that clogging along the median vertical line can take place. the occurrence of such clogging situations partly explain the not–monotonic behavior of the stationary flux with varying the visibility depth.

The emergence of the central clogging is related to the large value of the drift pointing towards the central direction. This phenomenon reminds the faster–is–slower behavior already pointed out in the literature [HFV00, KS02], even if in this case the origin of the phenomenon can be traced back to the intensity of the drift rather than to the pedestrian speed.

3.4.2 The room with an obstacle

Simulations similar with those described in Section 3.4.1 have been run in presence of a centered square obstacle made of 5×5 sites of the room not accessible by both active and passive particles. As before, we have computed the stationary flux and our results are reported in Figure 3.11.

The results plotted in Figures 3.11 and 3.12 are very similar to those shown in

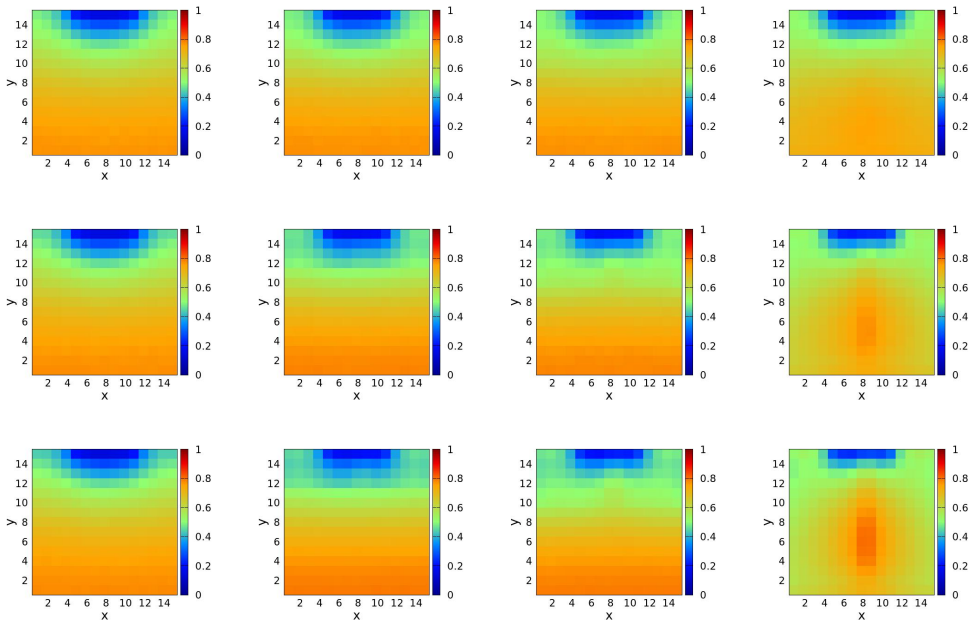

Figure 3.10: Occupation number profile at stationarity for $L = 15$, $w_{\text{ex}} = 7$, $x_{\text{ex}} = 5$, $N_A = N_P = 70$, $\varepsilon = 0.1, 0.3, 0.5$ (from the top to the bottom), $L_{\text{v}} = 2, 5, 7, 15$ (from the left to the right).

Figure 3.8 and 3.10. Our interpretation of the results is essentially the same. Mind though that, in order to reach the stationary state, we had to run the dynamics for a larger time than in the case of the empty room model (i.e., of order of 9.0×10^7 MC steps). Also from the point of view of the computed stationary flux measures, our results suggest that the presence of the obstacle slightly favors the exit of particles from the room. This was noted in Section 3.3.2 in connection with the evacuation time measurements; see also [CCCM18, CC18, CKMvS16b, CP17].

Comparing Figures 3.8 and 3.11 one realizes that the dependence of the stationary flux on the drift and on the visibility depth is milder. This fact can be explained remarking that the phenomenon of accumulation of particles along the median vertical line of the room discussed in Section 3.4.1 is less evident. Again, the obstacle seems to be keeping particles far apart so that clogging is reduced.

3.5 Discussion

We studied the problem of the evacuation of a crowd of pedestrians from an obscure region. We start from the assumption that the crowd is made of both active and passive pedestrians. The hazardous motion of pedestrians due to lack of light and, possibly, combined also to a high level of stress is modeled via a simple random walk with exclusion. The active (smart, informed, aware, ...) pedestrians, which are aware of the location of the exit, are supposed to be subject to a given drift towards the exit, while the passive (unaware, uninformed) pedestrians are

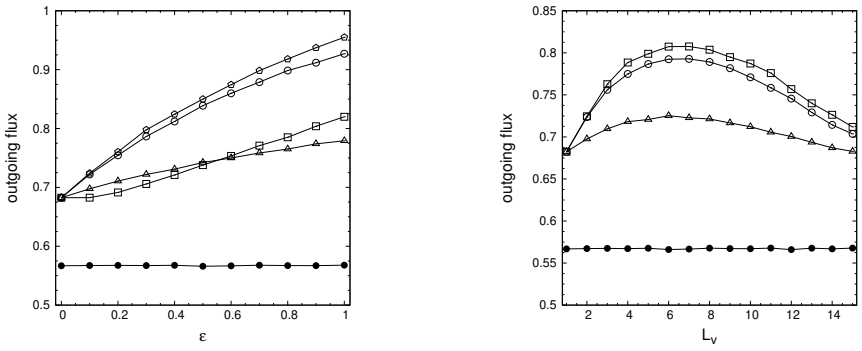

Figure 3.11: Stationary flux in a room with a 5×5 squared centered obstacle for $L = 15$, $w_{\rm ex} = 7$, $N_{\rm A} = 0$ and $N_{\rm P} = 70$ (solid disks) and $N_{\rm A} = N_{\rm P} = 70$ (open symbols). Left panel: $L_{\rm v} = 2$ (open triangles), $L_{\rm v} = 5$ (open circles), $L_{\rm v} = 7$ (open pentagons), $L_{\rm v} = 15$ (open squares). Right panel: $\varepsilon = 0.1$ (open triangles), $\varepsilon = 0.3$ (open circles), $\varepsilon = 0.5$ (open squares).

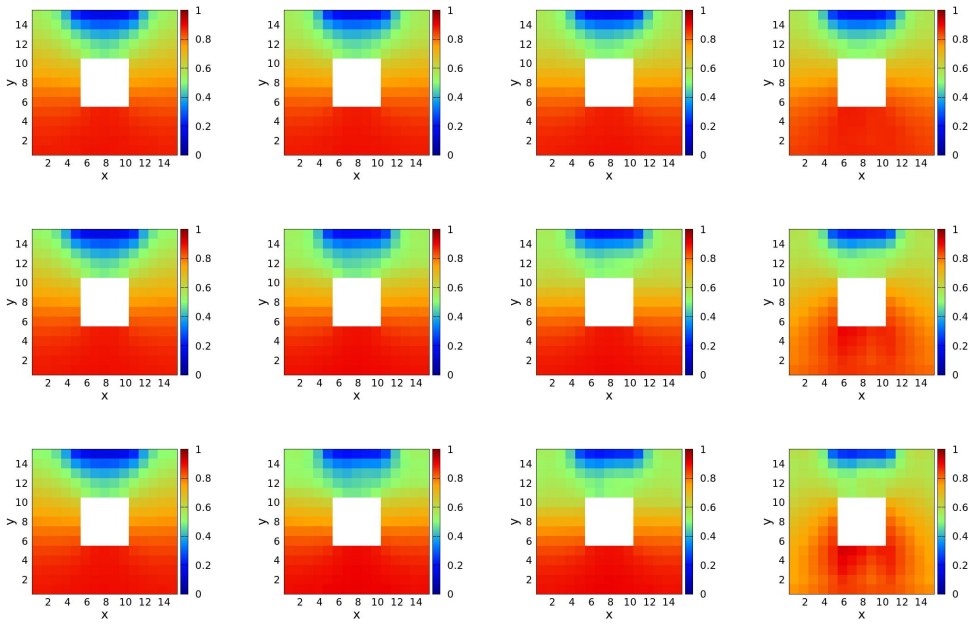

Figure 3.12: Occupation number profile at stationarity in presence of a 5×5 centered obstacle for $L = 15$, $w_{\rm ex} = 7$, $x_{\rm ex} = 5$, $N_A = N_P = 70$, $\varepsilon = 0.1, 0.3, 0.5$ (from the top to the bottom), $L_{\rm v} = 2, 5, 7, 15$ (from the left to the right).

performing a random walk within the walking geometry and eventually evacuate if they accidentally find the exit. The particle system is interacting via the site exclusion principle – each site can be occupied by only a single particle.

The main observable is the evacuation time as a function of the parameters caracterizing the motion of the aware pedestrians. We have found that the presence of the active pedestrians favors the evacuation of the passive ones. This is rather surprising since we explicitly do not allow for any communication among the pedestrians. This seems to be due to some sort of drafting effect. A drag seems to arise due to the empty spaces left behind by the active pedestrians moving towards the exit and naturally filled by the completely random moving unaware pedestrians.

We have also remarked that too smart active pedestrians can limit the drafting effect: indeed, if they exit the room too quickly the unaware pedestrian do not have the time to take profit of the wakes of empty side that they left during their motion towards the exit.

A promising research line concerns the investigation of evacuation times when different species of particles are assumed to choose among different exit doors. Such topic is relevant not only for urban situations but also for tunnel fires or for forrest fires expanding towards the neighborhood of inhabited regions.

The main open question in this context is the model validation. A suitable experiment design is needed to make any progress in this sense. This will be our target in forthcoming work.

With regards to the building up of the aerodynamic drag, it would also be interesting to verify the onset of the drafting phenomenon in lattice gas models in the presence of non–standard transport regimes leading to uphill diffusion of particles; see [CMP17] (and references cited therein) for the study of such transport mechanisms.

Chapter 4

When diffusion faces drift: consequences of exclusion processes for bi–directional pedestrian flows

Stochastic particle–based models are useful tools for describing the collective movement of large crowds of pedestrians in crowded confined environments. Using descriptions based on the simple exclusion process, two populations of particles, mimicking pedestrians walking in a built environment, enter a room from two opposite sides. One population is *passive* – being unaware of the local environment; particles belonging to this group perform a symmetric random walk. The other population has information on the local geometry in the sense that as soon as particles enter a visibility zone, a drift activates them. Their self–propulsion leads them towards the exit. This second type of species is referred here as *active*. The assumed crowdedness corresponds to a near–jammed scenario. The main question we ask in this chapter is: *Can we induce modifications of the dynamics of the active particles to improve the outgoing current of the passive particles?* To address this question, we compute occupation number profiles and currents for both populations in selected parameter ranges. Besides observing the more classical faster–is–slower effect, new features appear as prominent like the non–monotonicity of currents, self–induced phase separation within the active population, as well as acceleration of passive particles for large–drift regimes of active particles. This is based on [CCMT20].

4.1 Introduction

The pedestrian flows in agglomerated urban environments and the dynamics of microscopic constituents in cellular membranes, glasses, or supercooled liquids share an important feature: the dynamics takes place in a crowded environment with obstacles that are often active (i.e., not necessarily fixed in space and time). The management of the dynamics in these kinds of systems is far from being understood mainly due to the fact that the interplay between transport and

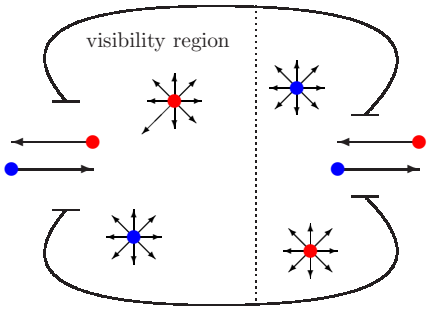

Figure 4.1: Qualitative description of the model: red and blue dots represent active and passive particles, respectively. Active particles are pushed toward the exit in the visibilty zone. Outside the visibility region all particles move isotropically. Active particles enter the room through the right door and exit through the left one, while passive particles enter through the left door and exit trough the right one.

particle–particle as well as particle–obstacle interactions is very complex; see, e.g., [GCM15, SLH09, CCMT19, WWLS19] and references cited therein.

Exploring by means of computer simulations is an efficient tool to shed light on the qualitative behavior of systems experiencing countercurrent–like behavior, that are found extensively in nature (think, for instance, of the heat exchange mechanism, called *rete mirabile*, in biological systems) and are advocated in a variety of engineering applications, e.g. in liquid chromatography (in which the stationary phase is held in place by an external force field), and in membrane–based gas separation technologies.

Depending on the level of observation, the modeling descriptions refer to micro–, meso–, macro–levels, or to suitable (multiscale) combinations thereof (see, e.g., [MCKB, E11]). In this framework, we consider a microscopic approach based on a modification of the classical simple exclusion[1] process formulated for two different populations of interacting pedestrians (particles). Essentially, two populations of particles, mimicking pedestrians walking in a built environment, enter a room from two opposite sides with the intention to cross the room and then exit from the door on the opposite side of the room.

Because of its own unawareness or lack of prior knowledge of the local environment, one population is *passive*, and hence particles belonging to this population perform a symmetric random walk. On the other hand, the second population has information on the local geometry, in the sense that as soon as particles enter a visibility zone, a drift activates them by sending them towards the exit door, see Figure 4.1. This type of particles is referred here as *active*. The assumed crowdedness corresponds to a near–jammed scenario. To fix ideas, the number of

[1] A simple exclusion process refers to the stochastic motion of interacting particles on a lattice where the interaction is given by the exclusion (excluded “volume" constraints) property, i.e., two particles may not occupy the same site simultaneously. We refer the reader to [MPS89] for rigorous considerations on the simple exclusion model and its hydrodynamic limits and to [GFP16] for a basic modeling perspective.

occupied sites in the room is chosen to be of the order of the 60% from the total number of available sites[2].

In an evacuation due to an emergency situation (like fire and smoke propagating in the building), the *a priori* knowledge of the environment is certainly an advantage (cf., e.g., [RJM19]). Hence, from this perspective, if a quick evacuation is needed, then the passive population has a disadvantage compared to the active population. We are wondering whether we can compensate at least partly this drawback, by managing intelligently the motion of the active population. In other words, the main question we ask in this chapter is:

> Q. Can we induce modifications of the dynamics of active particles to improve the outgoing current of passive particles?

The ingredients we have at our disposal are alterations either in the drift parameter of the active particles, or in their visibility zone by fine–tuning a parameter for a nonlocal interaction that activates the drift–towards–exit. It is worth noting that the latter feature is different from the nonlocal shoving of particles proposed in [APHL15].

To address the above question, we compute occupation number profiles and currents for both populations in selected parameter ranges. Our numerical results exhibit the classical faster–is–slower effect (see, e.g., [GZP$^+$14] for experimental evidence and [STU13] for numerical simulations exhibiting this effect using Helbing's social force model) and point out as well new prominent features like the non–monotonicity of currents, the self–induced phase separation within the active population, as well as an acceleration of passive particles induced by a large drift and a large visibility zone of active particles.

This research was initiated in [CKMvS16b, CKMvS16a], motivated by our intention to estimate the mean residence time of particles undergoing an asymmetric simple exclusion within a room in perfect contact with two infinite reservoirs of particles. Recent developments reported in [CCMT19] brought us to study drafting effects via the dynamics of mixed active–passive pedestrian populations in confined domains with obstacles and exit doors, which mimicks a built complex environment.

4.2 Model description

We consider a square lattice $\Lambda = \{1, \dots, L\} \times \{1, \dots, L\}$ with L a positive odd integer. The set Λ is referred in this context as *room* and its points $x = (x_1, x_2)$ as *sites*. Two sites at Euclidean distance one are called *nearest neighbors*. We call *horizontal* and *vertical* the first and the second coordinate axes, respectively. The horizontal and the veritical axes are, respectively, right and up oriented.

[2]Museums in highly touristic cities are examples of crowded areas; compare, e.g., with the situation of Galleria Borghese in Rome as described in [CCCO19].

The *doors* are the sets made of w_{L} and w_{R} neighboring sites in the left–most and right–most columns of the room, respectively, and symmetric with respect to its median row. This mimics the presence of two distinct doors on the left and right boundary of the room. The odd positive integers $w_{\mathrm{L}}, w_{\mathrm{R}}$ smaller than L will be called *width* of the doors. Inside the room we define a rectangular driven zone, namely, the *visibility region* V, made of the first L_{v} left columns of Λ, with the positive integer $L_{\mathrm{v}} \leq L$ called *depth* of the visibility region. By writing $L_{\mathrm{v}} = 0$, we refer to the case in which no visibility region is considered.

The dynamics will be defined so that particles will be able to exit the room only from sites belonging to the doors: jumps from other sites to the exterior of Λ will be forbidden.

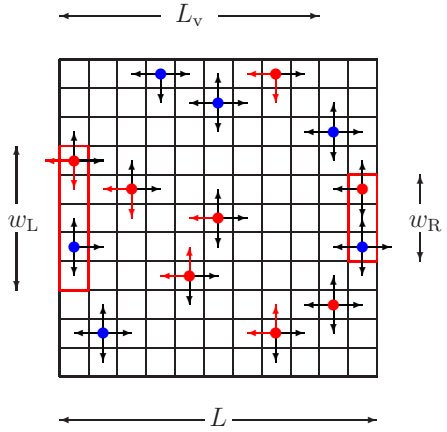

Figure 4.2: Schematic representation of our lattice model. Blue and red disks denote passive and active particles, respectively. The rectangles of sites delimited by the red contour denote the exit doors. Black and red arrows (color online) denote transitions performed with rates 1 and $1 + \varepsilon_1$ or $1 + \varepsilon_2$, respectively.

We consider two different species of particles, i.e., *active* and *passive* (we shall sometimes use in the notation the symbols A and P to refer to them), moving inside Λ with different dynamics. The interaction of particles inside the room is modelled via a simple exclusion random walk.

The passive particles enter through the left door and exit through the right door. They perform a symmetric simple exclusion dynamics on the whole lattice. Simultaneously, the active particles enter through the right door and exit through the left door. They perform a symmetric simple exclusion walk outside the visibility region, whereas inside such a region they experience also a drift pushing them towards the left door. In other words, the whole room is *obscure*[3] for the passive particles, while, for the active ones, only the region outside the visibility region[4] is obscure. The model also includes two external particle waiting lists, each of which is designed to collect particles of a given species when these move

[3]We refer the reader to [CKMvS16b], where the authors discuss the gregarious behavior of crowds moving in the dark.

[4]The concept of visibility region was introduced by the authors in [CCMT19].

out from the lattice Λ through their exit door and to reinsert them back on the lattice through their entrance door.

More precisely, we consider $N_{\rm A}$ active particles and $N_{\rm P}$ passive ones randomly distributed in the room at time zero, one per site. The motion of the particles is described by a continuous time Markov chain that is rigorously defined in the Appendix. In more simple words, the dynamics is defined as follows: we first pick two non–negative numbers $\varepsilon_1, \varepsilon_2 \geq 0$ called the *horizontal* and the *vertical drift* and, for any pair $x = (x_1, x_2), y = (y_1, y_2)$ of nearest neighbor sites in Λ we set $\epsilon(x, y) = 0$, excepting for the following cases:

- $\epsilon(x, y) = \varepsilon_1$ if $x, y \in V$ and $y_1 = x_1 - 1$, namely, x and y belong to the visibility region and x is to the right with respect to y;
- $\epsilon(x, y) = \varepsilon_2$ if $x, y \in V$ and $y_2 = x_2 + 1 \leq (L + 1)/2$, namely, x belongs to the bottom part of the visibility region and x is below y;
- $\epsilon(x, y) = \varepsilon_2$ if $x, y \in V$ and $y_2 = x_2 - 1 \geq (L + 1)/2$, namely, x belongs to the top part of the visibility region and x is above y.

Next, we assume that particles move with the following rates:

- a passive particle leave the room from a site in the right door with rate 1;
- an active particle leave the room from a site in the left door with rate $1+\epsilon_1$;
- if the number $n_{\rm A}$ of active particles in the room is smaller than $N_{\rm A}$ and the number of empty sites $m_{\rm R}$ in the right door is not zero then an active particle is added to a randomly chosen empty site of the right door with rate $[N_{\rm A} - n_{\rm A}]/m_{\rm R}$;
- if the number $n_{\rm P}$ of passive particles in the room is smaller than $N_{\rm P}$ and the number of empty sites $m_{\rm L}$ in the left door is not zero then a passive particle is added to a randomly chosen empty site of the left door with rate $[N_{\rm P} - n_{\rm P}]/m_{\rm L}$;
- a passive particle moves inside Λ from a site to one of its empty nearest neighbors with rate 1;
- an active particle moves from the site x inside Λ to its empty nearest neighbor y inside Λ with rate $1 + \epsilon(x, y)$.

We note that the quantities $N_{\rm A} - n_{\rm A}$ and $N_{\rm P} - n_{\rm P}$ represent the number of active, and, respectively, passive particles that exited the room and entered their own waiting list at the considered time, whereas $m_{\rm L} > 0$ and $m_{\rm R} > 0$ are the number of empty sites of the left and right doors at the same time.

The system will reach a stationary state, since passive particles exiting the domain via the right door are introduced back in one site randomly chosen among possible empty sites of the left door, while active particles leaving the system

through the left door are introduced back also at one random site chosen among possible empty sites of the right door. The total number of active and passive particles in the room Λ is only approximatively constant during the evolution. It slightly fluctuates due to the fact that particles may enter waiting lists. On the other hand, the total number of particles N in the system (considering both the room and the waiting lists) is conserved.

In the study of this dynamics, the main quantity of interest are the stationary *outgoing fluxes* or *currents of active and passive particles* which are the values approached in the infinite time limit by the ratio between the total number of active and passive particles, respectively, that in the interval $(0, t)$ exited through the left and the right door and entered the waiting lists and the time t. In order to discuss and to understand the behavior of currents with respect to the model parameters, we shall also look at the active and passive particles *occupation number profiles* of active and passive particles, namely, we evaluate the stationary mean value of the occupation numbers of active and passive particles which is equal to one if a site is occupied by a particle of the considered species or zero otherwise.

4.3 Numerical results

We compute the currents by applying directly the definition given at the end of Section 4.2 and the occupation number profiles as follows: we run the dynamics for a sufficiently long time (order of 9×10^7 MC steps) so that the system reaches the stationary state and then we average the occupation numbers for each site of the room for the following 9×10^7 MC steps; we thus obtain a function of $x \in \Lambda$ taking values in the interval $[0, 1]$.

The presence of two species fighting to get to opposing exit doors reasonably reduces the intensity of the current that we would expect to measure if a single species were present in the room. We have tested this fact by running simulations for one single species with the some dynamics as the one defined above and with the same choice of parameters and we have found currents that are typically three or four time larger.

In the following discussion the parameters are $L = 30$ and $N_{\mathrm{A}} = N_{\mathrm{P}} = 280$ and all of the simulations are done starting the system from the same initial configuration chosen once for all by distributing the particles at random with uniform probability. With such a choice of the parameters the number of occupied sites in the room is of the order of the 60% of the total; indeed, our study, as explained in the introduction, aims at understanding the behavior of the model in a crowded regime.

4.3.1 The corridor model

In this subsection, the width of the doors is set equal to the size of the lattice, namely, $w_{\mathrm{L}} = w_{\mathrm{R}} = L$. In this case, it is natural to limit the discussion to the

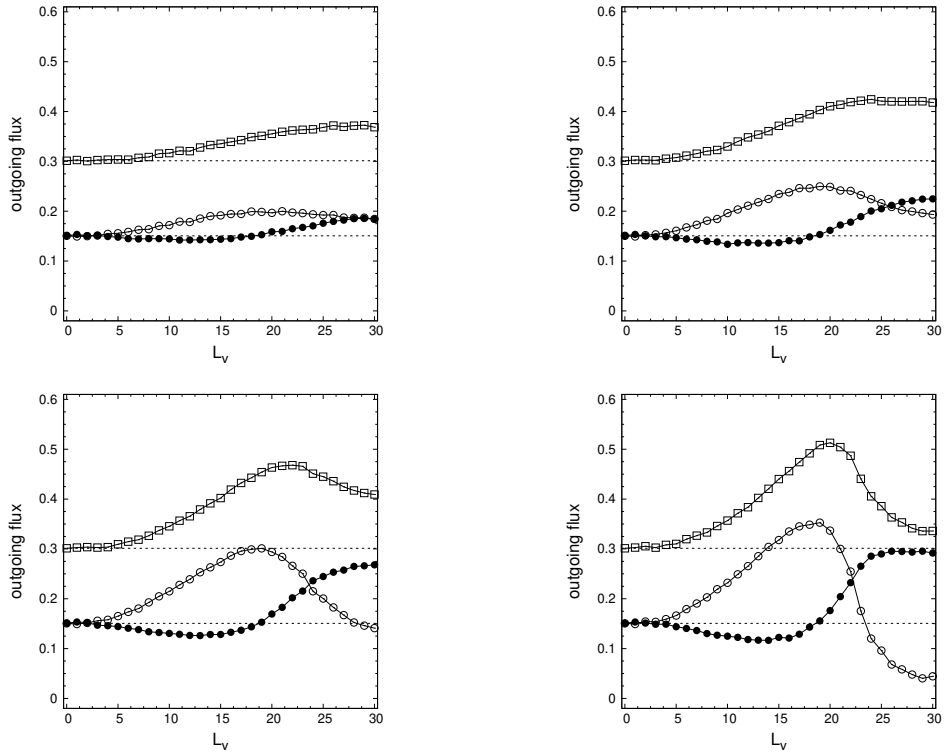

Figure 4.3: Corridor model: wide doors. Stationary currents of active (empty circles) and passive particles (solid disks) and cumulative current (empty squares) as functions of $L_{\rm v}$ for $\varepsilon = 0.05, 0.1, 0.15, 0.2$ (lexicographical order). The black dashed lines are eye guides showing the value measured in the zero drift case.

scenario in which $\varepsilon_2 = 0$, namely only the horizontal (longitudinal with respect to the position of the doors) component of the drift is considered. To simplify the notation, we shall also denote the longitudinal drift ε_1 simply by ε.

Among the different interesting results that we will discuss in this section, we want to single out a very peculiar behavior: since only active particles experience the drift, changes of the parameters $L_{\rm v}$ and ε act directly only on the active species. Nevertheless, due to the exclusion interaction between the two different species, also the passive particles behavior will be affected. In particular, we will see that a robust increase of the visibility length $L_{\rm v}$ and the longitudinal drift ε will induce a significant increase of the passive particle current.

In Figure 4.3, we plot the passive and active particle currents for four different values of the drift, i.e., $\varepsilon = 0.05, 0.1, 0.15, 0.2$, when the visibility length $L_{\rm v}$ is varied from 0 to L. We note that the active particles current (open circles) increases with $L_{\rm v}$ up to some value where it attains a maximum. This effect is visible in all of the panels of Figure 4.3, but the position and size of the maximum changes. This effect is more prominent for the largest value of considered ε (see bottom right panel in Figure 4.3). Moreover, excepting the smallest value of the drift $\varepsilon = 0.05$, soon after the active particle current reaches its maximum, the passive and active particle currents intersect so that, for the largest value of the

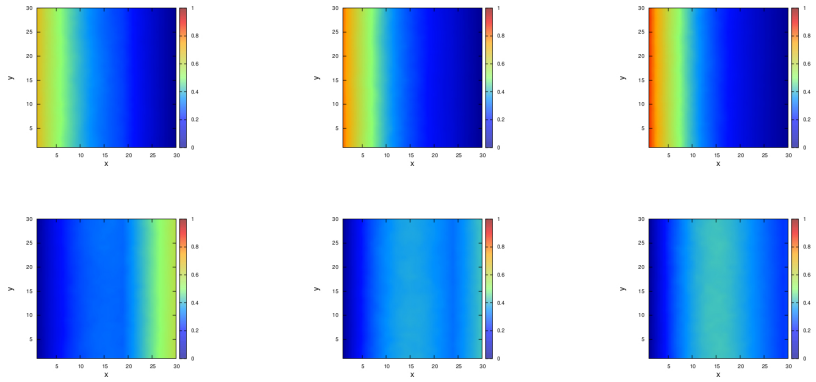

Figure 4.4: Corridor model: wide doors. Occupation number profile of passive (top row) and active (bottom row) particles at stationarity for $\varepsilon = 0.15$ and $L_{\mathrm{v}} = 20, 25, 30$ (from left to right).

visibility length, the transport of passive particles becomes more efficient than that of active ones.

This behavior is interesting and not trivial for two reasons: i) only active particles are driven and, hence, the parameters we play with directly act only on their dynamics; ii) when ε and L_{v} are increased, the active particle transport throughout the corridor is expected to become more and more efficient. To explain such an effect, we look at the stationary occupation profiles. In particular, we focus our attention to the case $\varepsilon = 0.15$, namely, we closely analyze the bottom left panel in Figure 4.3 and the corresponding occupation number profiles plotted in Figure 4.4. In this figure, we have considered the cases $L_{\mathrm{v}} = 20, 25, 30$ since the switch in the active and passive particle currents is observed around $L_{\mathrm{v}} = 25$.

Looking at Figure 4.4, we note that for $L_{\mathrm{v}} = 20$, passive and active particles mainly distributed close to their relative entrance doors, namely, passive particles on the left and active particle on the right. Nevertheless, a small depletion layer in the active particle distribution can be observed around $x = 20$, which is precisely the place where those particles enter the visibility regions. This is an expected behavior: active particle entering such a region from the right are accelerated towards the left and start to accumulate when they meet the passive particles standing at their left entrance. This behavior becomes more and more prominent when the visibility length is increased; see the panels corresponding to $L_{\mathrm{v}} = 25, 30$, where the presence of the depletion region and the accumulation of the active particles in the middle of the room is more evident. As a consequence, when the visibility length is increased, the right entrance is no more occupied by active particles. This explains the observed increase in the passive particle current.

Similar occupation profiles are found for the other values of the longitudinal drift considered in Figure 4.3. Hence, the behavior of currents can be explained similarly. We do not report such pictures because they do not add anything new to the understanding of the behavior of our model.

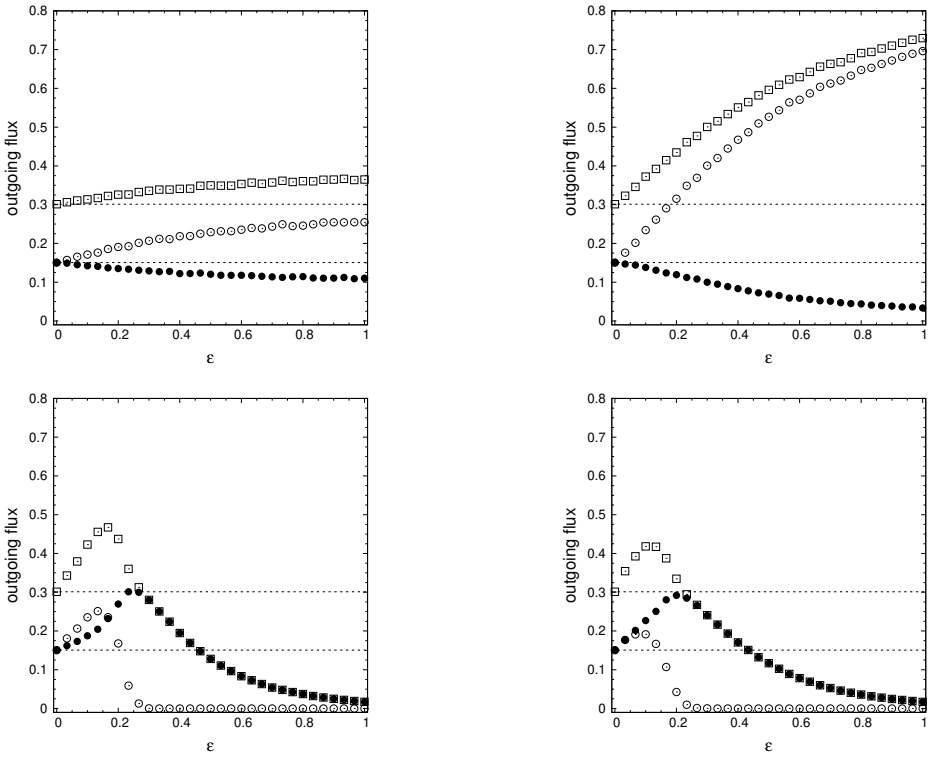

Figure 4.5: Corridor model: wide doors. Stationary currents of active (empty circles) and passive particles (solid disks) and cumulative current (empty squares) as functions of ε for $L_{\mathrm{v}} = 7, 15, 23, 30$ (lexicographical order). The black dashed lines are as in Figure 4.3.

In Figure 4.5, we consider larger values of ε for a fixed visibility length $L_{\mathrm{v}} = 7, 15, 23, 30$. If L_{v} is smaller than 15, the passive and, respectively, active particle currents decrease and increase monotonically with respect to the drift $\varepsilon \in [0, 1]$. Moreover, to a high current of active particle it corresponds a small current of passive ones. This behavior is coherent with the occupation number profiles reported in Figure 4.6. We see an accumulation of active particles at the right door, which prevents high passive particle currents, as well as a rather spread distribution of passive particles in the left part of the room with minor accumulation at the entrance, which allows high active particle currents.

The scenario changes drastically for larger values of the visibility length, see the bottom panels in Figure 4.5 and, in particular, focus the attention on the left one corresponding to $L_{\mathrm{v}} = 23$. Currents are not anymore monotonic functions of the drift, and, at very low values of ε, the active particle current is higher than the passive particle one, as soon as the drift exceeds a certain value the latter overtakes the former. Consequently, we see again that by increasing the drift of active particles, the transport of passive ones is favored. This behavior can be explained as before referring to the occupation number profiles reported in Figure 4.7. The first three columns are similar to those shown in Figure 4.4 so that the phenomenon can be explained similarly. However, in the fourth column

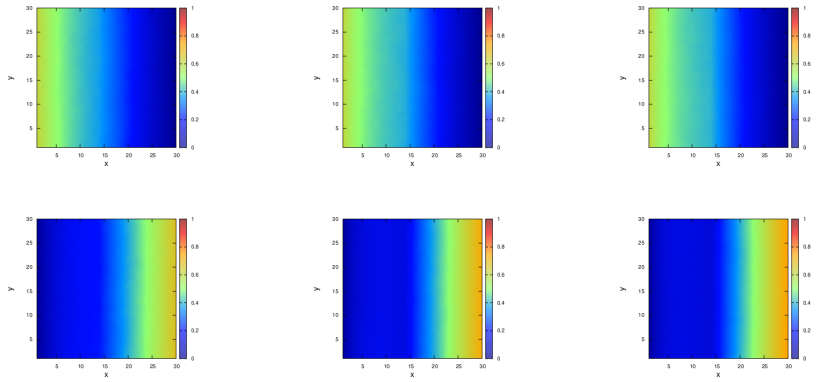

Figure 4.6: Corridor model: wide doors. Occupation number profile of passive (top row) and active (bottom row) particles at stationarity for $L_{\mathrm{v}} = 15$ and $\varepsilon = 0.2, 0.4, 0.48$ (from left to right).

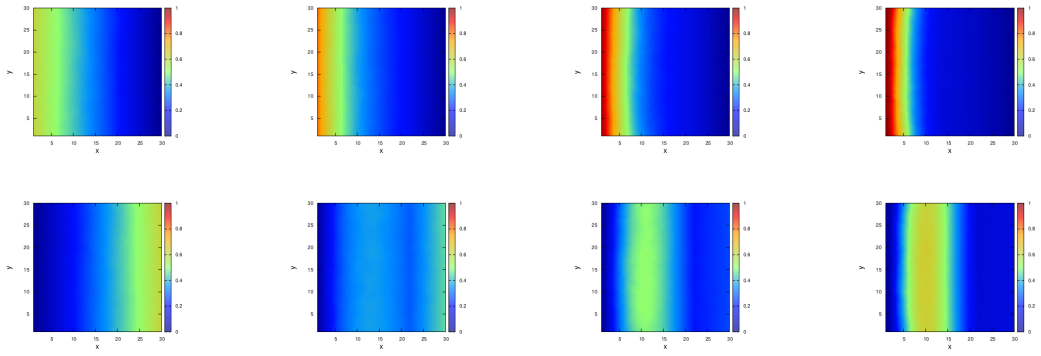

Figure 4.7: Corridor model: wide doors. Occupation number profile of passive (top row) and active (bottom row) particles at stationarity for $L_{\mathrm{v}} = 23$ and $\varepsilon = 0, 0.18, 0.25, 0.35$ (from left to right).

corresponding to $\varepsilon = 0.35$, a supplementary increase in the occupation number profile of the active particles in the middle region of the room is observed and this explains why for ε large also the passive particle currents becomes negligible. In this regime, a clogged configuration is eventually reached.

4.3.2 Room model: effect of the doors

In this section, we discuss the effect of the doors on the dynamics of our model. In the sequel, the width of the doors is taken to be smaller than the side length of the lattice. In particular, we consider the case in which the doors have equal widths $w_{\mathrm{L}} = w_{\mathrm{R}} = 14$, hence their capacity is reduced compared to the corridor model described in Subsection 4.3.1. Longitudinal and transversal (i.e., vertical) components of the drift, namely, ε_1 and ε_2 are chosen equal and will be simply denoted by ε.

Since the results are similar to those that we have found in the corridor case

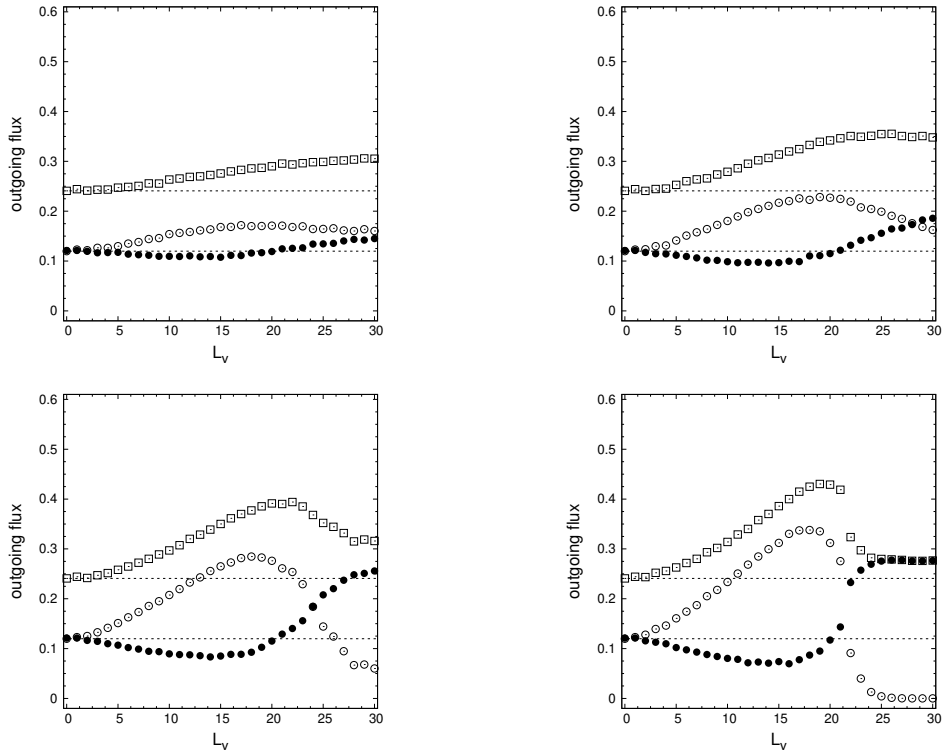

Figure 4.8: Room model: smaller doors. Stationary currents of active (empty circles) and passive particles (solid disks) and cumulative current (empty squares) as functions of L_v for $\varepsilon = 0.05, 0.1, 0.15, 0.2$ (lexicographical order). The black dashed lines are as in Figure 4.3

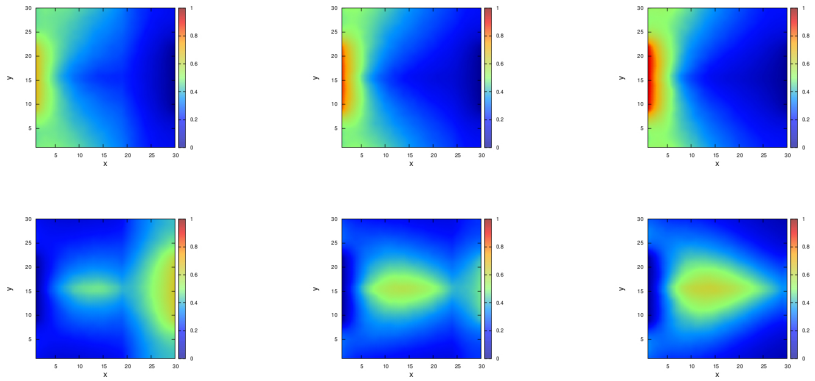

Figure 4.9: Room model: smaller doors. Occupation number profile of passive (top row) and active (bottom row) particles at stationarity for $\varepsilon = 0.15$ and $L_v = 21, 25, 30$ (from left to right).

of Subsection 4.3.1, we do not repeat the discussion in detail. Instead, we bound ourselves to highlight the few key differences that can be observed.

Figures 4.8 and 4.9 are analogous to Figures 3.5 and 4.4. The only difference is the shape of the region where particles accumulate which is strongly influenced

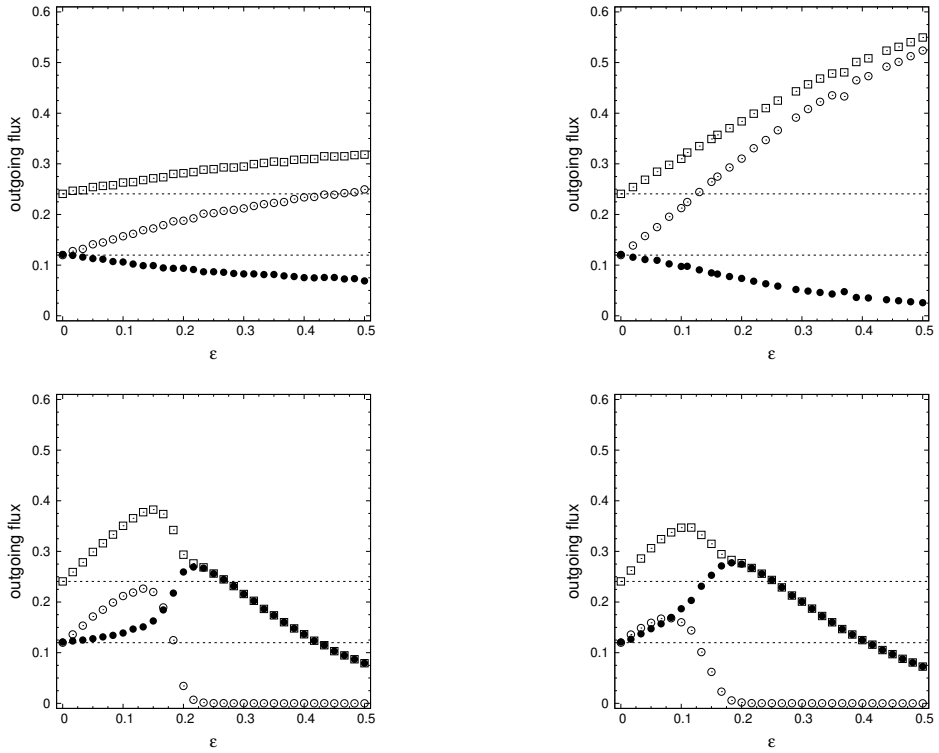

Figure 4.10: Room model: smaller doors. Stationary currents of active (empty circles) and passive particles (solid disks) and cumulative current (empty squares) as functions of ε for $L_{\mathrm{v}} = 7, 15, 23, 30$ (lexicographical order). The black dashed lines are as in Figure 4.3.

by the presence of the door and by the presence of the transversal drift. The door gives the rounded shape to the occupation number profile of active particles close to their entrance, whereas the transversal drift induces the formation of a “droplet" in the central region of the room.

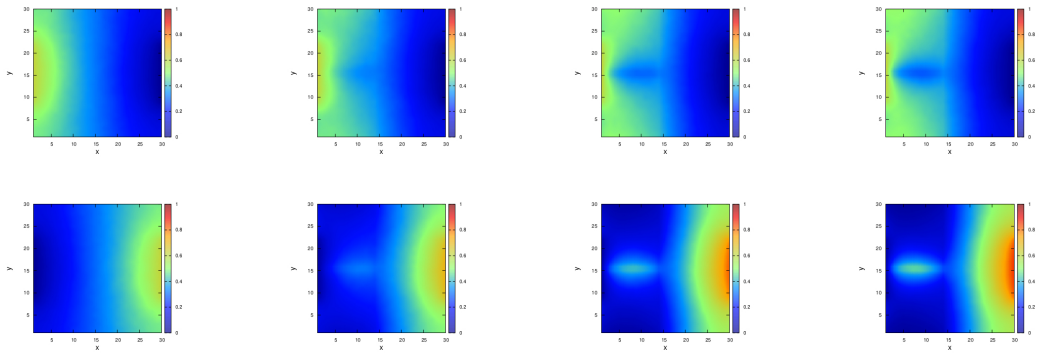

Figure 4.11: Room model: smaller doors. Occupation number profile of passive (top row) and active (bottom row) particles at stationarity for $L_{\mathrm{v}} = 15$ and $\varepsilon = 0, 0.15, 0.35, 0.45$ (from left to right).

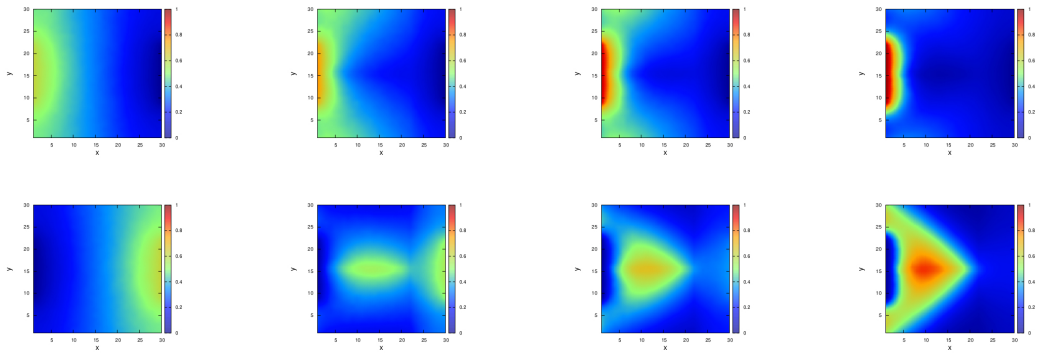

Figure 4.12: Room model: smaller doors. Occupation number profile of passive (top row) and active (bottom row) particles at stationarity for $L_{\mathrm{v}} = 23$ and $\varepsilon = 0, 0.15, 0.2, 0.3$ (from left to right).

Figures 4.10–4.12 are analogous to Figures 3.7–4.7. It appears that active particles separate in two distinct groups. It looks to be a self–induced phase separation within the own population. The shape of the droplet is very much affected by the geometry of the room and the size of the door.

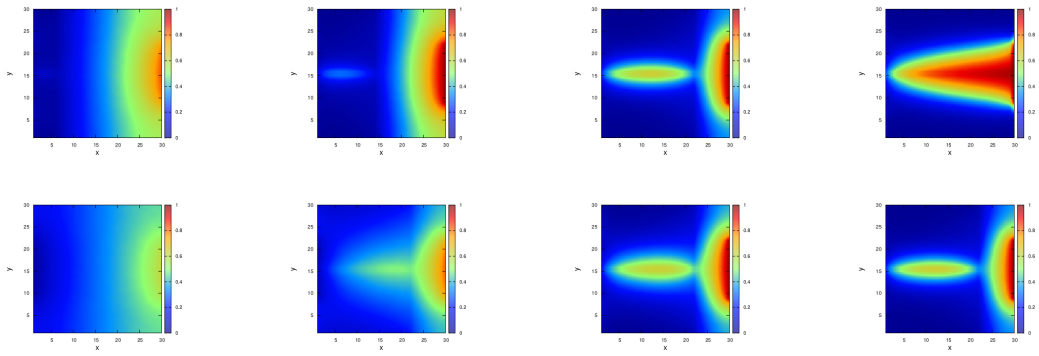

Figure 4.13: Room model: smaller doors. Occupation number profile at stationarity in a simulation without passive particles. Top row: $\varepsilon = 0.8$ and $L_{\mathrm{v}} = 7, 15, 23, 30$ (from left to right). Bottom row: $L_{\mathrm{v}} = 23$ and $\varepsilon = 0, 0.15, 0.5, 0.8$ (from left to right).

As a final comment, we report that, as we already mentioned at the very beginning of Section 4.3, we have performed some simulations of the model in absence of passive particles, namely, when just active particles are present in the lattice. The behavior of the current that we find is absolutely standard: the current increases monotonically both with respect to the drift and to the visibility length.

We find an interesting effect to point out, see Figure 4.13: due to the transverse component of the drift, we see particles tending to accumulate in the central part of the room. Moreover, depending on the visibility length, they can form a central droplet detached from the inlet right door. Additionally, we also remark

that it would be worth investigating the highlighted sensitivity of the stationary currents to changes of either the drift parameter or the length of the visibility region from the point of view of statistical mechanics. In particular, an open question is whether the observed presence of a non–monotonicity in the behavior of the current as a function of ε and L_{v} is compatible with the validity of standard fluctuation–response relations [MPRV08, CR12].

As closing note for this discussion, we mention the reference [CMLT16]. Here the authors have collected pedestrian traffic data in a railways station which contains detailed information on the dynamics of single and bi–directional flows. As further research, it would be interesting not only to attempt to identify based on the recorded Kinect images from [CMLT16], which pedestrian is active and which one is in fact passive, but also to measure in a suitable way the overall effect of the dynamics of active pedestrians on the passive ones. A suitable clustering of such sets of data could provide us with a concrete framework to bring our model towards the experimental range opening up this way possibilities for an automatic pedestrian traffic management designed for mixed populations of pedestrians.

4.4 Discussion

Based on the results detailed in Section 4.3, we see that if active particles undergo a non–zero drift and the visibility zone is sufficiently large, then the outgoing flux of passive particles improves. This is essentially the answer to the question Q. posed in the introduction. It is due to the fact that, in this regime, active particles move quickly far from their entrance door. In this way their entrance door becomes a free exit for the passive particles. The dynamics is still slow mainly because active particles succeed to jam around the center part of the room, slowing down the overall dynamics.

The population of active particles segregates in two different structures: one is an agglomeration located in the proximity of the entrance door, the other is a droplet in the center of the visibility zone. This is a consequence of the combined action of longitudinal and transversal drifts. On the other hand, if the transversal drift is not active, we still have an agglomeration in the central part of the visibility region, as we have observed in the corridor model. Its shape is not anymore a droplet but a vertical strip.

The fact that the flux of passive particles can be controlled via the active particle dynamics has been observed for a specific geometry and for a specific dynamics. The same kind of analysis can be done for concrete urban geometries, multiple populations of pedestrians, and different dynamics, providing potentially useful information for large crowd management.

Chapter 5

A fluid-like driven system for active–passive pedestrian dynamics

In this chapter, we study the question of well-posedness for a nonlinear coupled parabolic system that models the evolution of a complex pedestrian flow. The main feature is that the flow is composed of a mix of densities of active and passive pedestrians that are moving with different velocities. We rely on special energy estimates and on the use a Schauder's fixed point argument to tackle the existence of solutions to our evolution problem. Moreover, the structure of the nonlinearity of the coupling allows us to prove the uniqueness of solutions. We provide also the stability estimate of solutions with respect to selected parameters. This is based on [TCM19] and [TCM20].

5.1 Introduction

In this chapter, we study well-posedness of a coupled system of parabolic equations which are meant to describe the motion of a pedestrian flow in a heterogeneous environment. From the crowd dynamics perspective, the standing assumption is that our pedestrian flow is composed of two distinct populations: an *active* population – pedestrians are aware of the details of the environment and move rather fast, and a *passive* population – pedestrians are not aware of the details of the environment and move therefore rather slow. See also Figure 5.1, where we make the analogy with flow in a structured porous media, following an idea by Barenblatt and co-authors cf. [BZK60]. Mathematically, we investigate an evolution system where a Forchheimer-like equation is nonlinearly-coupled to a diffusion-like equation. For more details on the modeling of the situation, we refer the reader to Section 2.3 and references mentioned there.

Let a bounded set $\Omega \neq \emptyset$, $\Omega \subseteq \mathbb{R}^2$ a domain such that $\partial\Omega = \Gamma^N \cup \Gamma^R$, $\Gamma^N \cap \Gamma^R = \emptyset$ with $\mathcal{H}(\Gamma^N) \neq \emptyset$ and $\mathcal{H}(\Gamma^R) \neq \emptyset$, where $\mathcal{H}$ denotes the surface measure on Γ^N, Γ^R and take $S = (0, T)$. Find the pair (u, v), where $u : S \times \Omega \longrightarrow$

$\mathbb{R}^2$ and $v : S \times \Omega \longrightarrow \mathbb{R}^2$, satisfying the following model equations

$$\begin{cases} \partial_t(u^\lambda) + \operatorname{div}(-K_1(|\nabla u|)\nabla u) = -b(u-v) \ \text{ in } S \times \Omega, \\ \partial_t v - K_2 \Delta v = b(u-v) \ \text{ in } S \times \Omega, \\ -K_1(|\nabla u|)\nabla u \cdot \mathbf{n} = \varphi u^\lambda \ \text{ at } S \times \Gamma^R, \\ -K_1(|\nabla u|)\nabla u \cdot \mathbf{n} = 0 \ \text{ at } S \times \Gamma^N, \\ -K_2 \nabla v \cdot \mathbf{n} = 0 \ \text{ at } S \times \partial\Omega, \\ u(t=0,x) = u_0(x), \ x \in \bar{\Omega}, \\ v(t=0,x) = v_0(x), \ x \in \bar{\Omega}. \end{cases} \tag{5.1}$$

Here $K_2 > 0$, while the function K_1 is linked to the derivation of a nonlinear version of Darcy's law involving a polynomial with non-negative coefficients in velocities. This choice is rather non-standard, see e.g. the works [HI11], [ABHI09], [CHK16] and references cited therein for more details in this sense. In addition, $\lambda \in (0, 1]$ is a fixed number and $b(\cdot)$ is a sink/source term. The nonlinear structure of K_1 is described in Section 5.3 together with the remaining model parameters entering (5.1) which are not explained here, as well as with the assumptions needed to ensure the existence of solutions to our problem.

In model (5.1), the dynamics of interacting pedestrians involves the evolution of two distinct populations behaving very differently from each other. Seen at a microscopic level, the motion takes place in an heterogeneous domain - obstacles are obstructing the sight of the exit. The active pedestrians follow a predetermined velocity field (the map of the location is known), while the passive agents that have no preferred direction of motion. We assume that the size of the overall population is significantly large so that using macroscopic models makes sense. In this context, we consider that the active population of pedestrians follows velocity fields similar to a generalized Darcy flow, namely, a Forchheimer flow typically applicable for slightly compressible fluids in porous media, while the passive population is governed macroscopically by some averaged diffusion equation. To build this model, we took inspiration from the field of reactive flows in porous media (see, e.g., [Bea72]). It is worth pointing out that both reactive flows in porous media as well as pedestrian flows in heterogeneous domains are able to produce coherent flow patterns, manifestation of some sort of built-in self-organization mechanisms. Cf. e.g. [DHJW05, ECT15], either uniform or not, pedestrian flows can form collective patterns of motion. For instance, one notices circulating flows at intersections, lane formation, local clogging due a complex geometry (typically caused by walls and obstacles under normal walking conditions or when the evacuation of pedestrians takes place during an emergency situation). If the pedestrian flow is composed of mixed active-passive populations, then we see that often groups of passive pedestrians block the motion of the active ones. This effect was pointed out by the numerical results reported in [RJM19, CCMT19] and [CCMT20]. Of course, to get the needed trust in our model, equations (5.1) have to be approximated numerically and the corresponding numerical output has to be confronted with suitable statistics of experimental results. This will be one of our next steps in this investigation, which will be studied elsewhere.

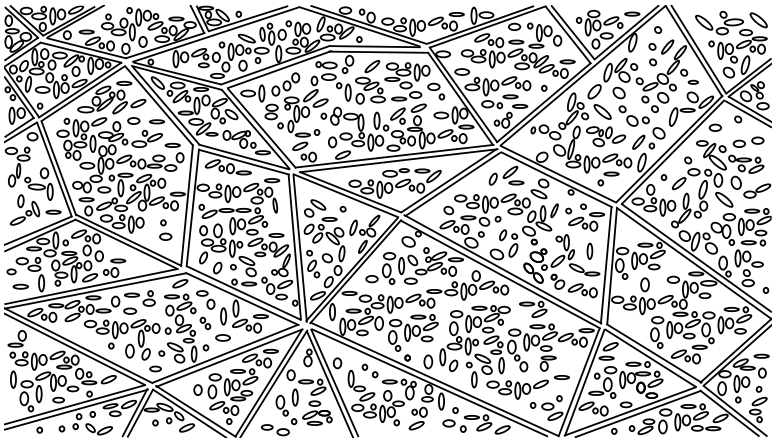

Figure 5.1: Sketch of a distributed flow through a fissured rock, scenario mimicking Fig.1 from [BZK60]. The fissured rock consists of pores and permeable blocks, generally speaking blocks are separated from each other by a system of fissures. Through the fissures, the flow is faster compared to the rest of the media.

5.2 Some background on the problem (5.1)

The modeling, analysis and simulation of pedestrian flows offers many challenging questions to science and technology in general, and to mathematics in particular. Our interest in this context is to study mixed pedestrian flows where the dynamics of interacting agents stems from two distinct populations: active agents that follow a predetermined velocity field and passive agents that have no preferred direction of motion.

There are several ways to approach such scenarios. One possible route has been studied in [RJM19, CMRT19], where the authors considered a non-linear system SDEs coupled with a linear parabolic equation to describe the escape evacuation dynamics of active and passive pedestrians moving through smoke (i.e. through regions with reduced visibility). A lattice model is explored in [CCMT19] to search for eventual drafting/aerodynamic drag effects.

In this chapter, we imagine that the active population of pedestrians have velocities similar to a non-Darcy flow, namely, a generalized Forchheimer flow as for slightly compressible fluids. Some of the mathematical properties of this type of flow have been already investigated, for instance, in [ABHI09, HI11, CHK16], and we are benefitting here of this background. On the other hand, we consider flow of the passive population as a diffusion process, hence no predetermined flow directions are prefered. The coupling between the two flows is done like in [BZK60].

From a micro-to-macro perspective, it is worth also noting that a generalized Forchheimer flow model (i.e. the first partial differential equation in (5.1)) can be obtained in principle via homogenization techniques (like in [LLPW11], e.g.), but it is not clear at this stage how a suitable microscopic model, defined at the level of the geometry depicted in Figure 5.1, would look like.

The aim of this chapter is to complete the proof of the well-posedness of the system (5.1) by showing the existence, uniqueness and stability of solutions with respect to parameters. In particular, we rely on special energy estimates and on the use a Schauder's fixed point argument to tackle the existence of solutions to our evolution problem. The nonlinear structure in the transport term where the Forchheimer polynomial appears, allows us to establish the wanted uniqueness and stability estimates. This work focuses on the structural stability of solution with respect to initial and boundary data, nonlinear coupling coefficient, and to the difussion coeficient from the semi-linear equation. We also provide a stability-like estimate for the gradient of the solutions. To obtain such control on the gradients, the structure of the system has an important degenerate monotonicity property[1], which allows us to compare the difference between pairs of parametrized solutions and their gradients (see in [HI11]).

A number of relevant results are available on structural stability topics. In particular, standard nonlinear energy stability results have been presented in [Str14] for convection problems, where the author dealt with an integral inequality technique referred to as the energy method. The structral stability of solutions to generalized Forchheimer equations (introduced in [CHK16]) has been provided in [ABHI09], where the authors investigated the uniqueness, the Lyapunov asymptotic stability together with the large time behavior features of the corresponding initial boundary value problems. A structural stability with respect to boundary data and the coefficients of Forchheimer is considered in [HI11]. In [WN19], a stability estimate is introduced by considering a nonlinear drag force term corresponding to the Forchheimer term in a Navier–Stokes type model of flow in non-homogeneous porous media. Such investigations on stability estimates not only contribute to the understanding of the well-posedness of model equations, but also can point out inherent delimitations of the parameters regions outside which it makes no sense to search for solutions, see e.g. [VVM19].

5.3 Preliminaries. List of assumptions

We list in this section a couple of preliminary results (mostly inequalities and compactness results) as well as our assumption on data and parameters.

Lemma 5.1. *Let $x, y \geq 0$. Then the following elementary inequalities hold:*

$$(x+y)^p \leq 2^p(x^p + y^p) \text{ for all } p > 0, \tag{5.2}$$

$$(x+y)^p \leq x^p + y^p \text{ for all } 0 < p \leq 1, \tag{5.3}$$

$$(x+y)^p \leq 2^{p-1}(x^p + y^p) \text{ for all } p \geq 1, \tag{5.4}$$

$$x^\beta \leq x^\alpha + x^\gamma \text{ for all } 0 \leq \alpha \leq \beta \leq \gamma, \tag{5.5}$$

$$x^\beta \leq 1 + x^\gamma \text{ for all } 0 \leq \beta \leq \gamma. \tag{5.6}$$

[1]This terminalogy is taken from [HI11] and refers to the assumption (A_5).

Lemma 5.2 (**A trace inequality**). *Let* $\lambda \in (0,1]$, $\delta = 1-\lambda$, $a \in (0,1)$, $a > \delta$, $\alpha \geq 2-\delta$, $\alpha \leq 2$, $\mu_0 = \frac{a-\delta}{1-a}$, $\alpha_\star = \frac{n(a-\delta)}{2-a}$ *and*

$$\theta = \theta_\alpha := \frac{1}{(1-a)(\alpha/\alpha_\star - 1)} \in (0,1). \tag{5.7}$$

Then it exists $C > 0$ *such that the following estimate holds*

$$\begin{aligned}\int_{\Gamma^R} |u|^\alpha d\sigma \leq 2\varepsilon \int_\Omega |u|^{\alpha+\delta-2} |\nabla u|^{2-a} dx + C\|u\|^\alpha_{L^\alpha(\Omega)} \\ + C\varepsilon^{-\frac{1}{1-a}} \|u\|^{\alpha+\mu_0}_{L^\alpha(\Omega)} + C\varepsilon^{-\mu_2} \|u\|^{\alpha+\mu_1}_{L^\alpha(\Omega)},\end{aligned} \tag{5.8}$$

where

$$\mu_1 = \mu_{1,\alpha} := \frac{\mu_0(1+\theta(1-a))}{1-\theta}, \tag{5.9}$$

$$\mu_2 = \mu_{2,\alpha} := \frac{1}{1-a} + \frac{\theta(2-a)}{(1-\theta)(1-a)}. \tag{5.10}$$

For the proof of Lemma 2.2, see Lemma 2.2 in [CHK16]. Here $a = \frac{\alpha_N}{\alpha_N+1} \in (0,1)$, with α_N cf. (5.11).

Theorem 5.3 (**Rellich-Kondrachov Compactness Theorem [Eva98]**). *Suppose* Ω *is a bounded open subset of* $\mathbb{R}^d$ *and the boundary* $\partial\Omega$ *is* C^1. *If* $1 \leq p < d$, *then* $W^{1,p}(\Omega) \hookrightarrow\hookrightarrow L^q(\Omega)$ *for each* $1 \leq q < p^\star$ *with* $p^\star = \frac{pd}{d-p}$.

Theorem 5.4 (**Aubin-Lions compactness Theorem [Aub63]**). *Let* $E_0 \hookrightarrow\hookrightarrow E \hookrightarrow E_1$ *be three Banach spaces. Suppose that* E_0 *is compactly embedded in* E *and* E *is continuously embedded in* E_1. *Then*

$$W = \{u \in L^p(S; E_0) \text{ and } u_t \in L^q(S; E_1)\}$$

is compactly embedded into $L^p(S; E)$.

Theorem 5.5 (**Schauder's Fixed Point Theorem [Zei86]**). *Let* B *be a nonempty, closed, bounded, convex subset of a Banach space* X, *and suppose:* $\mathcal{T} : B \longrightarrow B$ *is a compact operator. Then* $\mathcal{T}$ *has a fixed point.*

In the sequel, we recall some definitions on the constructions on the nonlinear Darcy equation and its monotonicity properties as they have been presented in [ABHI09]. First of all, we introduce the function $K_1 : \mathbb{R}^+ \longrightarrow \mathbb{R}^+$ defined for $\xi \geq 0$ by $K_1(\xi) = \frac{1}{g(s(\xi))}$ being the unique non-negative solution of the equation $sg(s) = \xi$, where $g : \mathbb{R}^+ \to \mathbb{R}^+$ is a polynomial with positive coefficients defined by

$$g(s) = a_0 s^{\alpha_0} + a_1 s^{\alpha_1} + \ldots + a_N s^{\alpha_N} \quad \text{for } s \geq 0, \tag{5.11}$$

where $\alpha_k \in \mathbb{R}_+$ with $k \in \{0, \ldots, N\}$.
The function g is independent of the spatial variables. Thus, we may have

$$G(|v|) = g(|v|)|v| = |\nabla p|, \tag{5.12}$$

where $G(s) = sg(s)$ for $s \geq 0$. From now on we use the following notation for the function G and its inverse G^{-1}, namely, $G(s) = sg(s) = \xi$ and $s = G^{-1}(\xi)$. To be successful in the analysis below, we impose the following condition, referred to as (G).

(G_1) $g \in C([0,\infty)) \cap C^1((0,\infty))$ such that

$$g(0) > 0 \text{ and } g'(s) \geq 0 \text{ for all } s \geq 0.$$

(G_2) It exists $\theta > 0$ with $g \in C([0,\infty)) \cap C^1((0,\infty))$ such that

$$g(s) \geq \theta s g'(s) \text{ for all } s > 0. \tag{5.13}$$

To be able to ensure the uniqueness of solution to the system (2.4), we use the monotonicity properties of the function $F : \mathbb{R}^d \longrightarrow \mathbb{R}^d$ such that $F(y) = K_1(|y|)y$. This is related to the nonlinear Darcy structure (5.12). Furthermore, we recall the following basic essential ingredients:

Definition 5.6. *Let $F : \mathbb{R}^d \longrightarrow \mathbb{R}^d$ be a given mapping.*

- *F is monotone if*

$$(F(y') - F(y)) \cdot (y' - y) \geq 0 \text{ for all } y', y \in \mathbb{R}^d. \tag{5.14}$$

- *F is strictly monotone if there is $c > 0$, such that*

$$(F(y') - F(y)) \cdot (y' - y) \geq c|y' - y|^2 \text{ for all } y', y \in \mathbb{R}^d. \tag{5.15}$$

- *F is strictly monotone on bounded sets if for any $R > 0$, there is a positive number $c_R > 0$, such that*

$$(F(y') - F(y)) \cdot (y' - y) \geq c_R|y' - y|^2 \text{ for all } |y'| \leq R, |y| \leq R. \tag{5.16}$$

See Definition III.3 in [ABHI09] for more details.

We introduce a useful formulation by defining the following function $\Phi : \mathbb{R}^d \times \mathbb{R}^d \longrightarrow \mathbb{R}$ as follow

$$\Phi(y, y') = (K_1(|y'|)y' - K_1(|y|)y) \cdot (y' - y) \text{ for } y, y' \in \mathbb{R}^d. \tag{5.17}$$

Proposition 5.7. *Let g satisfy (G_1). Then $F(y) = K_1(|y|)y$ is monotone, hence $\Phi(y, y') \geq 0$ for all $y, y' \in \mathbb{R}^d$, where Φ is defined as in (5.17).*

For the proof of Proposition 5.7, see Proposition III.4 in [ABHI09].

Lemma 5.8. *Let g satisfies (G_1). The function $K_1(\cdot) = K_{1g}(\cdot) = \frac{1}{g(s(\cdot))}$, is well defined, belongs to $C^1([0,\infty))$, and is decreasing. Moreover, for any $\xi \geq 0$, let $s = G^{-1}(\xi)$, then one has*

$$K_1'(\xi) = -K_1(\xi)\frac{g'(s)}{\xi g'(s) + g^2(s)} \leq 0. \tag{5.18}$$

For the proof of Lemma 5.8, see Lemma III.2 in [ABHI09].

Proposition 5.9. *Let g satisfies (G_1) and (G_2). Then $F(y) = K_1(|y|)y$ is strictly monotone on bounded sets. More precisely,*

$$\Phi(y, y') \geq \frac{\lambda}{\lambda + 1} K_1(\max\{|y|, |y'|\})|y' - y|^2 \text{ for all } y, y' \in \mathbb{R}^d. \tag{5.19}$$

For the proof 5.9, see Proposition III.6 in [ABHI09].

5.3.1 Assumptions

We make the following choices on the structure of the nonlinearities.

(A_1) The structure of $K_1(\xi)$ has the following properties hold $K_1 : [0,\infty) \longrightarrow (0, \frac{1}{a_0}]$ such that K_1 is decreasing and

$$\frac{d_1}{(1+\xi)^a} \leq K_1(\xi) \leq \frac{d_2}{(1+\xi)^a}; \tag{5.20}$$

$$d_3(\xi^{2-a} - 1) \leq K_1(\xi)\xi^2 \leq d_2\xi^{2-a} \text{ for all } \xi \in [0,\infty). \tag{5.21}$$

In (5.20), d_1, d_2, d_3 are strictly positive constants depending on $g(s)$ and $a \in (0,1)$.

(A_2) The function $b : \mathbb{R} \longrightarrow \mathbb{R}$ satisfies the following structural condition: it exists $\hat{c} > 0$ such that $b(z) \leq \hat{c}|z|^\sigma$, with $\sigma \in (0,1)$.

(A_3) The source term $b : \mathbb{R} \longrightarrow \mathbb{R}$ is globally Lipschitz continuous.

(A_4) The boundary data satisfies $\varphi \in L^\infty(\Gamma^N)$.

(A_5) K_1 satisfies the degeneracy type

$$C_1(1+\xi)^{-a} \leq K_1(\xi) \leq C_2(1+\xi)^{-a},$$

where C_1 and C_2 are constants.

Assumptions (A_1)-(A_5) are all technical. The choice of (A_1) was inspired by Theorem III.10 in [ABHI09] and the choice of (A_5) corresponds to the setting in [HI11].

We can now define the following concept of solutions to (2.4).

Definition 5.10. *Find*

$$(u,v) \in \left(L^{\alpha}(S;L^{\alpha}(\Omega)) \cap L^{2-a}(S;W^{1,2-a}(\Omega))\right) \times L^{2}(S;W^{1,2}(\Omega))$$

satisfying the identities

$$\int_{\Omega} \partial_t(u^{\lambda})\psi dx + \int_{\Omega} K_1(|\nabla u|)\nabla u \nabla \psi dx + \int_{\Gamma^R} \varphi u^{\lambda}\psi d\gamma = -\int_{\Omega} b(u-v)\psi dx \tag{5.22}$$

and

$$\int_{\Omega} \partial_t v\phi dx + \int_{\Omega} K_2 \nabla v \nabla \phi dx = \int_{\Omega} b(u-v)\phi dx \tag{5.23}$$

for a.e $t \in S$ and for all $\psi \in L^{\alpha}(\Omega)$, $\phi \in W^{1,2}(\Omega)$.

5.3.2 Statement of the main result

The main result of this paper is stated in Theorem 5.11, Theorem 5.12, Theorem 5.13 and Theorem 5.14.

Theorem 5.11. *Assume that (A_1)-(A_2) hold. Let $\lambda \in (0,1]$, $\delta = 1-\lambda$, $a = \frac{\alpha_N}{\alpha_N+1} \in (0,1)$, $a > \delta$, $\alpha \geq 2-\delta$, $\alpha \leq 2$, $\sigma \leq \frac{\alpha}{2}$, $\sigma \in (0,1)$ and $u_0 \in L^{\alpha}(\Omega)$, $v_0 \in L^2(\Omega)$. Then the problem (2.4) has at least a weak solution $(u,v) \in (L^{\alpha}(S;L^{\alpha}(\Omega)) \cap L^{2-a}(S;W^{1,2-a}(\Omega))) \times L^2(S;W^{1,2}(\Omega))$ in the sense of Definition 5.10.*

Theorem 5.12. *Assume that (A_1)-(A_4) hold. Let $a = \frac{\alpha_N}{\alpha_N+1} \in (0,1)$, $a > \delta$, $\alpha \geq 2-\delta$, $\alpha \leq 2$ and $\sigma \leq \frac{\alpha}{2}$, $\sigma \in (0,1)$. Then, the problem (2.4) admits at most a weak solution in the sense of Definition 5.10.*

We look for the case when the coupling is linear, i.e $b : \mathbb{R} \longrightarrow \mathbb{R}$ is a given function such that $b(s) = rB(s)$, where $r \in (0,\infty)$. Here, B is fixed and B is taken such that (A_2) and (A_3) are satisfied. We call $S_1 = (0,T_1)$, $S_2 = (0,T_2)$ and $\mathcal{S} = (0,\min\{T_1,T_2\}) = (0,\tau)$. Let (u_i,v_i) be weak solutions to (2.4) corresponding to the choices of data $(\tilde{D}_i,\varphi_i,r_i,u_{0i},v_{0i}), i \in \{1,2\}$. We define a triplet $(u_i,v_i,\mathcal{D}_i)$, where $(u_i,v_i) \in (L^{\alpha}(S;L^{\alpha}(\Omega)) \cap L^{2-a}(S;W^{1,2-a}(\Omega))) \times L^2(S;W^{1,2}(\Omega))$ and $\mathcal{D}_i = (D_i,r_i,u_{0i},v_{0i}) \in (0,\infty)\times(0,\infty)\times L^{\alpha}(\Omega)\times L^2(\Omega)$. To avoid the use of multiple indices, we denote $\tilde{D} := K_2$, where $K_2 > 0$ is entering (2.4). We give stability estimates of the solutions with respect to initial and boundary data, nonlinear coupling coefficient r_i and the diffusion coefficient $\tilde{D}$.

Theorem 5.13. *Assume that (A_1)-(A_4) hold, where (A_2) and (A_3) hold for the function $B(s)$. For $i \in \{1,2\}$, (D_i,r_i,u_{0i},v_{0i}) belong to a fixed compact subset $K \subset (0,\infty)\times(0,\infty)\times L^{\alpha}(\Omega)\times L^2(\Omega)$, $\lambda = 1$, $\bar{r} \geq |r_1 - r_2| > 0$. Then, the following stability estimate holds*

$$\|u_1-u_2\|^{\alpha}_{L^{\alpha}(\Omega)} + \|v_1-v_2\|^2_{L^2(\Omega)} \leq e^{C(\alpha,\lambda,\hat{c},\bar{r})|r_1-r_2|t}\Big[\|u_{01}-u_{02}\|^{\alpha}_{L^{\alpha}(\Omega)}$$
$$+\|v_{01}-v_{02}\|^2_{L^2(\Omega)} + Ct(|D_1-D_2| + |r_1-r_2| - \|\varphi_1-\varphi_2\|^2_{L^{\infty}(\Gamma^R)})\Big], \tag{5.24}$$

for $t \in \mathcal{S}$.

Theorem 5.14. *Assume that* (A_1)*-*(A_5) *hold, where* (A_2) *and* (A_3) *hold for the function* $B(s)$*. For* $i \in \{1,2\}$*, let* $(D_i, r_i, u_{0i}, v_{0i})$ *belong to a fixed compact subset* $K \subset (0,\infty)\times(0,\infty)\times L^\alpha(\Omega)\times L^2(\Omega)$*,* $\bar{r} \geq |r_1 - r_2| > 0$*. Let* (u_i, v_i) *be weak solutions to* (2.4) *corresponding to the choices of data* $(D_i, r_i, u_{0i}, v_{0i})$*. Then, the following estimate holds*

$$\int_\Omega |\nabla u_1 - \nabla u_2|^{2-a}dx + \int_\Omega |\nabla v_1 - \nabla v_2|^2 dx \leq C + C(|D_1 - D_2| - \|\varphi_1 - \varphi_2\|^2_{L^\infty(\Gamma^R)}) + \left(\left(t + \frac{1}{2}\right) + |r_1 - r_2|\frac{\hat{c}}{2\bar{r}}\right) e^{C(\alpha,\lambda,\hat{c},\bar{r})|r_1 - r_2|t}\Big(\|u_{01} - u_{02}\|^2_{L^2(\Omega)} + \|v_{01} - v_{02}\|^2_{L^2(\Omega)} + Ct\left(|D_1 - D_2| + |r_1 - r_2| - \|\varphi_1 - \varphi_2\|^2_{L^\infty(\Gamma^R)}\right)\Big). \tag{5.25}$$

for $t \in \mathcal{S}$*.*

The proofs of Theorem 5.11, Theorem 5.12, Theorem 5.13 and Theorem 5.14 are given in Section 5.11, Section 5.6, Section 5.7 and Section 5.8, respectively.

5.4 Energy estimates

In this section, we provide the energy estimates for the solutions in the sense of Definition 5.10 to our problem (2.4). This is a crucial step, which in fact allows the Schauder-fixed point Theorem to work in our case.

5.4.1 L^α - L^2 estimates

Proposition 5.15. *Assume that* (A_1)*-*(A_2) *hold and let* $\lambda \in (0,1]$*,* $\delta = 1 - \lambda$*,* $a = \frac{\alpha_N}{\alpha_N + 1} \in (0,1)$*,* $a > \delta$*,* $\alpha \geq 2 - \delta$*,* $\alpha \leq 2$*,* $\sigma \leq \frac{\alpha}{2}$*,* $\sigma \in (0,1)$ *and* $u_0 \in L^\alpha(\Omega)$*,* $v_0 \in L^2(\Omega)$*. Then, for any* $t \in S$*, the following estimates hold*

$$\frac{d}{dt}\int_\Omega |u|^\alpha dx + \int_\Omega |\nabla u|^{2-a}|u|^{\alpha+\delta-2}dx \leq C_1 + \Big(\frac{3}{2C_2}\hat{c} + \frac{d_3(\alpha-\lambda)}{C_2}\Big)\|u\|^\alpha_{L^\alpha(\Omega)} + \frac{\hat{c}}{2C_2}\|v\|^2_{L^2(\Omega)}. \tag{5.26}$$

$$\int_\Omega |u|^\alpha dx + \int_\Omega v^2 dx \leq e^{C_3 t}\left(1 + \|u_0\|^\alpha_{L^\alpha(\Omega)} + \|v_0\|^2_{L^2(\Omega)}\right), \tag{5.27}$$

$$\int_0^T\int_\Omega |u|^{\alpha+\delta-2}|\nabla u|^{2-a}dxdt + \int_0^T\int_\Omega |\nabla v|^2 dxdt \leq C_5 + C_6\left(\|u_0\|^\alpha_{L^\alpha(S;L^\alpha(\Omega))} + \|v_0\|^2_{L^2(S;L^2(\Omega))}\right), \tag{5.28}$$

where $C_1 := \frac{d_3(\alpha-\lambda)+\hat{c}}{C_5}|\Omega|$*,* $C_2 := \min\left\{\frac{\lambda}{\alpha}, d_3(\alpha-\lambda)\right\}$*,* $C_3 := \max\left\{\frac{5}{2}\tilde{\underline{c}}\hat{c}|\Omega|, 2\tilde{\underline{c}}\hat{c}\right\}$*,* $C_4 := \min\{\alpha - \lambda, K_2\}$*,* $C_5 := \frac{5T}{2C_4}\hat{c}|\Omega| + \frac{2T\hat{c}e^{C_3 t}}{C_4}$*, and* $C_6 := \frac{2\hat{c}e^{C_3 t}}{C_2}$ *with* $\tilde{\underline{c}} := \frac{1}{\min\left\{\frac{\lambda}{\alpha}, \frac{1}{2}\right\}}$ *and* $\hat{c}$ *as in* (A_2)*, respectively.*

Proof. To prove (5.27), we proceed as follows. We consider firstly the following sub-problem to which we refer to as (P_1): For a given $v \in L^2(S; L^2(\Omega))$, search for $u \in L^\alpha(S; L^\alpha(\Omega)) \cap L^{2-a}(S; W^{1,2-a}(\Omega))$ such that (5.29) is fulfilled, viz.

$$\begin{cases} \partial_t(u^\lambda) + \operatorname{div}(-K_1(|\nabla u|)\nabla u) = -b(u-v) \ \text{ in } S \times \Omega, \\ -K_1(|\nabla u|)\nabla u \cdot \mathbf{n} = \varphi u^\lambda \ \text{ at } S \times \Gamma^R, \\ -K_1(|\nabla u|)\nabla u \cdot \mathbf{n} = 0 \ \text{ at } S \times \Gamma^N, \\ u(0,x) = u_0(x) \ \text{ for all } x \in \bar{\Omega}. \end{cases} \tag{5.29}$$

Multiplying both sides of the first equation in (P_1) by $|u|^{\alpha+\delta-1}$ and integrating the result over Ω, we obtain

$$\int_\Omega \partial_t(u^\lambda)|u|^{\alpha+\delta-1}dx + \int_\Omega \operatorname{div}(-K_1(|\nabla u|)\nabla u)|u|^{\alpha+\delta-1}dx = -\int_\Omega b(u-v)|u|^{\alpha+\delta-1}dx.$$

Integrating by parts the last identity, and using the boundary conditions, it yields:

$$\begin{aligned} &\frac{\lambda}{\alpha}\frac{d}{dt}\int_\Omega |u|^\alpha dx + (\alpha-\lambda)\int_\Omega K_1(|\nabla u|)|\nabla u|^2 u^{\alpha+\delta-2}dx \\ &\qquad + \int_{\Gamma^R} |u|^\alpha \varphi d\gamma = -\int_\Omega b(u-v)|u|^{\alpha+\delta-1}dx. \end{aligned}$$

Using (A_2), we get the following estimate:

$$\begin{aligned} \frac{\lambda}{\alpha}\frac{d}{dt}\int_\Omega |u|^\alpha dx + (\alpha-\lambda)\int_\Omega K_1(|\nabla u|)|\nabla u|^2|u|^{\alpha+\delta-2}dx &\le \int_\Omega \hat{c}|u-v|^\sigma |u|^{\alpha+\delta-1}dx \\ &\le \int_\Omega \hat{c}|u+v|^\sigma |u|^{\alpha+\delta-1}dx \\ &\le \hat{c}\int_\Omega |u|^\sigma |u|^{\alpha+\delta-1}dx + \hat{c}\int_\Omega |v|^\sigma |u|^{\alpha+\delta-1}dx, \end{aligned} \tag{5.30}$$

where we used the inequality $|u+v|^\sigma \le |u|^\sigma + |v|^\sigma$ for $\sigma \in (0,1)$.

By choosing $\sigma = 1-\delta$ and $\sigma \le \frac{\alpha}{2}$ such that $\sigma \in (0,1)$ and $1 < \alpha \le 2$, the inequality (5.30) becomes

$$\begin{aligned} &\frac{\lambda}{\alpha}\frac{d}{dt}\int_\Omega |u|^\alpha dx + (\alpha-\lambda)\int_\Omega K_1(|\nabla u|)|\nabla u|^2|u|^{\alpha+\delta-2}dx \\ &\qquad \le \frac{\hat{c}}{2}\int_\Omega (1+|u|^\alpha)dx + \frac{\hat{c}}{2}\int_\Omega (1+|v|^2)dx + \hat{c}\int_\Omega |u|^\alpha dx \\ &\qquad \le \frac{\hat{c}}{2}|\Omega| + \frac{\hat{c}}{2}\int_\Omega |u|^\alpha dx + \hat{c}\int_\Omega |u|^\alpha dx + \frac{\hat{c}}{2}|\Omega| + \frac{\hat{c}}{2}\int_\Omega |v|^2 dx \\ &\qquad \le \hat{c}|\Omega| + \frac{3\hat{c}}{2}\|u\|^\alpha_{L^\alpha(\Omega)} + \frac{\hat{c}}{2}\|v\|^2_{L^2(\Omega)}. \end{aligned} \tag{5.31}$$

(5.31) also leads to

$$\begin{aligned} \frac{d}{dt}\int_\Omega |u|^\alpha dx + \int_\Omega |\nabla u|^{2-a}|u|^{\alpha+\delta-2}dx &\le \frac{d_3(\alpha-\lambda)+\hat{c}}{C_2}|\Omega| \\ &\quad + \left(\frac{3}{2C_2}\hat{c} + \frac{d_3(\alpha-\lambda)}{C_2}\right)\|u\|^\alpha_{L^\alpha(\Omega)} + \frac{\hat{c}}{2C_2}\|v\|^2_{L^2(\Omega)}, \end{aligned} \tag{5.32}$$

where we use the property of K_1 as indicated in (5.20).

Now, we consider a second sub-problem which prefer to as (P_2): For given $u \in L^\alpha(S; L^\alpha(\Omega))$, search for $v \in L^2(S; W^{1,2}(\Omega))$ such that

$$\begin{cases} \partial_t v - K_2 \Delta v = b(u-v) \ \text{ in } S \times \Omega, \\ -K_2 \nabla v \cdot \mathbf{n} = 0 \ \text{ at } S \times \partial\Omega, \\ v(0,x) = v_0(x) \ \text{ for all } x \in \bar{\Omega}. \end{cases} \tag{5.33}$$

Multiplying the first equation of (P_2) by v and integrating the result over Ω lead to

$$\int_\Omega \partial_t v v dx - \int_\Omega K_2 \Delta v v dx = \int_\Omega b(u-v) v dx.$$

Integrating by parts this expression and using the corresponding boundary conditions ensure the identity:

$$\frac{1}{2}\frac{d}{dt}\int_\Omega |v|^2 dx + K_2 \int_\Omega |\nabla v|^2 dx = \int_\Omega b(u-v) v dx. \tag{5.34}$$

Then, by (A_2), we have the following estimates

$$\begin{aligned} \frac{1}{2}\frac{d}{dt}\int_\Omega v^2 dx + K_2 \int_\Omega |\nabla v|^2 dx &\le \int_\Omega \hat{c}|u-v|^\sigma v dx \\ &\le \hat{c}\int_\Omega |u|^\sigma v dx + \hat{c}\int_\Omega |v|^\sigma v dx \\ &\le \frac{\hat{c}}{2}\int_\Omega |u|^{2\sigma} dx + \frac{\hat{c}}{2}\int_\Omega v^2 dx + \hat{c}\int_\Omega (1+v^2) dx \\ &\le \frac{\hat{c}}{2}\int_\Omega (1+|u|^\alpha) dx + \frac{3\hat{c}}{2}\|v\|^2_{L^2(\Omega)} + \hat{c}|\Omega| \\ &\le \frac{3}{2}\hat{c}|\Omega| + \frac{\hat{c}}{2}\|u\|^\alpha_{L^\alpha(\Omega)} + \frac{3}{2}\hat{c}\|v\|^2_{L^2(\Omega)}. \end{aligned} \tag{5.35}$$

Combining (5.31) and (5.35) together with neglecting the gradient terms from both these inequalities, we have

$$\frac{\lambda}{\alpha}\frac{d}{dt}\int_\Omega |u|^\alpha dx + \frac{1}{2}\frac{d}{dt}\int_\Omega |v|^2 dx \le \frac{5}{2}\hat{c}|\Omega| + 2\hat{c}\|u\|^\alpha_{L^\alpha(\Omega)} + 2\hat{c}\|v\|^2_{L^2(\Omega)}. \tag{5.36}$$

Setting $\tilde{c} := \min\left\{\frac{\lambda}{\alpha}, \frac{1}{2}\right\}$, we rewrite (5.36) as

$$\frac{d}{dt}\int_\Omega |u|^\alpha dx + \frac{d}{dt}\int_\Omega |v|^2 dx \le \frac{5}{2}\tilde{\underline{c}}\hat{c}|\Omega| + 2\tilde{\underline{c}}\hat{c}\|u\|^\alpha_{L^\alpha(\Omega)} + 2\tilde{\underline{c}}\hat{c}\|v\|^2_{L^2(\Omega)}, \tag{5.37}$$

where $\tilde{\underline{c}} := \frac{1}{\tilde{c}}$.

For any $t \in S$, take $V(t) := 1 + \int_\Omega (|u|^\alpha + v^2) dx$ and $C_3 := \max\left\{\frac{5}{2}\tilde{\underline{c}}\hat{c}|\Omega|, 2\tilde{\underline{c}}\hat{c}\right\}$. Then the inequality (5.37) becomes

$$\frac{d}{dt}V(t) \le C_3 V(t) \ \text{ for all } t \in S. \tag{5.38}$$

(5.38) leads to

$$V(t) \leq V(0) \exp\left(\int_0^t C_3 ds\right), \text{ and hence, we get}$$

$$\int_\Omega |u|^\alpha dx + \int_\Omega v^2 dx \leq e^{C_3 t}\left(1 + \|u_0\|^\alpha_{L^\alpha(\Omega)} + \|v_0\|^2_{L^2(\Omega)}\right). \tag{5.39}$$

Now we prove (5.28). Combining (5.31) and (5.35) yields

$$\begin{aligned}\frac{d}{dt}\int_\Omega |u|^\alpha dx + \frac{d}{dt}\int_\Omega |v|^2 dx + (\alpha - \lambda)\int_\Omega K_1(|\nabla u|)|\nabla u|^2 |u|^{\alpha+\delta-2} dx \\ + K_2 \int_\Omega |\nabla v|^2 dx \leq \frac{5}{2}\hat{c}|\Omega| + 2\hat{c}\|u\|^\alpha_{L^\alpha(\Omega)} + 2\hat{c}\|v\|^2_{L^2(\Omega)}.\end{aligned} \tag{5.40}$$

Set $C_4 := \min\{\alpha - \lambda, K_2\}$. Using (5.27) and integrating (5.40) over the time interval S, we are led to

$$\begin{aligned}\int_0^T \int_\Omega K_1(|\nabla u|)|\nabla u|^2 |u|^{\alpha+\delta-2} dx dt + \int_0^T \int_\Omega |\nabla v|^2 dx dt \leq \frac{5T}{2C_4}\hat{c}|\Omega| + \frac{2T\hat{c}e^{C_3 t}}{C_4} \\ + \frac{2\hat{c}e^{C_3 t}}{C_4}(\|u_0\|^\alpha_{L^\alpha(S,L^\alpha(\Omega))} + \|v_0\|^2_{L^2(S,L^2(\Omega))}).\end{aligned}$$

Therefore, the inequality (5.28) holds. □

5.4.2 Gradient and time derivative estimates

We consider the following function $H : \Omega \longrightarrow \mathbb{R}$ given by

$$H(\xi) = \int_0^{\xi^2} K_1(\sqrt{s}) ds \quad \text{for } \xi \geq 0. \tag{5.41}$$

We have the following structural inequality between $H(\xi)$ and $K_1(\xi)\xi^2$, i.e.

$$K_1(\xi)\xi^2 \leq H(\xi) \leq 2K_1(\xi)\xi^2 \text{ for all } \xi \geq 0. \tag{5.42}$$

By combining (5.20) and (5.42), we deduce also that

$$d_3(\xi^{2-a} - 1) \leq H(\xi) \leq 2d_2\xi^{2-a}, \tag{5.43}$$

where d_2, d_3 and a are defined as in (A_1).

Proposition 5.16. *Assume that (A_1)-(A_2) hold. Let $\lambda \in (0, 1]$, $\delta = 1 - \lambda$, $a = \frac{\alpha_N}{\alpha_N + 1}$, $a > \delta$, $\alpha \geq 2 - \delta$, $\alpha \leq 2$ and $\sigma \leq \frac{\alpha}{2}$. Furthermore, suppose that*

$\nabla u_0 \in L^\alpha(\Omega) \cap L^{2-a}(\Omega)$, $u_0 \in L^\alpha(\Omega)$, $v_0 \in H^1(\Omega)$ *and* $\varphi \in L^\infty(\Gamma^R)$. *Then, for any* $t \in S$, *the following estimates hold*

$$\int_\Omega |\nabla u|^{2-a} dx + \int_\Omega |\nabla v|^2 dx \leq C(\hat{c}, \lambda, a) \Bigg[\Lambda(0) + \int_0^t (1 + \|u\|^\alpha_{L^\alpha(\Omega)})^\beta ds + \int_0^t \|v\|^2_{L^2(\Omega)} ds + \int_0^t \int_{\Gamma^R} |\varphi_t|^{\frac{\alpha}{\alpha-\lambda-1}} d\sigma ds \Bigg] + \int_\Omega |\nabla v_0|^2 dx + \frac{\hat{c}^2}{C_2} |\Omega| t + \frac{\hat{c}^2}{2C_2} e^{C_3 t} \left(1 + \|u_0\|^\alpha_{L^\alpha(S, L^\alpha(\Omega))} + \|v_0\|^2_{L^2(S, L^2(\Omega))} \right). \quad (5.44)$$

$$\int_\Omega |(u^\lambda)_t|^2 dx + \int_\Omega |v_t|^2 dx \leq C(\hat{c}, \lambda, a) \Bigg[1 + (1 + \|u\|^\alpha_{L^\alpha(\Omega)})^\beta + \|v\|^2_{L^2(\Omega)} + \int_{\Gamma^R} |\varphi_t|^{\frac{\alpha}{\alpha-\lambda-1}} d\sigma \Bigg] + \frac{\hat{c}^2}{C_2} |\Omega| + \frac{\hat{c}^2}{2C_2} e^{C_3 t} \left(1 + \|u_0\|^\alpha_{L^\alpha(\Omega)} + \|v_0\|^2_{L^2(\Omega)} \right), \quad (5.45)$$

where $C(\hat{c}, \lambda, a) > 0$ *is a constant and*

$$\Lambda(0) := \frac{\lambda + 1}{2} \int_\Omega H(|\nabla u_0|) dx + \int_\Omega |u_0|^\alpha dx.$$

Proof. We begin with studying the sub-problem (P_1) for a given choice of $v \in L^2(S; L^2(\Omega))$. Multiplying the first equation in (P_1) by $u_t = \frac{1}{\lambda}(u^\lambda)_t u^{1-\lambda}$ (note that $\frac{1}{\lambda}(u^\lambda)_t u^{1-\lambda} = \frac{1}{\lambda}\lambda u^{\lambda-1} u_t u^{1-\lambda} = u_t$) and integrating the result over Ω, we have

$$\int_\Omega \partial_t(u^\lambda) u_t dx + \int_\Omega \operatorname{div}(-K_1(|\nabla u|)\nabla u) u_t dx = -\int_\Omega b(u - v) u_t dx. \quad (5.46)$$

By integrating (5.46) by parts and using the property of the function H as stated in (5.42), yields:

$$\frac{1}{\lambda} \int_\Omega u_t (u^\lambda)_t dx + \frac{1}{2} \frac{d}{dt} \int_\Omega H(|\nabla u|) dx + \int_{\Gamma^R} \varphi u^\lambda u_t d\sigma = -\int_\Omega b(u - v) u_t dx. \quad (5.47)$$

Using the assumption (A_2) together with the integration by parts the term $\int_{\Gamma^R} \varphi u^\lambda u_t d\sigma$ and by applying afterwards the Cauchy-Schwarz's inequality, we

get the upper bound

$$\begin{aligned}
\frac{1}{\lambda}\int_\Omega |u_t(u^\lambda)_t|dx + \frac{1}{2}\frac{d}{dt}\int_\Omega H(|\nabla u|)dx &\le -\int_{\Gamma^R}\varphi u^\lambda u_t d\sigma + \hat{c}\int_\Omega |u-v|^\sigma u_t dx \\
&\le -\int_{\Gamma^R}\varphi|u|^\lambda|u_t|d\sigma + \hat{c}\int_\Omega |u+v|^\sigma|u_t|dx \\
&\le -\frac{1}{\lambda+1}\frac{d}{dt}\int_{\Gamma^R}|u|^{\lambda+1}\varphi d\sigma + \frac{1}{\lambda+1}\int_{\Gamma^R}|u|^{\lambda+1}\varphi_t d\sigma + \\
&\hat{c}\int_\Omega |u|^\sigma|u_t|dx + \hat{c}\int_\Omega |v|^\sigma|u_t|dx \\
&\le -\frac{1}{\lambda+1}\frac{d}{dt}\int_{\Gamma^R}|u|^{\lambda+1}\varphi d\sigma + \frac{1}{\lambda+1}\int_{\Gamma^R}|u|^{\lambda+1}\varphi_t d\sigma + \frac{\hat{c}}{4\varepsilon}\int_\Omega |u|^{2\sigma}dx \\
&+ 2\varepsilon\hat{c}\int_\Omega |u_t|^2dx + \frac{\hat{c}}{4\varepsilon}\int_\Omega |v|^{2\sigma}dx \\
&\le -\frac{1}{\lambda+1}\frac{d}{dt}\int_{\Gamma^R}|u|^{\lambda+1}\varphi d\sigma + \frac{1}{\lambda+1}\int_{\Gamma^R}|u|^{\lambda+1}\varphi_t d\sigma \\
&+ \frac{\hat{c}}{2\varepsilon}|\Omega| + \frac{\hat{c}}{4\varepsilon}\int_\Omega |u|^\alpha dx + \frac{\hat{c}}{4\varepsilon}\int_\Omega |v|^2dx + 2\varepsilon\hat{c}\int_\Omega |u_t|^2dx. \qquad (5.48)
\end{aligned}$$

Multiplying the inequality (5.48) by $\lambda+1$ and applying Young's inequality to the term $\frac{1}{\lambda+1}\int_{\Gamma^R}|u|^{\lambda+1}\varphi_t d\sigma$ yield the estimate

$$\begin{aligned}
&\frac{\lambda+1}{\lambda}\int_\Omega |u|^{1-\lambda}|(u^\lambda)_t|^2dx + \frac{d}{dt}\left(\frac{\lambda+1}{2}\int_\Omega H(|\nabla u|)dx + \int_{\Gamma^R}|u|^{\lambda+1}\varphi d\sigma\right) \\
&\le \int_{\Gamma^R}|u|^\alpha d\sigma + \int_{\Gamma^R}|\varphi_t|^{\frac{\alpha}{\alpha-\lambda-1}}d\sigma + \frac{\hat{c}}{2\varepsilon}|\Omega|(\lambda+1) + (\lambda+1)\frac{\hat{c}}{4\varepsilon}\int_\Omega |u|^\alpha dx \\
&\qquad +(\lambda+1)\frac{\hat{c}}{4\varepsilon}\int_\Omega |v|^2dx + (\lambda+1)2\varepsilon\hat{c}\int_\Omega |u_t|^2dx. \qquad (5.49)
\end{aligned}$$

Using the trace inequality (5.8), we obtain

$$\begin{aligned}
\int_{\Gamma^R}|u|^\alpha d\sigma &\le 2\tilde{\varepsilon}\int_\Omega |\nabla u|^{2-a}|u|^{\alpha+\delta-2}dx + C\|u\|^\alpha_{L^\alpha(\Omega)} \\
&\quad +C\tilde{\varepsilon}^{-\frac{1}{1-a}}\|u\|^{\alpha+\mu_0}_{L^\alpha(\Omega)} + C\tilde{\varepsilon}^{-\mu_2}\|u\|^{\alpha+\mu_1}_{L^\alpha(\Omega)}. \qquad (5.50)
\end{aligned}$$

By (5.50) and (5.49), we obtain

$$\begin{aligned}
&\frac{\lambda+1}{\lambda}\int_\Omega |u|^{1-\lambda}|(u^\lambda)_t|^2dx + \frac{d}{dt}\left(\frac{\lambda+1}{2}\int_\Omega H(|\nabla u|)dx + \int_{\Gamma^R}|u|^{\lambda+1}\varphi d\sigma\right) \\
&\le 2\tilde{\varepsilon}\int_\Omega |\nabla u|^{2-a}|u|^{\alpha+\delta-2}dx + C\|u\|^\alpha_{L^\alpha(\Omega)} + C\tilde{\varepsilon}^{-\frac{1}{1-a}}\|u\|^{\alpha+\mu_0}_{L^\alpha(\Omega)} + C\tilde{\varepsilon}^{-\mu_2}\|u\|^{\alpha+\mu_1}_{L^\alpha(\Omega)} \\
&\qquad + \int_{\Gamma^R}|\varphi_t|^{\frac{\alpha}{\alpha-\lambda-1}}d\sigma + \frac{\hat{c}}{2\varepsilon}|\Omega|(\lambda+1) + (\lambda+1)\frac{\hat{c}}{4\varepsilon}\int_\Omega |u|^\alpha dx \\
&\qquad +(\lambda+1)\frac{\hat{c}}{4\varepsilon}\int_\Omega |v|^2dx + (\lambda+1)2\varepsilon\hat{c}\int_\Omega |u_t|^2dx. \qquad (5.51)
\end{aligned}$$

We denote

$$\Lambda(t) := \frac{\lambda+1}{2}\int_\Omega H(|\nabla u|)dx + \int_\Omega |u|^\alpha dx \text{ for all } t \in S.$$

Note that

$$\Lambda(0) := \frac{\lambda+1}{2}\int_\Omega H(|\nabla u_0|)dx + \int_\Omega |u_0|^\alpha dx.$$

Then, by using (5.26), we have the following estimate

$$\begin{aligned}
&\frac{\lambda+1}{\lambda}\int_\Omega |u|^{1-\lambda}|(u^\lambda)_t|^2dx - 2\varepsilon\hat{c}\frac{\lambda+1}{\lambda}\int_\Omega |u|^{2(1-\lambda)}|(u^\lambda)_t|^2dx + \frac{d}{dt}\Lambda(t)\\
&+(1-2\tilde{\varepsilon})\int_\Omega |u|^{\alpha+\delta-2}|\nabla u|^{2-a}dx \le \left(\frac{d_3(\alpha-\lambda)+\hat{c}}{C_2} + \frac{(\lambda+1)\hat{c}}{2\varepsilon}\right)|\Omega|\\
&+\left(\frac{3}{2C_2}\hat{c} + \frac{d_3(\alpha-\lambda)}{C_2} + C + \frac{(\lambda+1)\hat{c}}{4\varepsilon}\right)\|u\|^\alpha_{L^\alpha(\Omega)} + \left(\frac{\hat{c}}{2C_2} + \frac{\hat{c}(\lambda+1)}{4\varepsilon}\right)\|v\|^2_{L^2(\Omega)}\\
&+C\tilde{\varepsilon}^{-\frac{1}{1-a}}\|u\|^{\alpha+\mu_0}_{L^\alpha(\Omega)} + C\tilde{\varepsilon}^{-\mu_2}\|u\|^{\alpha+\mu_1}_{L^\alpha(\Omega)} + \int_{\Gamma^R}|\varphi_t|^{\frac{\alpha}{\alpha-\lambda-1}}d\sigma.
\end{aligned}$$

Based on (A_3), after choosing $\tilde{\varepsilon} = \frac{1}{4}$ and $\varepsilon = \frac{1}{4\hat{c}}$, we obtain

$$\begin{aligned}
\int_\Omega |(u^\lambda)_t|^2dx + \frac{d}{dt}\Lambda(t) \le C(\hat{c},\lambda,a)\Big[&1 + \|u\|^\alpha_{L^\alpha(\Omega)} + \|v\|^2_{L^2(\Omega)}\\
&+ \|u\|^{\alpha+\mu_0}_{L^\alpha(\Omega)} + \|u\|^{\alpha+\mu_1}_{L^\alpha(\Omega)} + \int_{\Gamma^R}|\varphi_t|^{\frac{\alpha}{\alpha-\lambda-1}}d\sigma\Big].
\end{aligned} \tag{5.52}$$

We denote $\beta := \alpha + \mu_1$, and β is the maximum allowed power of $\|u\|_{L^\alpha(\Omega)}$ when considering the right hand side of (5.52). Now, using the inequality (5.6) leads to

$$\begin{aligned}
\int_\Omega |(u^\lambda)_t|^2dx + \frac{d}{dt}\Lambda(t) \le C(\hat{c},\lambda,a)\Bigg[&1 + (1+\|u\|^\alpha_{L^\alpha(\Omega)})^\beta\\
&+\|v\|^2_{L^2(\Omega)} + \int_{\Gamma^R}|\varphi_t|^{\frac{\alpha}{\alpha-\lambda-1}}d\sigma\Bigg].
\end{aligned} \tag{5.53}$$

Integrating (5.53) over the time interval $(0,t)$, we are led to

$$\begin{aligned}
\int_0^t\int_\Omega |(u^\lambda)_t|^2dx + \frac{\lambda+1}{2}\int_\Omega H(|\nabla u|)dx + \int_\Omega |u|^\alpha dx \le C(\hat{c},\lambda,a)\Bigg[&\Lambda(0)\\
+\int_0^t(1+\|u\|^\alpha_{L^\alpha(\Omega)})^\beta ds + \int_0^t\|v\|^2_{L^2(\Omega)}ds + \int_0^t\int_{\Gamma^R}|\varphi_t|^{\frac{\alpha}{\alpha-\lambda-1}}d\sigma ds\Bigg].
\end{aligned} \tag{5.54}$$

This fact also implies

$$\begin{aligned}
\int_0^t\int_\Omega |(u^\lambda)_t|^2dx + \int_\Omega H(|\nabla u|)dx + \int_\Omega |u|^\alpha dx \le C(\hat{c},\lambda,a)\Bigg[&\Lambda(0)\\
+\int_0^t(1+\|u\|^\alpha_{L^\alpha(\Omega)})^\beta ds + \int_0^t\|v\|^2_{L^2(\Omega)}ds + \int_0^t\int_{\Gamma^R}|\varphi_t|^{\frac{\alpha}{\alpha-\lambda-1}}d\sigma ds\Bigg].
\end{aligned} \tag{5.55}$$

Employing (5.43) yields

$$\int_0^t \int_\Omega |(u^\lambda)_t|^2 dx + \int_\Omega |\nabla u|^{2-a} dx \le C(\hat{c}, \lambda, a) \Bigg[\Lambda(0) + \int_0^t (1 + \|u\|^\alpha_{L^\alpha(\Omega)})^\beta ds + \int_0^t \|v\|^2_{L^2(\Omega)} ds + \int_0^t \int_{\Gamma^R} |\varphi_t|^{\frac{\alpha}{\alpha-\lambda-1}} d\sigma ds \Bigg]. \tag{5.56}$$

Now, we consider the sub-problem (P_2): Take a fixed $u \in L^2(S; L^\alpha(\Omega))$. By multiplying the first equation of (P_2) by v_t and then integrating the result over Ω, we have

$$\int_\Omega |v_t|^2 dx + \frac{K_2}{2} \frac{d}{dt} \int_\Omega |\nabla v|^2 dx = \int_\Omega b(u - v) v_t dx. \tag{5.57}$$

By using (A_2) together with (5.3) and (5.6), it results in

$$\begin{aligned} \int_\Omega |v_t|^2 dx + \frac{K_2}{2} \frac{d}{dt} \int_\Omega |\nabla v|^2 dx &\le \hat{c} \int_\Omega |u - v|^\sigma |v_t| dx \\ &\le \hat{c} \int_\Omega |u + v|^\sigma |v_t| dx \\ &\le \hat{c} \int_\Omega |u|^\sigma |v_t| dx + \hat{c} \int_\Omega |v|^\sigma |v_t| dx \\ &\le \frac{\hat{c}}{4\varepsilon} \int_\Omega |u|^{2\sigma} dx + \frac{\hat{c}}{4\varepsilon} \int_\Omega |v|^{2\sigma} dx + 2\hat{c}\varepsilon \int_\Omega |v_t|^2 dx \\ &\le \frac{\hat{c}}{2\varepsilon} |\Omega| + \frac{\hat{c}}{4\varepsilon} \int_\Omega |u|^\alpha dx \\ &+ \frac{\hat{c}}{4\varepsilon} \int_\Omega |v|^2 dx + 2\hat{c}\varepsilon \int_\Omega |v_t|^2 dx. \end{aligned} \tag{5.58}$$

If we choose $\varepsilon = \frac{1}{4\hat{c}}$ such that $1 - 2\varepsilon\hat{c} > 0$, then (5.58) becomes

$$\frac{1}{2} \int_\Omega |v_t|^2 dx + \frac{K_2}{2} \frac{d}{dt} \int_\Omega |\nabla v|^2 dx \le 2\hat{c}^2 |\Omega| + \hat{c}^2 \int_\Omega |u|^\alpha dx + \hat{c}^2 \int_\Omega |v|^2 dx. \tag{5.59}$$

Putting $C_5 := \min\left\{\frac{1}{2}, \frac{K_2}{2}\right\}$, we get the following estimate

$$\int_\Omega |v_t|^2 dx + \frac{d}{dt} \int_\Omega |\nabla v|^2 dx \le \frac{\hat{c}^2}{C_2} |\Omega| + \frac{\hat{c}^2}{C_2} \int_\Omega |u|^\alpha dx + \frac{\hat{c}^2}{C_2} \int_\Omega |v|^2 dx. \tag{5.60}$$

Applying (5.27) to the right hand side of (5.60), we obtain

$$\int_\Omega |v_t|^2 dx + \frac{d}{dt} \int_\Omega |\nabla v|^2 dx \le \frac{\hat{c}^2}{C_2} |\Omega| + \frac{\hat{c}^2}{2C_2} e^{C_1 t} \left(1 + \|u_0\|^\alpha_{L^\alpha(\Omega)} + \|v_0\|^2_{L^2(\Omega)}\right). \tag{5.61}$$

The inequality (5.61) implies

$$\int_\Omega |v_t|^2 dx \le \frac{\hat{c}^2}{C_2}|\Omega| + \frac{\hat{c}^2}{2C_2} e^{C_3 t}\left(1 + \|u_0\|^\alpha_{L^\alpha(\Omega)} + \|v_0\|^2_{L^2(\Omega)}\right). \tag{5.62}$$

On the other hand, (5.61) also leads to

$$\frac{d}{dt}\int_\Omega |\nabla v|^2 dx \le \frac{\hat{c}^2}{C_2}|\Omega| + \frac{\hat{c}^2}{2C_2} e^{C_3 t}\left(1 + \|u_0\|^\alpha_{L^\alpha(\Omega)} + \|v_0\|^2_{L^2(\Omega)}\right). \tag{5.63}$$

Integrating (5.63) over the time interval $(0,t)$, we obtain the upper bound

$$\begin{aligned}\int_\Omega |\nabla v(t)|^2 dx \le \int_\Omega |\nabla v_0|^2 dx + \frac{\hat{c}^2}{C_2}|\Omega| t \\ + \frac{\hat{c}^2}{2C_2} e^{C_3 t}\left(1 + \|u_0\|^\alpha_{L^\alpha(S;L^\alpha(\Omega))} + \|v_0\|^2_{L^2(S;L^2(\Omega))}\right).\end{aligned} \tag{5.64}$$

Combining (5.56) and (5.64), we obtain

$$\begin{aligned}\int_\Omega |\nabla u|^{2-a} dx + \int_\Omega |\nabla v|^2 dx \le C(\hat{c},\lambda,a)\Bigg[\Lambda(0) + \int_0^t (1 + \|u\|^\alpha_{L^\alpha(\Omega)})^\beta ds \\ + \int_0^t \|v\|^2_{L^2(\Omega)} ds + \int_0^t \int_{\Gamma^R} |\varphi_t|^{\frac{\alpha}{\alpha-\lambda-1}} d\sigma ds\Bigg] \\ + \int_\Omega |\nabla v_0|^2 dx + \frac{\hat{c}^2}{C_2}|\Omega| t \\ + \frac{\hat{c}^2}{2C_2} e^{C_3 t}\left(1 + \|u_0\|^\alpha_{L^\alpha(S;L^\alpha(\Omega))} + \|v_0\|^2_{L^2(S;L^2(\Omega))}\right).\end{aligned} \tag{5.65}$$

Combining (5.54) and (5.62), we obtain

$$\begin{aligned}\int_\Omega |(u^\lambda)_t|^2 dx + \int_\Omega |v_t|^2 dx \le C\Big[1 + (1 + \|u\|^\alpha_{L^\alpha(\Omega)})^\beta + \|v\|^2_{L^2(\Omega)} + \int_{\Gamma^R} |\varphi_t|^{\frac{\alpha}{\alpha-\lambda-1}} d\sigma\Big] \\ + \frac{\hat{c}^2}{C_2}|\Omega| + \frac{\hat{c}^2}{2C_2} e^{C_3 t}\left(1 + \|u_0\|^\alpha_{L^\alpha(\Omega)} + \|v_0\|^2_{L^2(\Omega)}\right).\end{aligned} \tag{5.66}$$

This completes the proof of the theorem. □

5.5 Proof of Theorem 5.11

Proof. By using Schauder's fixed point argument (see e.g. Theorem 5.5), we show that there exist a pair (u,v) of weak solutions to problem (2.4) in the sense of Definition 5.10. First of all, let us define the operators:

$$\mathcal{T}_1 : L^2(S; L^\alpha(\Omega) \cap W^{1,2-a}(\Omega)) \longrightarrow L^2(S; L^2(\Omega))$$

by $\mathcal{T}_1(u) = v$ and

$$\mathcal{T}_2 : L^2(S; L^2(\Omega)) \longrightarrow L^\alpha(S; L^\alpha(\Omega) \cap W^{1,2-a}(\Omega))$$

by $\mathcal{T}_2(v) = w$. Then, consider the operator $\mathcal{T} : L^\alpha(S; L^\alpha(\Omega)) \longrightarrow L^\alpha(S; L^\alpha(\Omega) \cap W^{1,2-a}(\Omega))$ defined by

$$\mathcal{T}(w) = \mathcal{T}_2(\mathcal{T}_1(u)) = w. \tag{5.67}$$

Indeed, the estimates reported in Proposition 5.15 and Proposition 5.4.2 imply that the operators $\mathcal{T}_1$ and $\mathcal{T}_2$ are well-defined. Hence, the operator $\mathcal{T}$ is also well-defined.

In order to show the existence of solution to the problem (2.4), we wish to show that $\mathcal{T}$ admits a fixed point. Then, using Schauder's fixed point Theorem 5.5, we shall prove that there exits a set B such that

(1) $\mathcal{T} : B \to B$ is a compact operator;

(2) B is convex, closed, bounded set such that $\mathcal{T}(B) \subset B$.

In particular, to obtain the compactness of $\mathcal{T} = \mathcal{T}_2 \circ \mathcal{T}_1$, it is sufficient to demonstrate that $\mathcal{T}_1$ is compact and that $\mathcal{T}_2$ is continuous.

Recall that we have

$$\mathcal{T}_1 : L^2(S; L^\alpha(\Omega) \cap W^{1,2-a}(\Omega)) \longrightarrow L^2(S; L^2(\Omega)).$$

We assume in Proposition 5.15 that for given $u \in L^\alpha(S; L^\alpha(\Omega))$, we obtain $\mathcal{T}_1(u) = v \in L^2(S; W^{1,2}(\Omega))$ with $v_t \in L^2(S; L^2(\Omega))$. Hence,

$$\mathcal{T}_1(L^2(S; L^\alpha(\Omega) \cap L^2(\Omega))) \subset V,$$

where

$$V = \{\varphi : \varphi \in L^2(S; L^\alpha(\Omega) \cap W^{1,2-a}(\Omega)), \partial_t \varphi \in L^2(S; L^2(\Omega))\}.$$

By using Rellich-Kondrachov's Theorem (Theorem 5.3), we obtain

$$L^\alpha(\Omega) \cap W^{1,2-a}(\Omega) \hookrightarrow\hookrightarrow L^2(\Omega).$$

Applying Theorem 5.4 gives $V \hookrightarrow\hookrightarrow L^2(S; L^2(\Omega))$. Thus, for any bounded set $M \subset L^2(S; L^2(\Omega))$, then we have $\mathcal{T}_1(M) \subset V$. Since V is compactly embedded in $L^2(S; L^2(\Omega))$, then we have $\mathcal{T}_1(M)$ is precompact in $L^2(S; L^2(\Omega))$. Therefore, $\mathcal{T}_1$ is a compact operator.

Now, we prove that $\mathcal{T}_2$ is sequentially continuous. We proceed in a similar manner as in [AC10]. We recall first that

$$\mathcal{T}_2 : L^2(S; L^2(\Omega)) \longrightarrow L^\alpha(S; L^\alpha(\Omega) \cap W^{1,2-a}(\Omega)).$$

Let $v_n \longrightarrow v$ in $L^2(S; L^2(\Omega))$ as $n \longrightarrow \infty$ and with $u_n = \mathcal{T}(v_n)$ and $u = \mathcal{T}(v)$. We show that $u_n \longrightarrow u$ in $L^\alpha(S; L^\alpha(\Omega))$ as $n \longrightarrow \infty$.

We denote

$$E := \{\varphi : \varphi \in L^\alpha(S; L^\alpha(\Omega)) \cap L^{2-a}(S; W^{1,2-a}(\Omega))\}.$$

Since $L^\alpha(\Omega)$ and $W^{1,2-a}(\Omega)$ are reflexive Banach spaces, then also the Bochner spaces $L^\alpha(S; L^\alpha(\Omega))$ and $L^{2-a}(S; W^{1,2-a}(\Omega))$ are reflexive Banach spaces. Thus, E is a reflexive Banach space. We know that from a bounded sequence in a reflexive Banach space E, one can extract a subsequence that converges weakly in E in the weak topology (cf. Theorem 3.18, [Bre11]). Indeed, since we have (u_n) is bounded in E and $v_n \longrightarrow v$ as $n \to \infty$ in $L^2(S; L^2(\Omega))$, then we have $u_n \rightharpoonup u$ as $n \to \infty$ in E.

By the estimates (5.27), (5.44) and (5.45), we can extract two subsequences (u_{n_k}) and (v_{n_k}), still labeled by n instead of n_k for simplicity, such that as $n \to \infty$ it holds:

$$\begin{aligned}
\nabla v_n &\rightharpoonup \nabla v \text{ in } L^2(S; L^2(\Omega)),\\
(v_n)_t &\rightharpoonup v_t \text{ in } L^2(S; L^2(\Omega)),\\
u_n &\rightharpoonup u \text{ in } E,\\
(u_n^\lambda)_t &\rightharpoonup (u^\lambda)_t \text{ in } L^2(S; L^2(\Omega)),\\
\nabla u_n &\rightharpoonup \nabla u \text{ in } L^2(S; W^{1,2-a}(\Omega)).
\end{aligned}$$

Then, by using (A_1) and (A_2) and the fact that $b(u_n - v_n)$ and $K_1(|\nabla u_n|)|\nabla u_n|^2$ are bounded in E, it leads to

$$\begin{aligned}
b(u_n - v_n) &\rightharpoonup b(u - v) \text{ in } E,\\
K_1(|\nabla u_n|)|\nabla u_n|^2 &\rightharpoonup K_1(|\nabla u|)|\nabla u|^2 \text{ in } E.
\end{aligned}$$

We re-write (2.4) formulated for the sequences $(u_n) \in L^\alpha(S; L^\alpha(\Omega))$ and $(v_n) \in L^2(S; L^2(\Omega))$

$$\begin{cases}
\partial_t(u_n^\lambda) + \operatorname{div}(-K_1(|\nabla u_n|)\nabla u_n) = -b(u_n - v_n) \ \text{ in } S \times \Omega,\\
\partial_t v_n - K_2 \Delta v_n = b(u_n - v_n) \ \text{ in } S \times \Omega,\\
-K_1(|\nabla u_n|)\nabla u_n \cdot \mathbf{n} = \varphi u_n^\lambda \ \text{ at } S \times \Gamma^R,\\
-K_1(|\nabla u_n|)\nabla u_n \cdot \mathbf{n} = 0 \ \text{ at } S \times \Gamma^N,\\
-K_2 \nabla v_n \cdot \mathbf{n} = 0 \ \text{ at } S \times \partial\Omega,\\
u_n(t = 0, x) = u_{0_n}(x), \ x \in \bar{\Omega},\\
v_n(t = 0, x) = v_{0_n}(x), \ x \in \bar{\Omega}.
\end{cases} \tag{5.68}$$

Clearly, if $n \longrightarrow \infty$ in the weak form of (5.68) recovers the weak form of (2.4). Essentially, we have shown that $u_n \rightharpoonup u$ in E. Moreover, the embedding $E \hookrightarrow L^\alpha(S; L^\alpha(\Omega))$ is compact, this implies that $u_n \longrightarrow u$ in $L^\alpha(S; L^\alpha(\Omega))$. Therefore, $\mathcal{T}_2$ is continuous.

Let us fix $K > 0$ to be specified later and we denote by B_K the collection of functions $u \in L^\alpha(S; L^\alpha(\Omega) \cap W^{1,2-a}(\Omega))$ such that

$$\max\{\|u\|_{L^\alpha(S;L^\alpha(\Omega))}, \|\nabla u\|_{L^{2-a}(S;L^{2-a}(\Omega))}\} \le K.$$

For each choice of K, the set

$$B_K \subset L^\alpha(S; L^\alpha(\Omega) \cap W^{1,2-a}(\Omega))$$

is convex, closed, and bounded. We aim to show that we may select a $K > 0$ such that

$$\mathcal{T}(B_K) \subset B_K.$$

Indeed, by using the estimates (5.27), (5.44) as well as the fact that

$$L^2(S; L^\alpha(\Omega) \cap W^{1,2-a}(\Omega)) \subset \left(L^\alpha(S; L^\alpha(\Omega)) \cap L^{2-a}(S; W^{1,2-a}(\Omega))\right)$$

together with knowing that $\mathcal{T}_1(B_K)$ is bounded subset of $L^2(S; L^2(\Omega))$ and that $\mathcal{T}_2(\mathcal{T}_1(u))$ is a bounded subset of $L^\alpha(S; L^\alpha(\Omega) \cap W^{1,2-a}(\Omega))$, we have

$$\max\{\|u\|_{L^\alpha(S;L^\alpha(\Omega))}, \|\nabla u\|_{L^{2-a}(S;L^{2-a}(\Omega))}\} \leq K.$$

Here $K > 0$ is chosen such that

$$\begin{aligned} K := \max\Big\{ & e^{C_3 T}\left(1 + \|u_0\|^\alpha_{L^\alpha(0,T;L^\alpha(\Omega))} + \|v_0\|^2_{L^2(0,T;L^2(\Omega))}\right), \\ & C(\hat{c}, \lambda, a)\Big[\Lambda(0) + \int_0^t (1 + \|u\|^\alpha_{L^\alpha(\Omega)})^\beta ds \\ & + \int_0^t \|v\|^2_{L^2(\Omega)} ds + \int_0^t \int_{\Gamma^R} |\varphi_t|^{\frac{\alpha}{\alpha-\lambda-1}} d\sigma ds\Big] + \int_\Omega |\nabla v_0|^2 dx \\ & + \frac{\hat{c}^2}{C_2}|\Omega| t + \frac{\hat{c}^2}{2C_2} e^{C_3 t}\left(1 + \|u_0\|^\alpha_{L^\alpha(0,T;L^\alpha(\Omega))} + \|v_0\|^2_{L^2(0,T;L^2(\Omega))}\right)\Big\}. \end{aligned} \tag{5.69}$$

Hence, $\mathcal{T}(B_K) \subset B_K$.

We have shown that $\mathcal{T} : B_k \longrightarrow B_k$ is a compact operator with B_K a convex, closed, bounded set and also that $\mathcal{T}(B_K) \subset B_K$. Then, by Theorem 5.5 there exists at least a pair

$$(u, v) \in \left(L^\alpha(S; L^\alpha(\Omega)) \cap L^{2-a}(S; W^{1,2-a}(\Omega))\right) \times L^2(S; W^{1,2}(\Omega))$$

satisfying the problem (2.4) in the sense of Definition 5.10. □

5.6 Proof of Theorem 5.12

Proof. To prove the uniqueness of solutions in the sense of Definition 5.10, we adapt the arguments by E. Aulisa et. al (cf. Section IV, [ABHI09]) to our setting. Essentially, we are using the monotonicity properties of the term $K_1(y)y$ as stated in Proposition 5.7 and Proposition 5.9.

Let $(u_i, v_i), i \in \{1, 2\}$ be two arbitrary weak solutions to problem (2.4) in the sense of Definition 5.10, where the initial data is take $u_i(t = 0, x) = u_{i0}(x)$ and

$v_i(t=0,x) = v_{i0}(x)$ for all $x \in \bar{\Omega}$. We denote $w = u_1 - u_2$ and $z = v_1 - v_2$. If we substitute the pair (w, z) into (5.22)-(5.23), we obtain

$$\int_\Omega \partial_t(u_1^\lambda - u_2^\lambda)\psi dx + \int_\Omega \partial_t z\phi dx + \int_\Omega \left(K_1(|\nabla u_1|)\nabla u_1 - K_1(|\nabla u_2|)\nabla u_2\right)\nabla\psi dx +$$
$$+K_2\int_\Omega \nabla z\nabla\phi dx = -\int_{\Gamma^R}\varphi(u_1^\lambda - u_2^\lambda)\psi d\gamma - \int_\Omega (b(u_1 - v_1) - b(u_2 - v_2))(\psi - \phi)dx \tag{5.70}$$

Now, choosing the test function

$$(\psi, \phi) := (|w|^{\alpha+\delta-1}, z) \in \left(\left(L^\alpha(\Omega) \cap W^{1,2-a}(\Omega)\right) \times W^{1,2}(\Omega)\right)$$

leads to

$$\frac{\lambda}{\alpha}\frac{d}{dt}\int_\Omega |w|^\alpha dx + \frac{1}{2}\frac{d}{dt}\int_\Omega z^2 dx +$$
$$\int_\Omega \Big(K_1(|\nabla u_1|)\nabla u_1 - K_1(|\nabla u_2|)\nabla u_2\Big)\nabla w|w|^{\alpha+\delta-2}dx + K_2\int_\Omega |\nabla z|^2 dx$$
$$+\int_{\Gamma^R}\varphi(u_1^\lambda - u_2^\lambda)|w|^{\alpha+\delta-1}d\gamma = -\int_\Omega (b(u_1 - v_1) - b(u_2 - v_2))(|w|^{\alpha+\delta-1} - z)dx. \tag{5.71}$$

Using assumption (A_3) to handle the right hand side of (5.71), we have the following estimate

$$\begin{aligned}
&\frac{\lambda}{\alpha}\frac{d}{dt}\int_\Omega |w|^\alpha dx + \frac{1}{2}\frac{d}{dt}\int_\Omega z^2 dx + \int_\Omega \Phi(\nabla u_1, \nabla u_2)|w|^{\alpha+\delta-2}dx \\
&+ K_2\int_\Omega |\nabla z|^2 dx + \int_{\Gamma^R}|\varphi||u_1^\lambda - u_2^\lambda||w|^{\alpha+\delta-1}d\gamma \\
&\le \left|\int_\Omega (b(u_1 - v_1) - b(u_2 - v_2))(|w|^{\alpha+\delta-1} - z)dx\right| \\
&\le \left|\int_\Omega (|u_1 - u_2| + |v_1 - v_2|)(|w|^{\alpha+\delta-1} - z)dx\right| \\
&\le \left|\int_\Omega |w|^{\alpha+\delta}dx - \int_\Omega |w||z|dx - \int_\Omega |v_1 - v_2||w|^{\alpha+\delta-1}dx + \int_\Omega z^2 dx\right| \\
&\le \int_\Omega |w|^{\alpha+\delta}dx + \frac{1}{2}\int_\Omega |w|^{2(\alpha+\delta-1)}dx + \frac{1}{2}\int_\Omega |w|^2 dx + C\int_\Omega z^2 dx.
\end{aligned} \tag{5.72}$$

Since $\Phi(\nabla u_1, \nabla u_2) \ge 0$, (5.72) becomes

$$\begin{aligned}
\frac{\lambda}{\alpha}\frac{d}{dt}\int_\Omega |w|^\alpha dx + \frac{1}{2}\frac{d}{dt}\int_\Omega z^2 dx \le \int_\Omega |w|^{\alpha+\delta}dx + \frac{1}{2}\int_\Omega |w|^{2(\alpha+\delta-1)}dx \\
+ C\int_\Omega |w|^2 dx + C\int_\Omega |z|^2 dx.
\end{aligned} \tag{5.73}$$

We set $\delta = 0$ and use the inequality (5.5) to rewrite (5.73) as

$$\frac{d}{dt}\left(\int_\Omega |w|^\alpha dx + \int_\Omega z^2 dx\right) \leq C(\alpha,\lambda) + C(\alpha,\lambda)\left(\int_\Omega |w|^\alpha dx + \int_\Omega z^2 dx\right). \quad (5.74)$$

It is convenient to introduce the notation:

$$W(t) := \int_\Omega |w|^\alpha dx + \int_\Omega |z|^2 dx \text{ for } t \in S.$$

Hence, the inequality (5.74) becomes

$$\frac{d}{dt}W(t) \leq C(\alpha,\lambda)W(t), \quad (5.75)$$

for $t \in S$ with $W(0) = \int_\Omega |w_0|^\alpha dx + \int_\Omega |z_0|^2 dx$, where $w_0 := u_{01} - u_{02}$ and $z_0 := v_{01} - v_{02}$. Here we consider $u_{01}, u_{02} \in L^\alpha(\Omega)$ and $v_{01}, v_{02} \in L^2(\Omega)$.
By using Gronwall's inequality, (5.75) yields

$$W(t) \leq W(0)e^{tC(\alpha,\lambda)} \text{ for all } t \in S. \quad (5.76)$$

This also implies

$$\int_\Omega |w|^\alpha dx + \int_\Omega |z|^2 dx \leq (\|w_0\|^\alpha_{L^\alpha(\Omega)} + \|z_0\|^2_{L^2(\Omega)})e^{tC(\alpha,\lambda)}. \quad (5.77)$$

Clearly, if $w_0 = z_0 = 0$, then the weak solution of (2.4) is unique. □

5.7 Proof of Theorem 5.13

Proof. Let us recall the weak formulation corresponding to the different choices of data: $(u_{0i}, v_{0i}, D_i, \varphi_i), i \in \{1,2\}$. We denote $D = D_1 - D_2$, $\tilde{\varphi} = \varphi_1 - \varphi_2$, $\tilde{r} = r_1 - r_2$, $\tilde{u}_0 = u_{01} - u_{02}$ and $\tilde{v}_0 = v_{01} - v_{02}$. We denote also $w := u_1 - u_2$ and $z := v_1 - v_2$. Multiplying the first and the second equations of (2.4) with $\psi := |w|^{\alpha+\delta-1}, \phi := z$, respectively and interating the result by parts over Ω together with combining the two equations, one gets

$$\begin{aligned}
&\int_\Omega \partial_t(u_1^\lambda - u_2^\lambda)\psi dx + \int_\Omega \partial_t(v_1 - v_2)\phi dx + \int_\Omega \Big(K_1(|\nabla u_1|)\nabla u_1 \\
&- K_1(|\nabla u_2|)\nabla u_2\Big)\nabla\psi dx + \int_\Omega (D_1\nabla v_1 - D_2\nabla v_2)\nabla\phi dx + \int_{\Gamma^R}\left(\varphi_1 u_1^\lambda - \varphi_2 u_2^\lambda\right)\psi d\gamma \\
&= -\int_\Omega [r_1 B(u_1 - v_1)(\psi - \phi) - r_2 B(u_2 - v_2)(\psi - \phi)]\, dx, \quad (5.78)
\end{aligned}$$

Regarding (5.78), note that

$$\int_\Omega (D_1\nabla v_1 - D_2\nabla v_2)\nabla\phi dx = D_1\|\nabla\phi\|^2_{L^2(\Omega)} + (D_1 - D_2)\int_\Omega \nabla v_2\nabla\phi dx, \quad (5.79)$$

$$\int_{\Gamma^R}\left(\varphi_1 u_1^\lambda-\varphi_2 u_2^\lambda\right)\psi d\gamma=\int_{\Gamma^R}\varphi_1(u_1^\lambda-u_2^\lambda)\psi d\gamma+\int_{\Gamma^R}(\varphi_1-\varphi_2)u_2^\lambda\psi d\gamma \tag{5.80}$$

and

$$\begin{aligned}&\int_\Omega\left[r_1B(u_1-v_1)(\psi-\phi)-r_2B(u_2-v_2)(\psi-\phi)\right]dx\\&=\int_\Omega r_1\left(B(u_1-v_1)-B(u_2-v_2)\right)(\psi-\phi)dx+(r_1-r_2)\int_\Omega B(u_2-v_2)(\psi-\phi)dx.\end{aligned} \tag{5.81}$$

Using now (5.79), (5.81), as well as Young's inequality applied to the last terms of (5.79), (5.80) together with the assumption (A_2) and (A_3), we use that (5.78) becomes

$$\begin{aligned}&\frac{\lambda}{\alpha}\frac{d}{dt}\int_\Omega|u_1-u_2|^\alpha dx+\frac{1}{2}\frac{d}{dt}\int_\Omega\phi^2dx+\int_\Omega\Phi(\nabla u_1,\nabla u_2)|u_1-u_2|^{\alpha+\delta-2}dx+\\&+D_1\int_\Omega|\nabla\phi|^2dx+\int_{\Gamma^R}\varphi_1|u_1^\lambda-u_2^\lambda|\psi d\gamma\le C\varepsilon_1\int_\Omega|\nabla\phi|^2dx+\\&+C|D_1-D_2|\int_\Omega|\nabla v_2|^2dx-\frac{1}{2}\int_{\Gamma^R}|\varphi_1-\varphi_2|^2|u_2|^{2\lambda}d\gamma\\&-\frac{1}{2}\int_{\Gamma^R}|u_1-u_2|^{2(\alpha+\delta-1)}d\gamma+\int_\Omega r_1(|u_1-u_2|+|v_1-v_2|)(\psi-\phi)dx\\&+|r_1-r_2|\frac{\hat{c}}{\bar{r}}\int_\Omega|u_2-v_2|^\sigma(\psi-\phi)dx.\end{aligned} \tag{5.82}$$

Using the inequality (5.3), (5.82) receives the form

$$\begin{aligned}&\frac{\lambda}{\alpha}\frac{d}{dt}\int_\Omega|u_1-u_2|^\alpha dx+\frac{1}{2}\frac{d}{dt}\int_\Omega\phi^2dx+\int_\Omega\Phi(\nabla u_1,\nabla u_2)|u_1-u_2|^{\alpha+\delta-2}dx+\\&+D_1\int_\Omega|\nabla\phi|^2dx+\int_{\Gamma^R}\varphi_1|u_1^\lambda-u_2^\lambda|\psi d\gamma\le C\varepsilon_1\int_\Omega|\nabla\phi|^2dx+\\&+C|D_1-D_2|\int_\Omega|\nabla v_2|^2dx-\frac{1}{2}\int_{\Gamma^R}|\varphi_1-\varphi_2|^2|u_2|^{2\lambda}d\gamma\\&-\frac{1}{2}\int_{\Gamma^R}|u_1-u_2|^{2(\alpha+\delta-1)}d\gamma+\int_\Omega r_1|u_1-u_2|\psi dx-\int_\Omega r_1|u_1-u_2|\phi dx+\\&\int_\Omega r_1|v_1-v_2|\psi dx-\int_\Omega r_1|v_1-v_2|\psi dx+|r_1-r_2|\frac{\hat{c}}{\bar{r}}\int_\Omega(|u_2|^\sigma+|v_2|^\sigma)(\psi-\phi)dx.\end{aligned} \tag{5.83}$$

Applying the trace inequality (5.8) together with Cauchy-Schwarz's inequality, we obtain the following estimate

$$\begin{aligned}
&\frac{\lambda}{\alpha}\frac{d}{dt}\int_\Omega |u_1-u_2|^\alpha dx + \frac{1}{2}\frac{d}{dt}\int_\Omega \phi^2 dx + \int_\Omega \Phi(\nabla u_1,\nabla u_2)|u_1-u_2|^{\alpha+\delta-2}dx\\
&+ D_1\int_\Omega |\nabla\phi|^2dx + \int_{\Gamma^R}\varphi_1|u_1^\lambda - u_2^\lambda|\psi d\gamma \le C\varepsilon_1\int_\Omega |\nabla\phi|^2dx +\\
&+ C|D_1-D_2|\int_\Omega |\nabla v_2|^2dx - \frac{1}{2}\int_{\Gamma^R}|\varphi_1-\varphi_2|^2|u_2|^{2\lambda}d\gamma\\
&- \frac{1}{2}\Big(2\varepsilon_2\int_\Omega |\nabla u_1-\nabla u_2|^{2-a}|u_1-u_2|^{\alpha+\delta-2}dx + C\int_\Omega |u_1-u_2|^\alpha dx\\
&+ C\int_\Omega |u_1-u_2|^{\alpha+\mu_0}dx + C\int_\Omega |u_1-u_2|^{\alpha+\mu_1}dx\Big)\\
&+ r_1\int_\Omega |u_1-u_2|^{\alpha+\delta}dx - \frac{r_1}{2}\int_\Omega |u_1-u_2|^2dx - \frac{r_1}{2}\int_\Omega |v_1-v_2|^2dx\\
&+ \frac{r_1}{2}\int_\Omega |v_1-v_2|^2dx + \frac{r_1}{2}\int_\Omega |u_1-u_2|^{2(\alpha+\delta-1)}dx - r_1\int_\Omega |v_1-v_2|^2dx\\
&+ |r_1-r_2|\frac{\hat{c}}{2\bar{r}}\int_\Omega |u_2|^{2\sigma}dx + |r_1-r_2|\frac{\hat{c}}{2\bar{r}}\int_\Omega |u_1-u_2|^{2(\alpha+\delta-1)}dx\\
&- |r_1-r_2|\frac{\hat{c}}{2\bar{r}}\int_\Omega |u_2|^{2\sigma}dx - |r_1-r_2|\frac{\hat{c}}{2\bar{r}}\int_\Omega |v_1-v_2|^2dx\\
&+ |r_1-r_2|\frac{\hat{c}}{2\bar{r}}\int_\Omega |v_2|^{2\sigma}dx + |r_1-r_2|\frac{\hat{c}}{2\bar{r}}\int_\Omega |u_1-u_2|^{2(\alpha+\delta-1)}dx\\
&- |r_1-r_2|\frac{\hat{c}}{2\bar{r}}\int_\Omega |v_2|^{2\sigma}dx - |r_1-r_2|\frac{\hat{c}}{2\bar{r}}\int_\Omega |v_1-v_2|^2dx. \qquad (5.84)
\end{aligned}$$

Choosing $\varepsilon_1 = \frac{D_1}{C}$ and $\varepsilon_2 = 1$, we have

$$\begin{aligned}
&\frac{\lambda}{\alpha}\frac{d}{dt}\int_\Omega |u_1-u_2|^\alpha dx + \frac{1}{2}\frac{d}{dt}\int_\Omega \phi^2 dx \le C|D_1-D_2|\int_\Omega |\nabla v_2|^2dx -\\
&\frac{1}{2}\int_{\Gamma^R}|\varphi_1-\varphi_2|^2|u_2|^{2\lambda}d\gamma + r_1\int_\Omega |u_1-u_2|^{\alpha+\delta}dx - \frac{r_1}{2}\int_\Omega |u_1-u_2|^2dx\\
&+\frac{r_1}{2}\int_\Omega |u_1-u_2|^{2(\alpha+\delta-1)}dx - r_1\int_\Omega |v_1-v_2|^2dx\\
&+|r_1-r_2|\frac{\hat{c}}{\bar{r}}\int_\Omega |u_1-u_2|^{2(\alpha+\delta-1)}dx - |r_1-r_2|\frac{\hat{c}}{\bar{r}}\int_\Omega |v_1-v_2|^2dx. \qquad (5.85)
\end{aligned}$$

Moreover, if we assume that $\delta = 0$, then the maximum allowed power of $\|w\|$ is α. As next step, we use the inequality (5.6) together with the energy estimates (5.27), (5.44) to deal with the terms $\int_\Omega |u_2|^\alpha dx$, $\int_\Omega |v_2|^2dx$ and $\int_\Omega |\nabla u_2|^2dx$. Furthermore,

we use also the trace inequality (5.8). It yields

$$\frac{d}{dt}\Big(\int_\Omega |u_1-u_2|^\alpha dx+\int_\Omega |v_1-v_2|^2dx\Big)\le C(\alpha,\lambda,\hat{c},\bar{r})(|D_1-D_2|+|r_1-r_2|$$
$$-\|\varphi_1-\varphi_2\|^2_{L^\infty(\Gamma^R)})+C(\alpha,\lambda,\hat{c},\bar{r})|r_1-r_2|\left(|u_1-u_2\|^\alpha_{L^\alpha(\Omega)}+\|v_1-v_2\|^2_{L^2(\Omega)}\right). \tag{5.86}$$

Denoting

$$Z(t):=\int_\Omega |u_1-u_2|^\alpha dx+\int_\Omega |v_1-v_2|^2dx \text{ for any } t\in S, \tag{5.87}$$

The expansion (5.86) can be rewritten as follows

$$\frac{d}{dt}Z(t)\le C(\alpha,\lambda,\hat{c},\bar{r})(|D_1-D_2|+|r_1-r_2|-\|\varphi_1-\varphi_2\|^2_{L^\infty(\Gamma^R)})$$
$$+C(\alpha,\lambda,\hat{c},\bar{r})|r_1-r_2|Z(t), \tag{5.88}$$

for $t\in S$. It holds $Z(0)=\int_\Omega |u_{01}-u_{02}|^\alpha dx+\int_\Omega |v_{01}-v_{02}|^2dx$.
Appying the Grönwall's inequality to (5.87), we obtain

$$Z(t)\le e^{\int_0^t C(\alpha,\lambda,\hat{c},\bar{r})|r_1-r_2|ds}\Big[Z(0)+\int_0^t C(\alpha,\lambda,\hat{c},\bar{r})(|D_1-D_2|+|r_1-r_2|$$
$$-\|\varphi_1-\varphi_2\|^2_{L^\infty(\Gamma^R)})ds\Big]. \tag{5.89}$$

(5.89) implies

$$\|u_1-u_2\|^\alpha_{L^\alpha(\Omega)}+\|v_1-v_2\|^2_{L^2(\Omega)}\le e^{C(\alpha,\lambda,\hat{c},\bar{r})|r_1-r_2|t}\Big[\|u_{01}-u_{02}\|^\alpha_{L^\alpha(\Omega)}$$
$$+\|v_{01}-v_{02}\|^2_{L^2(\Omega)}+Ct(|D_1-D_2|+|r_1-r_2|-\|\varphi_1-\varphi_2\|^2_{L^\infty(\Gamma^R)})\Big], \tag{5.90}$$

which is precisely the kind of stability estimate with respect to data and parameters we are looking for. □

5.8 Proof of Theorem 5.14

Proof. We keep the same notations as in Theorem 5.13. Multiplying the first and the second equation of (2.4) with $\psi:=(u_1-u_2)_t$ and $\phi:=(v_1-v_2)_t$, respectively. Integrating the results by parts over Ω and combining the two equations, we obtain

$$\int_\Omega \partial_t(u_1^\lambda-u_2^\lambda)\psi dx+\int_\Omega \partial_t(v_1-v_2)\phi dx+\int_\Omega \Big(K_1(|\nabla u_1|)\nabla u_1$$
$$-K_1(|\nabla u_2|)\nabla u_2\Big)\nabla\psi dx+\int_\Omega (D_1\nabla v_1-D_2\nabla v_2)\nabla\phi dx$$
$$+\int_{\Gamma^R}\varphi\left(u_1^\lambda-u_2^\lambda\right)\psi d\gamma=-\int_\Omega\Big[r_1B(u_1-v_1)(\psi-\phi)$$
$$-r_2B(u_2-v_2)(\psi-\phi)\Big]dx. \tag{5.91}$$

Note that

$$\int_\Omega (D_1\nabla v_1 - D_2\nabla v_2)\nabla\phi dx = \int_\Omega D_1\nabla(v_1 - v_2)\nabla\phi dx + \int_\Omega (D_1 - D_2)\nabla v_2\nabla\phi dx$$
$$= \frac{1}{2}\frac{d}{dt}\int_\Omega D_1|\nabla(v_1 - v_2)|^2 dx + \int_\Omega (D_1 - D_2)\nabla v_2\nabla\phi dx, \tag{5.92}$$

$$\int_{\Gamma^R} (\varphi_1 u_1^\lambda - \varphi_2 u_2^\lambda)\psi d\gamma = \int_{\Gamma^R} \varphi_1(u_1^\lambda - u_2^\lambda)\psi d\gamma + \int_{\Gamma^R} (\varphi_1 - \varphi_2)u_2^\lambda\psi d\gamma \tag{5.93}$$

and

$$\int_\Omega \left[r_1 B(u_1 - v_1)(\psi - \phi) - r_2 B(u_2 - v_2)(\psi - \phi)\right] dx =$$
$$\int_\Omega r_1(B(u_1 - v_1) - B(u_2 - v_2))(\psi - \phi)dx + (r_1 - r_2)\int_\Omega B(u_2 - v_2)(\psi - \phi)dx. \tag{5.94}$$

Then, (5.91) becomes

$$\frac{d}{dt}\int_\Omega (u_1 - u_2)^2 dx + \int_\Omega (K_1(|\nabla u_1|)\nabla u_1 - K_1(|\nabla u_2|)\nabla u_2)\cdot\frac{\partial}{\partial t}(\nabla u_1 - \nabla u_2)dx$$
$$+\frac{1}{2}\frac{d}{dt}\int_\Omega |v_1 - v_2|^2 dx + \int_\Omega (D_1\nabla v_1 - D_2\nabla v_2)\nabla\phi dx + \int_{\Gamma^R} (\varphi_1 u_1^\lambda - \varphi_2 u_2^\lambda)\psi d\gamma$$
$$= \int_\Omega \left[r_1 B(u_1 - v_1)(\psi - \phi) - r_2 B(u_2 - v_2)(\psi - \phi)\right] dx$$
$$+(r_1 - r_2)\int_\Omega B(u_2 - v_2)(\psi - \phi)dx. \tag{5.95}$$

Using (5.92)-(5.94), as a result of applying the Young's inequality to the last terms of the right hand side of (5.92) and (5.93), we have

$$
\begin{aligned}
&\frac{d}{dt}\int_\Omega (u_1-u_2)^2dx + \int_\Omega K_1(|\nabla u_1|)\nabla u_1\cdot\frac{\partial}{\partial t}(\nabla u_1)dx + \int_\Omega K_1(|\nabla u_2|)\nabla u_2\cdot\frac{\partial}{\partial t}(\nabla u_2)dx\\
&-\int_\Omega K_1(|\nabla u_1|)\nabla u_1\cdot\frac{\partial}{\partial t}(\nabla u_2)dx - \int_\Omega K_1(|\nabla u_2|)\nabla u_2\cdot\frac{\partial}{\partial t}(\nabla u_1)dx\\
&+\frac{1}{2}\frac{d}{dt}\int_\Omega |v_1-v_2|^2dx + \frac{1}{2}\frac{d}{dt}\int_\Omega D_1|\nabla(v_1-v_2)|^2dx + \int_{\Gamma^R}\varphi_1|u_1^\lambda-u_2^\lambda|\psi d\gamma\\
&\le C\varepsilon_3\frac{d}{dt}\int_\Omega |\nabla v_1-\nabla v_2|^2dx + C|D_1-D_2|\int_\Omega |\nabla v_2|^2dx\\
&-\frac{1}{2}\|\varphi_1-\varphi_2\|^2_{L^\infty(\Gamma^R)}\int_{\Gamma^R}|u_2|^{2\lambda}d\gamma - \frac{1}{2}\frac{d}{dt}\int_{\Gamma^R}|u_1-u_2|^2d\gamma + \int_\Omega r_1B(u_1-v_1)\psi dx\\
&-\int_\Omega r_1B(u_1-v_1)\phi dx - \int_\Omega r_2B(u_2-v_2)\psi dx\\
&+\int_\Omega r_2B(u_2-v_2)\phi dx + |r_1-r_2|\int_\Omega B(u_2-v_2)\psi dx\\
&-|r_1-r_2|\int_\Omega B(u_2-v_2)\phi dx. \qquad (5.96)
\end{aligned}
$$

By the assumption (A_3), we are led to

$$
\begin{aligned}
&\frac{d}{dt}\int_\Omega (u_1-u_2)^2dx + \frac{d}{dt}\int_\Omega K_1(|\nabla u_1|)|\nabla u_1|^2dx + \frac{d}{dt}\int_\Omega K_1(|\nabla u_2|)|\nabla u_2|^2dx\\
&-\frac{d}{dt}\int_\Omega K_1(|\nabla u_1|)\nabla u_1\cdot\nabla u_2dx - \frac{d}{dt}\int_\Omega K_1(|\nabla u_2|)\nabla u_2\cdot\nabla u_1dx\\
&+\frac{1}{2}\frac{d}{dt}\int_\Omega |v_1-v_2|^2dx + \frac{1}{2}\frac{d}{dt}\int_\Omega D_1|\nabla(v_1-v_2)|^2dx + \int_{\Gamma^R}\varphi_1|u_1^\lambda-u_2^\lambda|\psi d\gamma\\
&\le C\varepsilon_3\frac{d}{dt}\int_\Omega |\nabla v_1-\nabla v_2|^2dx + C|D_1-D_2|\int_\Omega |\nabla v_2|^2dx\\
&-\frac{1}{2}\|\varphi_1-\varphi_2\|^2_{L^\infty(\Gamma^R)}\int_{\Gamma^R}|u_2|^{2\lambda}d\gamma - \frac{1}{2}\frac{d}{dt}\int_{\Gamma^R}|u_1-u_2|^2d\gamma\\
&+\int_\Omega r_1(B(u_1-v_1)-B(u_2-v_2))\psi dx + \int_\Omega r_1(B(u_1-v_1)-B(u_2-v_2))\phi dx\\
&+\frac{\hat{c}}{\bar{r}}|r_1-r_2|\int_\Omega |u_2-v_2|^\sigma\psi dx - \frac{\hat{c}}{\bar{r}}|r_1-r_2|\int_\Omega |u_2-v_2|^\sigma\phi dx \qquad (5.97)
\end{aligned}
$$

By using the assumption (A_2) together with (5.3), it leads to

$$\begin{aligned}
&\frac{d}{dt}\int_\Omega (u_1-u_2)^2dx+\frac{d}{dt}\int_\Omega K_1(|\nabla u_1|)|\nabla u_1|^2dx+\frac{d}{dt}\int_\Omega K_1(|\nabla u_2|)|\nabla u_2|^2dx\\
&-\frac{d}{dt}\int_\Omega K_1(|\nabla u_1|)\nabla u_1\cdot\nabla u_2dx-\frac{d}{dt}\int_\Omega K_1(|\nabla u_2|)\nabla u_2\cdot\nabla u_1dx\\
&+\frac{1}{2}\frac{d}{dt}\int_\Omega |v_1-v_2|^2dx+\frac{1}{2}\frac{d}{dt}\int_\Omega D_1|\nabla(v_1-v_2)|^2dx+\int_{\Gamma^R}\varphi_1|u_1^\lambda-u_2^\lambda|\psi d\gamma\\
&\le C\varepsilon_3\frac{d}{dt}\int_\Omega |\nabla v_1-\nabla v_2|^2dx+C|D_1-D_2|\int_\Omega |\nabla v_2|^2dx\\
&-\frac{1}{2}\|\varphi_1-\varphi_2\|^2_{L^\infty(\Gamma^R)}\int_{\Gamma^R}|u_2|^{2\lambda}d\gamma-\frac{1}{2}\frac{d}{dt}\int_{\Gamma^R}|u_1-u_2|^2d\gamma\\
&+\int_\Omega r_1|u_1-v_1-u_2+v_2|\psi dx+\int_\Omega r_1|u_1-v_1-u_2+v_2|\phi dx+\frac{\hat c}{\bar r}|r_1-r_2|\int_\Omega(|u_2|^\sigma\\
&+|v_2|^\sigma)\psi dx-\frac{\hat c}{\bar r}|r_1-r_2|\int_\Omega(|u_2|^\sigma+|v_2|^\sigma)\phi dx. \qquad (5.98)
\end{aligned}$$

Then, via Cauchy-Schwarz's inequality, we obtain the following estimate

$$\begin{aligned}
&\frac{d}{dt}\int_\Omega (u_1-u_2)^2dx+\frac{d}{dt}\int_\Omega K_1(|\nabla u_1|)|\nabla u_1|^2dx+\frac{d}{dt}\int_\Omega K_1(|\nabla u_2|)|\nabla u_2|^2dx\\
&-\frac{d}{dt}\int_\Omega K_1(|\nabla u_1|)\nabla u_1\cdot\nabla u_2dx-\frac{d}{dt}\int_\Omega K_1(|\nabla u_2|)\nabla u_2\cdot\nabla u_1dx\\
&+\frac{1}{2}\frac{d}{dt}\int_\Omega |v_1-v_2|^2dx+\frac{1}{2}\frac{d}{dt}\int_\Omega D_1|\nabla(v_1-v_2)|^2dx+\int_{\Gamma^R}\varphi_1|u_1^\lambda-u_2^\lambda|\psi d\gamma\\
&\le C\varepsilon_3\frac{d}{dt}\int_\Omega |\nabla v_1-\nabla v_2|^2dx+C|D_1-D_2|\int_\Omega |\nabla v_2|^2dx\\
&-\frac{1}{2}\|\varphi_1-\varphi_2\|^2_{L^\infty(\Gamma^R)}\int_{\Gamma^R}|u_2|^{2\lambda}d\gamma-\frac{1}{2}\frac{d}{dt}\int_{\Gamma^R}|u_1-u_2|^2d\gamma\\
&+r_1\int_\Omega |u_1-u_2|\psi dx+r_1\int_\Omega |v_1-v_2|\psi dx+r_1\int_\Omega |u_1-u_2|\phi dx+r_1\int_\Omega |v_1-v_2|\phi dx\\
&+\frac{\hat c}{2\bar r}|r_1-r_2|\int_\Omega |u_2|^{2\sigma}dx+\frac{\hat c}{4\bar r}|r_1-r_2|\frac{d}{dt}\int_\Omega |u_1-u_2|^2dx\\
&+\frac{\hat c}{2\bar r}|r_1-r_2|\int_\Omega |v_2|^{2\sigma}dx+\frac{\hat c}{4\bar r}|r_1-r_2|\frac{d}{dt}\int_\Omega |u_1-u_2|^2dx\\
&-\frac{\hat c}{2\bar r}|r_1-r_2|\int_\Omega |u_2|^{2\sigma}dx-\frac{\hat c}{4\bar r}|r_1-r_2|\frac{d}{dt}\int_\Omega |v_1-v_2|^2dx\\
&-\frac{\hat c}{2\bar r}|r_1-r_2|\int_\Omega |v_2|^{2\sigma}dx-\frac{\hat c}{4\bar r}|r_1-r_2|\frac{d}{dt}\int_\Omega |v_1-v_2|^2dx. \qquad (5.99)
\end{aligned}$$

In other words, (5.98) can be written as follow

$$\begin{aligned}
&\frac{d}{dt}\int_\Omega (u_1-u_2)^2dx+\frac{d}{dt}\int_\Omega K_1(|\nabla u_1|)|\nabla u_1|^2dx+\frac{d}{dt}\int_\Omega K_1(|\nabla u_2|)|\nabla u_2|^2dx\\
&-\frac{d}{dt}\int_\Omega K_1(|\nabla u_1|)\nabla u_1\cdot\nabla u_2dx-\frac{d}{dt}\int_\Omega K_1(|\nabla u_2|)\nabla u_2\cdot\nabla u_1dx\\
&+\frac{1}{2}\frac{d}{dt}\int_\Omega |v_1-v_2|^2dx+\frac{1}{2}\frac{d}{dt}\int_\Omega D_1|\nabla(v_1-v_2)|^2dx+\int_{\Gamma^R}\varphi_1|u_1^\lambda-u_2^\lambda|\psi d\gamma\\
&\le C\varepsilon_3\frac{d}{dt}\int_\Omega|\nabla v_1-\nabla v_2|^2dx+C|D_1-D_2|\int_\Omega|\nabla v_2|^2dx\\
&-\frac{1}{2}\|\varphi_1-\varphi_2\|^2_{L^\infty(\Gamma^R)}\int_{\Gamma^R}|u_2|^{2\lambda}d\gamma-\frac{1}{2}\frac{d}{dt}\int_{\Gamma^R}|u_1-u_2|^2d\gamma+r_1\int_\Omega|u_1-u_2|^2dx\\
&+\frac{1}{2}\frac{d}{dt}\int_\Omega|u_1-u_2|^2dx+r_1\int_\Omega|v_1-v_2|^2dx+\frac{r_1}{2}\frac{d}{dt}\int_\Omega|v_1-v_2|^2dx\\
&+|r_1-r_2|\frac{\hat c}{2\bar r}\frac{d}{dt}\int_\Omega|u_1-u_2|^2dx-|r_1-r_2|\frac{\hat c}{2\bar r}\frac{d}{dt}\int_\Omega|v_1-v_2|^2dx. \qquad (5.100)
\end{aligned}$$

Using the property of H in (5.43), (5.100) becomes

$$\begin{aligned}
&\frac{d}{dt}\int_\Omega(u_1-u_2)^2dx+\frac{1}{2}\frac{d}{dt}\int_\Omega(H(|\nabla u_1|)+H(|\nabla u_2|))dx+\frac{1}{2}\frac{d}{dt}\int_\Omega|v_1-v_2|^2dx\\
&+\frac{D_1}{2}\frac{d}{dt}\int_\Omega|\nabla u_1-\nabla u_2|^2dx\le\frac{d}{dt}\int_\Omega K_1(|\nabla u_1|)\nabla u_1\cdot\nabla u_2dx\\
&+\frac{d}{dt}\int_\Omega K_1(|\nabla u_2|)\nabla u_2\cdot\nabla u_1dx+C\varepsilon_3\frac{d}{dt}\int_\Omega|\nabla v_1-\nabla v_2|^2dx\\
&+C|D_1-D_2|\int_\Omega|\nabla v_2|^2dx-\frac{1}{2}\|\varphi_1-\varphi_2\|^2_{L^\infty(\Gamma^R)}\int_{\Gamma^R}|u_2|^{2\lambda}d\gamma\\
&-\frac{1}{2}\frac{d}{dt}\int_{\Gamma^R}|u_1-u_2|^2d\gamma+r_1\int_\Omega|u_1-u_2|^2dx+\frac{1}{2}\frac{d}{dt}\int_\Omega|u_1-u_2|^2dx\\
&+r_1\int_\Omega|v_1-v_2|^2dx+\frac{r_1}{2}\frac{d}{dt}\int_\Omega|v_1-v_2|^2dx+|r_1-r_2|\frac{\hat c}{2\bar r}\frac{d}{dt}\int_\Omega|u_1-u_2|^2dx\\
&-|r_1-r_2|\frac{\hat c}{2\bar r}\frac{d}{dt}\int_\Omega|v_1-v_2|^2dx. \qquad (5.101)
\end{aligned}$$

Integrating (5.101) over time interval $(0,t)$, it yields

$$\begin{aligned}
&\int_\Omega (u_1-u_2)^2dx+\frac{1}{2}\int_\Omega (H(|\nabla u_1|)+H(|\nabla u_2|))dx\\
&+\frac{D_1}{2}\int_\Omega |\nabla u_1-\nabla u_2|^2dx\le \int_\Omega K_1(|\nabla u_1|)\nabla u_1\cdot\nabla u_2dx\\
&+\int_\Omega K_1(|\nabla u_2|)\nabla u_2\cdot\nabla u_1dx+C\varepsilon_3\int_\Omega |\nabla v_1-\nabla v_2|^2dx\\
&+C|D_1-D_2|\int_0^t\int_\Omega |\nabla v_2|^2dxds-\frac{1}{2}\|\varphi_1-\varphi_2\|^2_{L^\infty(\Gamma^R)}\int_0^t\int_{\Gamma^R}|u_2|^{2\lambda}d\gamma ds\\
&-\frac{1}{2}\int_{\Gamma^R}|u_1-u_2|^2d\gamma+r_1\int_0^t\int_\Omega |u_1-u_2|^2dxds+\frac{1}{2}\int_\Omega |u_1-u_2|^2dx\\
&+r_1\int_0^t\int_\Omega |v_1-v_2|^2dxds+\frac{r_1}{2}\int_\Omega |v_1-v_2|^2dx+|r_1-r_2|\frac{\hat{c}}{2\bar{r}}\int_\Omega |u_1-u_2|^2dx\\
&-|r_1-r_2|\frac{\hat{c}}{2\bar{r}}\int_\Omega |v_1-v_2|^2dx. \qquad (5.102)
\end{aligned}$$

Next, we estimate the first term of the right hand side of (5.102) by using assumption (A_5) together with Holdër's inequality, one obtains

$$\begin{aligned}
\left|\int_\Omega K_1(|\nabla u_1|)\nabla u_1\cdot\nabla u_2dx\right| &\le C\int_\Omega |\nabla u_1|^{1-a}|\nabla u_2|dx\\
&\le C\left(\int_\Omega |\nabla u_1|^{2-a}dx\right)^{\frac{1-a}{2-a}}\left(\int_\Omega |\nabla u_2|^{2-a}dx\right)^{\frac{1}{2-a}}\\
&\le C\left(\int_\Omega (H(|\nabla u_1|)+1)dx\right)^{\frac{1-a}{2-a}}\left(\int_\Omega |\nabla u_2|^{2-a}dx\right)^{\frac{1}{2-a}}\\
&\le C\left(\int_\Omega H(|\nabla u_1|)dx\right)^{\frac{1-a}{2-a}}\left(\int_\Omega |\nabla u_2|^{2-a}dx\right)^{\frac{1}{2-a}}\\
&+C\left(\int_\Omega |\nabla u_2|^{2-a}dx\right)^{\frac{1}{2-a}}\\
&\le \varepsilon\int_\Omega H(|\nabla u_1|)dx+C\int_\Omega |\nabla u_2|^{2-a}dx\\
&+C\left(\int_\Omega |\nabla u_2|^{2-a}dx\right)^{\frac{1}{2-a}}. \qquad (5.103)
\end{aligned}$$

By using the same procedure for the second term of the right hand side of (5.102), we have

$$\begin{aligned}
\left|\int_\Omega K_1(|\nabla u_2|)\nabla u_2\cdot\nabla u_1dx\right| &\le \varepsilon\int_\Omega H(|\nabla u_2|)dx+C\int_\Omega |\nabla u_1|^{2-a}dx\\
&+C\left(\int_\Omega |\nabla u_1|^{2-a}dx\right)^{\frac{1}{2-a}}. \qquad (5.104)
\end{aligned}$$

Applying trace inequality (5.8) and using (5.103), (5.104), we obtain the following estimate

$$\begin{aligned}
&\int_\Omega (u_1-u_2)^2dx+\frac{1}{2}\int_\Omega (H(|\nabla u_1|)+H(|\nabla u_2|))dx\\
&+\frac{D_1}{2}\int_\Omega |\nabla u_1-\nabla u_2|^2dx\leq \varepsilon\int_\Omega (H(|\nabla u_1|)+H(|\nabla u_2|))dx\\
&+C\int_\Omega |\nabla u_1|^{2-a}dx+C\left(\int_\Omega |\nabla u_1|^{2-a}dx\right)^{\frac{1}{2-a}}\\
&+C\int_\Omega |\nabla u_2|^{2-a}dx+C\left(\int_\Omega |\nabla u_2|^{2-a}dx\right)^{\frac{1}{2-a}}\\
&+C\varepsilon_3\int_\Omega |\nabla v_1-\nabla v_2|^2dx+C|D_1-D_2|\int_0^t\int_\Omega |\nabla v_2|^2dxds-\\
&\frac{1}{2}\|\varphi_1-\varphi_2\|^2_{L^\infty(\Gamma^R)}\int_0^t\int_{\Gamma^R}|u_2|^{2\lambda}d\gamma ds-\frac{1}{2}\Big(2\varepsilon_4\int_\Omega |\nabla u_1-\nabla u_2|^{2-a}dx\\
&+C\int_\Omega |u_1-u_2|^{\alpha}dx+C\int_\Omega |u_1-u_2|^{\alpha+\mu_0}dx+C\int_\Omega |u_1-u_2|^{\alpha+\mu_1}dx\Big)\\
&+r_1\int_0^t\int_\Omega |u_1-u_2|^2dxds+\frac{1}{2}\int_\Omega |u_1-u_2|^2dx+r_1\int_0^t\int_\Omega |v_1-v_2|^2dxds\\
&+\frac{r_1}{2}\int_\Omega |v_1-v_2|^2dx+|r_1-r_2|\frac{\hat{c}}{2\bar{r}}\int_\Omega |u_1-u_2|^2dx\\
&-|r_1-r_2|\frac{\hat{c}}{2\bar{r}}\int_\Omega |v_1-v_2|^2dx.
\end{aligned}\tag{5.105}$$

Choosing $\varepsilon=\frac{1}{2}$, $\varepsilon_3=\frac{1}{4C}$ and $\varepsilon_4=1$, we are led to

$$\begin{aligned}
&\int_\Omega |\nabla u_1-\nabla u_2|^{2-a}dx+\int_\Omega |\nabla v_1-\nabla v_2|^2dx\leq \varepsilon\int_\Omega (H(|\nabla u_1|)+H(|\nabla u_2|))dx\\
&+C\int_\Omega |\nabla u_1|^{2-a}dx+C\left(\int_\Omega |\nabla u_1|^{2-a}dx\right)^{\frac{1}{2-a}}\\
&+C\int_\Omega |\nabla u_2|^{2-a}dx+C\left(\int_\Omega |\nabla u_2|^{2-a}dx\right)^{\frac{1}{2-a}}\\
&+C|D_1-D_2|\int_0^t\int_\Omega |\nabla v_2|^2dxds-\frac{1}{2}\|\varphi_1-\varphi_2\|^2_{L^\infty(\Gamma^R)}\int_0^t\int_{\Gamma^R}|u_2|^{2\lambda}d\gamma ds\\
&+r_1\int_0^t\int_\Omega |u_1-u_2|^2dxds+\frac{1}{2}\int_\Omega |u_1-u_2|^2dx+r_1\int_0^t\int_\Omega |v_1-v_2|^2dxds+\\
&\frac{r_1}{2}\int_\Omega |v_1-v_2|^2dx+|r_1-r_2|\frac{\hat{c}}{2\bar{r}}\int_\Omega |u_1-u_2|^2dx-|r_1-r_2|\frac{\hat{c}}{2\bar{r}}\int_\Omega |v_1-v_2|^2dx.
\end{aligned}\tag{5.106}$$

Now, we use the energy estimates (5.27), (5.44) and the stability-like estimate (5.24), we finally obtain the following structural-stability-like estimate

$$\int_\Omega |\nabla u_1 - \nabla u_2|^{2-a} dx + \int_\Omega |\nabla v_1 - \nabla v_2|^2 dx \leq C + C(|D_1 - D_2| - \|\varphi_1 - \varphi_2\|^2_{L^\infty(\Gamma^R)}) + \left(\left(t + \frac{1}{2}\right) + |r_1 - r_2|\frac{\hat{c}}{2\bar{r}}\right) e^{C(\alpha,\lambda,\hat{c},\bar{r})|r_1 - r_2|t}\Big(\|u_{01} - u_{02}\|^2_{L^2(\Omega)} + \|v_{01} - v_{02}\|^2_{L^2(\Omega)} + Ct\left(|D_1 - D_2| + |r_1 - r_2| - \|\varphi_1 - \varphi_2\|^2_{L^\infty(\Gamma^R)}\right)\Big). \tag{5.107}$$

□

5.9 Discussion

In this chapter, we have shown the well-posedness of a system of parabolic equations consisting of a double nonlinear parabolic equation of Forchheimer type coupled with a semilinear parabolic equation. The system describes a fluid-like driven system for active-passive pedestrian dynamics. Specifically, the pedestrian flow is composed of a mix of densities of active and passive pedestrians that are moving with different velocities. We used Schauder's fixed point argument to tackle the existence of solutions to the system. We proved the uniqueness of solutions by using the structure of the nonlinearity of the coupling. We provided also stability estimates of solutions with respect to selected parameters.

Note that our stability estimate for the gradient of the solutions is not optimal. This stability estimate can be eventually improved by studying the structural stability with respect to the Forchheimer polynomial $K_1(\cdot)$ (see e.g. [HI11]). From a micro-to-macro perspective, it is worth also noting that a generalized Forchheimer flow model can be obtained in principle via homogenization techniques (like in [LLPW11], e.g.). It would be interesting to see if we can build a suitable microscopic model defined at the level of the geometry depicted in Figure 2.5. An open question here would be to investigate the large time behavior of the solutions to our evolution system. Also, a convergent numerical approximation of solutions to (5.1) needs to be proposed. We plan to investigate these research directions in future works.

From a micro-to-macro perspective, it would be interesting to explore whether the structure of the nonlinearity arising in the Forchheimer polynomial can be related via a suitable hydrodynamic or mean-field limiting process to an interacting particle system. Such an investigation route would most probably use statistical mechanics-based techniques like the ones presented, for instance, in [Pre09]. Should such an approach be successful, then direct connections between microscopic (discrete, stochastic) models for pedestrian flows and macroscopic (continuum) models for pedestrian flows like the one presented in this chapter, will become clear.

Chapter 6

Solvability of a coupled nonlinear system of Skorohod-like stochastic differential equations modeling active–passive pedestrians dynamics through a heterogeneous domain and fire

In this chapter, we study the existence and uniqueness of solutions to a coupled nonlinear system of Skorohod-like stochastic differential equations with reflecting boundary condition. The setting describes the evacuation dynamics of a mixed crowd composed of both active and passive pedestrians moving through a domain with obstacles, fire and smoke. As main working techniques, we use compactness methods and the Skorohod's representation of solutions to SDEs posed in bounded domains. This functional setting is a new point of view in the field of modeling and simulation pedestrian dynamics. The main challenge is to handle the coupling and the nonlinearities present in the model equations together with the multiple-connectedness of the domain and the pedestrian-obstacle interaction. This is based on [TM20].

6.1 Introduction

In this chapter, we study the solvability of a coupled nonlinear system of Skorohod-like stochastic differential equations modeling the dynamics of pedestrians through a heterogenous domain in the presence of fire. From the modeling perspective, our approach is novel, opening many routes for investigation especially what concerns the computability of solutions and identification of model parameters. The standing assumption is that the crowd of pedestrians is composed of two distinct populations: an *active population* – these pedestrians are aware of the details

of the environment and move towards the exit door, and a *passive population* – these pedestrians are not aware of the details of the geometry and move randomly to explore the environment and eventually to find the exit. All pedestrians are seen as moving point particles driven by a suitable over-damped Langevin model, which will be described in Section 6.3. Our model belongs to the class of social-velocity models for crowd dynamics. It is posed in a two dimensional multiple connected region D, containing obstacles with a fixed location. Furthermore, a stationary fire, which produces smoke, is placed within the geometry forcing the pedestrians to choose a proper own velocity such that they evacuate. The fire is seen, as a first attempt, as a stationary obstacle.

To keep a realistic picture, the overall dynamics is restricted to a bounded "perforated" domain, i.e. all obstacles are seen as impenetrable regions. The geometry is described in Subsection 6.3.1; see Figure 6.1 to fix ideas. In this framework, we consider reflecting boundary conditions and plan, as further research, to treat the case of mixed reflection–flux boundary conditions so that the exits can allow for outflux. In this framework, we focus on the interior obstacles. To achieve a correct dynamics of dynamics of the pedestrians close to the boundary of the interior obstacles, we choose to work with the classical Skorohod's formulation of SDEs; we refer the reader to the textbook [Pil14] for more details on this subject. Note that this approach is needed especially because of the chosen dynamics for the passive particles, as the active pedestrians are able to avoid collisions with the obstacles by using a motion planning map (*a priori* given paths – solution to a suitable Eikonal-like equation; cf. Appendix A.2).

6.2 Related contributions. Main questions of this research

A number of relevant results are available on the dynamics of mixed active-passive pedestrian populations. As far as we are aware, the first questions in this context were posed in the modeling and simulation study [RJM19] while considering the evacuation dynamics of a mixed active-passive pedestrian populations in a complex geometry in the presence of a fire as well as of a slowly spreading smoke curtain. From a stochastic processes perspective, various lattice gas models for active-passive pedestrian dynamics have been recently explored in [CCMT19, CMRT19]. See also [TCM19] for a result on the weak solvability of a deterministic system of parabolic partial differential equations describing the interplay of a mixture of fluids for active–passive populations of pedestrians.

The discussion of the active-passive pedestrian dynamics at the level of SDEs is new and brings in at least a twofold challenge: (i) the evolution system is nonlinear and coupled and (ii) pedestrians have to cross a domain with forbidden regions (the obstacles). Various solution strategies have been already identified for deterministic crowd evolution equations. We mention here the two more prominent: a granular media approach, where collisions with obstacles are tackled with techniques of non-smooth analysis cf. e.g. [FM15], and a reflection-of-velocities

approach as it is done e.g. in [KvMY19]. If some level of noise affects the dynamics, then both these approaches fail to work. On the other hand, there are several results for stochastic differential equations with reflecting boundary conditions, one of them being the seminal contribution of Skorohod in [Sko61], where the author provided the existence and uniqueness to one dimensional stochastic equations for diffusion processes in a bounded region. A direct approach to the solution of the reflecting boundary conditions and reductions to the case including nonsmooth ones are reported in [Lio84]. Extending results by Tanaka, the author of [Sai87] proves the existence and uniqueness of solutions to the Skorohod equation posed in a bounded domain in $\mathbb{R}^d$ where a reflecting boundary condition is applied.

The main question we ask in this chapter is whether we can frame our crowd dynamics model as a well-posed system of stochastic evolution equations of Skorohod type. Provided suitable restrictions on the geometry of the domain, on the structure of nonlinearites as well as data and parameters, we provide in Section 6.6 a positive answer to this question. This study opens the possibility of exploring further our system from the numerical analysis perspective so that suitable algorithms can be designed to produce simulations forecasting the evacuation time based on our model. A couple of follow-up open questions are given in the conclusion; see Section 6.7.

6.3 Setting of the model equations

6.3.1 Geometry

We consider a two dimensional domain, which we refer to as Λ. As a building geometry, parts of the domain are filled with obstacles. Their collection is denoted by $G = \bigcup_{k=1}^{N_{\text{obs}}} G_k$, for all $k \in \{1, \dots, N_{\text{obs}} \in \mathbb{N}\}$. A fire F is introduced somewhere in this domain and is treated in this context as an obstacle for the motion of the crowd. Moreover, the domain has the exit denoted by E. Our domain represents the environment where the crowd of pedestrians is located. The crowd tries to find the fastest way to the exit, avoiding the obstacles and the fire. Let $D := \Lambda \backslash (G \cup E \cup F) \subset \mathbb{R}^2$ with the boundary ∂D such that $\partial\Lambda \cap \partial G_k = \emptyset$, $\partial\Lambda \cap \partial G_k = \emptyset$ and $F \cap G_k = \emptyset$, we also denote $S = (0, T)$ for some $T \in \mathbb{R}_+$. We refer to $\bar{D} \times S$ as D_T, note that $\bar{D}$ denotes the closure of D. Furthermore, N_A is the total number of active agents, N_P is the total number of passive particles with $N := N_A + N_P$ and $N_A, N_P, N \in \mathbb{N}$.

6.3.2 Active population

For $i \in \{1, \dots, N_A\}$ and $t \in S$, let $\mathbf{x}_{a_i}$ denote the position of the pedestrian i belonging to the active population at time t. We assume that the dynamics of

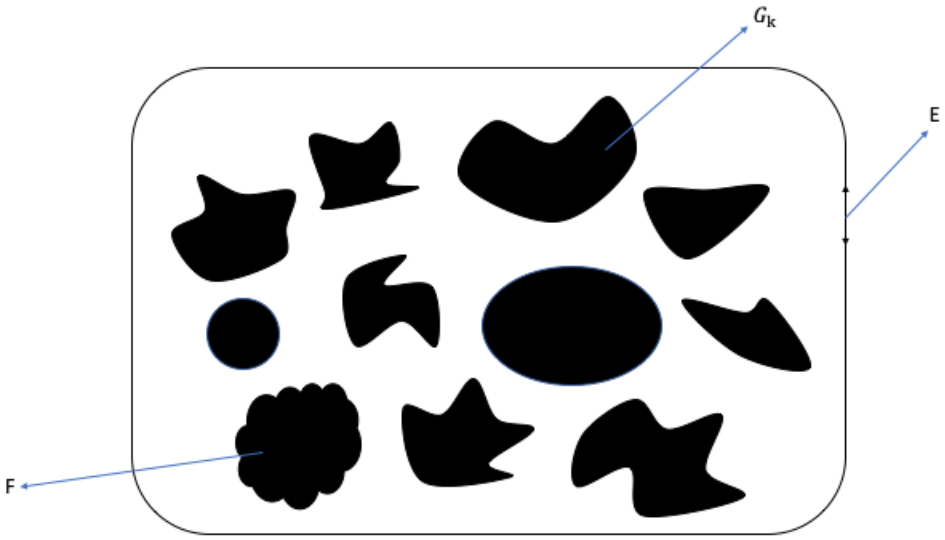

Figure 6.1: Basic geometry for our active-passive pedestrian model. Initially, pedestrians occupy some random position within a geometry with obstacles G_k. Because of the presence of the fire F, and presumably also of smoke, they wish to evacuate via the exit door E while avoiding the obstacles G_k and the fire F.

active pedestrians is governed by

$$\begin{cases} \frac{d\mathbf{x}_{a_i}(t)}{dt} = -\Upsilon(s(\mathbf{x}_{a_i}(t))\frac{\nabla\phi(\mathbf{x}_{a_i}(t))}{|\nabla\phi(\mathbf{x}_{a_i}(t))|}\left(p_{\max} - p(\mathbf{x}_{a_i}(t),t)\right), \\ \mathbf{x}_{a_i}(0) = \mathbf{x}_{a_{i0}}, \end{cases} \tag{6.1}$$

where $\mathbf{x}_{a_{i0}}$ represents the initial configuration of active pedestrians inside $\bar{D}$. In (6.1), $\nabla\phi$ is the minimal motion path of the distance between particle positions $\mathbf{x}_{a_i}$ and the exit location E (it solves the Eikonal-like equation). The function $\phi(\cdot)$ encodes the familiarity with the geometry; see also [YJQH16] for a related setting. We refer to it as the motion planning map. In this context, $p(\mathbf{x},t)$ is the local discomfort (a realization of the social pressure) so that

$$p(\mathbf{x},t) = \mu(t)\int_{D\cap B(\mathbf{x},\tilde{\delta})}\sum_{j=1}^{N}\delta(y-\mathbf{x}_{c_j}(t))dy, \tag{6.2}$$

for $\{\mathbf{x}_{c_j}\} := \{\mathbf{x}_{a_i}\}\cup\{\mathbf{x}_{b_k}\}$ for $i\in\{1,\ldots,N_A\}, k\in\{1,\ldots,N_P\}, j\in\{1,\ldots,N_A+N_P\}$. In (6.2), δ is the Dirac (point) measure and $B(\mathbf{x},\tilde{\delta})$ is a ball center $\mathbf{x}$ with small enough radius $\tilde{\delta}$ such that $\tilde{\delta}>0$. Hence, the discomfort $p(\mathbf{x},t)$ represents a finite measure on the set $D\cap B(\mathbf{x},\tilde{\delta})$. In addition, we assume the following structural relation between the smoke extinction and the walking speed (see in [Jin97], [RN19]) as a function $\Upsilon:\mathbb{R}^2_+\longrightarrow\mathbb{R}^2$ such that

$$\Upsilon(x) = -\zeta x + \eta, \tag{6.3}$$

where ζ, η are given real positive numbers. The dependence of the model coefficients on the local smoke density is marked via a smooth relationship with respect to an a priori given function $s(x,t)$ describing the distribution of smoke inside the geometry at position x and time t.

6.3.3 Passive population

For $k \in \{1, \dots, N_P\}$ and $t \in S$, let $\mathbf{x}_{p_k}$ denote the position of the pedestrian k belonging at time t to the passive population. The dynamics of the passive pedestrians is described here as a system of stochastic differential equations as follows:

$$\begin{cases} d\mathbf{x}_{p_k}(t) = \sum_{j=1}^{N} \frac{\mathbf{x}_{c_j} - \mathbf{x}_{p_k}}{\epsilon + |\mathbf{x}_{c_j} - \mathbf{x}_{p_k}|} \omega(|\mathbf{x}_{c_j} - \mathbf{x}_{p_k}|, s(\mathbf{x}_{p_k}, t))dt + \beta(s(\mathbf{x}_{p_k}, t))dB(t), \\ \mathbf{x}_{p_k}(0) = \mathbf{x}_{p_{k0}}, \end{cases} \tag{6.4}$$

where $\mathbf{x}_{p_{k0}}$ represents the initial configuration of passive pedestrians inside $\bar{D}$ and $\epsilon > 0$. In (6.4), ω is a Morse-like potential function (see e.g. Ref. [CMP13] for a setting where a similar potential has been used). We take $\omega : \mathbb{R} \times \mathbb{R}^2 \longrightarrow \mathbb{R}^2$ to be

$$\omega(x,y) = -\beta(y) \left(C_A e^{-\frac{x}{\ell_A}} + C_R e^{-\frac{x}{\ell_R}} \right) \text{ for } x, y \in \mathbb{R} \times \mathbb{R}^2, \tag{6.5}$$

while $C_A > 0, C_R > 0$ are the attractive and repulsive strengths and $\ell_A > 0, \ell_R > 0$ are the respective length scales for attraction and repulsion. Moreover, the coefficient β is a regularized version of the Heaviside step function. As in Subsection 2.4.2, the dependence of the model coefficients on the smoke is marked via a smooth relationship with respect to an a priori given function $s(x,t)$ describing the distribution of smoke inside the geometry at position x and time t. Note that the passive pedestrians do not posses any knowledge on the geometry of the walking space. In particular, the location of the exit is unknown; see [CP19] for a somewhat related context.

6.4 Technical preliminaries and assumptions

6.4.1 Technical preliminaries

We recall the classical Ascoli-Arzelà Theorem:
A family of functions $U \subset C(\bar{S}; \mathbb{R}^d)$ is relatively compact (with respect to the uniform topology) if

i. for every $t \in \bar{S}$, the set $\{f(t); f \in U\}$ is bounded.

ii. for every $\varepsilon > 0$ and $t, s \in \bar{S}$, there is $\bar{\delta} > 0$ such that

$$|f(t) - f(s)| \leq \varepsilon, \tag{6.6}$$

whenever $|t - s| \leq \bar{\delta}$ for all $f \subset U$.

For a function $f : \bar{S} \to \mathbb{R}^d$, we introduce the definition of Hölder seminorms as

$$[f]_{C^\alpha(S;\mathbb{R}^d)} = \sup_{t\neq s;t,s\in\bar{S}} \frac{|f(t)-f(s)|}{|t-s|^\alpha}, \tag{6.7}$$

for $\alpha \in (0,1)$ and the supremum norm as

$$\|f\|_{L^\infty(S;\mathbb{R}^d)} = \operatorname{ess\,sup}_{t\in\bar{S}} |f(t)|. \tag{6.8}$$

We refer to [AF03] and [GT77] for more details on these spaces.

Using Ascoli-Arzelà Theorem starting from the facts:

i'. there is $M_1 > 0$ such that $\|f\|_{L^\infty(S;\mathbb{R}^d)} \leq M_1$ for all $f \in U$,

ii'. for some $\alpha \in (0,1)$, there is an $M_2 > 0$ such that $[f]_{C^\alpha(\bar{S};\mathbb{R}^d)} \leq M_2$ for all $f \in U$,

we infer that the set

$$K_{M_1M_2} = \left\{ f \in C(\bar{S};\mathbb{R}^d); \|f\|_{L^\infty(S;\mathbb{R}^d)} \leq M_1, [f]_{C^\alpha(\bar{S};\mathbb{R}^d)} \leq M_2 \right\} \tag{6.9}$$

is relatively compact in $C(\bar{S};\mathbb{R}^d)$.

For $\alpha \in (0,1)$, $T > 0$ and $p > 1$, the space $W^{\alpha,p}(S;\mathbb{R}^d)$ is defined as the set of all $f \in L^p(S;\mathbb{R}^d)$ such that

$$[f]_{W^{\alpha,p}(S;\mathbb{R}^d)} := \int_0^T \int_0^T \frac{|f(t)-f(s)|^p}{|t-s|^{1+\alpha p}} dtds < \infty.$$

This space is endowed with the norm

$$\|f\|_{W^{\alpha,p}(S;\mathbb{R}^d)} = \|f\|_{L^p(S;\mathbb{R}^d)} + [f]_{W^{\alpha,p}(S;\mathbb{R}^d)}.$$

Moreover, we have the following embedding

$$W^{\alpha,p}(S;\mathbb{R}^d) \subset C^\gamma(\bar{S};\mathbb{R}^d) \quad \text{for } \alpha p - \gamma > 1$$

and $[f]_{C^\gamma(S;\mathbb{R}^d)} \leq C_{\gamma,\alpha,p}\|f\|_{W^{\alpha,p}(S;\mathbb{R}^d)}$. Relying on the Ascoli-Arzelà Theorem, we have the following situation:

ii". for some $\alpha \in (0,1)$ and $p > 1$ with $\alpha p > 1$, there is $M_2 > 0$ such that $[f]_{W^{\alpha,p}(S;\mathbb{R}^d)} \leq M_2$ for all $f \in U$.

If i' and ii" hold, then the set

$$K'_{M_1M_2} = \left\{ f \in C(\bar{S};\mathbb{R}^d); \|f\|_{L^\infty(S;\mathbb{R}^d)} \leq M_1, [f]_{W^{\alpha,p}(S;\mathbb{R}^d)} \leq M_2 \right\} \tag{6.10}$$

is relatively compact in $C(\bar{S};\mathbb{R}^d)$, if $\alpha p > 1$ (see e.g. [FG95], [CMRT19]).

6.4.2 Assumptions

To be successful with our analysis, we rely on the following assumptions:

(A_1) The functions $b : D_T \times D_T \longrightarrow \mathbb{R}^2 \times \mathbb{R}^2$, and $\sigma : D_T \times D_T \longrightarrow \mathbb{R}^{2\times 2} \times \mathbb{R}^{2\times 2}$ satisfy $|\sigma(x,t)| \leq L$, $|b(x,t)| \leq L$ for all $x \in \bar{D} \times \bar{D}$ and $t \in S$. Here σ and b incorporate the right-hand sides of the SDEs (6.1) and (6.4) in their respective dimensionless form indicated in Appendix A.3.

(A_2) $p_{\max} = N|\bar{D}|$, where $|\bar{D}|$ denotes the area of $\bar{D}$.

(A_3) $\Upsilon, \omega, \beta \in C^1(\mathbb{R}^2)$.

(A_4) $s \in C^1(\bar{S}; \mathbb{R}^2)$.

(A_5) ∂D is $C^{2,\alpha}$ with $\alpha \in (0,1)$, or at least satisfying the exterior sphere condition.

It is worth mentioning that assumptions (A_1) and (A_2) correspond to the modeling of the situation, while (A_3)-(A_5) are of technical nature, corresponding to the type of solution we are searching for; clarifications in this direction are given in the next Section.

6.5 The Skorohod equation

6.5.1 Concept of solution

Take $x \in \partial D$ arbitrarily fixed. We define the set $\mathcal{N}_x$ of inward normal unit vectors at $x \in \partial D$ by

$$\begin{aligned} \mathcal{N}_x &= \cup_{r>0} \mathcal{N}_{x,r}, \\ \mathcal{N}_{x,r} &= \left\{ \mathbf{n} \in \mathbb{R}^2 : |\mathbf{n}| = 1, B(x - r\mathbf{n}, r) \cap D = \emptyset \right\}, \end{aligned} \tag{6.11}$$

where $B(z,r) = \{y \in \mathbb{R}^2 : |y - z| < r\}, z \in \mathbb{R}^2, r > 0$. Mind that, in general, it can happen that $\mathcal{N}_x = \emptyset$. In this case, the uniform exterior sphere condition is not satisfied (see, for instance, the examples in [CFLPL16], Fig. 5 and in [Cho16], page 4).
We complement our list of assumptions (A_1)–(A_5) with three specific conditions on the geometry of the domain D:

(A_6) (Uniform exterior sphere condition). There exists a constant $r_0 > 0$ such that

$$\mathcal{N}_x = \mathcal{N}_{z,r_0} \neq \emptyset \text{ for any } z \in \partial D.$$

(A_7) There exits constants $\delta > 0$ and $\delta' \in [1, \infty)$ with the following property: for any $x \in \partial D$ there exists a unit vector $\mathbf{l}_x$ such that

$$\langle \mathbf{l}_x, \mathbf{n} \rangle \geq 1/\delta' \text{ for any } \mathbf{n} \in \bigcup_{y \in B(x,\delta) \cap \partial D} \mathcal{N}_y,$$

where $\langle \cdot, \cdot \rangle$ denotes the usual inner product in $\mathbb{R}^2$.

(A$_8$) There exist $\delta'' > 0$ and $\nu > 0$ such that for each $x_0 \in \partial D$ we can find a function $f \in C^2(\mathbb{R}^2)$ satisfying

$$\langle y - x, \mathbf{n}\rangle + \frac{1}{\nu}\langle \nabla f(x), \mathbf{n}\rangle |y - x|^2 \geq 0, \tag{6.12}$$

for any $x \in B(x_0, \delta'') \cap \partial D, y \in B(x_0, \delta'') \cap \partial \bar{D}$ and $\mathbf{n} \in \mathcal{N}_x$.

Let $W(\mathbb{R}^2)$ and $W(D)$ be the space of continuous paths in $\mathbb{R}^2$ and D, respectively. The following relation is called *the Skorohod equation*: Find $(\xi, \phi) \in W(\mathbb{R}^2)$ such that

$$\xi(t) = w(t) + \phi(t), \tag{6.13}$$

where $w \in W(\mathbb{R}^2)$ is given so that $w(0) \in \bar{D}$. The solution of (6.13) is a pair (ξ, ϕ), which satisfies the following two conditions:

(a) $\xi \in W(\bar{D})$;

(b) $\phi \in C(\bar{S})$ with bounded variation on each finite time interval satisfying $\phi(0) = 0$ and

$$\begin{aligned} \phi(t) &= \int_0^t \mathbf{n}(y) d|\phi|_y, \\ |\phi|_t &= \int_0^t \mathbb{1}_{\partial D}(\xi(y)) d|\phi|_y, \end{aligned} \tag{6.14}$$

where

$$\mathbf{n}(y) \in \mathcal{N}_{\xi(y)} \text{ if } \xi(y) \in \partial D, \tag{6.15}$$

$$\begin{aligned} |\phi|_t &= \text{ total variation of } \phi \text{ on } [0, t] \\ &= \sup_{\mathcal{T} \in \mathcal{G}([0,t])} \sum_{k=1}^{n_{\mathcal{T}}} |\phi(t_k) - \phi(t_k - 1)|. \end{aligned} \tag{6.16}$$

In (6.15), we denote by $\mathcal{G}([0, t])$ the family of all partitions of the interval $[0, t]$ and take a partition $\mathcal{T} = \{0 = t_0 < t_1 < \ldots < t_n = t\} \in \mathcal{G}([0, t])$. The supremum in (6.15) is taken over all partitions of type $0 = t_0 < t_1 < \ldots < t_n = t$.

Conditions (a) and (b) guarantee that ξ is a *reflecting process* on $\bar{D}$.

Theorem 6.1. *Assume conditions (a) and (b). Then for any $w \in W(\mathbb{R}^2)$ with $w(0) \in \bar{D}$, there exists a unique solution $\xi(t, w)$ of the equation* (6.13) *such that $\xi(t, w)$ is continuous in (t, w).*

For the proof of this Theorem, we refer the reader to Theorem 4.1 in [Sai87].

To come closer to the model equations for active-passive pedestrian dynamics described in Section 6.3, we introduce the mappings

$$b : D_T \times D_T \longrightarrow \mathbb{R}^2 \times \mathbb{R}^2, \quad \sigma : D_T \times D_T \longrightarrow \mathbb{R}^{2\times 2} \times \mathbb{R}^{2\times 2}$$

and consider a Skorohod-like system on the probability space $(\Omega, \mathcal{F}, P)$

$$dX_t = b(X_t(t))dt + \sigma(X_t(t))dB(t) + d\Phi_t, \tag{6.17}$$

or (6.17) can be written component-wise as

$$dX_t^{(I)} = b(X_t(t))_I dt + \sum_{J=1}^{2} \sigma_{IJ}(X_t(t))dB^{(J)}(t) + d\Phi_t^{(I)}, \text{ for } 1 \le I \le 4, 1 \le J \le 2$$

with

$$X(0) = X_0 \in \bar{D}, \tag{6.18}$$

where the inital value X_0 is assumed to be an $\mathcal{F}_0-$measurable random variable and $B(t)$ is a $2-$dimensional $\mathcal{F}_t-$Brownian motion with $B(0) = 0$. Here, $\{\mathcal{F}_t\}$ is a filtration such that $\mathcal{F}_0$ contains all $P-$negligible sets and $\mathcal{F}_t = \cap_{\varepsilon>0}\mathcal{F}_{t+\varepsilon}$. The structure of (6.17) is provided in Section 6.6.2. Similarly to the deterministic case, we can now define the following concept of solutions to (6.17). More details of the structure of (6.17)-(6.18) are listed in Section 6.6.2.

Definition 6.2. *A pair (X_t, Φ_t) is called solution to* (6.17)–(6.18) *if the following conditions hold:*

(i) *X_t is a $\bar{D}-$valued $\mathcal{F}_t-$adapted continuous process;*

(ii) *$\Phi(t)$ is an $\mathbb{R}^2-$valued $\mathcal{F}_t-$adapted continuous process with bounded variation on each finite time interval such that $\Phi(0) = 0$ with*

$$\Phi(t) = \int_0^t \boldsymbol{n}(y)d|\Phi|_y,$$
$$|\Phi|_t = \int_0^t \mathbb{1}_{\partial D}(X(y))d|\Phi|_y. \tag{6.19}$$

(iii) *$\boldsymbol{n}(s) \in \mathcal{N}_{X(s)} \in \partial D$.*

Note that the Definition 6.2 ensures that X_t entering (6.17) is a reflecting process on $\bar{D}$.

6.6 Solvability of Skorohod-like system

In this section, we establish the solvability of the Skorohod-like system by showing the existence and uniqueness of solutions in the sense of Definition 6.2 to the problem (6.17)–(6.18). It turns out that for completing the well-posedness study of our system, more work is required. We comment on this matter in Remark 6.7.

6.6.1 Statement of the main results

The main results of this chapter are stated in Theorem 6.3 and Theorem 6.4. In the frame of this chapter, the focus lies on ensuring the existence and uniqueness of Skorohod solutions to our crowd dynamics problem.

Theorem 6.3. *Assume that* (A_1)-(A_7) *hold. There exists at least a solution to the Skorohod-like system* (6.17)–(6.18) *in the sense of Definition 6.2.*

Theorem 6.4. *Assume that* (A_1)-(A_8) *hold. There is a unique strong solution to* (6.17)–(6.18).

These statements are proven in the next two subsections.

6.6.2 Structure of the proof of Theorem 6.3

For convenience, we rephrase the solution to the system (13) and (14) in terms of the vector X_t^n, $n \in \mathbb{N}$, such that

$$X_t^n := (X_{a_i}^n(t), X_{b_k}^n(t))^T \text{ for } i \in \{1, \dots, N_A\}, k \in \{1, \dots, N_P\}, \tag{6.20}$$

$$F_1(X_t^n, t) := \kappa \Upsilon(S(X_{a_i}^n(t))) \frac{\nabla_{X_{a_i}^n} \phi(X_{a_i}^n(t))}{|\nabla_{X_{a_i}^n} \phi(X_{a_i}^n(t))|} (p_{\max} - p(X_{a_i}^n(t), t)), \tag{6.21}$$

$$F_2(X_t^n, t) := \kappa \sum_{j=1}^{N} \frac{X_{c_j}^n(t) - X_{p_k}^n(t)}{\epsilon + |X_{c_j}^n(t) - X_{p_k}^n(t)|} \omega(|X_{c_j}^n(t) - X_{p_k}^n(t)|, S(X_{p_k}^n(t), t)), \tag{6.22}$$

$$\tilde{\sigma}(X_t^n, t) := \kappa \beta(S(X_{p_k}^n(t), t), t). \tag{6.23}$$

Furthermore, we set

$$b(X_t^n, t) := \begin{bmatrix} F_1(X_t^n, t) \\ F_2(X_t^n, t) \end{bmatrix} \text{ and } \sigma(X_t^n, t) := \begin{bmatrix} \mathbf{o} \\ \tilde{\beta} \end{bmatrix}, \tag{6.24}$$

with

$$\mathbf{o} := \begin{bmatrix} 0 & 0 \\ 0 & 0 \end{bmatrix} \quad \text{and } \tilde{\beta} := \begin{bmatrix} \tilde{\sigma}_{11} & \tilde{\sigma}_{12} \\ \tilde{\sigma}_{21} & \tilde{\sigma}_{22} \end{bmatrix}, \tag{6.25}$$

where $\tilde{\sigma}_{IJ} := (\tilde{\sigma}(X_t^n, t))_{IJ}$ for $1 \leq I, J \leq 2$ and the initial datum is

$$X^n(0) := X_0 := \begin{bmatrix} X_{a_i,0} \\ X_{b_k,0} \end{bmatrix}. \tag{6.26}$$

We denote by $\{\Phi_t^n\}$ the associated process of $\{X_t^n\}$ as in (6.17), viz.

$$\Phi_t^n := \begin{bmatrix} \Phi_1^n(t)) \\ \Phi_2^n(t) \end{bmatrix}. \tag{6.27}$$

We use the compactness method together with the continuity result of the deterministic case stated in Theorem 6.1 for proving the existence of solutions to (6.17)-(6.18). We follow the arguments by G. Da Prato and J. Zabczyk (2014) (cf. [PZ14], Section 8.3) and a result of F. Flandoli (1995) (cf. [FG95]) for martingale solutions. The starting point of this argument is based on considering a sequence $\{X_t^n\}$ of solutions of the following system of Skorohod-like stochastic differential equations

$$\begin{cases} dX_t^n = b(X_t^n(h^n(t))dt + \sigma(X_t^n(h^n(t))dB(t) + d\Phi_t^n, \\ X^n(0) = X_0 \in \bar{D}, \end{cases} \tag{6.28}$$

where $X_0^n \in \bar{D}$ is given, and

$$h^n(0) = 0, \tag{6.29}$$

$$h^n(t) = (k-1)2^{-n}, \quad (k-1)2^{-n} < t \leq k2^{-n}, \quad k = 1, 2, \ldots, n \text{ and } n \geq 1. \tag{6.30}$$

Moreover, by Theorem 6.1, we have a unique solution of (6.28). Hence, X_t^n obtained for $0 \leq t \leq k2^{-n}$ and for $k2^{-n} < t \leq (k+1)2^{-n}$ is uniquely determined as solution of the following Skohorod equation

$$X_t^n = X_t^n(k2^{-n}) + b(X_t^n(k2^{-n}))(t - k2^{-n}) + \sigma(X_t^n(k2^{-n}))\{B(t) - B(k2^{-n})\} + \Phi_t^n. \tag{6.31}$$

Let us call

$$Y_t^n := X_0 + \int_0^t b(X_y^n(h^n(y))dy + \int_0^t \sigma(X_y^n(h^n(y))dB(y). \tag{6.32}$$

We define the family of laws

$$\{\mathcal{P}(Y_t^n); 0 \leq t \leq T, n \geq 1\}. \tag{6.33}$$

(6.33) is a family of probability distributions of Y_t^n. Let $\mathcal{P}^n$ be the laws of Y_t^n.

The compactness argument proceeds as follows. We begin with $Y_t^n, n \in \mathbb{N}$, given cf. (6.32). The construction of Y_t^n is investigated on a probability space $(\Omega, \mathcal{F}, P)$ with a filtration $\{\mathcal{F}_t\}$ and a Brownian motion $B(t)$. Next, let $\mathcal{P}^n$ be the laws of Y_t^n which is defined cf. (6.33). Then, by using Prokhorov's Theorem (cf. [Bil99], Theorem 5.1), we can show that the sequence of laws $\{\mathcal{P}^n(Y_t^n)\}$ is weakly convergent as $n \to \infty$ to $\mathcal{P}(Y_t)$ in $C(\bar{S}; \mathbb{R}^2 \times \mathbb{R}^2)$. Then, by using the "Skorohod Representation Theorem"(cf. [PZ14], Theorem 2.4), this weak convergence holds in a new probability space with a new stochastic process, for a new filtration. This leads to some arguments for weak convergence results of two stochastic processes in two different probability spaces together with the continuity result in Theorem 6.1 that we need to use to obtain the existence of our Skorohod-like system (6.17). Finally, we prove the uniqueness of solutions to our system.

6.6.3 Proof of Theorem 6.3

Let us start with handling the tightness of the laws $\{\mathcal{P}^n\}$ through the following Lemma.

Lemma 6.5. *Assume that* (A_1)-(A_5) *hold. Then, the family* $\{\mathcal{P}^n\}$ *given by* (6.33) *is tight in* $C(\bar{S}, \mathbb{R}^2 \times \mathbb{R}^2)$.

Proof. To prove the wanted tightness, let us recall the following compact set in $C(\bar{S}, \mathbb{R}^2 \times \mathbb{R}^2)$

$$K_{M_1 M_2} = \left\{ f \in C(\bar{S}; \mathbb{R}^2 \times \mathbb{R}^2) : \|f\|_{L^\infty(S;\mathbb{R}^2\times\mathbb{R}^2)} \leq M_1, [f]_{C^\alpha(\bar{S};\mathbb{R}^2\times\mathbb{R}^2)} \leq M_2 \right\}. \tag{6.34}$$

Now, we show that for a given $\varepsilon > 0$, there are $M_1, M_2 > 0$ such that

$$P(Y_\cdot^n \in K_{M_1 M_2}) \leq \varepsilon, \text{ for all } n \in \mathbb{N}. \tag{6.35}$$

This means that

$$P(\|Y_t^n\|_{L^\infty(S;\mathbb{R}^2\times\mathbb{R}^2)} > M_1 \text{ or } [Y_\cdot^n]_{C^\alpha(\bar{S};\mathbb{R}^2\times\mathbb{R}^2)} > M_2) \leq \varepsilon. \tag{6.36}$$

A sufficient condition for this to happen is

$$P(\|Y_t^n\|_{L^\infty(S;\mathbb{R}^2\times\mathbb{R}^2)} > M_1) < \frac{\varepsilon}{2} \text{ and } P([Y_\cdot^n]_{C^\alpha(\bar{S};\mathbb{R}^2\times\mathbb{R}^2)} > M_2) < \frac{\varepsilon}{2}, \tag{6.37}$$

where $Y_\cdot$ denotes either Y_t or Y_r.

We consider first $P(\|Y_\cdot^n\|_{L^\infty(S,\mathbb{R}^2\times\mathbb{R}^2)} > M_1) < \frac{\varepsilon}{2}$. Using Markov's inequality (see e.g. [JP04], Corollary 5.1), we get

$$P(\|Y_t^n\|_{L^\infty(S;\mathbb{R}^2\times\mathbb{R}^2)} > M_1) \leq \frac{1}{M_1} E[\sup_{t\in S} |Y_t^n|], \tag{6.38}$$

but

$$\begin{aligned} \sup_{t\in S} |Y_t^n| = \sup_{t\in S} \Bigg\{ & \left| X_{a_i,0} + \int_0^t F_1(X_y^n(h^n(y)))dy \right| \\ & , \left| X_{p_k,0} + \int_0^t F_2(X_y^n(h^n(y)))dy + \int_0^t \sigma(X_y^n(h^n(y)))dB(y) \right| \Bigg\}. \end{aligned} \tag{6.39}$$

We estimate

$$\begin{aligned} \sup_{t\in S} |Y_t^n| = \sup_{t\in S} \Bigg\{ & |X_{a_i,0}| + \left| \int_0^t F_1(X_y^n(h^n(y)))dy \right| \\ & , |X_{p_k,0}| + \left| \int_0^t F_2(X_y^n(h^n(y)))dy \right| + \left| \int_0^t \sigma(X_y^n(h^n(y)))dB(y) \right| \Bigg\}. \end{aligned} \tag{6.40}$$

Since F_1, F_2 are bounded, then we have

$$\int_0^T F_1(X_y^n(h^n(y)))dy \leq C \text{ and } \int_0^T F_2(X_y^n(h^n(y)))dy \leq C. \tag{6.41}$$

Taking the expectation on (6.40), we are led to

$$E\left[\sup_{t\in S}|Y_t^n|\right] \leq C + E\left[\sup_{t\in S}\left|\int_0^t \sigma(X_y^n(h^n(y)))dB(y)\right|\right]. \tag{6.42}$$

On the other hand, the Burlkholder-Davis-Gundy's inequality [1] implies

$$E\left[\sup_{t\in S}\left|\int_0^t \sigma(X_y^n(h^n(y)))dB(y)\right|\right] \leq E\left[\int_0^t |\sigma(X_y^n(h^n(y)))|^2 dy\right]^{1/2}. \tag{6.43}$$

Then, we have the following estimate

$$E\left[\sup_{t\in S}|Y_t^n|\right] \leq C + E\left[\int_0^t |\sigma(X_y^n(h^n(y)))|^2 dy\right]^{1/2} \leq C \tag{6.44}$$

Hence, for $\varepsilon > 0$, we can choose $M_1 > 0$ such that $P(\|Y_t^n\|_{L^\infty(S;\mathbb{R}^2\times\mathbb{R}^2)} > M_1) < \frac{\varepsilon}{2}$.

In the sequel, we consider the second inequality $P([Y_\cdot^n]_{C^\alpha(\bar{S};\mathbb{R}^2\times\mathbb{R}^2)} > M_2) < \frac{\varepsilon}{2}$, this reads

$$P([Y_\cdot^n]_{C^\alpha(\bar{S};\mathbb{R}^2\times\mathbb{R}^2)} > M_2) = P\left(\sup_{t\neq r;t,r\in S}\frac{|Y_t^n - Y_r^n|}{|t-r|^\alpha} > M_2\right) \leq \frac{\varepsilon}{2}. \tag{6.45}$$

Let us introduce another class of compact sets now in the Sobolev space $W^{\alpha,p}(0,T;\mathbb{R}^2\times\mathbb{R}^2)$ (which for suitable exponents $\alpha p - \gamma > 1$ lies in $C^\gamma(\bar{S};\mathbb{R}^2\times\mathbb{R}^2)$). Additionally, we recall the relatively compact sets $K'_{M_1M_2}$, defined as in Section 6.4, such that

$$K'_{M_1M_2} = \left\{f \in C(\bar{S};\mathbb{R}^2\times\mathbb{R}^2) : \|f\|_{L^\infty(S;\mathbb{R}^2\times\mathbb{R}^2)} \leq M_1, [f]_{W^{\alpha,p}(S;\mathbb{R}^2\times\mathbb{R}^2)} \leq M_2\right\}. \tag{6.46}$$

A sufficient condition for $K'_{M_1M_2}$ to be a relative compact underlying space is $\alpha p > 1$ (see e.g. [FG95], [CMRT19]). Having this in mind, we wish to prove that there exits $\alpha \in (0,1)$ and $p > 1$ with $\alpha p > 1$ together with the property: given $\varepsilon > 0$, there is $M_2 > 0$ such that

$$P([Y_\cdot^n]_{W^{\alpha,p}(S;\mathbb{R}^2\times\mathbb{R}^2)} > M_2) < \frac{\varepsilon}{2} \text{ for every } n \in \mathbb{N}. \tag{6.47}$$

[1] See e.g. [KS00], Theorem 3.28 (The Burlkholder-Davis-Gundy's inequality). Let $M \in \mathcal{M}^{c,\text{loc}}$ and call $M_t^* := \max_{0\leq s\leq t}|M_s|$. For every $m > 0$, there exists universal positive constants k_m, K_m (depending only on m), such that the inequalities

$$k_m E(\langle M\rangle_T^m \leq E[(M_T^*)^{2m}] \leq K_m E(\langle M\rangle_T^m)$$

hold for every stopping time T. Note that $\mathcal{M}^{c,\text{loc}}$ denotes the space of continuous local martingales and $\langle X\rangle$ represents the quadratic variance process of $X \in \mathcal{M}^{c,\text{loc}}$.

Using Markov's inequality, we obtain

$$P([Y_\cdot^n]_{W^{\alpha,p}(S;\mathbb{R}^2\times\mathbb{R}^2)} > M_2) \leq \frac{1}{M_2} E\left[\int_0^T \int_0^T \frac{|Y_t^n - Y_r^n|^p}{|t-r|^{1+\alpha p}} dtdr\right]$$
$$= \frac{C}{M_2}\int_0^T \int_0^T \frac{E[|Y_t^n - Y_r^n|^p]}{|t-r|^{1+\alpha p}} dtdr. \tag{6.48}$$

For $t > r$, we have

$$Y_t^n - Y_r^n = \begin{bmatrix} \int_r^t F_1(X_y^n(h^n(y)))dy \\ \int_r^t F_2(X_y^n(h^n(y)))dy \end{bmatrix} + \begin{bmatrix} 0 \\ \int_r^t \sigma(X_y^n(h^n(y)))dB(y) \end{bmatrix}. \tag{6.49}$$

Let us introduce some further notation. For a vector $u = (u_1, u_2)$, we set $|u| := |u_1| + |u_2|$. At this moment, we consider the following expression

$$|Y_t^n - Y_r^n| = \left|\int_r^t F_1(X_y^n(h^n(y)))dy\right|$$
$$+ \left|\int_r^t F_2(X_y^n(h^n(y)))dy + \int_r^t \sigma(X_y^n(h^n(y)))dB(y)\right|. \tag{6.50}$$

Taking the modulus up to the power $p > 1$ together with applying Minkowski inequality, we have

$$|Y_t^n - Y_r^n|^p = \Bigg(\left|\int_r^t F_1(X_y^n(h^n(y)))dy\right|$$
$$+ \left|\int_r^t F_2(X_y^n(h^n(y)))dy + \int_r^t \sigma(X_y^n(h^n(y)))dB(y)\right| \Bigg)^p$$
$$\leq C\Bigg(\left|\int_r^t F_1(X_y^n(h^n(y)))dy\right|^p$$
$$+ \left|\int_r^t F_2(X_y^n(h^n(y)))dy\right|^p + \left|\int_r^t \sigma(X_y^n(h^n(y)))dB(y)\right|^p \Bigg)$$
$$\leq C\Bigg(\int_r^t |F_1(X_y^n(h^n(y)))|^p dy + \int_r^t |F_2(X_y^n(h^n(y)))|^p dy$$
$$+ \left|\int_r^t \sigma(X_y^n(h^n(y)))dB(y)\right|^p \Bigg). \tag{6.51}$$

Taking the expectation on (6.51), we obtain the following estimate

$$E[|Y_t^n - Y_r^n|^p] \leq C(t-r)^p + CE\left[\left|\int_r^t \sigma(X_y^n(h^n(y)))dB(y)\right|^p\right]. \tag{6.52}$$

Applying the Burkholder-Davis-Gundy's inequality to the second term of the right hand side of (6.52), we obtain

$$E\left[\left|\int_r^t \sigma(X_y^n(h^n(y)))dB(y)\right|^p\right] \leq CE\left[\left(\int_r^t dy\right)^{p/2}\right] \leq C(t-r)^{p/2}. \tag{6.53}$$

On the other hand, if $\alpha < \frac{1}{2}$, then

$$\int_0^T \int_0^T \frac{1}{|t-r|^{1+(\alpha-\frac{1}{2})p}} dtdr < \infty. \tag{6.54}$$

Consequently, we can pick $\alpha < \frac{1}{2}$. Taking now $p > 2$ together with the constraint $\alpha p > 1$, we can find $M_2 > 0$ such that

$$P([Y_t^n]_{W^{\alpha,p}(S;\mathbb{R}^2\times\mathbb{R}^2)} > M_2) < \frac{\varepsilon}{2}. \tag{6.55}$$

This argument completes the proof of this Lemma. □

From Lemma 6.5, we have obtained that the sequence $\{\mathcal{P}^n\}$ is tight in $C(\bar{S};\mathbb{R}^2\times\mathbb{R}^2)$. Applying the Prokhorov's Theorem, there are subsequences $\{\mathcal{P}^{n_k}\}$ which converge weakly to some $\mathcal{P}(Y_t)$ as $n \to \infty$. For simplicity of the notation, we denote these subsequences by $\{\mathcal{P}^n\}$. This means that we have $\{\mathcal{P}^n\}$ converging weakly to some probability measure $\mathcal{P}$ on Borel sets in $C(\bar{S};\mathbb{R}^2\times\mathbb{R}^2)$.

Since we have that $\mathcal{P}^n(Y_t^n)$ converges weakly to $\mathcal{P}(Y_t)$ as $n \to \infty$, by using the "Skorohod Representation Theorem", there exists a probability space $(\tilde{\Omega}, \tilde{\mathcal{F}}, \tilde{P})$ with the filtration $\{\tilde{\mathcal{F}}_t\}$ and $\tilde{Y}_t^n$, $\tilde{Y}_t$ belonging to $C(\bar{S};\mathbb{R}^2\times\mathbb{R}^2)$ with $n \in \mathbb{N}$, such that $\mathcal{P}(\tilde{Y}) = \mathcal{P}(Y)$, $\mathcal{P}(\tilde{Y}_t^n) = \mathcal{P}(Y_t^n)$, and $\tilde{Y}_t^n \to \tilde{Y}_t$ as $n \to \infty$, $\tilde{P}-$a.s. Moreover, let $(\tilde{X}_t^n, \tilde{\Phi}_t^n)$ and $(\tilde{X}_t, \tilde{\Phi}_t)$ be the solutions of the Skorohod equations

$$\begin{aligned} \tilde{X}_t^n &= \tilde{Y}_t^n + \tilde{\Phi}_t^n, \\ \tilde{X}_t &= \tilde{Y}_t + \tilde{\Phi}_t, \end{aligned} \tag{6.56}$$

respectively. Then the continuity result in Theorem 6.1 implies that the sequence $(\tilde{X}_t^n, \tilde{\Phi}_t^n)$ converges to $(\tilde{X}_t, \tilde{\Phi}_t) \in C(\bar{S};\bar{D}\times\bar{D})\times C(\bar{S})$ uniformly in $t \in \bar{S}$, $\tilde{P}-$a.s as $n \to \infty$. Hence, we still need to prove that $\tilde{Y}_t^n$ converges to $\tilde{Y}_t$ in some sense, where we denote

$$\tilde{Y}_t^n := \tilde{X}_0 + \int_0^t b(\tilde{X}_y^n(h_n(y))dy + \int_0^t \sigma(\tilde{X}_y^n(h_n(y))d\tilde{B}(y). \tag{6.57}$$

and

$$\tilde{Y}_t := \tilde{X}_0 + \int_0^t b(\tilde{X}_y^n((y))dy + \int_0^t \sigma(\tilde{X}_y^n((y))d\tilde{B}(y). \tag{6.58}$$

To complete the proof of the existence of solutions to the problem (6.17)-(6.18) in the sense of Definition 6.2, we consider the following Lemma.

Lemma 6.6. *The pair* $(\tilde{X}_t, \tilde{\Phi}_t) \in C(\bar{S}; \bar{D} \times \bar{D}) \times C(\bar{S})$ *cf.* (6.56) *is a solution of the Skorohod-like system*

$$\tilde{X}_t = \tilde{X}_0 + \int_0^t b(\tilde{X}_y(y))dy + \int_0^t \sigma(\tilde{X}_y(y))d\tilde{B}(y) + \tilde{\Phi}_t, \tag{6.59}$$

with $\tilde{X}_0 \in \bar{D}$.

Proof. We consider the term $\int_0^t \sigma(\tilde{X}_t^n(h_n(y))d\tilde{B}(y)$ with the step process $\sigma(\tilde{X}_t^n(h_n(y))$. Approximating this stochastic integral by Riemann-Stieltjes sums (see e.g. [Eva13]), it yields

$$\int_0^t \sigma(\tilde{X}_y^n(h_n(y))d\tilde{B}(y) = \sum_{k=0}^{n-1} \sigma(\tilde{X}_t^n(h_n(t)))(B(t_{k+1}^n) - B(t_k^n)). \tag{6.60}$$

This gives by taking the limit $n \to \infty$ in (6.60)

$$\begin{aligned}\lim_{n\to\infty} \int_0^t \sigma(\tilde{X}_y^n(h_n(y))d\tilde{B}(y) &= \lim_{n\to\infty} \sum_{k=0}^{n-1} \sigma(\tilde{X}_t^n(h_n(t)))(B(t_{k+1}^n) - B(t_k^n)) \\ &= \sum_{k=0}^{n-1} \sigma(\tilde{X}_t(t))(B(t_{k+1}) - B(t_k)) = \int_0^t \sigma(\tilde{X}_y(y))d\tilde{B}(y). \end{aligned} \tag{6.61}$$

By the fact that $(\tilde{X}_t^n, \tilde{\Phi}_t^n)$ converges to $(\tilde{X}_t, \tilde{\Phi}_t) \in C(\bar{S}; \bar{D} \times \bar{D}) \times C(\bar{S})$ uniformly in $t \in [0, T]$ $\tilde{P}-$a.s as $n \to \infty$ together with (6.61), we obtain that

$$\tilde{X}_t^n = \tilde{X}_0 + \int_0^t b(\tilde{X}_y^n(h^n(y)))dy + \int_0^t \sigma(\tilde{X}_y^n(h^n(y)))d\tilde{B}(y) + \tilde{\Phi}_t^n. \tag{6.62}$$

converges to

$$\tilde{X}_t = \tilde{X}_0 + \int_0^t b(\tilde{X}_y(y))dy + \int_0^t \sigma(\tilde{X}_y(y))d\tilde{B}(y) + \tilde{\Phi}_t, \quad \tilde{P} - \text{a.s as } n \to \infty. \tag{6.63}$$

□

Proof of Theorem 6.4

Proof. We take $X_t, X_t' \in C(\bar{S}; \bar{D} \times \bar{D})$ two solutions to (6.17)-(6.18) with the same initial values $X(0) = X'(0)$.

Moreover, suppose that the supports of b and σ is included in the ball $B(x_0, \delta)$ for some $x_0 \in \partial D$. We use the proof idea of the Lemma 5.3 in [Sai87]. Let us recall the assumption (A_8), where D satisfies the following condition: It exists a positive number ν such that for each $x_0 \in \partial D$ we can find $f \in C^2(\mathbb{R}^2 \times \mathbb{R}^2)$ satisfying

$$\langle y - x, \mathbf{n}\rangle + \frac{1}{\nu}\langle \nabla f(x), \mathbf{n}\rangle |y - x|^2 \geq 0.$$

for any $x \in B(x_0, \delta') \cap \partial D, y \in B(x_0, \delta'') \cap \partial \bar{D}$ and $\mathbf{n} \in \mathcal{N}_x$. Then, we have

$$\begin{aligned}\langle X_s - X'_s, d\Phi_s - d\Phi'_s\rangle - \frac{1}{\nu}|X_s - X'_s|^2\langle \mathbf{l}, d\Phi_s - d\Phi'_s\rangle \\ = -(\langle X_s - X'_s, d\Phi_s\rangle + \frac{1}{\nu}|X_s - X'_s|^2\langle \mathbf{l}, d\Phi_s\rangle) \\ -(\langle X_s - X'_s, d\Phi'_s\rangle + \frac{1}{\nu}|X_s - X'_s|^2\langle \mathbf{l}, d\Phi'_s\rangle) \leq 0, \end{aligned} \tag{6.64}$$

where $\mathbf{l}$ is the unit vector appearing in Condition (A_7).

Using similar ideas as in [Lio84], Proposition 4.1, we have the following estimate

$$\begin{aligned}&|X_t - X'_t|^2 \exp\left\{-\frac{1}{\nu}(\Phi(X_t) - \Phi'(X_t))\right\} \leq \\ &2\Bigg(\exp\left\{-\frac{1}{\nu}(\Phi(X_y) - \Phi'(X_y))\right\} \int_0^t (b(X_y(y)) - b(X'_y(y)))dy \\ &+ \exp\left\{-\frac{1}{\nu}(\Phi(X_y) - \Phi'(X_y))\right\} \int_0^t (\sigma(X_y(y)) - \sigma(X_y(y)))dB(y)\Bigg)^2 \\ &+ \exp\left\{-\frac{1}{\nu}(\Phi(X_y) - \Phi'(X_y))\right\} \int_0^t \left(2\langle X_y - X'_y, l\rangle - \frac{1}{\nu}|X_y - X'_y|^2\right) d\Phi_y \\ &+ \exp\left\{-\frac{1}{\nu}(\Phi(X_y) - \Phi'(X_y))\right\} \int_0^t \left(2\langle X_y - X'_y, l\rangle - \frac{1}{\nu}|X_y - X'_y|^2\right) d\Phi'_y \\ &2\int_0^t \left|b(X_y(y)) - b(X'_y(y))\right|^2 \exp\left\{-\frac{2}{\nu}(\Phi(X_y) - \Phi'(X_y))\right\} dy \\ &+ 2\int_0^t |\sigma(X_y(y)) - \sigma(X_y(y))|^2 \exp\left\{-\frac{2}{\nu}(\Phi(X_y) - \Phi'(X_y))\right\} dy \\ &+ \int_0^t \left(2\langle X_y - X'_y, l\rangle - \frac{1}{\nu}|X_y - X'_y|^2\right) \exp\left\{-\frac{1}{\nu}(\Phi(X_y) - \Phi'(X_y))\right\} d\Phi_y \\ &+ \int_0^t \left(2\langle X_y - X'_y, l\rangle - \frac{1}{\nu}|X_y - X'_y|^2\right) \exp\left\{-\frac{1}{\nu}(\Phi(X_y) - \Phi'(X_y))\right\} d\Phi'_y. \end{aligned} \tag{6.65}$$

On the other hand, taking the expectation are both sides of (6.65) and using the Lipschitz condidion to the first term of the right hand side together with (6.64), we are led to

$$\begin{aligned}E\left(|X_t - X'_t|^2 \exp\left\{-\frac{1}{\nu}(\Phi(X_t) - \Phi'(X_t))\right\}\right) \leq \\ C\int_0^t E\Big(|X_y - X'_y|^2 \exp\left\{-\frac{2}{\nu}(\Phi(X_y) - \Phi'(X_y))\right\}\Big)dy. \end{aligned} \tag{6.66}$$

This also implies that

$$E[|X_t - X'_t|^2] \leq C \int_0^t E[|X_y - X'_y|^2]dy. \tag{6.67}$$

Hence, $X_t = X'_t$ for all $t \in [0, T]$. Then, the pathwise uniqueness of solutions to (6.17) holds true. On the other hand, combining the Lemma 6.6 together with the fact that the pathwise uniqueness implies the uniqueness of strong solutions (see in [IW81], Theorem IV-1.1). Therefore, there is a unique solution $(X_t, \Phi_t) \in C(\bar{S}; \bar{D} \times \bar{D}) \times C(\bar{S})$ of (6.17). □

Remark 6.7. *What concerns the stability with respect to data and parameters of our concept of solution to the Skorohod-like system, we can show the stability with respect to the initial data via standard arguments (see e.g. [Eva13]). However, more work is needed, for instance in terms of energy-like estimates, to prove the structural stability with respect to the model nonlinearities and coefficients as there are no general known results in this direction. We expect however our problem to be well-posed in Hadamard's sense.*

6.7 Discussion

In this chapter, we have shown the existence and uniqueness of solutions to a system of Skorohod-like stochastic differential equations modeling the dynamics of a mixed population of active and passive pedestrians walking within a heterogenous environment in the presence of a stationary fire. Due to the discomfort pressure term as well as to the Morse potential preventing particles (pedestrians) to overlap, our model is nonlinearly coupled. The main feature of the model is that the dynamics of the crowd takes place in an heterogeneous domain, i.e. obstacles hinder the motion. Hence, to allow the SDEs to account for the presence of the obstacles, we formulate our crowd dynamics scenario as a Skorohod-like system with reflecting boundary condition posed in a bounded domain in $\mathbb{R}^2$. Then we use compactness methods to prove the existence of solutions. The uniqueness of solutions follows by standard arguments.

There are a number of open issues that are worth to be investigated for our system:

1. To obtain a better insight on how the solution of the SDEs behaves and how close is this behaviour to what is expected from standard evacuation scenarios, a convergent numerical approximation of solutions to (6.17)-(6.18) needs to be implemented. One possible route is to design an iterative weak approximation of the Skorohod system as it is done e.g. in [BGT04], [NO10], and in the references cited therein. The main challenge is to get fast and accurate numerical approximation of solutions so that an efficient parameter identification strategy can be proposed.

2. We did assume that the fire is a stationary obstacle, i.e. ∂F is independent on t. But, even if not evolving, this fire-obstacle should in fact have a time

dependent boundary. Using the working technique from [NO10], we expect that it is possible to handle the case of a time-evolving fire, provided the shape of the fire $\partial F(t)$ is sufficiently regular, fixed in space, and *a priori* prescribed.

3. From a mathematical point of view, the situation becomes a lot more challenging when there is a feedback mechanism between the pedestrian dynamics and the environment (fire and geometry). Empirically, such pedestrians-environment feedback was pointed out in [RN19]. An extension can be done in this context using the smoke observable $s(x,t)$. As a further development of our model, we intend to incorporate the "transport" of smoke eventually via a measure-valued equation (cf. e.g. [EHM16]), coupled with our SDEs for the pedestrian dynamics. In this case, besides the well-posedness question, it is interesting to study the large-time behavior of the system of evolution equations. Instead of a measure-valued equation for the smoke dynamics, one could also use a stochastically perturbed diffusion-transport equation. In this case, the approach from [CJK18] is potentially applicable, provided the coupling between the SDEs for the crowd dynamics and the SPDE for the smoke evolution is done in a well-posed manner. However, in both cases, it is not yet clear cut how to couple correctly the model equations.

4. From the modeling point of view, it would be very useful to find out to which extent the motion of active particles can affect the motion of passive particles so that the overall evacuation time is reduced. Note that our crowd dynamics context does not involve leaders, and besides the social pressure and the repelling from overlapping, there are no other imposed interactions between pedestrians. In this spirit, we are close to the setting described in [CTB$^+$18], where active and passive particles interplay together to find exists in a maze. Further links between maze-solving strategies and our crowd dynamics scenario would need to be identified to make progress in this direction.

5. Another interesting perspective would be to investigate systems of SDEs of mean-field type that model pedestrian motion. Based on the very recent work [AD20], it seems to be possible to consider a mean-field approach to our system of SDEs of Skorohod type where the pedestrians spend time at and move along walls by means of sticky boundaries and boundary diffusion.

6. It would be interesting to consider a hydrodynamic limit of our system of SDEs of Skorohod type to obtain a continuum system of PDEs. To study such PDEs, the boundary conditions need to be specific. For instance, in [FK17], there is an attempt to set boundary conditions for a swarming model in a continuum setup.

Chapter 7

On a pore-scale stationary diffusion equation: Scaling effects and correctors for the homogenization limit

In this chapter, we consider a microscopic semilinear elliptic equation posed in periodically perforated domains and associated with the Fourier-type condition on internal micro-surfaces. The first contribution of this work is the construction of a reliable linearization scheme that allows us, by a suitable choice of scaling arguments and stabilization constants, to prove the weak solvability of the microscopic model. Asymptotic behaviors of the microscopic solution with respect to the microscale parameter are thoroughly investigated in the second theme, based upon several cases of scaling. In particular, the variable scaling illuminates the trivial and non-trivial limits at the macroscale, confirmed by certain rates of convergence. Relying on classical results for homogenization of multiscale elliptic problems, we design a modified two-scale asymptotic expansion to derive the corresponding macroscopic equation, when the scaling choices are compatible. Moreover, we prove the high-order corrector estimates for the homogenization limit in the energy space H^1, using a large amount of energy-like estimates. A numerical example is provided to corroborate the asymptotic analysis. This is based on [KTI20].

7.1 Introduction

7.1.1 Background and statement of the problem

We assume that a porous medium $\Omega^\varepsilon \subset \mathbb{R}^d$ ($d \in \mathbb{N}^*$) possesses a uniformly periodic microstructure whose length scale is defined by a small parameter (microscale parameter) $0 < \varepsilon \ll 1$. In practice, ε is defined as the ratio of the characteristic length of the microstructure to a characteristic macroscopic length. In this chap-

ter, the porous medium of interest contains a large amount of very small holes and thus can be viewed as a perforated domain. Largely inspired by [KMK15], our work aims at understanding the spread of concentration of colloidal particles $u_\varepsilon : \Omega^\varepsilon \to \mathbb{R}$ in a saturated porous tissue Ω^ε with a cubic cell $Y = [0,1]^d$. This kind of tissues can be illustrated in Figure 7.1 as a schematic representation of a natural soil. Since the constitutive properties of the microstructure repeat periodically, the molecular diffusion coefficient $\mathbf{A} : Y \to \mathbb{R}^{d\times d}$ is assumed to vary in the cell or in a material point $x \in \Omega^\varepsilon$. Accordingly, it can be expressed as $\mathbf{A}(x/\varepsilon)$. We consider the presence of a volume reaction $\mathcal{R} : \mathbb{R} \to \mathbb{R}$ combined with an internal source $f : \Omega^\varepsilon \to \mathbb{R}$. Moreover, we also consider a chemical reaction $\mathcal{S} : \mathbb{R} \to \mathbb{R}$ for the immobile species along with deposition coefficients at the internal boundaries, denoted by Γ^ε. On the other hand, the colloidal species stay constant at the exterior boundary, denoted by Γ^{ext}. Mathematically, the governing equations describing this process is given by

$$(P_\varepsilon) : \begin{cases} \nabla \cdot (-\mathbf{A}(x/\varepsilon)\nabla u_\varepsilon) + \varepsilon^\alpha \mathcal{R}(u_\varepsilon) = f(x) & \text{in } \Omega^\varepsilon, \\ -\mathbf{A}(x/\varepsilon)\nabla u_\varepsilon \cdot \mathrm{n} = \varepsilon^\beta \mathcal{S}(u_\varepsilon) & \text{across } \Gamma^\varepsilon, \\ u_\varepsilon = 0 & \text{across } \Gamma^{\text{ext}}. \end{cases}$$

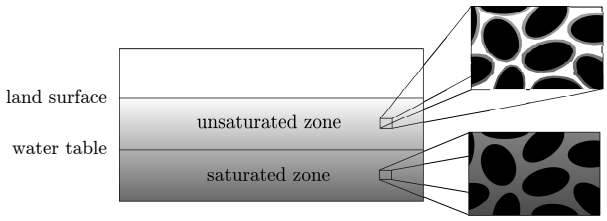

Figure 7.1: A schematic representation of a natural soil. The figure is followed from [Ray13].

Typically, the prototypical problem (P_ε) forms the standard model for diffusion, aggregation and surface deposition of a concentration in a porous and highly heterogeneous medium; cf. [HJ91, KAM14, KMK15]. Starting from the heat conduction problem in composite materials with inclusions (cf. [CJ99]), much of the current literature on the analysis of this elliptic model pays meticulous attention to different contexts involving rigorous mathematical treatments, physical modelling (e.g., [DHS16, SPPK12, GM18]) and numerical standpoints (e.g., [VS06]). Especially, understanding the asymptotic behaviors of solution of (P_ε) is essential in the studies of the classical spectral problems as investigated in, e.g., [CM12, Mel95].

7.1.2 Main goals

It is well known that due to the fast oscillation in the diffusion coefficient $\mathbf{A}(x/\varepsilon)$, the number of mesh-points at any discretization level is of the order ε^{-d}, which consequently reveals a huge complexity of computations as $\varepsilon \searrow 0^+$. Therefore,

when dealing with such multiscale problems, one usually targets the upscaled models where the oscillation is no longer involved, using different techniques of asymptotic analysis with respect to ε. In this work, our main finding is to point out the trivial and non-trivial macroscopic models, depending on every single case of α and β. Note that the major mathematical challenge we meet here is that α, β are real constants. We mention some physical implications of these parameters, although these variable scalings stem from our mathematical interest. The case $\alpha < 0$ and $\beta > 0$ implies that the volume reaction is large, while the surface reaction of the concentration is slow. Thus, u_ε can be expected to be slowly changing on Γ^ε. When $\alpha < 0$ and $\beta > 0$, we have a dominant surface reaction and the volume reaction is negligible. Meanwhile, on Γ^ε, this means that u_ε is rapidly changing. As to the literature on this topic, the reader can be referred to [RMK12, Ray13, KM19, FRK11, RvNFK12], where the variable scaling has been considered earlier in complex diffusion problems of charged colloidal particles. Besides, the case $\alpha > 0$ can be related to the context of low-cost control problems on perforated domains in [MN09].

The variable scaling not only requires a careful adaptation of classical homogenization results for elliptic problems, but also needs a particular investigation into the macroscopic problems obtained after the homogenization limit. When the limit function is non-trivial, we particularly design a new asymptotic expansion, which is needed by the presence of the scaling parameters. Aside from the derivation of the macroscopic problem, we delve into having the high-order corrector estimates, driven by a large amount of energy estimates. In the same manner, rates of convergence to the trivial limit function are under scrutiny. As the inception stage of this asymptotic analysis, we only focus on the speed of convergence when $\varepsilon \searrow 0^+$, while the regularity assumptions may not be minimal.

The high-order corrector estimates we prove in this chapter are involving the presence of the scaling parameters. This is the extended follow-up result of our earlier works [KM16a, KM16b, Kho17], where we wish to estimate the differences between micro–macro concentrations and micro–macro concentration gradients in the energy space of perforated domains. It is also in the same line with the theoretical findings in [KL18, CP99, AGK16, AA99, OV07, OV12, Gri04]. Our preceding works show that the macroscopic problem can be self-linear, albeit the semilinear microscopic problem. We find that this is caused by the scaled structure of the involved nonlinear reaction, which sometimes leads to the self-iterative auxiliary problems. However, there are somehow the cases that the auxiliary problems remain semilinear and thus, the fixed-point homogenization argument is required.

Another novelty we present here is the exploration of a linearization scheme for (P_ε) under a scaled Hilbert space. This scheme not only proves the weak solvability of (P_ε), but also provides an insight to expect the asymptotic analysis, due to the *a priori* estimates we obtain after the iteration limit. As far as the linearization-based algorithm is concerned, it has been profoundly developed for a long time in numerical methods for nonlinear PDEs. It is worth mentioning that the Jäger–Kačur scheme (see, e.g., [Kač99]) was investigated as the very first

contribution in this branch. It plays a vital role in solving some classes of one-dimensional parabolic problems, but it is not really effective in high dimensions. Using the same idea, Long et al. [LDD02] rigorously proved the local existence and uniqueness of a weak solution of a Kirchoff–Carrier wave equation in one-dimension. We also recall the linearization by the monotonicity of iterations, for example, introduced in the monograph [Pao93] involving the concepts of *sub-* and *super-solution*. However, its drawback comes from the way the initial loop is chosen, which must be far away from the true solution, whilst in general it can be taken by the already known initial or boundary information.

7.1.3 Outline

Our chapter is structured as follows. In Section 7.2, we provide the essential notation and working assumptions on data used in the analysis. In Section 7.3, we design a linearization scheme to prove the weak solvability of the microscopic model, where the main result in this part is stated in Theorem 7.5. In Section 7.4, we design several two-scale asymptotic expansions, corresponding to some particular microscopic models contained in (P_ε). Accordingly, we obtain distinctive convergence results. We conclude this paper by some numerical discussions included in Section 7.4.3.

7.2 Preliminaries

7.2.1 Geometrical description of a perforated medium

Let Ω be a bounded, open and connected domain in $\mathbb{R}^d$ with a Lipschitz boundary. Typically, we can consider it as a reservoir in three dimensions. Now, let Y be the unit cell defined by

$$Y := \left\{ \sum_{i=1}^{d} \lambda_i \vec{e}_i : 0 < \lambda_i < 1 \right\},$$

where $\vec{e}_i$ denotes the ith unit vector in $\mathbb{R}^d$. In addition, we assume that this cell is made up of two open sets: Y_l – the liquid part and Y_s – the solid part which is impermeable to solute concentrations satisfy $\bar{Y}_l \cup \bar{Y}_s = \bar{Y}$ and $Y_l \cap Y_s = \emptyset, \bar{Y}_l \cap \bar{Y}_s = \Gamma$ possessing a non-zero $(d-1)$-dimensional measure. On the other hand, suppose that the solid part Y_s stays totally inside in the cell Y, i.e. it does not intersect the cell's boundary ∂Y. Consequently, the liquid part Y_l is connected.

Let $Z \subset \mathbb{R}^d$ be a hypercube. For $X \subset Z$ we denote by X^k the shifted subset

$$X^k := X + \sum_{i=1}^{d} k_i \vec{e}_i,$$

where $k = (k_1, ..., k_d) \in \mathbb{Z}^d$ is a vector of indices.

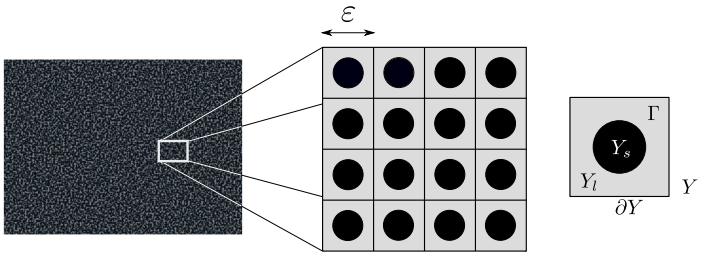

Figure 7.2: A schematic representation of the scaling procedure within a natural soil and the corresponding sample periodically perforated domain with its unit cell.

We scale this reservoir by a parameter $\varepsilon > 0$ which represents the ratio of the cell size to the size of the whole reservoir. Often, this scale factor is small. We further assume that Ω is completely covered by a regular mesh consisting of three ε-scaled and shifted cells: the scaled liquid, solid parts and boundary. More precisely, the solid part is defined as the union of the cell regions εY_s^k, i.e.

$$\Omega_0^\varepsilon := \bigcup_{k\in\mathbb{Z}^d} \varepsilon Y_s^k,$$

while the liquid part is given by

$$\Omega^\varepsilon := \bigcup_{k\in\mathbb{Z}^d} \varepsilon Y_l^k,$$

and we denote the micro-surface by $\Gamma^\varepsilon := \partial\Omega_0^\varepsilon$.

Note that we now assume $\partial\Omega \equiv \Gamma^{\text{ext}}$ and our perforated domain Ω^ε is bounded, connected and possesses C^2-internal boundary. We also denote throughout this paper $\mathrm{n} := (n_1, ..., n_d)$ as the unit outward normal vector on the boundary Γ^ε. In Figure 7.2, we show an illustration of scales from a soil structure and the perforated domain with its unit cell. The representation of the periodic geometries is in line with [KM16a, RMK12] and references therein.

7.2.2 Notation and assumptions on data

We denote by $x \in \Omega^\varepsilon$ the macroscopic variable and by $y = x/\varepsilon$ the microscopic variable representing fast variations at the microscopic geometry. With this convention, we write $\mathbf{A}(x/\varepsilon) = \mathbf{A}_\varepsilon(x) = \mathbf{A}(y)$. Let us define the function space

$$V^\varepsilon := \{v \in H^1(\Omega^\varepsilon) | v = 0 \text{ on } \Gamma^{\text{ext}}\},$$

which is a closed subspace of the Hilbert space $H^1(\Omega^\varepsilon)$, and thus endowed with the semi-norm

$$\|v\|_{V^\varepsilon} := \left(\sum_{i=1}^d \int_{\Omega^\varepsilon} \left|\frac{\partial v}{\partial x_i}\right|^2 dx\right)^{1/2} \text{ for all } v \in V^\varepsilon.$$

Obviously, this norm is equivalent (uniformly in ε) to the usual H^1-norm by the Poincaré inequality (cf. [CJ99, Lemma 2.1]).

Let us define the function space $\mathcal{W}_\varepsilon := L^2(\Gamma^\varepsilon) \cap L^2(\Omega^\varepsilon)$ with the inner product

$$\langle u, v\rangle_{\mathcal{W}_\varepsilon} := \langle u, v\rangle_{L^2(\Gamma^\varepsilon)} + \langle u, v\rangle_{L^2(\Omega^\varepsilon)} \qquad \text{for } u, v \in \mathcal{W}_\varepsilon,$$

and with the corresponding norm $\|u\|^2_{\mathcal{W}_\varepsilon} := \|u\|^2_{L^2(\Gamma^\varepsilon)} + \|u\|^2_{L^2(\Omega^\varepsilon)}$. Then for each $\varepsilon > 0$ we introduce the function space $\widetilde{\mathcal{W}}_\varepsilon$ equipped with the following inner product

$$\langle u, v\rangle_{\widetilde{\mathcal{W}}_\varepsilon} := \langle \nabla u, \nabla v\rangle_{L^2(\Omega^\varepsilon)} + (\varepsilon^\alpha + \varepsilon^\beta)\langle u, v\rangle_{\mathcal{W}_\varepsilon} \quad \text{ for } u, v \in \widetilde{\mathcal{W}}_\varepsilon,$$

and the corresponding norm is given by $\|u\|^2_{\widetilde{\mathcal{W}}_\varepsilon} := \|\nabla u\|^2_{L^2(\Omega^\varepsilon)} + (\varepsilon^\alpha + \varepsilon^\beta)\|u\|^2_{\mathcal{W}_\varepsilon}$. This space can be considered as the intersection between V^ε and the ε-scaled $\mathcal{W}_\varepsilon$. Hereby, $\widetilde{\mathcal{W}}_\varepsilon$ is a Hilbert space.

We introduce a bilinear form $a : \widetilde{\mathcal{W}}_\varepsilon \times \widetilde{\mathcal{W}}_\varepsilon \to \mathbb{R}$ by

$$a(u, \varphi) := \int_{\Omega^\varepsilon} \mathbf{A}_\varepsilon(x)\nabla u \cdot \nabla \varphi dx. \tag{7.1}$$

To be successful with our analysis below, we need the following assumptions:

(A_1) The diffusion coefficient $\mathbf{A}(y) \in L^\infty(\mathbb{R}^d)$ is Y-periodic and symmetric. It satisfies the uniform ellipticity condition, i.e there exists positive constants $\underline{\gamma}, \overline{\gamma}$ independent of ε such that

$$\underline{\gamma}\,|\xi|^2 \le \mathbf{A}(y)\xi_i\xi_j \le \overline{\gamma}\,|\xi|^2 \text{ for any } \xi \in \mathbb{R}^d.$$

(A_2) The reaction terms $\mathcal{S} : \mathbb{R} \to \mathbb{R}$ and $\mathcal{R} : \mathbb{R} \to \mathbb{R}$ are Carathéodory functions and globally Lipschitz.

(A_3) $\mathcal{S}$ and $\mathcal{R}$ do not degenerate, i.e there exist positive constants δ_0 and δ_1 independent of ε such that $0 < \delta_0 \le \mathcal{S}', \mathcal{R}' \le \delta_1$ a.e. in $\mathbb{R}$.

(A_4) The internal source f is a smooth function in Ω.

In the sequel, all the constants C are independent of the scale factor ε, but their precise values may differ from line to line and may change even within a single chain of estimates.

7.3 Weak solvability of (P_ε)

Obviously, solvability of microscopic problems is of great importance in mathematical analysis; see e.g. [OSY92, PBL78, Sch13]. In this section, we design a linearization scheme in line with [Slo01] to investigate the well-posedness of (P_ε). To do so, we accordingly need to derive the weak formulation of (P_ε). Multiplying (P_ε) by a test function $\varphi \in \widetilde{\mathcal{W}}_\varepsilon$ and using Green's formula, we arrive at the following definition of a weak solution of (P_ε).

Definition 7.1. *For each $\varepsilon > 0$, $u_\varepsilon \in \widetilde{\mathcal{W}}_\varepsilon$ is a weak solution to (P_ε), provided that*

$$a(u_\varepsilon, \varphi) + \varepsilon^\beta \langle \mathcal{S}(u_\varepsilon), \varphi \rangle_{L^2(\Gamma^\varepsilon)} + \varepsilon^\alpha \langle \mathcal{R}(u_\varepsilon), \varphi \rangle_{L^2(\Omega^\varepsilon)} = \langle f, \varphi \rangle_{L^2(\Omega^\varepsilon)} \quad \text{for all } \varphi \in \widetilde{\mathcal{W}}_\varepsilon. \tag{7.2}$$

Let us now introduce the definition of an approximation of (7.2).

Definition 7.2. *For each $\varepsilon > 0$, a linearization scheme for the weak formulation in Definition 7.1 is defined by*

$$\begin{aligned} (P_\varepsilon^k) :\ & a(u_\varepsilon^k, \varphi) + L\langle u_\varepsilon^k, \varphi \rangle_{L^2(\Gamma^\varepsilon)} + M\langle u_\varepsilon^k, \varphi \rangle_{L^2(\Omega^\varepsilon)} \\ & = \langle f, \varphi \rangle_{L^2(\Omega^\varepsilon)} + L\langle u_\varepsilon^{k-1}, \varphi \rangle_{L^2(\Gamma^\varepsilon)} \\ & \quad + M\langle u_\varepsilon^{k-1}, \varphi \rangle_{L^2(\Omega^\varepsilon)} - \varepsilon^\beta \langle \mathcal{S}(u_\varepsilon^{k-1}), \varphi \rangle_{L^2(\Gamma^\varepsilon)} - \varepsilon^\alpha \langle \mathcal{R}(u_\varepsilon^{k-1}), \varphi \rangle_{L^2(\Omega^\varepsilon)} \end{aligned} \tag{7.3}$$

for all $\varphi \in \widetilde{\mathcal{W}}_\varepsilon$ and $k \in \mathbb{N}^*$ with the initial guess $u_\varepsilon^0 \in \mathcal{W}_\varepsilon$ chosen as 0 and the stabilization constants $L, M > 0$ chosen later.

Lemma 7.3. *Suppose (A_1) and (A_4) hold. Assume further that there exist constants $\underline{c}_L, \overline{c}_L, \underline{c}_M, \overline{c}_M > 0$ independent of ε such that*

$$\underline{c}_L(\varepsilon^\alpha + \varepsilon^\beta) \le L \le \overline{c}_L(\varepsilon^\alpha + \varepsilon^\beta),\ \underline{c}_M(\varepsilon^\alpha + \varepsilon^\beta) \le M \le \overline{c}_M(\varepsilon^\alpha + \varepsilon^\beta). \tag{7.4}$$

Denote by (P_ε^1) the first-loop problem for (P_ε^k) defined in Definition 7.2. Then it admits a unique solution $u \in \widetilde{\mathcal{W}}_\varepsilon$ for each $\varepsilon > 0$.

Proof. Due to (A_4) and the choice of u_ε^0, the problem (P_ε^1) reads as

$$\begin{aligned} & a(u_\varepsilon^1, \varphi) + L\langle u_\varepsilon^1, \varphi \rangle_{L^2(\Gamma^\varepsilon)} + M\langle u_\varepsilon^1, \varphi \rangle_{L^2(\Omega^\varepsilon)} \\ & \qquad = \langle f, \varphi \rangle_{L^2(\Omega^\varepsilon)} - \varepsilon^\beta \langle \mathcal{S}(0), \varphi \rangle_{L^2(\Gamma^\varepsilon)} - \varepsilon^\alpha \langle \mathcal{R}(0), \varphi \rangle_{L^2(\Omega^\varepsilon)} \end{aligned}$$

for all $\varphi \in \widetilde{\mathcal{W}}_\varepsilon$. Let us put $K_\varepsilon : \widetilde{\mathcal{W}}_\varepsilon \times \widetilde{\mathcal{W}}_\varepsilon \to \mathbb{R}$ given by

$$K_\varepsilon(u, \varphi) := a(u, \varphi) + L\langle u, \varphi \rangle_{L^2(\Gamma^\varepsilon)} + M\langle u, \varphi \rangle_{L^2(\Omega^\varepsilon)} \quad \text{for } u, \varphi \in \widetilde{\mathcal{W}}_\varepsilon.$$

Clearly, this form is bilinear in $\widetilde{\mathcal{W}}_\varepsilon$ and its coerciveness is easily guaranteed. Therefore, by the Lax–Milgram argument there exists a unique $u \in \widetilde{\mathcal{W}}_\varepsilon$ satisfies (P_ε^1). □

As a consequence of Lemma 7.3, the sequence $\left\{u_\varepsilon^k\right\}_{k \in \mathbb{N}^*}$ is well-defined in $\widetilde{\mathcal{W}}_\varepsilon$ under condition (7.4). The notion of having this assumption is transparent in the next theorem, where the choice of our stabilization terms is included.

Theorem 7.4. *Assume (A_1)–(A_4) hold. There exists a choice of L and M such that (7.4) holds and the sequence of solution $\{u_\varepsilon^k\}_{k \in \mathbb{N}^*}$ to (P_ε^k) defined in (7.2) is Cauchy in $\widetilde{\mathcal{W}}_\varepsilon$. Moreover, the following estimate holds*

$$\|u_\varepsilon^{k+r+1} - u_\varepsilon^{k+1}\|_{\widetilde{\mathcal{W}}_\varepsilon} \le \frac{\eta^k(1-\eta^r)C}{1-\eta} \|u_\varepsilon^1\|_{\widetilde{\mathcal{W}}_\varepsilon},$$

where $\eta \in (0,1)$ is ε-independent and $k, r \in \mathbb{N}^*$.

Proof. Define $v_\varepsilon^k := u_\varepsilon^k - u_\varepsilon^{k-1} \in \widetilde{\mathcal{W}}_\varepsilon$ where u_ε^k and u_ε^{k-1} correspond to the solution of (P_ε^k) and (P_ε^{k-1}), respectively. Then we have the following difference equation

$$a(v_\varepsilon^k,\varphi) + L\langle v_\varepsilon^k,\varphi\rangle_{L^2(\Gamma^\varepsilon)} + M\langle v_\varepsilon^k,\varphi\rangle_{L^2(\Omega^\varepsilon)} = -\varepsilon^\beta\langle \mathcal{S}(u_\varepsilon^{k-1}) - \mathcal{S}(u_\varepsilon^{k-2}),\varphi\rangle_{L^2(\Gamma^\varepsilon)} \tag{7.5}$$
$$-\varepsilon^\alpha\langle \mathcal{R}(u_\varepsilon^{k-1}) - \mathcal{R}(u_\varepsilon^{k-2}),\varphi\rangle_{L^2(\Omega^\varepsilon)} \text{ for all } \varphi \in \widetilde{\mathcal{W}}_\varepsilon.$$

Choosing a test function $\varphi = v_\varepsilon^k \in \widetilde{\mathcal{W}}_\varepsilon$ in (7.5), we see that

$$\int_{\Omega^\varepsilon} \mathbf{A}_\varepsilon(x)\left|\nabla v_\varepsilon^k\right|^2 dx + L\|v_\varepsilon^k\|^2_{L^2(\Gamma^\varepsilon)} + M\|v_\varepsilon^k\|^2_{L^2(\Omega^\varepsilon)} = \varepsilon^\beta\langle \mathcal{S}(u_\varepsilon^{k-2}) \tag{7.6}$$
$$-\mathcal{S}(u_\varepsilon^{k-1}), v_\varepsilon^k\rangle_{L^2(\Gamma^\varepsilon)} + \varepsilon^\alpha\langle \mathcal{R}(u_\varepsilon^{k-2}) - \mathcal{R}(u_\varepsilon^{k-1}), v_\varepsilon^k\rangle_{L^2(\Omega^\varepsilon)}.$$

Now, we define $h(t) := \varepsilon^\beta\mathcal{S}(t) - Lt$ and $g(t) := \varepsilon^\alpha\mathcal{R}(t) - Mt$. Then taking the first-order derivative of h and g with respect to t, we get

$$h'(t) = \varepsilon^\beta\mathcal{S}'(t) - L \text{ and } g'(t) = \varepsilon^\alpha\mathcal{R}'(t) - M. \tag{7.7}$$

Notice that because of the structure of h and g, (7.6) becomes

$$\int_{\Omega^\varepsilon} \mathbf{A}_\varepsilon(x)\left|\nabla v_\varepsilon^k\right|^2 dx + L\|v_\varepsilon^k\|^2_{L^2(\Gamma^\varepsilon)} + M\|v_\varepsilon^k\|^2_{L^2(\Omega^\varepsilon)} \tag{7.8}$$
$$= -\langle h(u_\varepsilon^{k-1}) - h(u_\varepsilon^{k-2}), v_\varepsilon^k\rangle_{L^2(\Gamma^\varepsilon)} - \langle g(u_\varepsilon^{k-1}) - g(u_\varepsilon^{k-2}), v_\varepsilon^k\rangle_{L^2(\Omega^\varepsilon)}.$$

At this stage, we have to choose L and M such that

$$L \geq \delta_1\varepsilon^\beta \text{ and } M \geq \delta_1\varepsilon^\alpha. \tag{7.9}$$

As a result, h' and g' computed in (7.7) can be bounded with the help of (A_3) by

$$\varepsilon^\beta\delta_0 - L \leq h'(t) \leq 0, \varepsilon^\beta\delta_0 - M \leq g'(t) \leq 0 \quad \text{a.e in } \mathbb{R},$$

or it is equivalent to

$$|h'(t)| \leq L - \varepsilon^\beta\delta_0 \text{ and } |g'(t)| \leq M - \varepsilon^\beta\delta_0 \quad \text{a.e in } \mathbb{R}. \tag{7.10}$$

Combining (7.10) and (A_1), (7.8) leads to the following estimate:

$$\underline{\gamma}\|\nabla v_\varepsilon^k\|^2_{L^2(\Omega^\varepsilon)} + L\|v_\varepsilon^k\|^2_{L^2(\Gamma^\varepsilon)} + M\|v_\varepsilon^k\|^2_{L^2(\Omega^\varepsilon)}$$
$$\leq (L - \delta_0\varepsilon^\beta)\|v_\varepsilon^{k-1}\|_{L^2(\Gamma^\varepsilon)}\|v_\varepsilon^k\|_{L^2(\Gamma^\varepsilon)} + (M - \delta_0\varepsilon^\beta)\|v_\varepsilon^{k-1}\|_{L^2(\Omega^\varepsilon)}\|v_\varepsilon^k\|_{L^2(\Omega^\varepsilon)}.$$

Using the Cauchy–Schwarz inequality, we have that

$$\underline{\gamma}\|\nabla v_\varepsilon^k\|^2_{L^2(\Omega^\varepsilon)} + \frac{L + \delta_0\varepsilon^\beta}{2}\|v_\varepsilon^k\|^2_{L^2(\Gamma^\varepsilon)} + \frac{M + \delta_0\varepsilon^\alpha}{2}\|v_\varepsilon^k\|^2_{L^2(\Omega^\varepsilon)} \tag{7.11}$$
$$\leq \frac{L - \delta_0\varepsilon^\beta}{2}\|v_\varepsilon^{k-1}\|^2_{L^2(\Gamma^\varepsilon)} + \frac{M - \delta_0\varepsilon^\alpha}{2}\|v_\varepsilon^{k-1}\|^2_{L^2(\Omega^\varepsilon)}.$$

Omitting the first term of the left-hand side of (7.11), we obtain

$$\|v_\varepsilon^k\|^2_{L^2(\Gamma^\varepsilon)} + \|v_\varepsilon^k\|^2_{L^2(\Omega^\varepsilon)} \leq \frac{L-\delta_0\varepsilon^\beta}{\min\{L+\delta_0\varepsilon^\beta, M+\delta_0\varepsilon^\alpha\}}\|v_\varepsilon^{k-1}\|^2_{L^2(\Gamma^\epsilon)} + \frac{M-\delta_0\varepsilon^\alpha}{\min\{L+\delta_0\varepsilon^\beta, M+\delta_0\varepsilon^\alpha\}}\|v_\varepsilon^{k-1}\|^2_{L^2(\Omega^\varepsilon)}. \tag{7.12}$$

Rewriting (7.12), we thus have

$$\|v_\varepsilon^k\|^2_{L^2(\Gamma^\varepsilon)} + \|v_\varepsilon^k\|^2_{L^2(\Omega^\varepsilon)} \leq \eta_\varepsilon^2(\alpha,\beta)\left(\|v_\varepsilon^{k-1}\|^2_{L^2(\Gamma^\epsilon)} + \|v_\varepsilon^{k-1}\|^2_{L^2(\Omega^\varepsilon)}\right), \tag{7.13}$$

where we have denoted by

$$\eta_\varepsilon(\alpha,\beta) := \left(\max\left\{\frac{L-\delta_0\varepsilon^\beta}{L+\delta_0\varepsilon^\beta}, \frac{L-\delta_0\varepsilon^\beta}{M+\delta_0\varepsilon^\alpha}, \frac{M-\delta_0\varepsilon^\alpha}{M+\delta_0\varepsilon^\alpha}, \frac{M-\delta_0\varepsilon^\alpha}{L+\delta_0\varepsilon^\beta}\right\}\right)^{1/2}.$$

According to the linearization procedures, we need to find an ε-independent bound for η_ε in (7.13) such that it is strictly less than 1. Accordingly, we choose the stabilization constants L and M such that $\eta_\varepsilon < 1$ for all $\varepsilon > 0$ and $\alpha, \beta \in \mathbb{R}$. Now, we may write $\eta_\varepsilon = \eta$, i.e. it is independent of ε by suitable choices of L, M. Note that

$$\frac{L-\delta_0\varepsilon^\beta}{L+\delta_0\varepsilon^\beta} < 1 \text{ and } \frac{M-\delta_0\varepsilon^\alpha}{M+\delta_0\varepsilon^\alpha} < 1 \tag{7.14}$$

because of the choice (7.10). Therefore, we target the following cases:

$$\frac{L-\delta_0\varepsilon^\beta}{M+\delta_0\varepsilon^\alpha} < 1 \quad \text{and} \quad \frac{M-\delta_0\varepsilon^\alpha}{L+\delta_0\varepsilon^\alpha} < 1.$$

From (7.14), a suitable choice of L, M is taking

$$M+\delta_0\varepsilon^\alpha \geq L+\delta_0\varepsilon^\beta \text{ and } L+\delta_0\varepsilon^\beta \geq M+\delta_0\varepsilon^\alpha,$$

which leads to $M-L = \delta_0(\varepsilon^\beta - \varepsilon^\alpha)$. Hence, in accordance with (7.9) the suitable choice we eventually obtain is provided as follows:

$$L = L(\varepsilon) := \begin{cases} \delta_1\varepsilon^\alpha + \delta_0\left(\varepsilon^\alpha - \varepsilon^\beta\right) & \text{if } \alpha \leq \beta, \\ \delta_1\varepsilon^\beta & \text{if } \alpha \geq \beta, \end{cases} \tag{7.15}$$

$$M = M(\varepsilon) := \begin{cases} \delta_1\varepsilon^\alpha & \text{if } \alpha \leq \beta, \\ \delta_1\varepsilon^\beta + \delta_0\left(\varepsilon^\beta - \varepsilon^\alpha\right) & \text{if } \alpha \geq \beta. \end{cases} \tag{7.16}$$

Interestingly, this choice works for all real scaling parameters α, β. It also agrees with (7.9) and guarantees the positivity of such stabilization constants. In addition, we now observe that (7.15) and (7.16) are well-suited to the condition (7.4) in Lemma 7.3, where the well-posedness of the first-loop problem of (P_ε^k) is proven. Collectively, we have demonstrated that there exists a choice of L and

M satisfying (7.9) such that $\eta_\varepsilon = \eta < 1$ for all scaling factor $\varepsilon > 0$ and scaling parameters $\alpha, \beta \in \mathbb{R}$.

As a consequence of (7.13) and (7.15)–(7.16), we conclude that for every $\varepsilon > 0$ and $k \in \mathbb{N}^*$, the following estimate holds

$$(\varepsilon^\alpha + \varepsilon^\beta)\|v_\varepsilon^k\|^2_{\mathcal{W}_\varepsilon} \leq \eta^2(\varepsilon^\alpha + \varepsilon^\beta)\|v_\varepsilon^{k-1}\|^2_{\mathcal{W}_\varepsilon}. \tag{7.17}$$

On the other hand, for any $k, r \in \mathbb{N}^*$ we have

$$\begin{aligned}
&\sqrt{\varepsilon^\alpha + \varepsilon^\beta}\|u_\varepsilon^{k+r} - u_\varepsilon^k\|_{\mathcal{W}_\varepsilon} \qquad (7.18)\\
&\leq \sqrt{\varepsilon^\alpha + \varepsilon^\beta}\|u_\varepsilon^{k+r} - u_\varepsilon^{k+r-1}\|_{\mathcal{W}_\varepsilon} + \ldots + \sqrt{\varepsilon^\alpha + \varepsilon^\beta}\|u_\varepsilon^{k+1} - u_\varepsilon^k\|_{\mathcal{W}_\varepsilon}\\
&\leq \sqrt{\varepsilon^\alpha + \varepsilon^\beta}(\eta^{k+r-1} + \ldots + \eta^k)\|u_\varepsilon^1 - u_\varepsilon^0\|_{\mathcal{W}_\varepsilon} \leq \frac{\eta^k(1-\eta^r)}{1-\eta}\sqrt{\varepsilon^\alpha + \varepsilon^\beta}\|u_\varepsilon^1\|_{\mathcal{W}_\varepsilon}.
\end{aligned}$$

From now on, it remains to estimate the difference gradient we omitted in (7.11). Once again, it follows from (7.11) and (7.15)–(7.16) that

$$\begin{aligned}
\underline{\gamma}\|\nabla v_\varepsilon^k\|^2_{L^2(\Omega^\varepsilon)} &\leq \frac{L - \delta_0\varepsilon^\beta}{2}\|v_\varepsilon^{k-1}\|^2_{L^2(\Gamma^\varepsilon)} + \frac{M - \delta_0\varepsilon^\alpha}{2}\|v_\varepsilon^{k-1}\|^2_{L^2(\Omega^\varepsilon)}\\
&\leq \frac{\delta_1 + \delta_0}{2}(\varepsilon^\alpha + \varepsilon^\beta)\|v_\varepsilon^{k-1}\|^2_{\mathcal{W}_\varepsilon}.
\end{aligned}$$

We then combine this with (7.17) to get

$$\|\nabla v_\varepsilon^{k+1}\|^2_{L^2(\Omega^\varepsilon)} \leq \eta^2\frac{\delta_1 + \delta_0}{2\underline{\gamma}}(\varepsilon^\alpha + \varepsilon^\beta)\|v_\varepsilon^k\|^2_{\mathcal{W}_\varepsilon},$$

and as a by-product, it yields

$$\|v_\varepsilon^{k+1}\|^2_{\widetilde{\mathcal{W}}_\varepsilon} \leq \eta^2\left(\frac{\delta_1 + \delta_0}{2\underline{\gamma}} + 1\right)\|v_\varepsilon^k\|^2_{\widetilde{\mathcal{W}}_\varepsilon}.$$

At this moment, we proceed as in (7.18) to arrive at

$$\|u_\varepsilon^{k+r+1} - u_\varepsilon^{k+1}\|_{\widetilde{\mathcal{W}}_\varepsilon} \leq \frac{\eta^k(1-\eta^r)}{1-\eta}\left(\frac{\delta_1 + \delta_0}{2\underline{\gamma}} + 1\right)^{1/2}\|u_\varepsilon^1\|_{\widetilde{\mathcal{W}}_\varepsilon}. \tag{7.19}$$

This completes the proof of the theorem. □

It is worth noting that from (7.18), the iterative sequence $\{u_\varepsilon^k\}_{k\in\mathbb{N}^*}$ is Cauchy in $\mathcal{W}_\varepsilon$ for any $\varepsilon > 0$ when $\alpha = \beta = 0$. From (7.19), this sequence is Cauchy in $\widetilde{\mathcal{W}}_\varepsilon$. Consequently, there exists a unique $u_\varepsilon \in \widetilde{\mathcal{W}}_\varepsilon$ such that $u_\varepsilon^k \to u_\varepsilon$ as $k \to \infty$ and for each $\varepsilon > 0$. On the other side, using the Lipschitz properties of the volume and surface reaction rates assumed in (A_2), we have

$$\varepsilon^\beta\mathcal{S}\left(u_\varepsilon^k\right) \to \varepsilon^\beta\mathcal{S}\left(u_\varepsilon\right) \text{ strongly in } L^2\left(\Gamma^\varepsilon\right), \tag{7.20}$$

$$\varepsilon^\alpha\mathcal{R}\left(u_\varepsilon^k\right) \to \varepsilon^\alpha\mathcal{R}\left(u_\varepsilon\right) \text{ strongly in } L^2\left(\Omega^\varepsilon\right) \text{ as } k \to \infty. \tag{7.21}$$

Hence, u_ε is a unique solution of the microscopic model (P_ε) in the sense of Definition 7.1. Besides, when taking $r \to \infty$ in (7.19), its stability is confirmed by

$$\|u_\varepsilon^k - u_\varepsilon\|_{\widetilde{\mathcal{W}}_\varepsilon}^2 \leq C\eta^{2(k-1)}\|u_\varepsilon^1\|_{\widetilde{\mathcal{W}}_\varepsilon}^2.$$

As a result, we state the following theorem.

Theorem 7.5. *Assume (A_1)–(A_4) hold. Then for each $\varepsilon > 0$ there exists a unique solution of (P_ε) in the sense of Definition 7.1.*

Remark 7.6. *Compared to the mild restriction in [KM16b,KM16a], we no longer rely on the Poincaré constant and the lower bound of the diffusion. However, information of reaction terms in this context is further required as specified in (A_3).*

7.4 Asymptotic behaviors and convergence results

7.4.1 Volume reaction and surface reaction

In this subsection, we aim to see the asymptotic behaviors of the microscopic solution of (P_ε), when the volume and surface reactions are involved separately. In other words, as the starting point we consider the following problems:

$$\left(P_\varepsilon^R\right): \begin{cases} \nabla \cdot \left(-\mathbf{A}\left(x/\varepsilon\right)\nabla u_\varepsilon\right) + \varepsilon^\alpha \mathcal{R}\left(u_\varepsilon\right) = f & \text{in } \Omega^\varepsilon, \\ -\mathbf{A}\left(x/\varepsilon\right)\nabla u_\varepsilon \cdot \mathrm{n} = 0 & \text{across } \Gamma^\varepsilon, \\ u_\varepsilon = 0 & \text{across } \Gamma^{\text{ext}}, \end{cases}$$

$$\left(P_\varepsilon^S\right): \begin{cases} \nabla \cdot \left(-\mathbf{A}\left(x/\varepsilon\right)\nabla u_\varepsilon\right) = f & \text{in } \Omega^\varepsilon, \\ -\mathbf{A}\left(x/\varepsilon\right)\nabla u_\varepsilon \cdot \mathrm{n} = \varepsilon^\beta \mathcal{S}\left(u_\varepsilon\right) & \text{across } \Gamma^\varepsilon, \\ u_\varepsilon = 0 & \text{across } \Gamma^{\text{ext}}. \end{cases}$$

Volume reaction

The case $\alpha > 0$

Given a natural constant $\theta \geq 2$, we define the index set

$$\mathcal{M}_{\alpha,\theta} := \left\{k, l \in [0, \theta] : k\alpha + l \geq 1 \text{ and } k + l \leq \theta\right\}. \tag{7.22}$$

The asymptotic expansion we consider here is structured as follows:

$$u_\varepsilon\left(x\right) = u_0\left(x, y\right) + \varepsilon^\alpha u_{1,-1}\left(x, y\right) + \sum_{(k,l)\in\mathcal{M}_{\alpha,\theta}} \varepsilon^{k\alpha+l} u_{k,l}\left(x, y\right) + \mathcal{O}\left(\varepsilon^{\theta+1}\right), \tag{7.23}$$

where $x \in \Omega^\varepsilon, y \in Y_l$ and all components $u_{k,l}$ are periodic in y.

Remark 7.7. *This ansatz essentially mimics the standard two-scale asymptotic expansions used in the homogenization theory for second-order elliptic equations. Since the diffusion coefficient of the PDE is periodic in y, it is reasonable to require that all $u_{k,l}$ are periodic functions of y. For $\varepsilon \ll 1$ the microscopic variable y changes much more rapidly than x and heuristically, the macroscopic variable can be viewed as a "constant", when looking at the microscopic problem. This is why the method is expected to treat the "slow" variable x and the "fast" one y independently. Furthermore, this way the gradient operator and the gradient of the fluxes can be evaluated according to the rule $\nabla = \nabla_x + \varepsilon^{-1}\nabla_y$. With this essence in mind, our designation of asymptotic expansions in this work are such that we are able to handle variable scalings α and β in the PDE in the rigorous asymptotic analysis. From the physical point of view, the use of asymptotic expansions in understanding size effects in periodic media was studied in e.g. [TB96].*

Assume that there exists a Lipschitz-continuous function $\bar{\mathcal{R}}$ such that

$$\mathcal{R}(u^\varepsilon) = \bar{\mathcal{R}}(u_0) + \varepsilon^\alpha \bar{\mathcal{R}}(u_{1,-1}) + \sum_{(k,l)\in\mathcal{M}_{\alpha,\theta}} \varepsilon^{k(\alpha+1)+l}\bar{\mathcal{R}}(u_{k,l}) + \mathcal{O}(\varepsilon^{\theta+1}). \tag{7.24}$$

This corresponds to the fact that there exists $\mathbf{L}_{\mathcal{R}} > 0$ such that

$$\left\|\bar{\mathcal{R}}(u) - \bar{\mathcal{R}}(v)\right\|_{L^2(\Omega^\varepsilon)} \leq \mathbf{L}_{\mathcal{R}} \left\|u - v\right\|_{L^2(\Omega^\varepsilon)} \text{ for } u, v \in \mathbb{R}. \tag{7.25}$$

Remark 7.8. *In the sequel, our new assumptions* (7.24) *and* (7.25) *on the reaction rate $\mathcal{R}$ are termed as (A_5) and (A_6), respectively. It resembles the definition of almost additive functions with positive homogeneity in stochastic processes (see, e.g., [SSV17]).*

Due to the simple relation $\nabla = \nabla_x + \varepsilon^{-1}\nabla_y$, it follows that

$$\begin{aligned}\nabla u_\varepsilon = {} & \varepsilon^{-1}\nabla_y u_0 + \varepsilon^{\alpha-1}\nabla_y u_{1,-1} + \varepsilon^0\left(\nabla_x u_0 + \nabla_y u_{0,1}\right) \\ & + \varepsilon^\alpha\left(\nabla_x u_{1,-1} + \nabla_y u_{1,0}\right) + \sum_{(k,l)\in\mathcal{N}_{\alpha,\theta}} \varepsilon^{k\alpha+l}\left(\nabla_x u_{k,l} + \nabla_y u_{k,l+1}\right) + \mathcal{O}\left(\varepsilon^\theta\right),\end{aligned}$$

where $\mathcal{N}_{\alpha,\theta} = \mathcal{M}_{\alpha,\theta}\backslash\{(0,1)\}$. Hereafter, the diffusion term involved in $\left(P_\varepsilon^R\right)$ is expressed as

$$\begin{aligned}& \nabla\cdot\left(-\mathbf{A}\left(y\right)\nabla u_\varepsilon\right) \\ & = \varepsilon^{-2}\nabla_y\cdot\left(-\mathbf{A}\left(y\right)\nabla_y u_0\right) + \varepsilon^{\alpha-2}\nabla_y\cdot\left(-\mathbf{A}\left(y\right)\nabla_y u_{1,-1}\right) \\ & + \varepsilon^{-1}\left(\nabla_x\cdot\left(-\mathbf{A}\left(y\right)\nabla_y u_0\right) + \nabla_y\cdot\left(-\mathbf{A}\left(y\right)\left(\nabla_x u_0 + \nabla_y u_{0,1}\right)\right)\right) \\ & + \varepsilon^{\alpha-1}\left(\nabla_x\cdot\left(-\mathbf{A}\left(y\right)\nabla_y u_{1,-1}\right) + \nabla_y\cdot\left(-\mathbf{A}\left(y\right)\left(\nabla_x u_{1,-1} + \nabla_y u_{1,0}\right)\right)\right) \\ & + \varepsilon^0\left(\nabla_x\cdot\left(-\mathbf{A}\left(y\right)\left(\nabla_x u_0 + \nabla_y u_{0,1}\right)\right) + \nabla_y\cdot\left(-\mathbf{A}\left(y\right)\left(\nabla_x u_{0,1} + \nabla_y u_{0,2}\right)\right)\right) \\ & + \varepsilon^\alpha\left(\nabla_x\cdot\left(-\mathbf{A}\left(y\right)\left(\nabla_x u_{1,-1} + \nabla_y u_{1,0}\right)\right) + \nabla_y\cdot\left(-\mathbf{A}\left(y\right)\left(\nabla_x u_{1,0} + \nabla_y u_{1,1}\right)\right)\right) \\ & + \sum_{(k,l)\in\mathcal{N}_{\alpha,\theta}} \varepsilon^{k(\alpha+1)+l}\left[\nabla_x\cdot\left(-\mathbf{A}\left(y\right)\left(\nabla_x u_{k,l} + \nabla_y u_{k,l+1}\right)\right)\right. \\ & \left. + \nabla_y\cdot\left(-\mathbf{A}\left(y\right)\left(\nabla_x u_{k,l+1} + \nabla_y u_{k,l+2}\right)\right)\right] + \mathcal{O}\left(\varepsilon^{\theta-1}\right),\end{aligned} \tag{7.26}$$

while relying on (A_5), the reaction term can be decomposed as

$$\varepsilon^{\alpha}\mathcal{R}(u^{\varepsilon}) = \varepsilon^{\alpha}\bar{\mathcal{R}}(u_0) + \varepsilon^{2\alpha}\bar{\mathcal{R}}(u_{1,-1}) + \sum_{(k,l)\in\mathcal{M}_{\alpha,\theta}} \varepsilon^{k(\alpha+1)+l+\alpha}\bar{\mathcal{R}}(u_{k,l}) + \mathcal{O}(\varepsilon^{\theta+1}). \tag{7.27}$$

In the same vein, the term on internal micro-surfaces are determined by

$$\begin{aligned} -\mathbf{A}(y)\nabla u_{\varepsilon}\cdot \mathrm{n} = &-\varepsilon^{-1}\mathbf{A}(y)u_0\cdot \mathrm{n} - \varepsilon^{\alpha-1}\mathbf{A}\nabla_y u_{1,-1}\cdot \mathrm{n} \\ &- \varepsilon^{0}\mathbf{A}(y)(\nabla_x u_0 + \nabla_y u_{0,1})\cdot \mathrm{n} - \varepsilon^{\alpha}\mathbf{A}(y)(\nabla_x u_{1,-1} + \nabla_y u_{1,0})\cdot \mathrm{n} \\ &- \varepsilon\mathbf{A}(y)(\nabla_x u_{0,1} + \nabla_y u_{0,2})\cdot \mathrm{n} - \varepsilon^{\alpha+1}\mathbf{A}(y)(\nabla_x u_{1,0} + \nabla_y u_{1,1})\cdot \mathrm{n} \\ &- \sum_{(k,l)\in\mathcal{K}_{\alpha,\theta}} \varepsilon^{k(\alpha+1)+l}\mathbf{A}(y)\left(\nabla_x u_{k,l} + \nabla_y u_{k,l+1}\right)\cdot \mathrm{n} + \mathcal{O}(\varepsilon^{\theta}), \end{aligned} \tag{7.28}$$

where $\mathcal{K}_{\alpha,\theta} = \mathcal{N}_{\alpha,\theta}\backslash\{(1,0)\}$. From now on, we set:

$$\begin{aligned} &\mathcal{A}_0 := \nabla_y\cdot(-\mathbf{A}(y)\nabla_y), \\ &\mathcal{A}_1 := \nabla_x\cdot(-\mathbf{A}(y)\nabla_y) + \nabla_y\cdot(-\mathbf{A}(y)\nabla_x), \\ &\mathcal{A}_2 := \nabla_x\cdot(-\mathbf{A}(y)\nabla_x). \end{aligned} \tag{7.29}$$

We obtain the following auxiliary problems from (7.26) and (7.28):

$$(\varepsilon^{-2}): \quad \begin{cases} \mathcal{A}_0 u_0 = 0 \quad \text{in } Y_l, \\ -\mathbf{A}(y)\nabla_y u_0\cdot \mathrm{n} = 0 \quad \text{on } \Gamma, \\ u_0 \text{ is periodic in } y, \end{cases} \tag{7.30}$$

$$(\varepsilon^{\alpha-2}): \quad \begin{cases} \mathcal{A}_0 u_{1,-1} = 0 \quad \text{in } Y_l, \\ -\mathbf{A}(y)\nabla_y u_{1,-1}\cdot \mathrm{n} = 0 \quad \text{on } \Gamma, \\ u_{1,-1} \text{ is periodic in } y, \end{cases} \tag{7.31}$$

$$(\varepsilon^{-1}): \quad \begin{cases} \mathcal{A}_0 u_{0,1} = -\mathcal{A}_1 u_0 \quad \text{in } Y_l, \\ -\mathbf{A}(y)(\nabla_x u_0 + \nabla_y u_{0,1})\cdot \mathrm{n} = 0 \quad \text{on } \Gamma, \\ u_{0,1} \text{ is periodic in } y, \end{cases} \tag{7.32}$$

$$(\varepsilon^{\alpha-1}): \quad \begin{cases} \mathcal{A}_0 u_{1,0} = -\mathcal{A}_1 u_{1,-1} \quad \text{in } Y_l, \\ -\mathbf{A}(y)(\nabla_x u_{1,-1} + \nabla_y u_{1,0}) \cdot \mathrm{n} = 0 \quad \text{on } \Gamma, \\ u_{1,0} \text{ is periodic in } y, \end{cases} \tag{7.33}$$

$$(\varepsilon^{0}): \quad \begin{cases} \mathcal{A}_0 u_{0,2} = f - \mathcal{A}_1 u_{0,1} - \mathcal{A}_2 u_0 \quad \text{in } Y_l, \\ -\mathbf{A}(y)(\nabla_x u_{0,1} + \nabla_y u_{0,2}) \cdot \mathrm{n} = 0 \quad \text{on } \Gamma, \\ u_{0,2} \text{ is periodic in } y, \end{cases} \tag{7.34}$$

$$(\varepsilon^{\alpha}): \quad \begin{cases} \mathcal{A}_0 u_{1,1} = -\mathcal{A}_1 u_{1,0} - \mathcal{A}_2 u_{1,-1} \quad \text{in } Y_l, \\ -\mathbf{A}(y)(\nabla_x u_{1,0} + \nabla_y u_{1,1}) \cdot \mathrm{n} = 0 \quad \text{on } \Gamma, \\ u_{1,1} \text{ is periodic in } y. \end{cases} \tag{7.35}$$

$$\vdots$$

$$(\varepsilon^{k(\alpha+1)+l}): \quad \begin{cases} \mathcal{A}_0 u_{k,l+2} = -\mathcal{A}_1 u_{k,l+1} - \mathcal{A}_2 u_{k,l} \quad \text{in } Y_l, \\ -\mathbf{A}(y)(\nabla_x u_{k,l+1} + \nabla_y u_{k,l+2}) \cdot \mathrm{n} = 0 \quad \text{on } \Gamma, \\ u_{k,l+2} \text{ is periodic in } y, \end{cases} \tag{7.36}$$

for all pairs $(k,l) \in \mathcal{K}_{\alpha,\theta-2}$.

By classical arguments in homogenization procedures, one has from (7.30) and (7.31) that u_0 and $u_{1,-1}$ are independent of y. Without loss of generality, we take $u_{1,-1} \equiv 0$ and by substitution, we also get $u_{1,0} \equiv 0$ in (7.33). Besides, we write

$$u_0(x,y) = \tilde{u}_0(x). \tag{7.37}$$

Therefore, the auxiliary problem (7.32) is solvable with respect to $u_{0,1}$. Plugging all auxiliary solutions that have been deduced above into (7.34) and (7.35), we easily obtain $u_{0,2}$ and $u_{1,1}$. On the whole, we repeat the same strategy and ensure the solvability of the high-order auxiliary problem (7.36). From e.g. [CJ99], the existence and uniqueness results for (7.32) are trivial and the solution $u_{0,1}$ is sought in the sense of separation of variables. In other words, we have that

$$u_{0,1}(x,y) = -\chi_{0,1}(y) \cdot \nabla_x \tilde{u}_0(x). \tag{7.38}$$

Hereby, the following cell problem for the field $\chi_{0,1}(y)$ is obtained:

$$\begin{cases} \mathcal{A}_0 \chi^j_{0,1} = \dfrac{\partial \mathbf{A}_{ij}}{\partial y_i} & \text{in } Y_l, \\ -\mathbf{A}\,(y)\,\nabla_y \chi^j_{0,1} \cdot \mathrm{n} = \mathbf{A}\,(y) \cdot \mathrm{n}_j & \text{on } \Gamma, \\ \chi^j_{0,1} \text{ is periodic,} \end{cases} \tag{7.39}$$

where $\mathbf{A}_{ij}$ are elements of the second-order tensor $\mathbf{A}$ with $1 \leq i,j \leq d$ and $\chi^j_{0,1} = \chi^j_{0,1}(y)$ are elements in the cell vector-valued function $\chi_{0,1}$. Remarkably, classical results provide that $\chi_{0,1} \in [H^1_{\#}(Y_l)/\mathbb{R}]^d$ exists uniquely in these cell problems.

From the cell function $\chi_{0,1}$ in (7.38), we obtain the limit equation by taking into account the auxiliary problem (7.34). In fact, the limit equation is of the

following structure:

$$-\bar{\mathbf{A}}\Delta_x\tilde{u}_0 = \frac{|Y_l|}{|Y|}f \quad \text{in } \Omega, \tag{7.40}$$

where the coefficient $|Y_l|/|Y|$ is referred to as the volumetric porosity and $\bar{\mathbf{A}}$ given by

$$\bar{\mathbf{A}} = \frac{1}{|Y|}\int_{Y_l}\left(-\nabla_y\chi_{0,1}(y) + \mathbb{I}\right)\mathbf{A}(y)\,dy, \tag{7.41}$$

is the effective diffusion coefficient corresponding to $\mathbf{A}$ with $\mathbb{I}$ being the identity matrix.

Obviously, this limit equation is supplemented with the zero Dirichlet boundary condition on Γ^{ext} and $\bar{\mathbf{A}}$ satisfies the ellipticity condition (cf. [CJ99, Proposition 2.6]).

Remark 7.9. *We recall from [Kho17] that when $\alpha = 0$, the limit equation becomes semi-linear, i.e.*

$$-\bar{\mathbf{A}}\Delta_x\tilde{u}_0 - \frac{|Y_l|}{|Y|}\bar{\mathcal{R}}(\tilde{u}_0) = 0 \quad \textit{in } \Omega, \tag{7.42}$$

where we have omitted f, for simplicity. Based on the Lax–Milgram argument, the limit problem (7.42) *with the homogeneous Dirichlet boundary condition admits a unique solution $\tilde{u}_0 \in H_0^1(\Omega)$ due to the Lipschitz reaction term. Moreover, from [GMRL09, Lemma 5], it is essentially bounded and the following estimate holds*

$$\|\tilde{u}_0\|_{L^\infty(\Omega)} \le C(\|\tilde{u}_0\|_{L^2(\Omega)} + 1).$$

Accordingly, these results can be applied to the limit problem (7.40)*, including the existence and uniqueness of $\tilde{u}_0 \in H_0^1(\Omega)$ for any $f \in L^2(\Omega)$. From [GT83, Corollary 8.11], if $f \in C^\infty(\Omega)$, this solution $\tilde{u}_0$ belongs to $C^\infty(\Omega)$.*

Due to the structure of the auxiliary problems (7.30)–(7.36), we get $u_{k,l} \equiv 0$ for all $k \ge 1$ and $(k,l) \in \mathcal{K}_{\alpha,\theta}$. In line with [Kho17], we obtain when $k = 0$ that

$$u_{0,l} = (-1)^l\chi_{0,l}(y)\cdot\nabla_x^l\tilde{u}_0(x). \tag{7.43}$$

Thus, we obtain the following high-order cell problems in this case:

$$\begin{cases} \nabla_y\cdot\left(-\mathbf{A}(y)\left(\nabla_y\chi_{0,l+2} - \chi_{0,l+1}\right)\right)\nabla_x^{l+2}\tilde{u}_0 \\ = (-1)^l\bar{\mathcal{R}}\left((-1)^l\chi_{0,l}\nabla_x^l\tilde{u}_0\right) - \left(\mathbf{A}(y) - \mathbb{I}\right)\nabla_y\chi_{0,l+1}\nabla_x^{l+2}\tilde{u}_0 & \text{in } Y_l, \\ -\mathbf{A}(y)\left(\nabla_y\chi_{0,l+2} - \chi_{0,l+1}\right)\nabla_x^{l+2}\tilde{u}_0\cdot\mathrm{n} = 0 & \text{on } \Gamma, \\ \chi_{0,l+2} \text{ is periodic.} \end{cases} \tag{7.44}$$

Combining (7.37), (7.38) and (7.43) we recover the structure of the asymptotic expansion for u^ε defined in (7.23), as follows:

$$u_\varepsilon(x) = \tilde{u}_0(x) - \varepsilon\chi_{0,1}\left(\frac{x}{\varepsilon}\right)\cdot\nabla_x\tilde{u}_0(x) + \sum_{l=2}^{\theta}(-1)^l\varepsilon^l\chi_{0,l}\left(\frac{x}{\varepsilon}\right)\cdot\nabla_x^l\tilde{u}_0(x) + \mathcal{O}(\varepsilon^{\theta+1}) \tag{7.45}$$

with the cell functions $\chi_{0,l}$ for $1 \leq l \leq \theta$ satisfying the cell problems defined in (7.39) and (7.44).

At this point, we have derived the structure of two-scale asymptotic expansions where the scaling parameter α is positive. In the following, we show that the speed of convergence can be accelerated if the high-order asymptotic expansion is chosen appropriately. In addition, this questions how much regularity on the involved data we require to achieve the desired order of expansion as well as the rate of convergence.

We introduce a smooth cut-off function $m^\varepsilon \in \mathcal{D}(\Omega)$ such that $0 \leq m^\varepsilon \leq 1$ with

$$m^\varepsilon = \begin{cases} 0 & \text{if } \operatorname{dist}(x,\partial\Omega) \leq \varepsilon, \\ 1 & \text{if } \operatorname{dist}(x,\partial\Omega) \geq 2\varepsilon, \end{cases} \quad \text{and} \quad \varepsilon\left|\nabla m^\varepsilon\right| \leq C,$$

for which the following helpful estimates hold (cf. e.g. [CJ99]):

$$\left\|1 - m^\varepsilon\right\|_{L^2(\Omega^\varepsilon)} \leq C\varepsilon^{\frac{1}{2}}, \quad \varepsilon\left\|\nabla m^\varepsilon\right\|_{L^2(\Omega^\varepsilon)} \leq C\varepsilon^{\frac{1}{2}}. \tag{7.46}$$

Remark 7.10. *The use of this cut-off function to prove the convergence rates is not only seen in elliptic problems that we have taken into consideration, but also can be found in some particular multiscale models. Aside from our earlier works [Kho17, KM16a], this technique is applied in the works [Sch12, KM19] for a nonlinear drift-reaction-diffusion model in a heterogeneous solid-electrolyte composite and in [SK17] in the context of phase field equations. Besides, we single out the survey [ZP16] and the work [Sus13] for a concrete background of the so-called operator corrector estimates related to this approach.*

Given a natural number $\mu \in [0, \theta-1]$, we define the function ψ_ε by

$$\psi_\varepsilon := u_\varepsilon - \left(\tilde{u}_0 + \sum_{(k,l)\in\mathcal{M}_{\alpha,\mu}} \varepsilon^{k(\alpha+1)+l}u_{k,l}\right) - m^\varepsilon \sum_{(k,l)\in\mathcal{M}_{\alpha,\theta}\setminus\mathcal{M}_{\alpha,\mu}} \varepsilon^{k(\alpha+1)+l}u_{k,l}.$$

Observe that ψ_ε can be decomposed further as

$$\psi_\varepsilon = \underbrace{u_\varepsilon - \tilde{u}_0 - \sum_{(k,l)\in\mathcal{M}_{\alpha,\theta}} \varepsilon^{k(\alpha+1)+l}u_{k,l}}_{:=\varphi_\varepsilon} + \underbrace{(1-m^\varepsilon)\sum_{(k,l)\in\mathcal{M}_{\alpha,\theta}\setminus\mathcal{M}_{\alpha,\mu}} \varepsilon^{k(\alpha+1)+l}u_{k,l}}_{:=\sigma_\varepsilon}. \tag{7.47}$$

Now, we state our convergence result.

Theorem 7.11. *Assume* (A_1), (A_5) *and* (A_6) *hold. Furthermore, suppose that* $f \in C^\infty(\Omega)$ *and let* $\mathcal{M}_{\alpha,\theta}$ *be defined as in* (7.43) *for given parameters* $\alpha > 0$ *and* $2 \leq \theta \in \mathbb{N}$. *Let* u_ε *and* $\tilde{u}_0$ *be unique weak solutions of the microscopic problem* $\left(P_\varepsilon^R\right)$ *and the limit problem* (7.40), *respectively. Let* $u_{k,l}$ *be defined as in* (7.43) *for* $(k,l) \in \mathcal{M}_{\alpha,\theta}$. *Then, for any* $\mu \in [0, \theta-1]$ *the following high-order corrector estimate holds:*

$$\left\| u_\varepsilon - \tilde{u}_0 - \sum_{(k,l)\in\mathcal{M}_{\alpha,\mu}} \varepsilon^{k(\alpha+1)+l} u_{k,l} - m^\varepsilon \sum_{(k,l)\in\mathcal{M}_{\alpha,\theta}\setminus\mathcal{M}_{\alpha,\mu}} \varepsilon^{k(\alpha+1)+l} u_{k,l} \right\|_{V^\varepsilon} \leq C\left(\varepsilon^{\theta-1+\alpha} + \varepsilon^{\mu+1/2}\right).$$

Proof. From the auxiliary problems (7.30)–(7.36) and the operators defined in (7.29), one can deduce, after some rearrangements, the following equation for φ_ε in (7.47), which we refer to as the first difference equation:

$$\begin{aligned} \nabla\cdot(-\mathbf{A}_\varepsilon(x)\nabla\varphi_\varepsilon) &= \varepsilon^\alpha \mathcal{R}(u_\varepsilon) - \sum_{\substack{(k,l)\in\mathcal{M}_{\alpha,\theta}\\ l\leq\theta-2}} \varepsilon^{k(\alpha+1)+l+\alpha}\bar{\mathcal{R}}(u_{k,l}) \\ &\quad - \sum_{\substack{(k,l)\in\mathcal{M}_{\alpha,\theta}\\ l=\theta-1}} \varepsilon^{k(\alpha+1)+l}(\mathcal{A}_1 u_{k,l+1} + \mathcal{A}_2 u_{k,l}) - \sum_{\substack{(k,l)\in\mathcal{M}_{\alpha,\theta}\\ l=\theta}} \varepsilon^{k(\alpha+1)+l}\mathcal{A}_2 u_{k,l}, \end{aligned} \tag{7.48}$$

associated with the boundary condition at Γ^ε:

$$\begin{aligned} &-\mathbf{A}_\varepsilon(x)\nabla\varphi_\varepsilon\cdot\mathrm{n} \\ &= -\mathbf{A}_\varepsilon(x)\nabla u_\varepsilon\cdot\mathrm{n} - \mathbf{A}_\varepsilon(x)\sum_{\substack{(k,l)\in\mathcal{M}_{\alpha,\theta}\\ l\leq\theta-1}} \varepsilon^{k(\alpha+1)+l}(\nabla_x u_{k,l} + \nabla_y u_{k,l+1})\cdot\mathrm{n} \\ &- \mathbf{A}_\varepsilon(x)\sum_{\substack{(k,l)\in\mathcal{M}_{\alpha,\theta}\\ l=\theta}} \varepsilon^{k(\alpha+1)+l}\nabla_x u_{k,l}\cdot\mathrm{n}. \end{aligned} \tag{7.49}$$

From the auxiliary problem (7.36), the first term and the second term of the right-hand side of (7.49) vanishes naturally on the micro-surface Γ^ε. Thus, it yields

$$-\mathbf{A}_\varepsilon(x)\nabla\varphi_\varepsilon\cdot\mathrm{n} = -\mathbf{A}_\varepsilon(x)\sum_{\substack{(k,l)\in\mathcal{M}_{\alpha,\theta}\\ l=\theta}} \varepsilon^{k(\alpha+1)+l}\nabla_x u_{k,l}\cdot\mathrm{n}. \tag{7.50}$$

Multiplying (7.48) by a test function $\varphi \in V^\varepsilon$, integrating the resulting equation by parts and then using the boundary information (7.50) together with the

zero Dirichlet exterior condition, we get

$$
\begin{aligned}
a(\varphi_\varepsilon,\varphi) = & \underbrace{\left\langle \varepsilon^{\alpha}\mathcal{R}(u_\varepsilon) - \sum_{(k,l)\in\mathcal{M}_{\alpha,\theta},l\le\theta-2} \varepsilon^{k(\alpha+1)+l+\alpha}\bar{\mathcal{R}}(u_{k,l}),\varphi\right\rangle_{L^2(\Omega^\varepsilon)}}_{:=\mathcal{I}_1} \\
& - \underbrace{\sum_{(k,l)\in\mathcal{M}_{\alpha,\theta},l=\theta-1} \varepsilon^{k(\alpha+1)+l}\left\langle \mathcal{A}_1 u_{k,l+1} + \mathcal{A}_2 u_{k,l},\varphi\right\rangle_{L^2(\Omega^\varepsilon)}}_{:=\mathcal{I}_2} \\
& - \underbrace{\sum_{(k,l)\in\mathcal{M}_{\alpha,\theta},l=\theta} \varepsilon^{k(\alpha+1)+l}\left\langle \mathcal{A}_2 u_{k,l},\varphi\right\rangle_{L^2(\Omega^\varepsilon)}}_{:=\mathcal{I}_3} \\
& + \underbrace{\int_{\Gamma^\varepsilon}\sum_{(k,l)\in\mathcal{M}_{\alpha,\theta}} \varepsilon^{k(\alpha+1)+l}\mathbf{A}_\varepsilon(x)\nabla u_{k,l}\cdot \mathrm{n}\varphi dS_\varepsilon}_{:=\mathcal{I}_4},
\end{aligned}
\tag{7.51}
$$

where $a : V^\varepsilon \times V^\varepsilon \to \mathbb{R}$ is the bilinear form defined in (7.1).

In order to find the upper bound of ψ_ε, we need to estimate from above all terms on the right-hand side of (7.51). We begin with the estimate for $\mathcal{I}_1$ by the following structural inequality:

$$
\|\bar{\mathcal{R}}(u_{k,l})\|_{L^2(\Omega^\varepsilon)} \le \mathbf{L}_{\mathcal{R}}\|u_{k,l}\|_{L^2(\Omega^\varepsilon)} + \|\bar{\mathcal{R}}(0)\|_{L^2(\Omega^\varepsilon)} \text{ for all } (k,l)\in\mathcal{M}_{\alpha,\theta}, \tag{7.52}
$$

by virtue of the globally Lipschitz function $\bar{\mathcal{R}}$. Due to (7.52), one can estimate from above $\mathcal{I}_1$ by

$$
\begin{aligned}
|\mathcal{I}_1| \le & \mathbf{L}_{\mathcal{R}} \sum_{\substack{(k,l)\in\mathcal{M}_{\alpha,\theta}\\ l=\theta-1}} \varepsilon^{k(\alpha+1)+l+\alpha}(\|u_{k,l}\|_{L^2(\Omega^\varepsilon)} + \|\bar{\mathcal{R}}(0)\|_{L^2(\Omega^\varepsilon)})\|\varphi\|_{L^2(\Omega^\varepsilon)} \\
& + \mathbf{L}_{\mathcal{R}} \sum_{\substack{(k,l)\in\mathcal{M}_{\alpha,\theta}\\ l=\theta}} \varepsilon^{k(\alpha+1)+l+\alpha}(\|u_{k,l}\|_{L^2(\Omega^\varepsilon)} + \|\bar{\mathcal{R}}(0)\|_{L^2(\Omega^\varepsilon)})\|\varphi\|_{L^2(\Omega^\varepsilon)} \\
& \le C\varepsilon^{\theta-1+\alpha}\|\varphi\|_{V^\varepsilon}.
\end{aligned}
\tag{7.53}
$$

By the definition of the operators $\mathcal{A}_1$ and $\mathcal{A}_2$, we get for $(k,l)\in\mathcal{M}_{\alpha,\theta}$,

$$
\begin{aligned}
& \mathcal{A}_1 u_{k,l+1} \\
& = \begin{cases} 0 & \text{if } k\neq 0, \\ (-1)^{l+1}\left[-\mathbf{A}(y)\nabla_y\chi_{0,l+1}(y) + \nabla_y(-\mathbf{A}(y)\chi_{0,l}(y))\right]\cdot\nabla_x^{l+2}\tilde{u}_0(x) & \text{if } k=0. \end{cases}
\end{aligned}
\tag{7.54}
$$

$$
\mathcal{A}_2 u_{k,l} = \begin{cases} 0 & \text{if } k\neq 0, \\ (-1)^{l+1}\mathbf{A}(y)\chi_{0,l}(y)\nabla_x^{l+2}\tilde{u}_0(x) & \text{if } k=0. \end{cases} \tag{7.55}
$$

As stated in Remark 7.9, we only need the source f to be very smooth, says $f\in C^\infty(\Omega)$, to guarantee the uniform bound (with respect to ε) of all the

involved derivatives of $\tilde{u}_0$ in (7.54) and (7.55). We combine this with the fact that $\chi_{k,l} \in H^1_{\#}(Y_l)/\mathbb{R}$ and the assumptions (A_1) and $P_{k,l} \in W^{2,\infty}(\Omega)$ for all $(k,l) \in \mathcal{M}_{\alpha,\theta}$ to get

$$|\mathcal{I}_2 + \mathcal{I}_3| \leq C\varepsilon^{\theta-1+\alpha}\|\varphi\|_{V^\varepsilon} \text{ for all } \varphi \in V^\varepsilon, \tag{7.56}$$

where we have used the Poincaré inequality.

To estimate $\mathcal{I}_4$, we note that by the change of variables $x = \varepsilon y$, the following estimate holds

$$\int_{\Gamma^\varepsilon} \left|\chi_{0,\theta}\left(\frac{x}{\varepsilon}\right) \nabla_x^{\theta+1}\tilde{u}_0(x) \cdot \mathrm{n}\right|^2 dS_\varepsilon \leq C\varepsilon^{d-1} \int_\Gamma |\chi_{0,\theta}(y)|^2 dS_y.$$

Since $|\Omega| \geq \varepsilon^d|Y|$ (due to our choice of perforated domains that $\varepsilon Y \subset \Omega$) together with the fact that the trace inequality in Y_l is uniform with respect to ε, we estimate the above inequality as

$$\int_{\Gamma^\varepsilon} \left|\chi_{0,\theta}\left(\frac{x}{\varepsilon}\right) \nabla_x^{\theta+1}\tilde{u}_0(x) \cdot \mathrm{n}\right|^2 dS_\varepsilon \leq C\varepsilon^{-1}\|\chi_{0,\theta}\|^2_{H^1(Y_l)} \leq C\varepsilon^{-1}. \tag{7.57}$$

Combining (7.57) with assumption (A_1), the trace inequality (cf. [ADN59, Lemma 2.31]) for Γ^ε and the Poincaré inequality, we obtain

$$|\mathcal{I}_4| \leq \varepsilon^\theta \|\chi_{0,\theta}\nabla_x^{\theta+1}\tilde{u}_0 \cdot \mathrm{n}\|_{L^2(\Gamma^\varepsilon)}\|\varphi\|_{L^2(\Gamma^\varepsilon)} \leq C\varepsilon^{\theta-1}\|\varphi\|_{V^\varepsilon}. \tag{7.58}$$

It now remains to estimate the second part σ_ε of the decomposition (7.47). Similar to the above estimates of φ_ε, we consider the following quantity $\langle \sigma_\varepsilon, \varphi\rangle_{V^\varepsilon}$ for any $\varphi \in V^\varepsilon$. Observe that by the definition of V^ε and by using the simple chain rule of differentiation, the estimate for σ_ε is given by

$$\begin{aligned}
&\left|\left\langle (1-m^\varepsilon) \sum_{(k,l)\in\mathcal{M}_{\alpha,\theta}\setminus\mathcal{M}_{\alpha,\mu}} \varepsilon^{k(\alpha+1)+l} u_{k,l}, \varphi \right\rangle_{V^\varepsilon}\right| \\
&\leq C \sum_{(k,l)\in\mathcal{M}_{\alpha,\theta}\setminus\mathcal{M}_{\alpha,\mu}} \varepsilon^{k(\alpha+1)+l}\|\nabla(1-m^\varepsilon)\|_{L^2(\Omega^\varepsilon)}\|\varphi\|_{V^\varepsilon} \\
&+ C \sum_{(k,l)\in\mathcal{M}_{\alpha,\theta}\setminus\mathcal{M}_{\alpha,\mu}} \varepsilon^{k(\alpha+1)+l}\|1-m^\varepsilon\|_{L^2(\Omega^\varepsilon)}\|\varphi\|_{V^\varepsilon} \\
&\leq C \sum_{(k,l)\in\mathcal{M}_{\alpha,\theta}\setminus\mathcal{M}_{\alpha,\mu}} (\varepsilon^{k(\alpha+1)+l-1/2} + \varepsilon^{k(\alpha+1)+l+1/2})\|\varphi\|_{V^\varepsilon}.
\end{aligned} \tag{7.59}$$

Consequently, we finalize the estimate in (7.59) by

$$\left|\left\langle (1-m^\varepsilon) \sum_{(k,l)\in\mathcal{M}_{\alpha,\theta}\setminus\mathcal{M}_{\alpha,\mu}} \varepsilon^{k(\alpha+1)+l} u_{k,l}, \varphi \right\rangle_{V^\varepsilon}\right| \leq C(\varepsilon^{\mu+1/2} + \varepsilon^{\mu+3/2})\|\varphi\|_{V^\varepsilon}. \tag{7.60}$$

Thanks to the triangle inequality, we combine (7.51), (7.53), (7.56), (7.58) and (7.60) to get

$$|\langle \psi_\varepsilon, \varphi \rangle_{V^\varepsilon}| \leq C(\varepsilon^{\theta-1+\alpha} + \varepsilon^{\mu+1/2} + \varepsilon^{\mu+3/2}) \|\varphi\|_{V^\varepsilon} \text{ for any } \varphi \in V^\varepsilon.$$

By choosing $\varphi = \psi_\varepsilon$ and then by simplifying both sides of the resulting estimate, we complete the proof of the theorem. □

The case $\alpha < 0$

Recalling Theorem 7.5, we have $u_\varepsilon \in \widetilde{\mathcal{W}}_\varepsilon$ for each $\varepsilon > 0$, i.e. $\|u_\varepsilon\|^2_{\widetilde{\mathcal{W}}_\varepsilon} \leq C$. Note that our the underlying problem (P^R_ε) is associated with the zero Neumann boundary condition on the micro-surfaces. Thus, the structure of $\widetilde{\mathcal{W}}_\varepsilon$-norm reduces to

$$\|u_\varepsilon\|^2_{\widetilde{\mathcal{W}}_\varepsilon} = \|\nabla u_\varepsilon\|^2_{L^2(\Omega^\varepsilon)} + \varepsilon^\alpha \|u_\varepsilon\|^2_{L^2(\Omega^\varepsilon)} \leq C. \tag{7.61}$$

As a result of (7.61), we get

$$\|u_\varepsilon\|_{L^2(\Omega^\varepsilon)} \leq C\varepsilon^{-\frac{\alpha}{2}}, \tag{7.62}$$

which proves the strong convergence in $L^2(\Omega^\varepsilon)$ of u_ε to zero as $\alpha < 0$ and $\varepsilon \searrow 0^+$.

Moreover, by using the trace inequality for hypersurfaces Γ^ε (cf. [HJ91, Lemma 3]), which reads as

$$\varepsilon \|u_\varepsilon\|^2_{L^2(\Gamma^\varepsilon)} \leq C \left(\|u_\varepsilon\|^2_{L^2(\Omega^\varepsilon)} + \varepsilon^2 \|\nabla u_\varepsilon\|^2_{L^2(\Omega^\varepsilon)} \right) \text{ for any } \varepsilon > 0, \tag{7.63}$$

we combine (7.62) with the fact that $\|\nabla u_\varepsilon\|^2_{L^2(\Omega^\varepsilon)} \leq C$ from (7.61) to obtain

$$\varepsilon \|u_\varepsilon\|^2_{L^2(\Gamma^\varepsilon)} \leq C \left(\varepsilon^{-\alpha} + \varepsilon^2 \right). \tag{7.64}$$

Consequently, it follows from (7.64) that

$$\|u_\varepsilon\|_{L^2(\Gamma^\varepsilon)} \leq C \max \left\{ \varepsilon^{-\frac{(\alpha+1)}{2}}, \varepsilon^{\frac{1}{2}} \right\} \text{ for any } \varepsilon > 0. \tag{7.65}$$

In conclusion, combining (7.62) and (7.64) we claim the following theorem for the limit behavior of solution to problem (P^R_ε) in the case $\alpha < 0$.

Theorem 7.12. *Assume* (A_1)*–*(A_4) *hold. Suppose that* $f \in L^2(\Omega^\varepsilon)$ *and* $\alpha < 0$. *Let* u_ε *be a unique solution in* $\widetilde{\mathcal{W}}_\varepsilon$ *of the problem* (P^R_ε). *Then it holds:*

$$\|u_\varepsilon\|_{L^2(\Omega^\varepsilon)} + \sqrt{\varepsilon} \|u_\varepsilon\|_{L^2(\Gamma^\varepsilon)} \leq C \left(\varepsilon^{-\frac{\alpha}{2}} + \varepsilon \right).$$

Remark 7.13. *From* (7.65), u_ε *converges strongly to zero in* $L^2(\Gamma^\varepsilon)$ *when* $\alpha < -1$ *and* $\varepsilon \searrow 0^+$. *We also remark that the internal source* f *in Theorem 7.12 just belongs to* $L^2(\Omega^\varepsilon)$, *which is quite different from the very smoothness of* f *in Theorem 7.11. It is because in Theorem 7.11 we need the boundedness of all the high-order derivatives of* $\tilde{u}_0$ *that solves* (7.40), *while the linearization in Section 7.3 only requires* $f \in L^2(\Omega^\varepsilon)$ *to fulfill the estimate* (7.61) *by the Lax–Milgram-based argument.*

Surface reaction

For the problem (P_ε^S), we can proceed as in [CP99]. If $\beta > 1$ we consider the following asymptotic expansion:

$$u_\varepsilon(x) = u_0(x,y) + \varepsilon^{\beta-1}u_{1,-1}(x,y) + \sum_{(k,l)\in\mathcal{Q}_{\beta,\theta}} \varepsilon^{k\beta+l}u_{k,l}(x,y) + \mathcal{O}(\varepsilon^{\theta+1}),$$

where $x \in \Omega^\varepsilon, y \in Y_l$, $u_{k,l}$ are periodic in y and for $2 \leq \theta \in \mathbb{N}$, we define

$$\mathcal{Q}_{\beta,\theta} := \{(k,l) \in [0,\theta] : k\beta + l \geq 1 \text{ and } k + l \leq \theta\}. \tag{7.66}$$

Taking assumptions on $\mathcal{S}$ as in (A_5)–(A_6) and the fact that $u_{k,l}$ can be obtained by a family of linear partial differential equations for $(k,l) \in \mathcal{Q}_{\beta,\theta}$, we thus state the following result.

Theorem 7.14. *Assume that (A_1) holds. Suppose that $f \in C^\infty(\Omega)$ and let $\mathcal{Q}_{\beta,\theta}$ be defined in (7.66) for given parameters $\beta > 1$ and $2 \leq \theta \in \mathbb{N}$. Let u_ε and $\tilde{u}_0$ be unique weak solutions of the microscopic problem (P_ε^R) and the limit problem (7.40), respectively. For any $\mu \in [0, \theta-1]$ the following higher-order corrector estimate holds*

$$\left\| u_\varepsilon - \tilde{u}_0 - \sum_{(k,l)\in\mathcal{Q}_{\beta,\mu}} \varepsilon^{k\beta+l}u_{k,l} - m^\varepsilon \sum_{(k,l)\in\mathcal{Q}_{\beta,\theta}\setminus\mathcal{M}_{\beta,\mu}} \varepsilon^{k\beta+l}u_{k,l} \right\|_{V^\varepsilon} \leq C\left(\varepsilon^{\theta+\beta-2} + \varepsilon^{\mu+1/2}\right).$$

One has immediately, by the same argument as in (7.62), that u_ε converges strongly in $L^2(\Omega^\varepsilon)$ to zero if $\beta < 0$ and hence, a similar result to Theorem 7.12 can be obtained. Moreover, it remains to derive the convergence for $0 \leq \beta < 1$. If for any f_1, $f_2 \in H^1(\Omega^\varepsilon) \cap L^\infty(\Omega^\varepsilon)$ with $0 < \underline{c} \leq f_1, f_2 \leq \overline{c} < \infty$, we can find a function $f_3 \in L^\infty(\Omega^\varepsilon)$ such that

$$\int_{\Omega^\varepsilon} f_1 u_\varepsilon dx = \int_{\Gamma^\varepsilon} f_2 \mathcal{S}(u_\varepsilon)\, dS_\varepsilon + \varepsilon f_3, \tag{7.67}$$

then one can prove that (cf. [KM17, Lemma 3.4]) for any $\varphi \in H^1(\Omega^\varepsilon)$,

$$\left| \int_{\Omega^\varepsilon} f_1 u_\varepsilon \varphi dx - \varepsilon \int_{\Gamma^\varepsilon} f_2 \mathcal{S}(u_\varepsilon)\, \varphi dS_\varepsilon \right| \leq C\varepsilon \left(\|\varphi\|_{H^1(\Omega^\varepsilon)} + \|f_3\|_{L^\infty(\Omega^\varepsilon)} \right). \tag{7.68}$$

Using (7.67) as an assumption, we state the following theorem.

Theorem 7.15. *Assume (A_1)–(A_4) and (7.67) hold. Suppose that $f \in L^2(\Omega^\varepsilon)$ and $\beta < 1$. Let u_ε be a unique solution in $\widetilde{\mathcal{W}}_\varepsilon$ of the problem (P_ε^S). Then it holds:*

$$\|u_\varepsilon\|_{L^2(\Omega^\varepsilon)} + \sqrt{\varepsilon}\|u_\varepsilon\|_{L^2(\Gamma^\varepsilon)} \leq C\left(\varepsilon^{\frac{1-\beta}{2}} + \varepsilon^{\frac{1}{2}} + \varepsilon\right).$$

Proof. By a simple decomposition with the choice $\varphi = u_\varepsilon$, one thus has

$$\begin{aligned}\int_{\Omega^\varepsilon} f_1 u_\varepsilon^2 dx &= \varepsilon \int_{\Gamma^\varepsilon} f_2 \mathcal{S}\left(u_\varepsilon\right) u_\varepsilon dS_\varepsilon + \int_{\Omega^\varepsilon} f_1 u_\varepsilon^2 dx - \varepsilon \int_{\Gamma^\varepsilon} f_2 \mathcal{S}\left(u_\varepsilon\right) u_\varepsilon dS_\varepsilon \\ &\leq \varepsilon \int_{\Gamma^\varepsilon} f_2 \mathcal{S}\left(u_\varepsilon\right) u_\varepsilon dS_\varepsilon + C\varepsilon \left(\|u_\varepsilon\|_{H^1(\Omega^\varepsilon)} + \|f_3\|_{L^\infty(\Omega^\varepsilon)} \right).\end{aligned} \tag{7.69}$$

We turn our attention to the weak formulation for (P_ε^S), which reads as

$$\int_{\Omega^\varepsilon} \mathbf{A}_\varepsilon\left(x\right) \nabla u_\varepsilon \cdot \nabla \varphi dx + \varepsilon^\beta \int_{\Gamma^\varepsilon} \mathcal{S}\left(u_\varepsilon\right) \varphi dS_\varepsilon = \int_{\Omega^\varepsilon} f \varphi dx \quad \text{for any } \varphi \in V^\varepsilon.$$

Therefore, by choosing $\varphi = u_\varepsilon$ and (A_1), one can estimate that

$$\varepsilon \int_{\Gamma^\varepsilon} f_2 \mathcal{S}\left(u_\varepsilon\right) u_\varepsilon dS_\varepsilon \leq C\varepsilon^{1-\beta} \left(\|f\|_{L^2(\Omega^\varepsilon)} \|u_\varepsilon\|_{L^2(\Omega^\varepsilon)} + \overline{\gamma} \|u_\varepsilon\|_{H^1(\Omega^\varepsilon)}^2 \right). \tag{7.70}$$

Combining (7.69) and (7.70) and thanks to the trace inequality (7.63), we obtain the corrector result for (P_ε^S). □

7.4.2 Volume-surfaces reactions

This part is devoted to tackling the pore-scale elliptic problem (P_ε), based upon the analysis we have done above. Let us start off with the case $\alpha > 0, \beta > 1$ and consider

$$\begin{aligned}u_\varepsilon(x) = u_0(x,y) &+ \varepsilon^\alpha u_{1,0,-1}(x,y) + \varepsilon^{\beta-1} u_{0,1,-1}(x,y) \\ &+ \sum_{(k,l,n)\in\mathcal{M}_\theta} \varepsilon^{k(\alpha+1)+l\beta+n} u_{k,l,n}(x,y) + \mathcal{O}(\varepsilon^{\theta+1}),\end{aligned} \tag{7.71}$$

where $x \in \Omega^\varepsilon, y \in Y_l$ and all components $u_{k,l,n}$ are periodic in y. For $\theta \geq 2$ we define the set $\mathcal{M}_\theta$ as

$$\mathcal{M}_\theta := \left\{(k,l,n) \in [0,\theta] : k(\alpha+1) + l\beta + n \geq 1 \text{ and } k+l+n \leq \theta\right\}, \tag{7.72}$$

inspired very much by (7.22) and (7.66). Moreover, we assume there exist Lipschitz-continuous functions $\bar{\mathcal{R}}$ and $\bar{\mathcal{S}}$ such that

$$\begin{aligned}\mathcal{R}(u_\varepsilon) &= \bar{\mathcal{R}}(u_0) + \varepsilon^\alpha \bar{\mathcal{R}}(u_{1,0,-1}) + \varepsilon^{\beta-1} \bar{\mathcal{R}}(u_{0,1,-1}) \\ &\quad + \sum_{(k,l,n)\in\mathcal{M}_\theta} \varepsilon^{k(\alpha+1)+l\beta+n} \bar{\mathcal{R}}(u_{k,l,n}) + \mathcal{O}(\varepsilon^{\theta+1}), \\ \mathcal{S}(u_\varepsilon) &= \bar{\mathcal{S}}(u_0) + \varepsilon^\alpha \bar{\mathcal{S}}(u_{1,0,-1}) + \varepsilon^{\beta-1} \bar{\mathcal{S}}(u_{0,1,-1}) \\ &\quad + \sum_{(k,l,n)\in\mathcal{M}_\theta} \varepsilon^{k(\alpha+1)+l\beta+n} \bar{\mathcal{S}}(u_{k,l,n}) + \mathcal{O}(\varepsilon^{\theta+1}).\end{aligned}$$

To avoid repeating cumbersome computations and unnecessary arguments, we only state the auxiliary problems and the limit system below, while the others

are left to the interested reader. Using the convention in (7.29), the auxiliary problems are given by

$$(\varepsilon^{-2}):\begin{cases}\mathcal{A}_0 u_0 = 0 \quad \text{in } Y_l,\\ -\mathbf{A}(y)\nabla_y u_0 \cdot \mathrm{n} = 0 \quad \text{on } \Gamma,\\ u_0 \text{ is periodic in } y,\end{cases} \tag{7.73}$$

$$(\varepsilon^{-1}):\begin{cases}\mathcal{A}_0 u_{0,0,1} = -\mathcal{A}_1 u_0 \quad \text{in } Y_l,\\ -\mathbf{A}(y)(\nabla_x u_0 + \nabla_y u_{0,0,1}) \cdot \mathrm{n} = 0 \quad \text{on } \Gamma,\\ u_{0,0,1} \text{ is periodic in } y,\end{cases} \tag{7.74}$$

$$(\varepsilon^{0}):\begin{cases}\mathcal{A}_0 u_{0,0,2} = f - \mathcal{A}_1 u_{0,0,1} - \mathcal{A}_2 u_0 \quad \text{in } Y_l,\\ -\mathbf{A}(y)(\nabla_x u_{0,0,1} + \nabla_y u_{0,0,2}) \cdot \mathrm{n} = 0 \quad \text{on } \Gamma,\\ u_{0,0,2} \text{ is periodic in } y,\end{cases} \tag{7.75}$$

$$(\varepsilon^{\alpha-2}):\begin{cases}\mathcal{A}_0 u_{1,0,-1} = 0 \quad \text{in } Y_l,\\ -\mathbf{A}(y)\nabla_y u_{1,0,-1} \cdot \mathrm{n} = 0 \quad \text{on } \Gamma,\\ u_{1,0,-1} \text{ is periodic in } y,\end{cases} \tag{7.76}$$

$$(\varepsilon^{\alpha-1}):\begin{cases}\mathcal{A}_0u_{1,0,0}=-\mathcal{A}_1u_{1,0,-1} & \text{in } Y_l,\\ -\mathbf{A}(y)(\nabla_x u_{1,0,-1}+\nabla_y u_{1,0,0})\cdot \mathrm{n}=0 \text{ on } \Gamma,\\ u_{1,0,0} \text{ is periodic in } y,\end{cases} \tag{7.77}$$

$$(\varepsilon^{\alpha}):\begin{cases}\mathcal{A}_0u_{1,0,1}+\mathcal{R}(u_0)=-\mathcal{A}_1u_{1,0,0}-\mathcal{A}_2u_{1,0,-1} \text{ in } Y_l,\\ -\mathbf{A}(y)(\nabla_x u_{1,0,0}+\nabla_y u_{1,0,1})\cdot \mathrm{n}=0 \quad \text{on } \Gamma,\\ u_{1,0,1}\text{is periodic in } y,\end{cases} \tag{7.78}$$

$$(\varepsilon^{\beta-3}):\begin{cases}\mathcal{A}_0u_{0,1,-1}=0 & \text{in } Y_l,\\ -\mathbf{A}(y)\nabla_y u_{0,1,-1}\cdot \mathrm{n}=0 & \text{on } \Gamma,\\ u_{0,1,-1} \text{ is periodic in } y,\end{cases} \tag{7.79}$$

$$(\varepsilon^{\beta-2}):\begin{cases}\mathcal{A}_0u_{0,1,0}=-\varepsilon^{\alpha}\mathcal{R}(u_{0,1,-1})-\mathcal{A}_1u_{0,1,-1} & \text{in } Y_l,\\ -\mathbf{A}(y)(\nabla_x u_{0,1,-1}+\nabla_y u_{0,1,0})\cdot n=0 \text{ on } \Gamma,\\ u_{0,1,0} \text{ is periodic in } y,\end{cases} \tag{7.80}$$

$$(\varepsilon^{\beta-1}):\begin{cases}\mathcal{A}_0u_{0,1,1}=-\mathcal{A}_1u_{0,1,0}-\mathcal{A}_2u_{0,1,-1} & \text{in } Y_l,\\ -\mathbf{A}(y)(\nabla_x u_{0,1,0}+\nabla_y u_{0,1,1})\cdot \mathrm{n}=\mathcal{S}(u_0) & \text{on } \Gamma,\\ u_{0,1,1} \text{ is periodic in } y,\end{cases} \tag{7.81}$$

$$\vdots$$

$$(\varepsilon^{k(\alpha+1)+l\beta+n}):\begin{cases}\mathcal{A}_0u_{k,l,n+2}=-\mathcal{A}_1u_{k,l,n+1}-\mathcal{A}_2u_{k,l,n} & \text{in } Y_l,\\ -\mathbf{A}(y)(\nabla_x u_{k,l,n+1}+\nabla_y u_{k,l,n+2})\cdot \mathrm{n}=0 & \text{on } \Gamma,\\ u_{k,l,n} \text{ is periodic in } y,\end{cases} \tag{7.82}$$

for all pairs $(k,l,n)\in\mathcal{K}_{\theta-2}:=\mathcal{M}_{\theta-2}\setminus\{(1,0,0);(0,1,0);(0,0,1)\}$.

Once again, we obtain from (7.73) that $u_0(x,y)=\tilde{u}_0(x)$, and hence the problems (7.74) and (7.75) are solvable in $u_{0,0,1}$ and $u_{0,0,2}$, respectively. On the other hand, from (7.76) and (7.79), we may take $u_{1,0,-1}$ and $u_{0,1,-1}$ as zero functions, without loss of generality. From (7.77) and (7.80), we have $u_{1,0,0}=u_{0,1,0}\equiv 0$ in accordance with (A_3) and so is the function $u_{0,1,1}$ in (7.81). Therefore, we conclude that the family of cell problems can be solved up to the high-order problems (7.82). As a consequence, the corresponding cell problems can be obtained.

From the auxiliary problems (7.73)–(7.75), we know that $u_{0,0,1}(x,y)=-\chi_{0,0,1}(y)\cdot\nabla_x\tilde{u}_0(x)$, where $\chi_{0,0,1}(y)$ is a field of cell functions whose cell problems are given by

$$\begin{cases}\mathcal{A}_0\chi^j_{0,0,1}=\dfrac{\partial\mathbf{A}_{ij}}{\partial y_i} & \text{in } Y_l,\\ -\mathbf{A}\,(y)\,\nabla_y\chi^j_{0,0,1}\cdot\mathrm{n}=\mathbf{A}\,(y)\cdot\mathrm{n}_j & \text{on } \Gamma,\\ \chi^j_{0,0,1} \text{ is periodic,}\end{cases} \tag{7.83}$$

which resembles the problem (7.39). These cell problems admit a unique weak solution $\chi_{0,0,1}\in[H^1_{\#}(Y_l)/\mathbb{R}]^d$.

As in (7.43), we get for $k=l=0$ that $u_{0,0,n}=(-1)^n\chi_{0,0,n}(y)\cdot\nabla^n_x\tilde{u}_0(x)$, and then the high-order cell problems for this case are also determined, similar to

(7.44). In this context, the limit problem remains unchanged and can be recalled from (7.40)–(7.41) with the zero Dirichlet boundary condition for the exterior boundary.

Let us now turn our attention to the corrector estimate in this case.

Theorem 7.16. *Assume* (A_1), (A_5) *and* (A_6) *hold. Assume that* $f \in C^\infty(\Omega)$ *and let* $\mathcal{M}_\theta$ *be defined as in* (7.72) *for given parameters* $\alpha > 0$, $\beta > 1$ *and* $2 \leq \theta \in \mathbb{N}$. *Let* u_ε *and* $\tilde{u}_0$ *be the unique weak solutions of the microscopic problem* (P_ε) *and the limit problem* (7.40), *respectively. Let* $u_{k,l,n}$ *be solutions to the cell problems determined by the auxiliary problems* (7.73)–(7.82) *for* $(k,l,n) \in \mathcal{M}_\theta$. *Then, for any* $\mu \in [0, \theta - 1]$ *the following high-order corrector estimate holds:*

$$\left\| u_\varepsilon - \tilde{u}_0 - \sum_{(k,l,n)\in\mathcal{M}_\mu} \varepsilon^{k(\alpha+1)+l\beta+n} u_{k,l,n} - m^\varepsilon \sum_{(k,l,n)\in\mathcal{M}_\theta\setminus\mathcal{M}_\mu} \varepsilon^{k(\alpha+1)+l\beta+n} u_{k,l,n} \right\|_{V^\varepsilon} \leq C(\varepsilon^{\theta-1+\alpha} + \varepsilon^{\theta+\beta-2} + \varepsilon^{\mu+\min\{\mu\alpha,0\}+1/2}).$$

Proof. We set $\psi_\varepsilon := \varphi_\varepsilon + \sigma_\varepsilon$, where

$$\varphi_\varepsilon = u_\varepsilon - \tilde{u}_0 - \sum_{(k,l,n)\in\mathcal{M}_\theta} \varepsilon^{k(\alpha+1)+l\beta+n} u_{k,l,n},$$
$$\sigma_\varepsilon = (1 - m^\varepsilon) \sum_{(k,l,n)\in\mathcal{M}_\theta\setminus\mathcal{M}_\mu} \varepsilon^{k(\alpha+1)+l\beta+n} u_{k,l,n}.$$

Therefore, we derive the difference equation for φ_ε as in (7.48), while the associated boundary condition is

$$-\mathbf{A}_\varepsilon(x)\nabla\varphi_\varepsilon \cdot \mathrm{n} = -\mathbf{A}_\varepsilon(x) \sum_{\substack{(k,l,n)\in\mathcal{M}_\theta \\ n=\theta}} \varepsilon^{k(\alpha+1)+l\beta+n} \nabla_x u_{k,l,n} \cdot \mathrm{n} + \varepsilon^\beta \left(\mathcal{S}(u_\varepsilon) - \sum_{\substack{(k,l,n)\in\mathcal{M}_\theta \\ n\leq\theta-2}} \varepsilon^{k(\alpha+1)+l\beta+n} \bar{\mathcal{S}}(u_{k,l,n}) \right).$$

For a test function $\varphi \in V^\varepsilon$, one can get the weak formulation of the difference

equation for φ_ε, as follows:

$$
\begin{aligned}
a(\varphi_\varepsilon,\varphi) = &\left\langle \varepsilon^{\alpha}\mathcal{R}(u_\varepsilon) - \sum_{(k,l,n)\in\mathcal{M}_\theta, l\leq\theta-2} \varepsilon^{k(\alpha+1)+l\beta+n+\beta}\bar{\mathcal{R}}(u_{k,l,n}),\varphi\right\rangle_{L^2(\Omega^\varepsilon)}\\
&- \sum_{(k,l,n)\in\mathcal{M}_\theta, n=\theta-1} \varepsilon^{k(\alpha+1)+l\beta+n}\left\langle \mathcal{A}_1 u_{k,l,n+1} + \mathcal{A}_2 u_{k,l,n},\varphi\right\rangle_{L^2(\Omega^\varepsilon)}\\
&- \sum_{(k,l,n)\in\mathcal{M}_\theta, n=\theta} \varepsilon^{k(\alpha+1)+l\beta+n}\left\langle \mathcal{A}_2 u_{k,l,n},\varphi\right\rangle_{L^2(\Omega^\varepsilon)}\\
&+ \int_{\Gamma^\varepsilon} \sum_{(k,l,n)\in\mathcal{M}_\theta} \varepsilon^{k(\alpha+1)+l\beta+n}\mathbf{A}_\varepsilon(x)\nabla u_{k,l,n}\cdot \mathrm{n}\varphi dS_\varepsilon\\
&+ \left\langle \varepsilon^{\beta}\left(\mathcal{S}(u_\varepsilon) - \sum_{\substack{(k,l,n)\in\mathcal{M}_\theta\\ n\leq\theta-2}} \varepsilon^{k(\alpha+1)+l\beta+n}\bar{\mathcal{S}}(u_{k,l,n})\right),\varphi\right\rangle_{L^2(\Gamma^\varepsilon)}.
\end{aligned}
\tag{7.84}
$$

At this stage, we observe that (7.84) resembles (7.51) except the last term on the right-hand side. Thus, it remains to estimate it from above. Clearly, using the Lipschitz property of $\mathcal{S}$ with the Poincaré inequality and the trace inequality on hypersurfaces, one gets

$$
\left|\left\langle \varepsilon^{\beta}\mathcal{S}(u_\varepsilon) - \sum_{\substack{(k,l,n)\in\mathcal{M}_\theta\\ n\leq\theta-2}} \varepsilon^{k(\alpha+1)+l\beta+n+\beta},\varphi\right\rangle_{L^2(\Gamma^\varepsilon)}\right| \leq C\varepsilon^{\theta+\beta-2}\|\varphi\|_{V^\varepsilon}. \tag{7.85}
$$

Following the same argument as for the estimate (7.60), we can bound the inner product of σ_ε from above:

$$
\begin{aligned}
&\left|\left\langle (1-m^\varepsilon)\sum_{(k,l,n)\in\mathcal{M}_\theta\setminus\mathcal{M}_\mu} \varepsilon^{k(\alpha+1)+l\beta+n}u_{k,l,n},\varphi\right\rangle\right|\\
&\qquad\leq C(\varepsilon^{\mu+\min\{\mu\alpha,0\}+1/2} + \varepsilon^{\mu+\min\{\mu\alpha,0\}+3/2}).
\end{aligned}
\tag{7.86}
$$

Thanks to the triangle inequality. By choosing $\varphi=\psi_\varepsilon$, we combine (7.84), (7.85) and (7.86) to get the corrector estimate

$$
\|\psi_\varepsilon\|_{V^\varepsilon} \leq C(\varepsilon^{\theta-1+\alpha} + \varepsilon^{\theta+\beta-2} + \varepsilon^{\mu+\min\{\mu\alpha,0\}+1/2} + \varepsilon^{\mu+\min\{\mu\alpha,0\}+3/2}).
$$

Hence, we complete the proof of the theorem. □

When either $\alpha<0$ or $\beta<0$ is satisfied, the asymptotic limit of u_ε is close to zero. Indeed, we recall from Section 7.2 that

$$
\|\nabla u_\varepsilon\|^2_{L^2(\Omega^\varepsilon)} + \left(\varepsilon^{\alpha}+\varepsilon^{\beta}\right)\left(\|u_\varepsilon\|^2_{L^2(\Omega^\varepsilon)} + \|u_\varepsilon\|^2_{L^2(\Gamma^\varepsilon)}\right) \leq C. \tag{7.87}
$$

Thanks to the elementary Bunyakovsky–Cauchy–Schwarz inequality, we deduce from (7.87) that

$$\varepsilon^{\frac{\alpha}{2}} \|u_\varepsilon\|_{L^2(\Omega^\varepsilon)} + \varepsilon^{\frac{\beta}{2}} \|u_\varepsilon\|_{L^2(\Gamma^\varepsilon)} \leq C,\ \varepsilon^{\frac{\beta}{2}} \|u_\varepsilon\|_{L^2(\Omega^\varepsilon)} + \varepsilon^{\frac{\alpha}{2}} \|u_\varepsilon\|_{L^2(\Gamma^\varepsilon)} \leq C.$$

Henceforth, the theorems for these cases can be stated as in Theorem 7.12.

When $\alpha > 0$ and $0 \leq \beta < 1$, we proceed as in Subsection 7.4.1: for any $f_1, f_2 \in H^1(\Omega^\varepsilon) \cap L^\infty(\Omega^\varepsilon)$ with $0 < \underline{c} \leq f_1, f_2 \leq \bar{c} < \infty$, assume that we can find a function $f_3 \in L^\infty(\Omega^\varepsilon)$ such that (7.67) holds. Then we are led to the estimates (7.68) and (7.69). Recalling the weak formulation of (P_ε), which reads as

$$\int_{\Omega^\varepsilon} \mathbf{A}_\varepsilon(x) \nabla u_\varepsilon \cdot \nabla \varphi dx + \varepsilon^\beta \int_{\Gamma^\varepsilon} \mathcal{S}(u_\varepsilon) \varphi d\mathcal{S}_\varepsilon + \varepsilon^\alpha \int_{\Omega^\varepsilon} \mathcal{R}(u_\varepsilon) \varphi dx = \int_{\Omega^\varepsilon} f \varphi dx$$

for any $\varphi \in H^1(\Omega^\varepsilon)$, by choosing $\varphi = u_\varepsilon$ and (A_1)–(A_4) one can get

$$\varepsilon \int_{\Gamma^\varepsilon} \mathcal{S}(u_\varepsilon) u_\varepsilon d\mathcal{S}_\varepsilon \leq \varepsilon^{1-\beta} (\bar{\gamma} \|u_\varepsilon\|^2_{H^1(\Omega^\varepsilon)} + \delta_1 \varepsilon^\alpha \|u_\varepsilon\|^2_{L^2(\Omega^\varepsilon)} + \|f\|_{L^2(\Omega^\varepsilon)} \|u_\varepsilon\|_{L^2(\Omega^\varepsilon)}). \tag{7.88}$$

Combining (7.69) and (7.88), we obtain

$$\|u_\varepsilon\|^2_{L^2(\Omega^\varepsilon)} \leq C(\varepsilon^{1-\beta}(1 + \varepsilon^\alpha) + \varepsilon). \tag{7.89}$$

Applying the trace inequality (7.63) to (7.89), we can finalize the corrector results for (P_ε) by the following theorem.

Theorem 7.17. *Assume (A_1)–(A_3) hold. Suppose that $f \in L^2(\Omega^\varepsilon)$ and $\alpha > 0, 0 \leq \beta < 1$. Let u_ε be a unique solution in $\widetilde{\mathcal{W}}_\varepsilon$ of the problem (P_ε). Then, the following estimate holds:*

$$\|u_\varepsilon\|_{L^2(\Omega^\varepsilon)} + \sqrt{\varepsilon} \|u_\varepsilon\|_{L^2(\Gamma^\varepsilon)} \leq C \left(\varepsilon^{\frac{1-\beta}{2}} (1 + \varepsilon^{\frac{\alpha}{2}}) + \varepsilon^{\frac{1}{2}} \right). \tag{7.90}$$

7.4.3 A numerical example

Here, we illustrate the asymptotic behaviors of the microscopic problem for different values of the scaling factors $\beta_1, \beta_2 \in \mathbb{R}$. For simplicity, we consider (P_ε) in two dimensions with the linear mappings $\mathcal{R}, \mathcal{S}$ of the form $\mathcal{R}(z) = C_1 z, \mathcal{S}(z) = C_2 z$ for $C_1 > 0$ and $C_2 \geq 0$. Taking $C_1 = 1$, we arrive at a modified Helmholtz-type equation. We choose the unit square $\Omega = (0,1) \times (0,1)$ the domain of interest and the oscillatory diffusion as

$$\mathbf{A}(x/\varepsilon) = \frac{1}{2 + \cos\left(\frac{2\pi x_1}{\varepsilon}\right) \cos\left(\frac{2\pi x_2}{\varepsilon}\right)}.$$

Moreover, we consider the unit cell $Y = (0,1) \times (0,1)$ with a reference circular hole of radius $r = 0.4$ and take the volumetric source $f = 1$ and define the volume porosity as $|Y_l| = 1 - \pi r^2 \approx 0.497$. According to (7.83), the effective diffusion coefficient is computed as

$$\bar{\mathbf{A}} = \begin{pmatrix} 0.191613 & 2.025 \times 10^{-9} \\ 2.025 \times 10^{-9} & 0.191613 \end{pmatrix}.$$

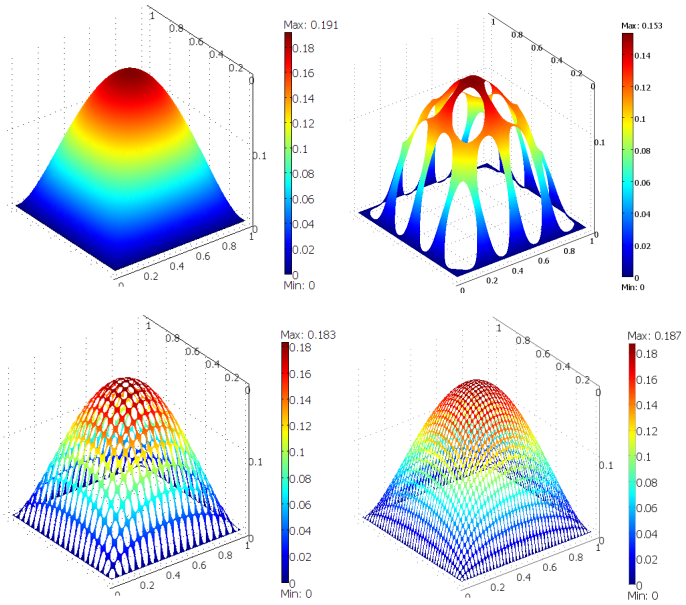

Figure 7.3: Comparison between the homogenized solution and the microscopic solution for $\varepsilon \in \{0.25, 0.05, 0.025\}$.

Comments on numerical results

To verify our theoretical results, we divide the scale factors β_1 and β_2 into three cases:

1. When $\beta_1 > 0$ and $\beta_2 > 1$, u_ε converges to $\tilde{u}_0$ of the homogenized problem (7.40)–(7.41).

2. When either $\beta_1 < 0$ or $\beta_2 < 0$, u_ε converges to 0.

3. When $\beta_1 > 0$ and $0 \leq \beta_2 < 1$, u_ε converges to 0.

Suppose we take $C_2 = 1$. We consider the first case by fixing $\beta_1 = 1$ and $\beta_2 = 2$. Here, we use the standard linear FEM with a mesh discretization, which is much more smaller than ε to solve the microscopic problem for various values of $\varepsilon \in \{0.25, 0.05, 0.025, 0.01, 0.005\}$. In Figure 7.3, we compare the homogenized solution $\tilde{u}_0$ with the microscopic solution u_ε at some chosen values of $\varepsilon \in \{0.25, 0.01, 0.025\}$. It can be seen that the microscopic solution converges to the homogenized solution as ε tends to 0. This confirms the usual performance of our homogenization procedure. Based on Table 7.1, it can also be seen that the homogenized solution $\tilde{u}_0$ is the excellent approximation candidate when ε gets smaller and smaller.

For the second case, we verify the sub-cases $\beta_1 = -1, \beta_2 = 1$ and $\beta_1 = 1, \beta_2 = -1$, respectively. As depicted in Figure 7.4, we find that u_ε converges to 0 as $\varepsilon \searrow 0^+$, which agrees with Theorem 7.12. Moreover, we have tabulated in Table 7.2 the smallness of the microscopic solution in ℓ^2-norm of these cases at various $\varepsilon \in \{0.25, 0.025, 0.00125, 0.001\}$. In the same spirit, choosing $\beta_1 = 1$ and $\beta_2 = 1/2$

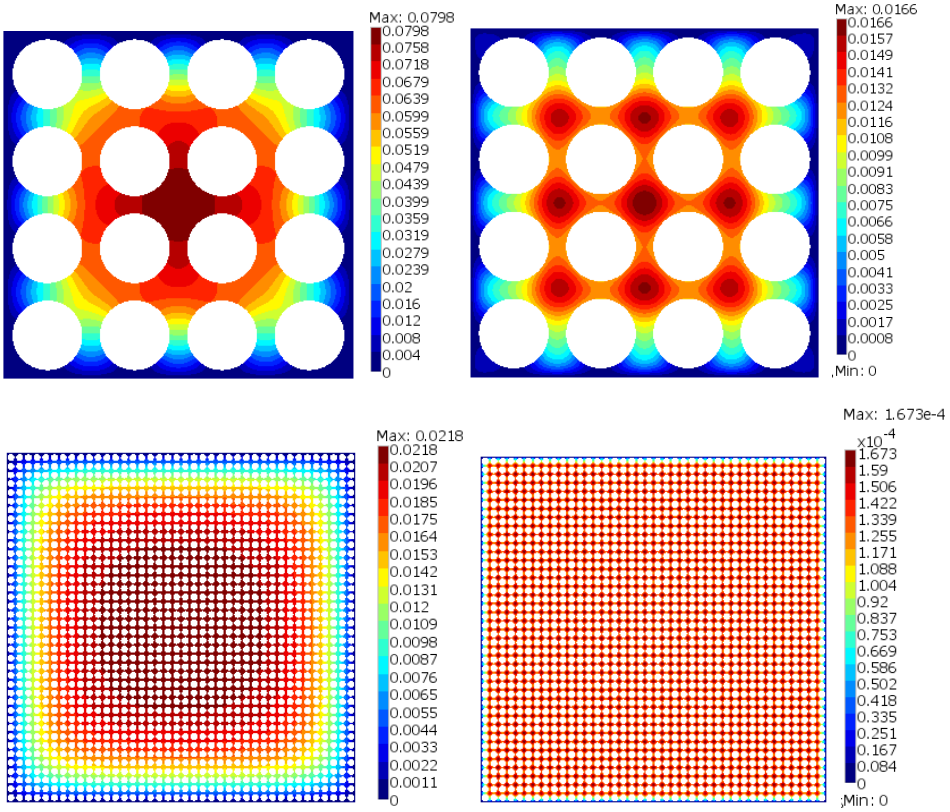

Figure 7.4: Behavior of the microscopic solution u_ε for the sub-cases $\beta_1 = -1, \beta_2 = 1$ and $\beta_1 = 1, \beta_2 = -1$ at $\varepsilon = 0.25$ (top) and $\varepsilon = 0.025$ (bottom).

the convergence to 0 of u_ε is guaranteed by Theorem 7.17 and this is verified by the numerical results tabulated in Table 7.3.

It is worth mentioning that we can also corroborate the case $\beta_1 < -1$ discussed in Remark 7.13 where u_ε converges to 0 at the micro-surfaces. Indeed, taking $C_2 = 0$ and $\beta_1 = -2$ we obtain the numerical results in Table 7.4, which are consistent with Theorem 7.12.

The convergence rates in Tables 7.1, 7.2, 7.3 and 7.4 are also depicted in Figure 7.5, where we show log-log plots of the numerical errors.

ε	0.25	0.05	0.025	0.01	0.005
$\|u_\varepsilon - \tilde{u}_0\|_{\ell^2}$	0.015219	0.003079	0.001550	0.000266	9.623×10^{-5}

Table 7.1: Numerical results in the ℓ^2-norm of u_ε in the microscopic domain for $\beta_1 = 1, \beta_2 = 2$ and choices of ε.

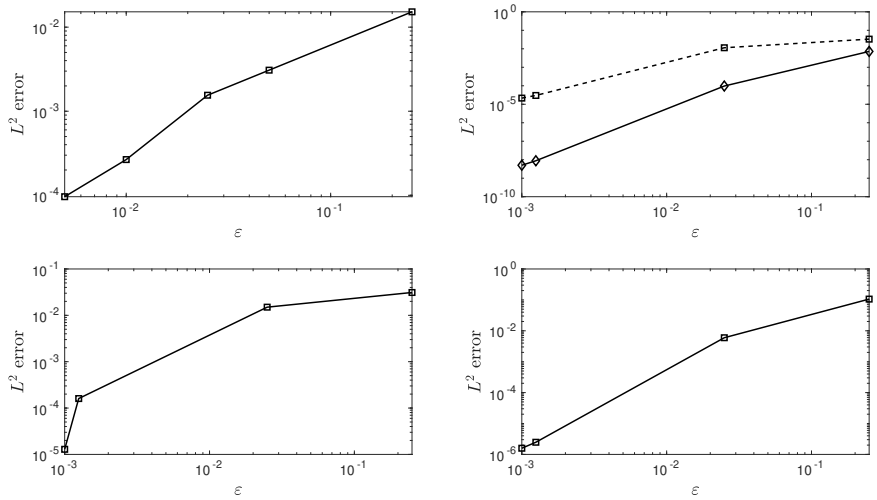

Figure 7.5: Convergence results in the ℓ^2-norm of u_ε in the microscopic domain for various combinations of the parameters β_1, β_2 and choices of ε. *First panel:* $\beta_1 = 1, \beta_2 = 2$. *Second panel:* $\beta_1 = -1, \beta_2 = 1$ (dashed square) and $\beta_1 = 1, \beta_2 = -1$ (solid diamond). *Third panel:* $\beta_1 = 1, \beta_2 = 1/2$. *Fourth panel:* convergence at the micro-surfaces for $\beta_1 = -2, C_2 = 0$.

ε	0.25	0.025	0.00125	0.001
$\beta_1 = -1, \beta_2 = 1$				
$\|u_\varepsilon\|_{\ell^2}$	0.0333	0.0114	2.9938×10^{-5}	2.1528×10^{-5}
$\beta_1 = 1, \beta_2 = -1$				
$\|u_\varepsilon\|_{\ell^2}$	0.0072	9.6755×10^{-5}	8.789×10^{-9}	5.0318×10^{-9}

Table 7.2: Numerical results in the ℓ^2-norm of u_ε in the microscopic domain for $\beta_1 = -1, \beta_2 = 1$ and $\beta_1 = 1, \beta_2 = -1$ and choices of ε.

ε	0.25	0.025	0.00125	0.001
$\|u_\varepsilon\|_{\ell^2}$	0.0311	0.0150	1.6029×10^{-4}	1.2887×10^{-5}

Table 7.3: Numerical results in the ℓ^2-norm of u_ε in the microscopic domain for $\beta_1 = 1, \beta_2 = 1/2$ and choices of ε.

ε	0.25	0.025	0.00125	0.001
$\|u_\varepsilon\|_{\ell^2(\Gamma^\varepsilon)}$	0.10589	0.00596	2.474×10^{-6}	1.584×10^{-6}

Table 7.4: Numerical results in the ℓ^2-norm of u_ε at the micro-surfaces for $\beta_1 = -2, C_2 = 0$.

7.5 Discussion

We studied a microscopic semilinear elliptic equation posed in periodically perforated domains. The structure of a linearization scheme together with a suitable

choice of scalings and stabilization constants allow us to prove the existence of the microscopic model. In this work, as main finding we point out the structure trivial and non-trivial macroscopic models, depending on the choice of β_1 and β_2. Moreover, we designed a new asymptotic expansion, which accounts for the presence of the scaling parameters. The high-order corrector estimates we provided in this chapter are involving the presence of such scaling parameters.

Note that our active–passive pedestrian dynamics discussed in Chapter 6 can, in principle, be formulated in a multiscale setting in perforated domains. Hence, this work basically gives us a fundamental homogenization background to study the asymptotics of a class of Langevin equations posed in perforated domains using the Skorohod formulation. In this context, we refer to the methods of averaging and of homogenization for SDEs (see e.g. in [PS07]) to tackle the following microscopic Langevin equations

$$dX_t^\varepsilon = b(X_t^\varepsilon, t)dt + \sigma(X_t^\varepsilon, t)dB_t + d\Phi_t^\varepsilon, \tag{7.91}$$

where b is a random force in terms of a confining potential representing the effect of interacting particles, while σ represents the diffusion coefficient. In addition, Φ_t is an associated process so that X_t^ε is a reflecting process and B_t is a standard Brownian motion.

A related possible direction is to study the combined mean field and homogenization limits for a system of interacting diffusions in a two-scale potential (see e.g. in [GP18]). We refer the reader also to [OP11, LW18] for remotely related settings.

Chapter 8

Concluding remarks. Outlook

In this dissertation, we studied various models aimed at describing crowds of mixed active–passive populations moving inside heterogenous environments. We addressed the subject from three different perspectives, driven by our main questions discussed in Chapter 1. Following these questions, the thesis is structured into three main parts in which we adopt approaches inspired by lattice gas models, a fluid-like driven system and by a system of Skorohod-like stochastic differential equations. This is the moment to review briefly what we have done in this thesis and point out to what remains to be done.

8.1 Summary

In Chapter 2, we introduced what we mean by the dynamics of active–passive pedestrian populations. Also, we provided our motivation to study this scenario as well as the mathematical structure of the involved models.

In Chapter 3, we studied the problem of the evacuation of a crowd of pedestrians from an obscure region. We started from the assumption that the crowd is made of both active and passive pedestrians. The hazardous motion of pedestrians due to lack of visibility and, possibly, combined also to a high level of stress is modeled via a simple exclusion process on a two-dimensional lattice equipped with appropriate boundary conditions. The particle system modeling the crowd is strongly interacting via the simple exclusion principle – each site can be occupied by only a single particle. The main observable is the evacuation time as a function of the parameters caracterizing the motion of the active pedestrians. We have found that the presence of the active pedestrians favors the evacuation of the passive ones. This is a rather surprising effect since we explicitly do not allow for any communication among the pedestrians. A similar effect is also observed when looking at the outgoing particle flux, when the system is in contact with an external particle reservoir that induces the onset of a steady state. We interpret this phenomenon as a discrete space counterpart of the so-called drafting effect, which typically is observed in a continuum set-up.

In Chapter 4, based again on the simple exclusion process, we studied the

dynamics of two populations of active–passive particles, mimicking pedestrians walking in a building environment, entering a room from two opposite sides. We see that if active particles undergo a non–zero drift and the visibility zone is sufficiently large, then the outgoing flux of passive particles improves.

We decided to study in Chapter 5 a macroscopic formulation of the dynamics of active–passive pedestrians. We provided the well-posedness of a system of parabolic equations consisting of a double nonlinear parabolic equation of Forchheimer type for the active population coupled with a semilinear parabolic equation for the passive population. The system describes the motion of a fast "fluid" combined with a "slow" fluid. We relied on special energy estimates and on the use a Schauder's fixed point argument to tackle the existence of weak solutions to our evolution problem. The structure of the nonlinearity of the coupling allowed us to prove also the uniqueness of solutions. Moreover, the stability estimates of solutions with respect to selected parameters are provided.

We turned the attention in Chapter 6 to a microscopic formulation of the active–passive population dynamics in a heterogenous environment with fire and smoke. We showed the existence and uniqueness of strong solutions to a coupled system of Skorohod-like stochastic differential equations with reflecting boundary condition. We used compactness methods together with the Skorohod's representation of solutions to ensure the solvability of the system. The proof of uniqueness of solutions is based on standard arguments.

In Chapter 7, we started to prepare a homogenization setting where later on our microscopic pedestrian dynamics can be studied. To fix ideas, we considered a semilinear elliptic equation posed in periodically perforated domains and associated with a Fourier-type condition on internal interfaces. In such a continuum-level description, this is seen as a microscopic problem to be upscaled. We provided a linearization scheme which by a suitable choice of scaling arguments and stabilization constants allowed us to prove the weak solvability of the microscopic model. Based on classical results for homogenization of multiscale elliptic problems, we designed a modified two-scale asymptotic expansion to derive the corresponding macroscopic equation, when the scaling choices are compatible. Furthermore, we proved high-order corrector estimates that involve the explicit presence of the scaling parameters. A numerical example is provided to confirm the asymptotic analysis.

8.2 Outlook

There are a few open questions that would need further investigation. We enumerate them here.

1. From the perspective of lattice models:

- The topic of "exit choices" is one of the interesting problems in the field of pedestrian evacuation. It would be e.g. interesting to find out to which extent the choice of the exit affects the overall evacuation time.

- In order to describe a realistic scenario, it would be very useful to find out an extended model where the active pedestrians can transmit to the passive population the information of the geometry, hoping that this way the evacuation time can be reduced.

- The model validation is an open question in this context. A suitable experiment design is needed to make any progress in this sense (see in e.g. [LRR$^+$20]).

- The flux of passive particles can be controlled via the active particle dynamics. This fact has been observed for a specific geometry and for a specific dynamics. Can perhaps our investigation be extended to concrete urban geometries, multiple populations of pedestrians, and different dynamics? This could provide potentially useful information for large crowd management.

- It would be interesting to study the inclusion of non-local interactions among particles, where the interaction range is considered as mesoscopic, namely it is much larger than the microscopic lattice unity (conventionally taken as the unity in statistical mechanics) and much less than the macroscopic size of the system. One promising candidate is the so-called Kac potential (see e.g. in [Pre09]) in which we may find the way to analytic calculations.

- Another open direction is the investigation of the hydrodynamic limit of the lattice dynamics (that might in fact be quite complicated due to the presence of two different species of particles and the geometry).

2. From the perspective of fluid-like driven systems:

- The structural stability with respect to the Forchheimer polynomial $K_1(\cdot)$ can be improved. Specifically, the estimate (5.25) needs to be much stronger to provide a full control on the gradient.

- A generalized Forchheimer flow model can inprinciple be obtained via homogenization techniques. Therefore, the structure of such models could be studied further for periodic geometries.

- We could formulate the model such that the pedestrian populations can interact with their surrounding environment (geometry, fire, smoke). Formulating this relationship mathematically would allow for an optimization approach, potentially in a multiscale setting.

- Like for all evacuation problems, the large time behavior of the weak solution to our fluid-like driven system would need to be investigated.

3. From the perspective a stochastic differential equations of Skorohod type:

- A convergent numerical approximation of solutions to (6.17)-(6.18) needs to be implemented. One possible route is to design an iterative weak approximation of the Skorohod system as it is done e.g. in [BGT04], [NO10], and in the references cited therein.

- We supposed that the fire is stationary, i.e. ∂F is independent on t. Trusting ideas from [NO10], we expect that it is possible to handle the case of a time-evolving fire, provided the shape of the fire $\partial F(t)$ is sufficiently regular and it is *a priori* prescribed.

- From a mathematical point of view, the situation becomes a lot more challenging when there is a feedback mechanism between the pedestrian dynamics and the environment (fire and geometry) (see e.g. in [RN19]). Taking into account the smoke observable $s(x,t)$, an extension can be done in this context. As a further development of our model, it would be interesting to study the "transport" of smoke eventually via a measure-valued equation (cf. e.g. [EHM16]), coupled with our SDEs for the pedestrian dynamics. The well-posedness of such model needs to be investigated. Again, it is also interesting to study the large-time behavior of the system of evolution equations. In this context, another direction is the use of a stochastically perturbed diffusion-transport equation instead of a measure-valued equation for the smoke dynamics. The coupling between the SDEs for the crowd dynamics and the SPDE for the smoke evolution potentially offers new challenges (see e.g. in [CJK18]). However, in both cases, it is not yet clear cut how to couple correctly the model equations.

- In our crowd dynamics model, besides the social pressure and the repelling from overlapping, there are no other imposed interactions between pedestrians. It would be interesting to build a model where there are additional interactions between active–passive pedestrians; we refer for instance to the setting described in [CTB$^+$18], where active and passive particles interplay together to find exits in a maze.

- Note that our crowd dynamics can be formulated in a multiscale setting for instance in perforated domains. Based on the methods of averaging and of the homogenization for SDEs (see e.g. in [PS07]), the asymptotic of a class of Langevin equations posed in perforated domains using a Skorohod formulation could be obtained. Some other possible directions would be a combine mean field and homogenization limits for a system of interacting diffusions in a two-scale potential (see e.g. in [GP18]); see also [OP11,LW18] for related situations.

- A novel trend promoted e.g. in [AD20], it would be interesting to take a mean-field game approach to our system of SDEs of Skorohod type that models pedestrian motion.

Appendix

A.1 Rigorous definition of the active–passive dynamics in Chapter 4

The state of the system is a *configuration* $\eta \in \mathcal{C} = \{-1, 0, 1\}^\Lambda$ and we say that the site x is *empty* if $\eta_x = 0$, *occupied by an active particle* if $\eta_x = 1$, and *occupied by a passive particle* if $\eta_x = -1$. The number of active (respectively, passive) particles in the configuration η is given by $n_{\mathrm{A}}(\eta) = \sum_{x\in\Lambda} \delta_{1,\eta_x}$ (respectively, $n_{\mathrm{P}}(\eta) = \sum_{x\in\Lambda} \delta_{-1,\eta_x}$), where $\delta_{\cdot,\cdot}$ is Kronecker's symbol. Their sum is the total number of particles in the configuration η.

Picked the positive integers N_{A} and N_{P} and set $N = N_{\mathrm{A}} + N_{\mathrm{P}}$, the dynamics is the continuous time Markov chain $\eta(t)$ on Ω with initial configuration $\eta(0)$ such that $n_{\mathrm{A}}(\eta(0)) = N_{\mathrm{A}}$ and $n_{\mathrm{P}}(\eta(0)) = N_{\mathrm{P}}$ and rates $c(\eta, \eta')$ defined as follows (recall the function $\epsilon(x, y)$ is defined in Section 2.2.2): we let the rate $c(\eta, \eta')$ be equal

- to 1 if η' can be obtained by η by replacing with 0 a -1 at the right door (passive particles leave the room);
- to $1 + \epsilon(x, y)$ if η' can be obtained by η by replacing with 0 a 1 at the left door (active particles leave the room);
- to $[N_{\mathrm{A}} - n_{\mathrm{A}}(\eta)]/m_{\mathrm{R}}$ if the number of empty sites in the right door is $m_{\mathrm{R}} > 0$ and η' can be obtained by η by adding a 1 at one of the empty sites of the right door;
- to $[N_{\mathrm{P}} - n_{\mathrm{P}}(\eta)]/m_{\mathrm{L}}$ if the number of empty sites in the left door is $m_{\mathrm{L}} > 0$ and η' can be obtained by η by adding a -1 at one of the empty sites of the left door;
- to 1 if η' can be obtained by η by exchanging a -1 with a 0 between two neighboring sites of Λ (motion of passive particles inside Λ);
- to $1 + \epsilon(x, y)$ if η' can be obtained by η by exchanging a $+1$ at site x with a 0 at site y, with x and y nearest neighbor sites of Λ (motion of active particles inside Λ);
- to 0 in all the other cases.

We stress that, at time t, the quantities $N_{\mathrm{A}} - n_{\mathrm{A}}(\eta(t))$ and $N_{\mathrm{P}} - n_{\mathrm{P}}(\eta(t))$ represent the number of active, and, respectively, passive particles that exited the room and entered their own waiting list at time t, whereas $m_{\mathrm{L}} > 0$ and $m_{\mathrm{R}} > 0$ are the number of empty sites of the left and right doors at time t.

We simulate the model introduced above and in Section 2.2.2 using the following scheme: at time t, we extract an exponential random time τ with parameter the total rate $\sum_{\zeta\in\Omega} c(\eta(t),\zeta)$ and set the time equal to $t+\tau$. We then select a configuration using the probability distribution $c(\eta(t),\xi)/\sum_{\zeta\in\Omega} c(\eta(t),\zeta)$ and then set $\eta(t+\tau)=\xi$.

A.2 Regularized Eikonal equation for motion planning

To describe how the active population moves within D, we use a motion planning in terms of the solution of the following regularized Eikonal equation:

$$\begin{cases} -\varsigma\Delta\phi_\varsigma + |\nabla\phi_\varsigma|^2 = f^2 & \text{in } D, \\ \phi_\varsigma = 0 & \text{at } E, \\ \nabla\phi_\varsigma\cdot\mathbf{n} = 0 & \text{at } \partial(\mathbb{O}\setminus(G\cup E\cup F)), \end{cases} \tag{1}$$

where $\varsigma > 0$ given sufficiently small. In fact, $|\nabla\phi_\varsigma|$ plays the role of *a priori* known guidance (navigation information). Inspired very much from the implementation of video games, this is a strategy commonly used in most major crowd evacuation softwares, i.e. the map of the building to be evacuated is built-in. An alternative motion guidance strategy is suggested in [YDW+14].

We point out the existence and uniqueness of classical solutions to the problem (1) in the following Lemma.

Lemma A.1. *Assume that $f \in C^{\bar\alpha}(D)$ with $0 < \bar\alpha < 1$. Let $D \subset \mathbb{R}^2$ be a bounded domain with $\partial D \cup \partial G \in C^{2,\bar\alpha}$. Then the problem (1) has a unique solution $\phi_\varsigma \in C(\overline{D}) \cap C^2(D)$.*

Proof. The idea of this proof comes from Theorem 2.1, p.10, in [Sch06] for the case of the Dirichlet problem. In fact, the semilinear viscous problem (1) can be transformed into a linear partial differential equation via $w_a : D \longrightarrow \mathbb{R}$ given by

$$w_a(\phi_\varsigma) := \exp(-\varsigma^{-1}\phi_\varsigma) - 1, \tag{2}$$

where $a = \frac{1}{\varsigma}$. Then $w_a \in C(\overline{D})\cap C^2(D)$ becomes a solution of the following linear partial differential equation with mixed Dirichlet-Neumann boundary conditions:

$$\begin{cases} -\Delta w_a + f^2a^2w_a + a^2 = 0 & \text{in } D, \\ w_a = 0 & \text{at } E, \\ \nabla w_a\cdot\mathbf{n} = 0 & \text{at } \partial D\cup\partial G. \end{cases} \tag{3}$$

Futhermore, there is a unique solution $w_a \in C(\overline{D}) \cap C^2(D)$ of the problem (3) (see in Theorem 1, [Lie86]). This also implies that there is a unique solution $\phi_\varsigma \in C(\overline{D}) \cap C^2(D)$ to the problem (1). □

A.3 Nondimensionalization of the system of SDEs (2.5) and (2.8)

In this section, we nondimensionalize the system (2.5)-(2.8). By this procedure, we aim to identify the relevant characteristic time and length scales involved in this crowd dynamics scenario. We introduce $x_{a_i}^{\text{ref}}, x_{p_k}^{\text{ref}}, x_{\text{ref}}$ and $t_{a_i}^{\text{ref}}, t_{p_k}^{\text{ref}}, t_{\text{ref}}$ as possible characteristic length and time scales, respectively. We choose

$X_{a_i}(t_{\text{ref}}\tau) := \frac{x_{a_i}(t)}{x_{a_i}^{\text{ref}}}, X_{p_k}(t_{\text{ref}}\tau) := \frac{x_{p_k}(t)}{x_{p_k}^{\text{ref}}}, z := \frac{x}{x_{\text{ref}}}$ and $\tau := \frac{t_{a_i}}{t_{a_i}^{\text{ref}}} = \frac{t_{p_k}}{t_{p_k}^{\text{ref}}} = \frac{t}{t_{\text{ref}}}$ where $x_{a_i}^{\text{ref}} = x_{p_k}^{\text{ref}} = x_{\text{ref}}$ and $t_{a_i}^{\text{ref}} = t_{p_k}^{\text{ref}} = t_{\text{ref}}$. Then, equations (2.5) and (2.8) become

$$\begin{cases} \frac{x_{\text{ref}}}{t_{\text{ref}}}\frac{d}{d\tau}X_{a_i}(t_{\text{ref}}\tau) & = \Upsilon_{\text{ref}} s_{\text{ref}} \tilde{\Upsilon}(S(x_{\text{ref}}X_{a_i}(t_{\text{ref}}\tau)))\frac{\phi_{\text{ref}}\nabla_{X_{a_i}}\tilde{\phi}(x_{\text{ref}}X_{a_i}(t_{\text{ref}}\tau))}{\phi_{\text{ref}}|\nabla_{X_{a_i}}\tilde{\phi}(x_{\text{ref}}X_{a_i}(t_{\text{ref}}\tau))|}(p_{\max} \\ & \quad -p_{\text{ref}}\tilde{p}(x_{\text{ref}}X_{a_i}(t_{\text{ref}}\tau), t_{\text{ref}}\tau)), \\ X_{a_i}(0) & = \frac{X_{a_i 0}}{x_{\text{ref}}}, \end{cases} \tag{4}$$

where

$$\begin{aligned} p(\mathbf{x}_{a_i}(t), t) &= p_{\text{ref}}\tilde{p}(x_{\text{ref}}X_{a_i}(t_{\text{ref}}\tau), t_{\text{ref}}\tau) \\ &= \mu_{\text{ref}}\tilde{\mu}(t_{\text{ref}}\tau_{a_i})\int_{\ddot{D}\cap B(x_{\text{ref}}X_{a_i}, \tilde{\delta}_{\text{ref}}\hat{\tilde{\delta}})}\sum_{j=1}^{N}\delta(y_{\text{ref}}Y - x_{\text{ref}}X_{c_j}(t_{\text{ref}}\tau)y_{\text{ref}}dY. \end{aligned} \tag{5}$$

$$\begin{cases} \frac{x_{\text{ref}}}{t_{\text{ref}}}\frac{d}{d\tau}X_{p_k}(t_{\text{ref}}\tau) & = \sum_{j=1}^{N}\frac{x_{\text{ref}}X_{c_j} - x_{\text{ref}}X_{p_k}}{\epsilon + |x_{\text{ref}}X_{c_j} - x_{\text{ref}}X_{p_k}|}\omega_{\text{ref}}\tilde{\omega}(|x_{\text{ref}}X_{c_j} \\ & \quad -x_{\text{ref}}X_{p_k}|, S(x_{\text{ref}}X_{p_k}, t_{\text{ref}}\tau)) \\ & \quad +\beta_{\text{ref}}\tilde{\beta}(S(x_{\text{ref}}X_{p_k}, t_{\text{ref}}\tau)))\sqrt{d\tau}\frac{d\tilde{B}(t_{\text{ref}}\tau)}{\sqrt{d\tau}}, \\ X_{p_k}(0) & = \frac{X_{p_k 0}}{x_{\text{ref}}}, \end{cases} \tag{6}$$

where

$$\omega(y, z) = \omega_{\text{ref}}\tilde{\omega}(y_{\text{ref}}\tilde{y}, z_{\text{ref}}\tilde{z}) = -\beta_{\text{ref}}\beta(z_{\text{ref}}\tilde{z})\left(C_A e^{-\frac{y_{\text{ref}}\tilde{y}}{\ell_A}} + C_R e^{-\frac{y_{\text{ref}}\tilde{y}}{\ell_R}}\right), \tag{7}$$

$$\beta(y) = \beta_{\text{ref}}\tilde{\beta}(y_{\text{ref}}M) = \begin{cases} 1, \text{ if } y_{\text{ref}}M < s_{\text{cr}}, \\ 0, \text{ if } y_{\text{ref}}M \geq s_{\text{cr}}. \end{cases} \tag{8}$$

Multiplying (4) by $\frac{t_{\text{ref}}}{x_{\text{ref}}}$, we are led to

$$\begin{cases} \frac{d}{d\tau}X_{a_i}(t_{\text{ref}}\tau) & = \frac{\Upsilon_{\text{ref}}t_{\text{ref}}s_{\text{ref}}}{x_{\text{ref}}}\tilde{\Upsilon}(S(x_{\text{ref}}X_{a_i}(t_{\text{ref}}\tau)))\frac{\phi_{\text{ref}}\nabla_{X_{a_i}}\tilde{\phi}(x_{\text{ref}}X_{a_i}(t_{\text{ref}}\tau))}{\phi_{\text{ref}}|x_{\text{ref}}\nabla_{X_{a_i}}\tilde{\phi}(X_{a_i}(t_{\text{ref}}\tau))|}(p_{\max} \\ & \quad -p_{\text{ref}}\tilde{p}(x_{\text{ref}}X_{a_i}(t_{\text{ref}}\tau), t_{\text{ref}}\tau)), \\ X_{a_i}(0) & = \frac{X_{a_i 0}}{x_{\text{ref}}}. \end{cases} \tag{9}$$

Similarly, we obtain

$$\begin{cases} \frac{d}{d\tau}X_{p_k}(t_{\rm ref}\tau) & = \frac{\omega_{\rm ref}t_{\rm ref}}{x_{\rm ref}}\sum_{j=1}^{N}\frac{x_{\rm ref}X_{c_j}-x_{\rm ref}X_{p_k}}{\epsilon+|x_{\rm ref}X_{c_j}-x_{\rm ref}X_{p_k}|}\tilde{\omega}(|x_{\rm ref}X_{c_j} \\ & \quad -x_{\rm ref}X_{p_k}|, S(x_{\rm ref}X_{p_k}, t_{\rm ref}\tau)) \\ & \quad +\frac{\beta_{\rm ref}t_{\rm ref}}{x_{\rm ref}}\tilde{\beta}(S(x_{\rm ref}X_{p_k}, t_{\rm ref}\tau)))\sqrt{d\tau}\frac{d\tilde{B}(t_{\rm ref}\tau)}{\sqrt{d\tau}}, \\ X_{p_k}(0) & = \frac{X_{p_k0}}{x_{\rm ref}}, \end{cases} \tag{10}$$

From (9) and (10) the following dimensionless numbers arise:

$$\frac{\Upsilon_{\rm ref}t_{\rm ref}s_{\rm ref}p_{\max}}{x_{\rm ref}}, \quad \frac{\Upsilon_{\rm ref}t_{\rm ref}s_{\rm ref}p_{\rm ref}}{x_{\rm ref}}, \quad \frac{\omega_{\rm ref}t_{\rm ref}}{x_{\rm ref}}, \quad \frac{\beta_{\rm ref}t_{\rm ref}}{x_{\rm ref}}. \tag{11}$$

These dimensionless numbers indicate four different choices of the characteristic time scale $t_{\rm ref}$. This is due to the complexity of our system: active and passive agents interplay within the domain geometry as well as the propagation of the smoke. The choice of the corresponding time scale can be the characteristic time capturing relation between the smoke extinction, the walking speed and the discomfort level to the overall population size or the local discomfort, the one for the drift from the smoke propagation, the one for the drift produced by the action of active and passive pedestrians and the one for the amplifying factor on the noise. Therefore, in order to cover the physical relevance of the whole system, we introduce the following rate

$$\kappa := \max\left\{\frac{\Upsilon_{\rm ref}t_{\rm ref}s_{\rm ref}p_{\max}}{x_{\rm ref}}, \frac{\Upsilon_{\rm ref}t_{\rm ref}s_{\rm ref}p_{\rm ref}}{x_{\rm ref}}, \frac{w_{\rm ref}t_{\rm ref}}{x_{\rm ref}}, \frac{\beta_{\rm ref}t_{\rm ref}}{x_{\rm ref}}\right\}. \tag{12}$$

On the other hand, a typical choice for the reference length scale is $x_{\rm ref} = \ell$, where $\ell := \mathrm{diam}(D)$. Finally, we obtain the following nondimensionalized equations

$$\begin{cases} \frac{d}{d\tau}X_{a_i}(\tau) & = \kappa\Upsilon(S(X_{a_i}(\tau)))\frac{\nabla_{X_{a_i}}\phi(X_{a_i}(\tau))}{\|\nabla_{X_{a_i}}\phi(X_{a_i}(\tau))\|}(p_{\max}-p(X_{a_i}(\tau),\tau)), \\ X_{a_i}(0) & = X_{a_i0},\ i\in\{1,\dots,N_A\}. \end{cases} \tag{13}$$

$$\begin{cases} \frac{d}{d\tau}X_{p_k}(\tau) & = \kappa\sum_{j=1}^{N}\frac{X_{c_j}-X_{p_k}}{\epsilon+\|X_{c_j}-X_{p_k}\|}w(\|X_{c_j}-X_{p_k}\|, S(X_{p_k},\tau)) \\ & \quad +\kappa\beta(S(X_{p_k},\tau),\tau)dB(\tau), \\ X_{p_k}(0) & = X_{p_k0},\ k\in\{1,\dots,N_P\}. \end{cases} \tag{14}$$

A.4 Higher regularity estimates for the smoke concentration

In this framework, we require the following assumptions:

($\bar{\rm A}_1$) The smoke matrix diffusion coefficient $D = \mathbf{D}(x) \in W^{m,\infty}(\Omega)$ satisfies the uniform ellipticity condition, i.e. there exists positive constants $\underline{\theta}, \overline{\theta}$ such that

$$\underline{\theta}|\xi|^2 \le \mathbf{D}(x)\xi_i\xi_j \le \overline{\theta}|\xi|^2 \text{ for any } \xi\in\Omega.$$

($\bar{\text{A}}_2$) The smoke interface exchange coefficient on the boundary of our domain $\lambda := \Lambda(x) \in W^{m,\infty}(\partial\Omega)$ is such that there exist positive constants $\underline{\gamma}, \overline{\gamma}$ satisfying

$$-\underline{\gamma}|\xi|^2 < \lambda(x)\xi_i\xi_j \leq \overline{\gamma}|\xi|^2 \text{ for any } \xi \in \partial\Omega.$$

Changing the functional framework will naturally lead to a reconsideration of these assumptions.

We introduce the evolution of fire throughout a diffusion-dominated convection process. The production and spreading of smoke, with the smoke density $s(\mathbf{x}, t)$, are described as the following diffusion-drift-reaction equation:

$$\begin{cases} \partial_t s + \operatorname{div}(-\hat{D}\nabla s + \mathbf{v}_d s) = y_s H(\mathbf{x}, t) & \text{in } D \times (0, T], \\ \left(-\hat{D}\nabla s + \mathbf{v}_d s\right) \cdot \mathbf{n} = 0 & \text{on } \partial D \cup \partial G \times (0, T], \\ \left(-\hat{D}\nabla s + \mathbf{v}_d s\right) \cdot \mathbf{n} = \lambda s & \text{at } \partial E \times (0, T], \\ s(x, 0) = s_0 & \text{in } D \times \{t = 0\}, \end{cases} \tag{15}$$

where $\hat{D}$ is the smoke diffusive coefficient, $\mathbf{v}_d$ is a given drift corresponding (e.g. wind's velocity,...), y_s is a smoke production coefficient, while H represents the shape and intensity of the fire. The center of the fire location is denoted by $\mathbf{x}_0$ with radius r_0. H reads

$$H(\mathbf{x}, t) = \begin{cases} R(\mathbf{x}, t) & \text{if } |\mathbf{x} - \mathbf{x}_0| < r_0, \\ 0 & \text{otherwise }, \end{cases} \tag{16}$$

where $R(\mathbf{x}, t)$ is defined by

$$R(\mathbf{x}, t) = c(t) \exp\left(-\kappa \frac{|\mathbf{x} - \mathbf{x}_0|}{L}\right).$$

Here, κ is the convection heat transfer constant coefficient, $c(t)$ is a constant function depending on t, L is the typical length of a stationary temperature distribution within the geometry and λ is an interface exchange smoke coefficient. For convenience, in order to take the gradient of H, we consider H_ϵ a suitable mollification of H. In our case, from now on, we consider the coefficient y_s as a constant c_y and put $f(x, t) := c_y H_\epsilon(x, t)$, then (15) becomes

$$\begin{cases} \partial_t s + \operatorname{div}(-\hat{D}\nabla s + \mathbf{v}_d s) = f(\mathbf{x}, t) & \text{in } D \times (0, T], \\ \left(-\hat{D}\nabla s + \mathbf{v}_d s\right) \cdot \mathbf{n} = 0 & \text{on } \partial D \cup \partial G \times (0, T], \\ \left(-\hat{D}\nabla s + \mathbf{v}_d s\right) \cdot \mathbf{n} = \lambda s & \text{at } \partial E \times (0, T], \\ s(\mathbf{x}, 0) = s_0 & \text{in } D \times \{t = 0\}, \end{cases} \tag{17}$$

In order to have a well-posed dynamics of pedestrians model, we need the solution of (17) to belong to $C([0, T]; C^1(D))$. Since the pedestrian dynamics system couple one way with the smoke equation, the solution s of (17) should be Lipschitz

to guarantee the well-posedness of the system. In the next part, we adapt the approach in [PM05] to get a short proof of increased parabolic regularity for a bounded domain D in $\mathbb{R}^d$. Moreover, from now on, we assume the boundaries $\partial D \cup \partial G$ and ∂E are C^2 (or, at least, they satisfy the exterior sphere condition).

Theorem A.2. *[Lower-order regularity] Assume* $(\bar{A}_1)$ *and* $(\bar{A}_2)$ *hold. Suppose* $f \in H^1(D)$ *and* $\boldsymbol{v}_d \in W^{1,\infty}(D)$. *Then, for any* $T > 0$, $t \in (0, T]$, *there exists a unique*

$$s \in C([0,T]; H^1(D)) \text{ and } s' \in L^2(0,T; H^{-1}(D))$$

that solves (17). *Furthermore, the following a priori estimates hold*

$$\sup_{t\in[0,T]} \|s\|^2_{L^2(D)} \leq C_T \left(\|s_0\|^2_{L^2(D)} + \|f\|^2_{L^2(D)} \right) \text{ and } \|\nabla s\|^2_{L^2(D)} \leq \frac{C_T}{t} \left(\|s_0\|^2_{L^2(D)} + \|f\|^2_{H^1(D)} \right).$$

Proof. We adapt the arguments from [PM05] to our setting and split the proof into fourth steps:

- Step 1: *Galerkin approximation*

  Firstly, we assume that the functions $w_k = w_k(x) (k \in \mathbb{N})$ are smooth and that

  $$\{w_k\}_{k=1}^{\infty} \text{ is an orthonormal basis of } H^1(D). \tag{18}$$

  We are looking for an approximation of (17) in the form

  $$s_m(t) := \sum_{k=1}^{m} d_n^k(t) w_k, \tag{19}$$

  where the coefficients d_m^k satisfy the following system

  $$\begin{cases} \langle s_m', w_k \rangle_{L^2(D)} + \langle \hat{D} \nabla s_m, \nabla w_k \rangle_{L^2(D)} - \langle \mathbf{v}_d s_m, \nabla w_k \rangle_{L^2(D)} \\ + \langle \lambda s_m, w_k \rangle_{L^2(\partial E)} = \langle f, w_k \rangle_{L^2(D)}, \\ s_m(0) = s_{0m} \text{ with } k = 1 \dots m, \end{cases} \tag{20}$$

  where

  $$s_{0m} = \sum_{k=1}^{m} c_m^k w_k \to s_0 \tag{21}$$

  strongly in $L^2(D)$.

- Step 2: *A priori estimates*

  The goal of this step is to obtain some useful a priori estimates. Multiplying (20) by $d_m^k(t)$, taking the summation for $k \in \{1, \dots, m\}$. Then recalling (19), using Green's formula together with the mixed boundary condition, we arrive at

$$\frac{1}{2}\frac{d}{dt}\|s_m(t)\|^2_{L^2(D)} + \int_D \nabla s_m \cdot \hat{D}\nabla s_m dx + \int_{\partial E} \lambda s_m^2 d\sigma(E) = \int_D s_m \mathbf{v}_d \cdot \nabla s_m dx + \int_D f s_m dx. \tag{22}$$

  Thanks to Cauchy-Schwarz's inequality ε for an $\varepsilon > 0$, we have

$$\frac{1}{2}\frac{d}{dt}\|s_m(t)\|^2_{L^2(D)} + \int_D \nabla s_m \cdot \hat{D}\nabla s_m dx + \int_{\partial E} \lambda s_m^2 d\sigma(E) \leq \|\mathbf{v}_d\|_{1,\infty}\Big(\varepsilon\|s_m\|^2_{L^2(D)} + \frac{1}{\varepsilon}\|\nabla s_m\|^2_{L^2(D)}\Big) + \frac{1}{2}\left(\|f\|^2_{L^2(D)} + \|s_m\|^2_{L^2(D)}\right).$$

  Next, by using the ellipticity property of the diffusion coefficient D and the assumption on the interface exchange coefficient, we obtain

$$\frac{1}{2}\frac{d}{dt}\|s_m(t)\|^2_{L^2(D)} \leq -\underline{\theta}\|\nabla s_m\|^2_{L^2(D)} + \underline{\gamma}\|s_m\|^2_{L^2(\partial E)} + \|\mathbf{v}_d\|_{1,\infty}\left(\frac{1}{\varepsilon}\|s_m\|^2_{L^2(D)} + \varepsilon\|\nabla s_m\|^2_{L^2(D)}\right) + \frac{1}{2}\left(\|f\|^2_{L^2(D)} + \|s_m\|^2_{L^2(D)}\right). \tag{23}$$

  By the trace inequality applied to $\|s_m\|^2_{L^2(\partial E)}$, (23) reads

$$\frac{1}{2}\frac{d}{dt}\|s_m(t)\|^2_{L^2(D)} \leq -\underline{\theta}\|\nabla s_m\|^2_{L^2(D)} + C(\underline{\gamma})\|s_m\|^2_{H^1(D)} + \|\mathbf{v}_d\|_{1,\infty}\left(\frac{1}{\varepsilon}\|s_m\|^2_{L^2(D)} + \varepsilon\|\nabla s_m\|^2_{L^2(D)}\right) + \frac{1}{2}\left(\|f\|^2_{L^2(D)} + \|s_m\|^2_{L^2(D)}\right).$$

  By choosing $\varepsilon = \underline{\theta}(2\|\mathbf{v}_d\|_{1,\infty})^{-1}$, we get the following estimate

$$\frac{1}{2}\frac{d}{dt}\|s_m(t)\|^2_{L^2(D)} \leq C\left(\|f\|^2_{L^2(D)} + \|s_m\|^2_{H^1(D)}\right) + \left(C(\underline{\gamma}) - \frac{\underline{\theta}}{2}\right)\|\nabla s_m\|^2_{L^2(D)}. \tag{24}$$

  Multiplying with $\varphi = \partial_x s_m$ (17) differentiated with respect to x, we obtain after integrating by part that

$$\frac{1}{2}\frac{d}{dt}\|\partial_x s_m\|^2_{L^2(D)} + \int_\Omega \nabla\partial_x s_m \cdot \hat{D}\nabla\partial_x s_m dx + \int_D \nabla\partial_x s_m \cdot \partial_x\hat{D}\nabla s_m dx - \int_D \nabla\partial_x s_m \cdot \mathbf{v}_d\partial_x s_m dx - \int_D \nabla\partial_x s_m \cdot \partial_x\mathbf{v}_d s_m dx + \int_{\partial E}\lambda|\partial_x s_m|^2 d\sigma(E) + \int_{\partial E}\partial_x(\lambda s_m)\partial_x s_m d\sigma(E) = \int_D \partial_x f \partial_x s_m dx.$$

This leads to

$$\frac{1}{2}\frac{d}{dt}\|\partial_x s_m\|^2_{L^2(D)} = -\int_D \nabla\partial_x s_m \cdot \hat{D}\nabla\partial_x s_m dx - \int_D \nabla\partial_x s_m \cdot \partial_x\hat{D}\nabla s_m dx + \int_D \nabla\partial_x s_m \cdot \mathbf{v}_d\partial_x s_m dx + \int_D \nabla\partial_x s_n \cdot \partial_x\mathbf{v}_d s_m dx - \int_{\partial E} \lambda|\partial_x s_m|^2 d\sigma(E) - \int_{\partial E} \partial_x(\lambda s_m)\partial_x s_m d\sigma(E) + \int_D \partial_x f\partial_x s_m dx. \tag{25}$$

Using the assumptions on $\hat{D}$ and λ as well as Cauchy-Schwarz' inequality for the right-hand side of (25), we obtain the following estimate

$$\begin{aligned}\frac{1}{2}\frac{d}{dt}\|\partial_x s_m\|^2_{L^2(D)} \leq -\underline{\theta}\|\nabla\partial_x s_m\|^2_{L^2(D)} + \|\hat{D}\|_{W^{1,\infty}}\Bigg(\varepsilon_1\|\nabla\partial_x s_m\|^2_{L^2(D)} \\ + \frac{1}{\varepsilon_1}\|\nabla s_m\|^2_{L^2(D)}\Bigg) + |\mathbf{v}_d|\left(\varepsilon_{2'}\|\nabla\partial_x s\|^2_{L^2(D)} + \frac{1}{\varepsilon_{2'}}\|\partial_x s\|^2_{L^2(D)}\right) \\ + \|\mathbf{v}_d\|_{1,\infty}\left(\varepsilon_2\|\nabla\partial_x s\|^2_{L^2(D)} + \frac{1}{\varepsilon_2}\|s\|^2_{L^2(D)}\right) + \underline{\gamma}\|\partial_x s_m\|^2_{L^2(\partial E)} \\ + \|\lambda\|_{1,\infty}\|\partial_x s_m\|^2_{L^2(\partial E)} + \frac{1}{2}\left(\|\partial_x f\|^2_{L^2(D)} + \|\partial_x s_m\|^2_{L^2(D)}\right).\end{aligned}$$

By choosing $\varepsilon_1 = \underline{\theta}(4\|D\|_{1,\infty})^{-1}$, $\varepsilon_{2'} = \underline{\theta}(8C)^{-1}$, $\varepsilon_2 = \underline{\theta}(8\|\mathbf{v}_d\|_{1,\infty})^{-1}$ together with the use of the trace inequality to handle the boundary terms, we arrive at

$$\begin{aligned}\frac{1}{2}\frac{d}{dt}\|\partial_x s_m\|^2_{L^2(D)} &\leq -\frac{\underline{\theta}}{2}\|\nabla\partial_x s_m\|^2_{L^2(D)} + C\|\nabla s_m\|^2_{L^2(D)} + C\|\partial_x s_m\|^2_{L^2(D)} \\ &\quad + C\|s_m\|^2_{L^2(D)} + C(\underline{\gamma})\left(\|\partial_x s_m\|^2_{L^2(D)} + \|\nabla\partial_x s_m\|^2_{L^2(D)}\right) \\ &\quad + \frac{1}{2}\left(\|\partial_x f\|^2_{L^2(D)} + \|\partial_x s_m\|^2_{L^2(D)}\right) \\ &\leq \left(-\frac{\underline{\theta}}{2} + C(\underline{\gamma})\right)\|\nabla\partial_x s_m\|^2_{L^2(D)} \\ &\quad + C\left(\|\nabla s_m\|^2_{L^2(D)} + \|\partial_x s_m\|^2_{L^2(D)} + \|s_m\|^2_{L^2(D)}\right).\end{aligned} \tag{26}$$

Taking the summation over all first order derivatives, we have

$$\frac{1}{2}\frac{d}{dt}\|\nabla s_m\|^2_{L^2(D)} \leq \left(C(\underline{\gamma}) - \frac{\underline{\theta}}{2}\right)\|\nabla^2 s_m\|^2_{L^2(D)} + C\left(\|s_m\|^2_{H^1(D)} + \|f\|^2_{H^1(D)}\right).$$

Let us introduce a linear expansion in t as follow

$$\zeta_1(t) = \|s_m\|^2_{L^2(D)} + \frac{C(\underline{\theta},\underline{\gamma})t}{2}\|\nabla s_m\|^2_{L^2(D)}. \tag{27}$$

Taking the derivative of (27) with respect to t, we obtain

$$\zeta_1'(t) = \frac{d}{dt}\|s_m\|^2_{L^2(D)} + \frac{C(\underline{\theta},\underline{\gamma})}{2}\|\nabla s_m\|^2_{L^2(D)} + \frac{C(\underline{\theta},\underline{\gamma})t}{2}\frac{d}{dt}\|\nabla s_m\|^2_{L^2(D)}.$$

Combining (24) and (26), we are led to the following estimate

$$\begin{aligned}\zeta'(t) \leq 2C\left(\|f\|^2_{L^2(D)} + \|s_m\|^2_{H^1(D)}\right) - 2\left(C(\underline{\gamma}) - \frac{\underline{\theta}}{2}\right)\|\nabla s_m\|^2_{L^2(D)} \\ + \frac{C(\underline{\theta},\underline{\gamma})}{2}\|\nabla s_m\|^2_{L^2(D)} + \frac{C(\underline{\theta},\underline{\gamma})t}{2}\Bigg[\left(C(\underline{\gamma}) - \frac{\underline{\theta}}{2}\right)\|\nabla^2 s_m\|^2_{L^2(D)} \\ + C\left(\|s_m\|^2_{H^1(D)} + \|f\|^2_{H^1(D)}\right)\Bigg].\end{aligned}$$

Choosing $\underline{\theta},\underline{\gamma}$ such that $-\frac{\underline{\theta}}{2} + C(\underline{\gamma}) < 0$ and put $-\frac{\underline{\theta}}{2} + C(\underline{\gamma}) =: -C(\underline{\theta},\underline{\gamma})$, we obtain

$$\zeta'(t) \leq C_T\left(\|f\|^2_{H^1(D)} + \zeta(t)\right) \text{ for a.e. } t \in (0,T). \tag{28}$$

Applying Grönwall's inequality to (28), we have the following estimate

$$\zeta(t) \leq C_T\left(\zeta(0) + \|f\|^2_{H^1(D)}\right) = C_T\left(\|s_0\|^2_{L^2(D)} + \|f\|^2_{H^1(D)}\right). \tag{29}$$

Combining (27) and (29) gives

$$\|s_m(t)\|^2_{L^2(D)} \leq C_T\left(\|s_0\|^2_{L^2(D)} + \|f\|^2_{H^1(D)}\right) \tag{30}$$

and

$$\|\nabla s_m\|^2_{L^2(D)} \leq \frac{C_T}{Ct}\left(\|s_0\|^2_{L^2(\Omega)} + \|f\|^2_{H^1(D)}\right). \tag{31}$$

The estimates (30) and (31) imply that s_m is a bounded sequence in $H^1(D)$ and a.e $t \in (0,T)$.

- Step 3: *Passage to the limit* $m \to \infty$

  Using the *a priori* estimates (30) and (31), we obtain the following inequality

$$\int_0^T \frac{1}{2}\frac{d}{dt}\|s_m(t)\|^2_{L^2(D)}dt + \int_0^T \|\nabla s_m\|^2_{L^2(D)}dt \leq C_T\int_0^T\left(\|f\|^2_{H^1(D)} + \|s_0\|^2_{L^2(D)}\right).$$

  This implies that (s_m) is a bounded sequence in $L^2(0,T;H^1(D))$.

  On the other hand, in order to use Aubin-Lions's lemma, we additionally need to prove $s_m' \in L^2(0,T;H^{-1}(D))$. Take an arbitrary $v \in H^1(D)$, with $\|v\|_{H^1(D)} \leq 1$. We can deduce for a.e. $0 < t < T$ that

$$\langle s_m', v\rangle_{L^2(D)} = \langle f, v\rangle_{L^2(D)} + \langle \mathbf{v}_d s_m, \nabla v\rangle_{L^2(D)} - \langle D\nabla s_m, \nabla v\rangle_{L^2(D)} - \langle \lambda s_m, v\rangle_{L^2(\partial E)}.$$

Then, we get

$$|\langle s'_m, v\rangle| \leq C\|s_m\|_{H^1(D)} + C\|f\|_{L^2(D)}. \tag{32}$$

for $\|v\|_{W^{1,2}(D)} \leq 1$. Moreover, (32) implies that

$$\|s'_m\|_{H^{-1}(D)} \leq C\left(\|s_m\|_{H^1(D)} + \|f\|_{L^2(D)}\right). \tag{33}$$

Integrating (33) on $(0,T)$, we obtain the following estimate

$$\begin{aligned}\int_0^T \|s'_m\|^2_{H^{-1}(D)}dt &\leq C\int_0^T \|s_m\|_{H^1(D)} + \|f\|_{L^2(D)}dt \\ &\leq C\left(\|s_0\|^2_{L^2(D)} + \|f\|_{L^2(0,T;L^2(D))}\right).\end{aligned} \tag{34}$$

Thus, $s'_m \in L^2(0,T;H^{-1}(D))$. Therefore, we conclude that

$$\begin{cases} s_m \rightharpoonup s \text{ weakly in } L^2(0,T;H^1(D)), \\ s'_m \rightharpoonup s' \text{ weakly in } L^2(0,T;H^{-1}(D)). \end{cases}$$

Relying on Aubin-Lions lemma in [BF12] with $p, q = 2$,

$$A_0 = H^1(D), \quad A = L^2(\Omega), \quad A_1 = H^{-1}(D)$$

together with Rellich theorem (cf. [Eva97], Section 5.7, Theorem 1) for the compactness embedding $H^1(D) \subset L^2(D)$, we have that the sequence $\{s_m\}$ is relatively compact in $L^2(0,T;L^2(D))$ in the strong topology. This sequence is also weakly relatively compact in $L^2(0,T;H^1(D))$ and weakly star relatively compact in $C([0,T];L^2(D))$. Hence, there exists a subsequence s_{m_k} (just for simplicity of notation, let us denote it by s_m) which converges to a function s belonging to $L^2(0,T;H^1(D))$ and $C([0,T];L^2(D))$. Therefore, we can conclude that there exists a solution $s \in L^2(0,T;H^1(D)) \cup C([0,T];L^2(D))$ satisfying (17).

- Step 4: *Uniqueness of solutions*

  Assume that (17) admits 2 solutions s_1 and s_2 belonging to $L^2(0,T;H^1(D)) \cup C([0,T];L^2(D))$. Denote $w = s_1 - s_2$. Then (17) becomes

$$\begin{cases} \partial_t w + \operatorname{div}(-\hat{D}\nabla w + \mathbf{v}_d w) = 0 \quad \text{in } D \times (0,T], \\ (-\hat{D}\nabla w + \mathbf{v}_d w)\cdot \mathbf{n} = 0 \quad \text{on } \partial D \cup \partial G \times (0,T], \\ (-D\nabla w + \mathbf{v}_d w)\cdot \mathbf{n} = \lambda w \quad \text{at } \partial E \times (0,T], \\ w(t=0) = 0 \quad \text{in } D \times \{t=0\}, \end{cases}$$

  Recalling (20), we note that

$$\frac{1}{2}\frac{d}{dt}\int_D w^2 dx + \int_D \hat{D}|\nabla w|^2 dx + \int_{\partial E} \lambda w^2 d\sigma(E) = \int_D w\mathbf{v}_d \cdot \nabla w dx,$$

which leads to

$$\frac{d}{dt}\left(\|w\|^2_{L^2(D)}\right) + \overline{\theta}\|\nabla w\|^2_{L^2(D)} + \overline{\gamma}\|w\|^2_{L^2(\partial E)} \leq C\|w\|^2_{L^2(D)}.$$

This also implies

$$\frac{d}{dt}\left(\|w\|^2_{L^2(D)}\right) \leq C\|w\|^2_{L^2(D)}. \tag{35}$$

Integrating (35) on $(0,T)$, gives

$$\|w\|^2_{L^2(D)} \leq \|w(0)\|^2_{L^2(D)} + C\int_0^t \|w\|^2_{L^2(D)}.$$

Grönwall's lemma ensure

$$\|w\|^2_{L^2(D)} \leq \|w(0)\|^2_{L^2(D)}(1 + Cte^{Ct}),$$

which for $w(0) = 0$, gives $\|w\|_{L^2(D)} = 0$. So, $w = 0$ a.e. in Ω and everywhere in $[0,T]$, which ensures the desired uniqueness.

Now, let us show that $s \in C([0,T]; H^1(D))$. We consider $w_r(t) = s(t+r) - s(t)$, then $w_r(t)$ satisfies (17) with $f = 0$, $w(0) = s_0 - s(r)$ and $\lambda s(t+r) - \lambda s(t) = \lambda w_r(t)$. By using a similar argument, we obtain

$$\|w_r(t)\|^2_{L^2(D)} + \frac{C(\underline{\theta},\underline{\gamma})t}{2}\|\nabla w_r(t)\|^2_{L^2(D)} \leq C_T\left(\|s_0 - s(r)\|^2_{L^2(D)}\right).$$

Since we have $s \in C([0,T]; L^2(D))$, then $\lim_{r\to\infty}\|s(t+r) - s(t)\| = 0$ and $\lim_{r\to\infty}\|\nabla s(t+r) - \nabla s(t)\| = 0$ for $t > 0$. Therefore, we obtain $s \in C([0,T]; H^1(D))$.

□

Theorem A.3. *[High-order regularity] Assume $(\bar{A}_1)$ and $(\bar{A}_2)$ hold. Suppose $f \in H^m(D)$ and $\boldsymbol{v}_d \in W^{m,\infty}(D)$ for every $m \in \mathbb{N}$, and $s_0 \in L^2(D)$. Then, for any $T > 0$, $t \in [0,T]$, the solution of (17) satisfies the following estimate*

$$\|\nabla^k s\|^2_{L^2(D)} \leq \frac{C_T}{t^k}\left(\|s_0\|^2_{L^2(D)} + \|f\|^2_{H^k(D)}\right) \text{ for } k = 0, 1, \ldots, m.$$

Proof. We use the method of induction on $m \in \mathbb{N}$, using the fact that we have done the first case $m = 1$ mathematically in Theorem A.2. We define the gradient of a function s as follows:

$$\|\nabla^k s\|^2_{L^2(D)} := \sum_{|\alpha|\leq k}\|\partial^\alpha_x s\|^2_{L^2(D)}.$$

Now, taking the $k-$order derivative with respect to x for $k \in \mathbb{N}$ which is denoted by ∂_x^α of (17), multiplying by $\partial_x^\alpha s$ and integrating the results by parts together with using Green's theorem for the equation, we obtain

$$\frac{1}{2}\frac{d}{dt}\|\partial_x^\alpha s(t)\|^2_{L^2(D)} + \int_D \nabla\partial_x^\alpha s \cdot \sum_{j=0}^{k} \sum_{|\beta|=j,\beta+\gamma=\alpha} \binom{\alpha}{\beta} \partial_x^\beta \hat{D} \nabla \partial_x^\gamma s dx$$
$$- \int_D \nabla\partial_x^\alpha s \cdot \sum_{j=0}^{k} \sum_{|\beta|=j,\beta+\gamma=\alpha} \binom{\alpha}{\beta} \partial_x^\beta \mathbf{v}_d \partial_x^\gamma s dx + \int_{\partial E} \partial_x^\alpha s \lambda \partial_x^\alpha s d\sigma(E)$$
$$+ \int_{\partial E} \partial_x^\alpha(\lambda s) \cdot \partial_x^\alpha s d\sigma(E) = \int_D \partial_x^\alpha f \partial_x^\alpha s dx,$$

and thus

$$\frac{1}{2}\frac{d}{dt}\|\partial_x^\alpha s(t)\|^2_{L^2(D)} = -\int_D \nabla\partial_x^\alpha s \cdot \sum_{j=0}^{k} \sum_{|\beta|=j,\beta+\gamma=\alpha} \binom{\alpha}{\beta} \partial_x^\beta \hat{D} \nabla \partial_x^\gamma s dx$$
$$+ \int_D \nabla\partial_x^\alpha s \cdot \sum_{j=0}^{k} \sum_{|\beta|=j,\beta+\gamma=\alpha} \binom{\alpha}{\beta} \partial_x^\beta \mathbf{v}_d \partial_x^\gamma s dx - \int_{\partial E} \partial_x^\alpha s \lambda \partial_x^\alpha s d\sigma(E)$$
$$- \int_{\partial E} \partial_x^\alpha(\lambda s) \cdot \partial_x^\alpha s d\sigma(E) + \int_D \partial_x^\alpha f \partial_x^\alpha s dx. \tag{36}$$

Denote

$$B_1 := -\int_D \nabla\partial_x^\alpha s \cdot \sum_{j=0}^{k} \sum_{|\beta|=j,\beta+\gamma=\alpha} \binom{\alpha}{\beta} \partial_x^\beta \hat{D} \nabla \partial_x^\gamma s dx$$
$$= -\int_D \nabla\partial_x^\alpha s \cdot \hat{D} \nabla \partial_x^\alpha s dx - \int_D \nabla\partial_x^\alpha s \cdot \sum_{j=1}^{k} \sum_{|\beta|=j,\beta+\gamma=\alpha} \binom{\alpha}{\beta} \partial_x^\beta \hat{D} \nabla \partial_x^\gamma s dx.$$

We can estimate $|A|$ from above:

$$|B_1| \le -\underline{\theta}\|\nabla\partial_x^\alpha s\|^2_{L^2(D)} + C\|\hat{D}\|_{1,\infty}\left(\varepsilon_1\|\nabla\partial_x^\alpha s\|^2_{L^2(D)} + \frac{1}{\varepsilon_1}\|s\|^2_{H^{k-1}(D)}\right)$$
$$\le \frac{-\theta}{2}\|\nabla\partial_x^\alpha s\|^2_{L^2(D)} + C\|s\|^2_{H^{k-1}(D)}, \tag{37}$$

where we choose $\varepsilon_1 = \underline{\theta}(4C\|D\|_{m,\infty})^{-1}$. Set

$$B_2 := \int_D \nabla\partial_x^\alpha s \cdot \sum_{j=0}^{k} \sum_{|\beta|=j,\beta+\gamma=\alpha} \binom{\alpha}{\beta} \partial_x^\beta \mathbf{v}_d \partial_x^\gamma s dx,$$

and obtain the upper bound

$$|B_2| \le C\|\mathbf{v}_d\|_{m,\infty}\left(\varepsilon_2\|\nabla\partial_x^\alpha s\|^2_{L^2(D)} + \frac{1}{\varepsilon_2}\|\partial_x^\alpha s\|^2_{H^{k-1}(D)}\right). \tag{38}$$

Now, let us label the third and fourth terms in the right hand side of (36) as follow

$$\tilde{C} := -\int_{\partial E} \partial_x^\alpha s \lambda \partial_x^\alpha s d\sigma(E) - \int_{\partial E} \partial_x^\alpha (\lambda s) \cdot \partial_x^\alpha s d\sigma(E).$$

Using the assumptions on λ together with applying Cauchy's inequality, trace inequality for $\tilde{C}$, we have the following estimate:

$$\tilde{C} \leq \underline{\gamma} \|\partial_x^\alpha s\|^2_{L^2(\partial E)} + \|\lambda\|_{m,\infty} \|\partial_x^\alpha s\|^2_{L^2(\partial E)} \leq C(\underline{\gamma}) \left(\|\nabla \partial_x^\alpha s\|^2_{L^2(D)} + \|\partial_x^\alpha s\|^2_{L^2(D)} \right). \tag{39}$$

Finally, we estimate the last term of (36), by using Cauchy's inequality, we obtain

$$\int_D \partial_x^\alpha f \partial_x^\alpha s dx \leq \frac{1}{2} \left(\|\partial_x^\alpha f\|^2_{L^2(D)} + \|\partial_x^\alpha s\|^2_{L^2(D)} \right). \tag{40}$$

Combining (37)-(40) and choosing $\varepsilon_2 = \underline{\theta}(4C\|\mathbf{v}_d\|_{1,\infty})^{-1}$, we have the following estimate

$$\begin{aligned} \frac{1}{2}\frac{d}{dt}\|\partial_x^\alpha s(t)\|^2_{L^2(D)} \leq \frac{-\underline{\theta}}{2}\|\nabla \partial_x^\alpha s\|^2_{L^2(D)} + C\|s\|^2_{H^{k-1}(D)} + C\|\partial_x^\alpha s\|^2_{H^{k-1}(D)} \\ + C(\underline{\gamma})\|\nabla \partial_x^\alpha s\|^2_{L^2(D)} + \|f\|^2_{H^k(D)}. \end{aligned}$$

Now, summing all of first-order derivatives, we obtain

$$\frac{1}{2}\frac{d}{dt}\|\nabla^k s(t)\|^2_{L^2(D)} \leq \left(C(\underline{\gamma}) - \frac{\underline{\theta}}{2} \right) \|\nabla^{k+1} s\|^2_{L^2(D)} + C\left(\|f\|^2_{H^k(D)} + \|s\|^2_{H^k(D)} \right). \tag{41}$$

Now, we aim to find $s \in C([0,T], H^{m-1}(D))$ using the induction hypothesis under the assumptions $f \in H^{m-1}(D)$ and $D, \lambda, \mathbf{v}_d \in W^{m,\infty}(0,T;D)$. Using the same argument as in the case $m = 1$, we define

$$\zeta_2(t) := \sum_{k=1}^{n} \frac{(C(\underline{\theta}, \underline{\gamma})t)^k}{2^k k!} \|\nabla^k s\|^2_{L^2(D)}. \tag{42}$$

Taking the derivative of (42) with respect to t, we obtain

$$\begin{aligned} \zeta_2'(t) &= \sum_{k=1}^{m} \frac{(C(\underline{\theta}, \underline{\gamma}))^k t^{k-1}}{2^k (k-1)!} \|\nabla^k s\|^2_{L^2(D)} + \sum_{k=0}^{m} \frac{(C(\underline{\theta}, \underline{\gamma}))^k}{2^k k!} \frac{d}{dt} \|\nabla^k s\|^2_{L^2(D)} \\ &:= G_1 + G_2. \end{aligned}$$

$$
\begin{aligned}
G_2 &\leq \sum_{k=0}^{m} \frac{(C(\underline{\theta},\underline{\gamma})t)^k}{2^k k!} \left(-C(\underline{\theta},\underline{\gamma}) \|\nabla^{k+1} s\|^2_{L^2(D)} + C \left(\|f\|^2_{H^k(D)} + \|s\|^2_{H^k(D)} \right) \right) \\
&= -2 \sum_{k=0}^{m} \frac{(C(\underline{\theta},\underline{\gamma}))^{k+1} t^k}{2^{k+1} k!} \|\nabla^{k+1} s\|^2_{L^2(D)} \\
&+ C \sum_{k=0}^{m} \frac{(C(\underline{\theta},\underline{\gamma}))^k}{2^k k!} \left(\|f\|^2_{H^k(D)} + \|s\|^2_{H^k(D)} \right) \\
&\leq -2G_1 - \frac{2(C(\underline{\theta},\underline{\gamma}))^{m+1} t^m}{2^{m+1} m!} \|\nabla^{m+1} s\|^2_{L^2(D)} \\
&+ C \sum_{k=0}^{m} \frac{(C(\underline{\theta},\underline{\gamma}))^k}{2^k k!} \left(\|f\|^2_{H^k(D)} + \|s\|^2_{H^k(D)} \right). \qquad (43)
\end{aligned}
$$

On the other hand, the induction hypothesis gives the following inequality

$$
\|s\|^2_{H^{k-1}(D)} \leq \frac{C_T}{t^{k-1}} \left(\|f\|^2_{H^{k-1}(D)} + \|s_0\|^2_{L^2(D)} \right). \qquad (44)
$$

Combining (43) and (44), we obtain

$$
\begin{aligned}
\zeta_2'(t) &\leq C \sum_{k=0}^{m} \frac{(C(\underline{\theta},\underline{\gamma}))^k}{2^k k!} \left(\|f\|^2_{H^k(D)} + \|s\|^2_{H^k(D)} \right) \\
&\leq C_T \left(\|f\|^2_{H^m(D)} + \sum_{k=0}^{m} \frac{(C(\underline{\theta},\underline{\gamma})t)^k}{2^k k!} \left[\|\nabla^k s\|^2_{L^2(D)} + \|s\|^2_{H^{k-1}(D)} \right] \right) \\
&\leq C_T \left(\|f\|^2_{H^m(D)} + \zeta_2(t) + \sum_{k=0}^{m} \frac{(C(\underline{\theta},\underline{\gamma})t)^k}{2^k k!} \frac{C_T}{t^{k-1}} \left[\|f\|^2_{H^{k-1}(D)} + \|s_0\|^2_{L^2(D)} \right] \right) \\
&\leq C_T \left(\|f\|^2_{H^m(D)} + \|s_0\|^2_{L^2(D)} + \zeta_2(t) \right).
\end{aligned}
$$

Grönwall's inequality yields

$$
\zeta_2(t) \leq C_T \left(\|f\|^2_{H^m(D)} + \|s_0\|^2_{L^2(D)} + \zeta_2(0) \right) \leq C_T \left(\|f\|^2_{H^m(D)} + \|s_0\|^2_{L^2(D)} \right).
$$

The bound on $\zeta_2(t)$ gives the following estimate

$$
\|\nabla^m s\|^2_{L^2(D)} \leq \frac{C_T}{(C(\underline{\theta},\underline{\gamma})t)^m},
$$

which completes the induction proof. □ □

Remark A.4. *From Theorem A.3, for $m = 3$, $D \subset \mathbb{R}^d$ with $d = 2$, there exists a unique solution $s \in C([0,T]; C^1(D))$ and $s' \in L^2(0,T; H^{-1}(D))$ that solves (17). By the same arguments as in Theorem A.2, this also implies that $s \in C([0,T]; H^m(D))$. In our model, we consider our domain in $D \subset \mathbb{R}^d$ with $d = 2$. Moreover, assume D satisfies the strong locally Lipschitz condition (cf. [AF03], Theorem 4.12), taking $m = 3$, hence $H^3(D)$ compact embedding into $C^1(D)$, i.e. $H^3(D) \subset C^1(D)$. As a conclusion, we obtain $s \in C([0,T]; C^1(D))$. This property ensures that the smoke concentration field s is Lipschitz with respect to the space variable – a fact needed to handle the well-posedness of our SDEs.*

Acknowledgement

First of all, I wish to express my sincere gratitude to my supervisors Prof. dr. habil. Adrian Muntean and Dr. Matteo Colangeli for their guidance, advices and the time they devoted to my research during my doctoral years. Many thanks also to Prof. Emilio N. M. Cirillo for useful discussion as well as guidance, advices to my research during the years. All of you have been supportive and have given me the freedom to pursue various projects without objection. Also, you have provided me insightful discussion about the research. I am fortunate to be one of your students, and I enjoy all of the meetings we had. You always bring new ideas and useful suggestions to my research that has helped significantly broaden my knowledge and the way I think scientifically. I would like to thanks also Prof. Rinaldo M. Colombo for useful discussion.

Besides my advisors, I would like to thank the rest of my thesis committee: Prof. Corrado Lattanzio (University of L'Aquila), Prof. Azmy S. Ackleh (University of Louisiana at Lafayette, USA), Prof. Emilio N. M. Cirillo (Sapienza University of Rome), Prof. Grigorios A. Pavliotis (London), Dr. Paolo Antonelli (GSSI) for their insightful comments and encouragement, but also for the hard question which incented me to widen my research from various perspectives.

I hereby express my gratitude to the Division of Mathematics at Gran Sasso Science Institute (GSSI), Italy for offering me a Ph.D. position since 2016. I owe big thanks to all members and staffs of the department, in particular, Prof. Pierangelo Marcati, Prof. Errico Presutti, Prof. Nicola Guglielmi and Dr. Paolo Antonelli for their invaluable help and screening my research progress through the years.

Next, I acknowledge the Departments of Mathematics and Computer Science of Karlstad University (Sweden) for offering me a double Ph.D. degree between GSSI and Karlstad University since 2018. My special thanks to Prof. Stefan Lindskog, Dr. Sorina Barza, Dr. Martin Lind, Dr. Anders Hedin and the secretaries Stina and Juliana for helping me during the period of my PhD at KAU.

I would like to thank my best friends (colleagues) who kindly help me during my PhD period. Specifically, thanks V. A. Khoa for helping me everything from the beginning of my research until now. Thanks Omar, Trung and Xuan for supporting me everytime when I have technical problems.

I would like also to acknowledge to all people with whom I had luck to collaborate with and whom I learned a lot: Dr. V. A. Khoa, Dr. E. R. Ijioma, O. Richardson. I am extremely thankful to my PhD mates: Fabio, Alessan-

dro, Roberta, Cristina, Roberto, Lorenzo, Antonio, Francesco, Luca, Carroline, Duyen, Phu, Surendra, Vishnu, Tam with whom I shared this mathematical path. Also, I would like to thank all of my friends for everything.

Last but not the least, I would like to thank my family: my parents and to my brother and sisters, thanks for being always with me and for supporting me spiritually throughout writing this thesis and my life in general.

List of publications

- T. K. T. Thieu, M. Colangeli and A. Muntean. Uniqueness and stability with respect to parameters of solutions to a fluid-like driven system for active–passive pedestrian dynamics, *Accepted for publication in Journal of Mathematical Analysis and Applications*, 2020.

- V. A. Khoa, T. K. T. Thieu and E. R. Ijioma. On a pore-scale stationary diffusion equation: scaling effects and correctors for the homogenization limit. *Accepted for publication in Discrete and Continuous Dynamical Systems Series B*, 2020.

- E. N. M. Cirillo, M. Colangeli, A. Muntean and T. K. T. Thieu. When diffusion faces drift: consequences of exclusion processes for bi–directional pedestrian flows. *Physica D: Nonlinear Phenomena*, Vol. 413, no. 132651, 2020.

- E. N. M. Cirillo, M. Colangeli, A. Muntean and T. K. T. Thieu. A lattice model for active - passive pedestrian dynamics: a quest for drafting effects. *Mathematical Biosciences and Engineering*, Vol. 17, 1, pp. 460-477, 2019.

- T. K. T. Thieu, M. Colangeli and A. Muntean. Weak solvability of a fluid-like driven system for active-passive pedestrian dynamics. *Nonlinear Studies*, Vol. 26, no. 4, pp. 991-1006, 2019.

- M. Colangeli, A. Muntean, O. Richardson and T. K. T. Thieu. Modeling Interactions Between Active and Passive Agents Moving Through Heterogeneous Environments. In G. Libelli, N. Bellomo (Eds), Crowd Dynamics, vol. 1: Theory, Models and Safety Problems (pp. 211–254). *Modeling and Simulation in Science, Engineering and Technology, Boston, Birkhauser, Springer*, 2019.

- T. K. T. Thieu and A. Muntean. Solvability of a coupled nonlinear system of Skorohod-like stochastic differential equations modeling active–passive pedestrians dynamics through a heterogeneous domain and fire, submitted, 2020.

My contributions to the manuscripts

This section is meant to clarify the contributions that I, Thoa Thieu, have made to the 7 manuscripts that are part of this dissertation.

1. Modelling Interactions Between Active and Passive Agents Moving Through Heterogeneous Environments [RJM19]:

In this work, I accomplished all proofs and mathematical derivations in the manuscript. Discussions and feedback was provided continuously by M. Colangeli, A. Muntean and O. Richardson.

2. A lattice model for active–passive pedestrian dynamics [CCMT19]:

In this work, M. Colangeli and I implemented the Monte Carlo code in Fortran. I performed data exploration. Discussions and feedback was provided continuously by E. N. M. Cirillo, M. Colangeli and A. Muntean. I drafted the manuscript, produced all figures and was responsible for the submission process to publication.

3. When diffusion faces drift: consequences of exclusion processes for bi–directional pedestrian flows [CCMT20]:

In this work, M. Colangeli and I implemented the Monte Carlo code in Fortran. I performed data exploration. Discussions and feedback was provided continuously by E. N. M. Cirillo, M. Colangeli and A. Muntean. I drafted the manuscript, produced all figures and was responsible for the submission process to publication.

4. Weak solvability of a fluid-like driven system for active–passive pedestrian dynamics [TCM19]:

In this work, I accomplished all proofs and mathematical derivations in the manuscript. Discussions and feedback was provided continuously by M. Colangeli and A. Muntean. I drafted the manuscript, produced all figures and was responsible for the submission process to publication.

5. Uniqueness and stability with respect to parameters of solutions to a fluid-like driven system for active–passive pedestrian dynamics [TCM20]:

In this work, I contributed with major, essential parts to all proofs and mathematical derivations in the manuscript. Discussions and feedback was provided continuously by M. Colangeli and A. Muntean. I drafted the manuscript and was responsible for the submission process to publication.

6. Solvability of a coupled nonlinear system of Skorohod-like stochastic dif-

ferential equations modeling active–passive pedestrians dynamics through a heterogenous domain and fire [TM20]:

In this work, I contributed with major, essential parts to all proofs and mathematical derivations in the manuscript. Discussions and feedback was provided continuously by A. Muntean. I drafted the manuscript and produced all figures and was responsible for the submission process to publication.

7. On a pore-scale stationary diffusion equation: Scaling effects and correctors for the homogenization limit [KTI20]:

In this work, I contributed to all proofs and mathematical derivations in the manuscript together with the co-authors. Simulations were produced by E. R. Ijioma. Discussions and feedback were provided continuously by V. A. Khoa and E. R. Ijioma.

List of Figures

List of Tables

Bibliography

[AA99] G. Allaire and M. Amar. Boundary layer tails in periodic homogenization. *ESAIM: Control, Optimisation and Calculus of Variations*, 4:209–243, 1999.

[ABCK16] G. Albi, M. Bongini, E. Cristiani, and D. Kalise. Invisible control of self-organizing agents leaving unknown environments. *SIAM J. Appl. Math.*, 76:1683–1710, 2016.

[ABHI09] E. Aulisa, L. Bloshanskaya, L. Hoang, and A. Ibragimov. Analysis of generalized Forchheimer flows of compressible fluids in porous media. *Journal of Mathematical Physics*, 50:103102, 2009.

[AC10] W. Arendt and R. Chill. Global existence for quasilinear diffusion equations in isotropic nondivergence form. *Ann. Scuola Norm. Sup. Pisa Cl. Sci.*, IX:523–539, 2010.

[ACK15] J.P. Agnelli, F. Colasuonno, and D. Knopoff. A kinetic theory approach to the dynamics of crowd evacuation from bounded domains. *Mathematical Models and Methods in Applied Sciences*, 25:109–129, 2015.

[AD20] A. Aurell and B. Djehiche. Behavior near walls in the mean-field approach to crowd dynamics. *SIAM J. Appl. Math.*, 80:1153–1174, 2020.

[ADN59] S. Agmon, A. Douglis, and L. Nirenberg. Estimates near the boundary for solutions of elliptic partial differential equations satisfying general boundary value conditions I. *Communications on Pure and Applied Mathematics*, 12:623–727, 1959.

[AF03] R. A . Adams and J. J. F. Fournier. *Sobolev Spaces*, volume 140. Academic Press, 2003.

[AGK16] S. Armstrong, A. Gloria, and T. Kuusi. Bounded correctors in almost periodic homogenization. *Archive for Rational Mechanics and Analysis*, 222(1):393–426, 2016.

[APHL15] A. A. Almet, M. Pan, B. D. Hughes, and K. A. Landman. When push comes to shove: Exclusion processes with nonlocal consequences. *Physica A: Statistical Mechanics and its Applications*, 437:119–129, 2015.

[Aub63] J. P. Aubin. Un théoreme de compacité. *C. R. Acad. Sci. Paris*, 256:5042–5044, 1963.

[BCG+16] N. Bellomo, D. Clarke, L. Gibelli, P. Townsend, and B. J. Vreugdenhil. Human behaviours in evacuation crowd dynamics: From modelling to "big data" toward crisis management. *Physics of Life Reviews*, 18:1–21, 2016.

[Bea72] J. Bear. *Dynamics of Fluids in Porous Media*, volume 1. American Elsevier Publishing Company, 1972.

[BF12] F. Boyer and P. Fabrie. *Mathematical Tools for the Study of the Incompressible Navier-Stokes Equations and Related Models*, volume 183. Springer Science & Business Media, 2012.

[BGT04] M. Bossy, E. Gobet, and D. Talay. A symmetrized Euler scheme for an efficient approximation of reflected diffusions. *Journal of Applied Probability*, 41:877–889, 2004.

[Bil99] P Billingsley. *Convergence of Probability Measures*. John Wiley & Sons, Inc, 1999.

[Bre11] H. Brezis. *Functional Analysis, Sobolev Spaces and Partial Differential Equations*. Springer, 2011.

[BTvDA18] B. Blocken, Y. Toparlar, T. van Druenen, and T. Andrianne. Aerodynamic drag in cycling team time trials. *Journal of Wind Engineering and Industrial Aerodynamics*, 182:128–145, 2018.

[BvDT+18] B. Blocken, T. van Druenen, Y. Toparlar, F. Malizia, P. Mannion, T. Andrianne, T. Marchal, G. J. Maas, and J. Diepens. Aerodynamic drag in cycling pelotons: new insights by CFD simulation and wind tunnel testing. *Journal of Wind Engineering and Industrial Aerodynamics*, 179:319–337, 2018.

[BZK60] G. I. Barenblatt, Iu. P. Zheltov, and I. N. Kochina. Basic concepts in the theory of seepage of homogeneous liquids in fissured rocks. *PMM*, 24:852–864, 1960.

[CC18] A. Ciallella and E. N. M. Cirillo. Linear Boltzmann dynamics in a strip with large reflective obstacles: stationary state and residence time. *Kinetic and Related Models*, 11:1475–1501, 2018.

[CCCM18] A. Ciallella, E. N. M. Cirillo, P. Curseu, and A. Muntean. Free to move or trapped in your group: Mathematical modeling of information overload and coordination in crowded populations. *Mathematical Models and Methods in Applied Sciences*, 28:1831–1856, 2018.

[CCCO19] P. Centorrino, A. Corbetta, E. Cristiani, and E. Onofri. Measurement and analysis of visitors' trajectories in crowded museums. *International Conference on Metrology for Archaeology and Cultural Heritage*, IMEKO TC-4, 2019.

[CCMT19] E. N. M. Cirillo, M. Colangeli, A. Muntean, and T. K. T. Thieu. A lattice model for active-passive pedestrian dynamics: a quest for drafting effects. *Mathematical Biosciences and Engineering*, 17:460–477, 2019.

[CCMT20] E. N. M. Cirillo, M. Colangeli, A. Muntean, and T. K. T. Thieu. When diffusion faces drift: consequences of exclusion processes for bi–directional pedestrian flows. *Physica D: Nonlinear Phenomena*, 413, 2020.

[CFL09] C. Castellano, S. Fortunato, and V. Loreto. Statistical physics of social dynamics. *Reviews of Modern Physics*, 81, 2009.

[CFLPL16] A. Cholaquidis, R. Fraiman, G. Lugosi, and B. Pateiro-López. Set estimation from reflected Brownian motion. *Journal of the Royal Statistical Society: Series B (Statistical Methodology)*, 78:1057–1078, 2016.

[CHK16] E. Celik, L. Hoang, and T. Kieu. Generalized Forchheimer flows of isentropic gases. *J. Math. Fluid Mech.*, 20:83–115, 2016.

[Cho16] M. Choulli. *Applications of Elliptic Carleman Inequalities to Cauchy and Inverse Problems*. Springer, 2016.

[CJ99] D. Cioranescu and J. Saint Jean Paulin. *Homogenization of Reticulated Structures*. Springer, 1999.

[CJK18] D. Crisan, C. Janjigian, and T. G. Kurtz. Particle representations for stochastic partial differential equations with boundary conditions. *Electronic Journal of Probability*, 23:1–29, 2018.

[CKMvS16a] E. N. M. Cirillo, O. Krehel, A. Muntean, and R. v. Santen. Lattice model of reduced jamming by barrier. *Physical Review E*, 94:042115, 2016.

[CKMvS16b] E. N. M. Cirillo, O. Krehel, A. Muntean, and R. van Santen. Lattice model of reduced jamming by a barrier. *Physical Review E*, 94:042115, 2016.

[CM12] G. A. Chechkin and T. A. Melnyk. Asymptotics of eigenelements to spectral problem in thick cascade junction with concentrated masses. *Applicable Analysis*, 91(6):1055–1095, 2012.

[CMLT16] A. Corbetta, J. A. Meeusen, C. Lee, and F. Toschi. Continuous measurements of real-life bidirectional pedestrian flows on a wide walkway. *Proceedings of Pedestrian and Evacuation Dynamics*, pages 18–24, 2016. (Special issue in "Collective Dynamics").

[CMP13] J. A. Carrillo, S. Martin, and V. Panferov. A new interaction potential for swarming models. *Physica D: Nonlinear Phenomena*, 260:112–126, 2013.

[CMP17] M. Colangeli, A. D. Masi, and E. Presutti. Microscopic models for uphill diffusion. *J. Phys. A: Math. Theor.*, 50:435002, 2017.

[CMRT19] M. Colangeli, A. Muntean, O. Richardson, and T. K. T. Thieu. *Modelling Interactions Between Active and Passive Agents Moving Through Heterogeneous Environments*, volume 1: Theory, Models and Safety Problems,. in G. Libelli, N. Bellomo (Eds), Crowd Dynamics, Modeling and Simulation in Science, Engineering and Technology, Boston, Birkhäuser, Springer, 2019.

[Cor15] A. Corbetta. *Multiscale Crowd Dynamics: Physical Analysis, Modeling and Applications*. PhD thesis, Eindhoven University of Technology, Netherlands, 2015.

[CP99] G. A. Chechkin and A. L. Piatnitski. Homogenization of boundary-value problem in a locally periodic perforated domain. *Applicable Analysis*, 71(1):215–235, 1999.

[CP17] E. Cristiani and D. Peri. Handling obstacles in pedestrian simulations: Models and optimization. *Applied Mathematical Modelling*, 45:285–302, 2017.

[CP19] E. Cristiani and D. Peri. Robust design optimization for egressing pedestrians in unknown environments. *Applied Mathematical Modelling*, 72:553–568, 2019.

[CPT14] E. Cristiani, B. Piccoli, and A. Tosin. *Multiscale Modeling of Pedestrian Dynamics, Series in Modeling, Simulation and Applications*, volume 12. Springer, 2014.

[CR12] M. Colangeli and L. Rondoni. Equilibrium, fluctuation relations and transport for irreversible deterministic dynamics. *Physica D*, 241:681–691, 2012.

[CTB+18] J. Cejkova, R. Toth, A. Braun, M. Branicki, D. Ueyama, and I. Lagzi. *Shortest path finding in mazes by active and passive particles*, volume 32. in Adamatzky A. (eds) Shortest Path Solvers. From Software to Wetware. Emergence, Complexity and Computation, Springer, Cham, 2018.

[DAM11] E. N. M. Cirillo D. Andreucci, D. Bellaveglia and S. Marconi. Monte Carlo study of gating and selection in potassium channels. *Physical Review E*, 84:021920, 2011.

[DHJW05] L. Buzna D. Helbing, A. Johansson, and T. Werner. Self-organized pedestrian crowd dynamics: Experiments, simulations, and design solutions. *Transportation science*, 39:1–24, 2005.

[DHS16] C. Dorlemann, M. Heida, and B. Schweizer. Transmission conditions for the Helmholtz-equation in perforated domains. *Vietnam Journal of Mathematics*, 45(1–2):241–253, 2016.

[E11] W. E. *Principles of Multiscale Modeling.* Cambridge University Press, 2011.

[ECT15] F. S. Priuli E. Cristiani and A. Tosin. Modeling rationality to control self-organization of crowds: An environmental approach. *SIAM Journal on Applied Mathematics*, 75:605–629, 2015.

[EHM16] J. H. M. Evers, S. C. Hille, and A. Muntean. Measure-valued mass evolution problems with flux boundary conditions and solution-dependent velocities. *SIAM J. Math. Anal.*, 48:1929–1953, 2016.

[Eva97] L. C. Evans. *Partial Differential Equations*, volume 19. American Mathematical Society, 1997.

[Eva98] L. C. Evans. *Partial Differential Equations.* American Mathematical Society, 1998.

[Eva13] L. C. Evans. *An Introduction to Stochastic Differential Equations*, volume 82. American Mathematical Soc., 2013.

[Eve15] J. Evers. *Evolution Equations for Systems Governed by Social Interactions.* PhD thesis, Eindhoven University of Technology, Netherlands, 2015.

[FG95] F. Flandoli and D. Gatarek. Martingale and stationary solutions for stochastic Navier-Stokes equations. *Probability Theory and Related Fields*, 102(3):367–391, 1995.

[FK17] R. C. Fetecau and M. Kovacic. Swarm Equilibria in Domains with Boundaries. *SIAM J. Applied Dynamical Systems*, 16:1260–1308, 2017.

[FM15] S. Faure and B. Maury. Crowd motion from the granular standpoint. *Mathematical Models and Methods in Applied Sciences (M3AS)*, 25:463–493, 2015.

[FRK11] F. Frank, N. Ray, and P. Knabner. Numerical investigation of homogenized Stokes-Nernst-Planck-Poisson systems. *Computing and Visualization in Science*, 14(8):385–400, 2011.

[FRNF13] K. Fridolf, E. Ronchi, D. Nilsson, and H. Frantzich. Movement speed and exit choice in smoke-filled rail tunnels. *Fire Safety Journal*, 59:8–21, 2013.

[GCM15] S. K. Ghosh, A. G. Cherstvy, and R. Metzler. Non-universal tracer diffusion in crowded media of non-inert obstacles. *Phys. Chem. Chem. Phys.*, 17:1847, 2015.

[GFP16] M. Galanti, D. Fanelli, and F. Piazza. Macroscopic transport equations in many-body systems from microscopic exclusion processes in disordered media: a review. *Frontiers in Physics*, 4:1–8, 2016.

[GM18] A. Gaudiello and T. Mel'nyk. Homogenization of a nonlinear monotone problem with nonlinear Signorini boundary conditions in a domain with highly rough boundary. *Journal of Differential Equations*, 265(10):5419–5454, 2018.

[GMRL09] J. Garcia-Melian, J. D. Rossi, and J. C. Sabina De Lis. Existence and uniqueness of positive solutions to elliptic problems with sublinear mixed boundary conditions. *Communications in Contemporary Mathematics*, 11(4):585–613, 2009.

[GP18] S. N. Gomes and G. A. Pavliotis. Mean field limits for interacting diffusions in a two-scale potential. *Journal of Nonlinear Science*, 28:905–941, 2018.

[Gri04] G. Griso. Error estimate and unfolding for periodic homogenization. *Asymptotic Analysis*, 40:269–286, 2004.

[GT77] D. Gilbarg and N. S. Trudinger. *Elliptic Partial Differential Equations of Second Order*, volume 224. Springer, 1977.

[GT83] D. Gilbarg and N. Trudinger. *Elliptic Partial Differential Equations of Second Order*. Springer-Verlag, 1983.

[GZP+14] A. Garcimartin, I. Zuriguel, J. M. Pastor, C. Martin-Gomez, and D. R. Parisi. Experimental evidence of the faster-is-slower effect. *Transportation Research Procedia*, 2:760–767, 2014.

[HFV00] D. Helbing, I. Farkas, and T. Vicsek. Simulating dynamical features of escape panic. *Nature*, 407:487–490, 2000.

[HI11] L. Hoang and A. Ibragimov. Structural stability of generalized Forchheimer equations for compressible fluids in porous media. *Nonlinearity*, 24:1–41, 2011.

[HJ91] U. Hornung and W. Jäger. Diffusion, convection, adsorption, and reaction of chemicals in porous media. *Journal of Differential Equations*, 92:199–225, 1991.

[IDCL05] N. R. Franks I. D. Couzin, J. Krause and S. A. Levin. Effective leadership and decision–making in animal groups on the move. *Nature*, 433:513–516, 2005.

[IW81] N. Ikeda and S. Watanabe. *Stochastic Differential Equations and Diffusion Processes.* Amsterdam-Tokyo: North Holland-Kodansha, 1981.

[Jin97] T. Jin. Studies on human behavior and tenability in fire smoke. *Fire Safety Science - Proceedings of the Fifth International Symposium*, 5:3–12, 1997.

[JP04] J. Jacod and P. Protter. *Probability Essentials.* Springer Science & Business Media, 2004.

[Kač99] J. Kačur. Solution to strongly nonlinear parabolic problems by a linear approximation scheme. *IMA Journal of Numerical Analysis*, 19:119–145, 1999.

[KAM14] O. Krehel, T. Aiki, and A. Muntean. Homogenization of a thermo-diffusion system with Smoluchowski interactions. *Networks and Heterogeneous Media*, 9(4):739–762, 2014.

[Kho17] V. A. Khoa. A high-order corrector estimate for a semi-linear elliptic system in perforated domains. *Comptes Rendus Mécanique*, 345(5):337–343, 2017.

[KL18] S. Kim and K. A. Lee. Higher order convergence rates in theory of homogenization III: Viscous Hamilton-Jacobi equations. *Journal of Differential Equations*, 265(10):5384–5418, 2018.

[KLSD08] H. Kuang, X. Li, T. Song, and S. Dai. Analysis of pedestrian dynamics in counter flow via an extended lattice gas model. *Physical Review E*, 78:066117, 2008.

[KM16a] V. A. Khoa and A. Muntean. Asymptotic analysis of a semi-linear elliptic system in perforated domains: Well-posedness and corrector for the homogenization limit. *Journal of Mathematical Analysis and Applications*, 439:271–295, 2016.

[KM16b] V. A. Khoa and A. Muntean. A note on iterations-based derivations of high-order homogenization correctors for multiscale semi-linear elliptic equations. *Applied Mathematics Letters*, 58:103–109, 2016.

[KM17] V. A. Khoa and A. Muntean. Correctors justification for a Smoluchowski-Soret-Dufour model posed in perforated domains. submitted (arXiv:1704.01790), 2017.

[KM19] V. A. Khoa and A. Muntean. Corrector homogenization estimates for a non-stationary Stokes–Nernst–Planck–Poisson system in perforated domains. *Communications in Mathematical Sciences*, 17(3):705–738, 2019.

[KMK15] O. Krehel, A. Muntean, and P. Knabner. Multiscale modeling of colloidal dynamics in porous media including aggregation and deposition. *Advances in Water Resources*, 86:209–216, 2015.

[KS00] I. Karatzars and S. E. Shreve. *Brownian Motion and Stochastic Calculus*. Second Edition, Graduate Texts in Mathematics, Springer, 2000.

[KS02] A. Kirchner and A. Schadschneider. Simulation of evacuation processes using a bionics–inspired cellular automaton model for pedestrian dynamics. *Physica A*, 312:260–276, 2002.

[KTI20] V. A. Khoa, T. K. T. Thieu, and E. R. Ijioma. On a pore-scale stationary diffusion equation: scaling effects and correctors for the homogenization limit. *Accepted for publication in Discrete & Continuous Dynamical Systems Series B (Doi: 10.3934/dcdsb.2020190)*, 2020.

[KvMY19] M. Kimura, P. van Meurs, and Z. Yang. Particle dynamics subject to impenetrable boundaries: Existence and uniqueness of mild solutions. *SIAM J. Math. Anal.*, 51:5049–5076, 2019.

[LDD02] N. T. Long, A. P. N. Dinh, and T. N. Diem. Linear recursive schemes and asymptotic expansion associated with the Kirchoff–Carrier operator. *Journal of Mathematical Analysis and Applications*, 267(1):116–134, 2002.

[Lie86] G. M. Lieberman. Mixed boundary value problems for elliptic and parabolic differential equations of second order. *Journal of Mathematical Analysis and Applications*, 113:422–440, 1986.

[Lio84] P. L. Lions. Stochastic differential equations with reflecting boundary conditions. *Communications on Pure and Applied Mathematics*, XXXVII:511–537, 1984.

[LLPW11] J. L. Lions, D. Lukkassen, L. E. Persson, and P. Wall. Reiterated homogenization of nonlinear monotone operators. *Chinese Annals of Mathematics*, 22:1–12, 2011.

[LRR+20] A. Larsson, E. Ranudd, E. Ronchi, A. Hunt, and S. Gwynne. The impact of crowd composition on egress performance. *Fire Safety Journal (Doi: https://doi.org/10.1016/j.firesaf.2020.103040)*, 2020.

[LW18] S. H. Lim and J. Wehr. Homogenization for a class of generalized langevin equations with an application to thermophoresis. *Journal of Statistical Physics*, 174:656–691, 2018.

[MCKB] A. Muntean, E. N. M. Cirillo, O. Krehel, and M. Böhm. Pedestrians moving in dark: Balancing measures and playing games on lattice. *In "Collective Dynamics from Bacteria to Crowds", An Excursion Through Modeling, Analysis and Simulation Series: CISM International Centre for Mechanical Sciences, Vol. 553 Muntean, Adrian, Toschi, Federico (Eds.) 2014, VII, 177 p. 29 illus, Springer, 2014.*

[Mel95] T. A. Melnik. Asymptotic expansion of eigenvalues and eigenfunctions for elliptic boundary-value problems with rapidly oscillating coefficients in a perforated cube. *Journal of Mathematical Sciences*, 75(3):1646–1671, 1995.

[MN09] T. Muthukumar and A. K. Nandakumaran. Homogenization of low-cost control problems on perforated domains. *Journal of Mathematical Analysis and Applications*, 351(1):29–42, 2009.

[MPRV08] U. M. B. Marconi, A. Puglisi, L. Rondoni, and A. Vulpiani. Fluctuation–dissipation: Response theory in statistical physics. *Phys. Rep.*, 461:111, 2008.

[MPS89] A. D. Masi, E. Presutti, and E. Scacciatelli. The weakly asymmetric simple exclusion process. *Annales de l'I.H.P. Probabilités et statistiques*, 25(1):1–38, 1989.

[MWS14] F. Müller, O. Wohak, and A. Schadschneider. Study of influence of groups on evacuation dynamics using a cellular automaton model. *Transportation Research Procedia*, 2:168–176, 2014.

[NO10] K. Nyström and T. Önskog. The Skorohod oblique reflection problem in time-dependent domains. *The Annals of Probability*, 38:2170–2223, 2010.

[Ö09] T. Önskog. *The Skorohod Problem and Weak Approximation of Stochastic Differential Equations in Time-dependent Domains*. PhD thesis, Umeå University, Sweden, 2009.

[OP11] M. Ottobre and G. A. Pavliotis. Asymptotic analysis for the generalized Langevin equation. *Nonlinearity*, 24:1629–1653, 2011.

[OP17] H. Oh and J. Park. Main factor causing "faster-is-slower" phenomenon during evacuation: rodent experiment and simulation. *Scientific Reports*, 7:13724, 2017.

[OSY92] O. A. Oleinik, A. S. Shamaev, and G. A. Yosifian. *Mathematical Problems in Elasticity and Homogenization*. North Holland, 1992.

[OV07] D. Onofrei and B. Vernescu. Error estimates in periodic homogenization with non-smooth coefficients. *Asymptotic Analysis*, 54:103–123, 2007.

[OV12] D. Onofrei and B. Vernescu. Asymptotic analysis of second-order boundary layer correctors. *Applicable Analysis*, 91(6):1097–1110, 2012.

[Pao93] C. V. Pao. *Nonlinear Parabolic and Elliptic Equations*. Springer, 1993.

[Pav14] G. A. Pavliotis. *Stochastic Processes and Applications: Diffusion Processes, the Fokker-Planck and Langevin Equations. Texts in Applied Mathematics*, volume 60. Springer Verlag, Berlin, 2014.

[PBL78] G. Papanicolau, A. Bensoussan, and J.-L. Lions. *Asymptotic Analysis for Periodic Structures*. North Holland, 1978.

[Pil14] A. Pilipenko. *An Introduction to Stochastic Differential Equations with Reflection*. Lectures in Pure and Applied Mathematics. Institutional Repository of the University of Potsdam, Germany, 2014.

[PM05] S. Pankavich and N. Michalowski. A short proof of increased parabolic regularity. *Electronic Journal of Differential Equations*, 205, 2005.

[Pre09] E. Presutti. *Scaling Limits in Statistical Mechanics and Microstructures in Continuum Mechanics*. Springer, 2009.

[PS07] G. A. Pavliotis and A. M. Stuart. *Multiscale Methods: Averaging and Homogenization*. Springer, 2007.

[PZ14] G. D. Prato and J. Zabczyk. *Stochastic Equations in Infinite Dimensions*. Cambridge University Press, 2014.

[Ray13] N. Ray. *Colloidal Transport in Porous Media Modeling and Analysis*. PhD thesis, University of Erlangen-Nuremberg, 2013.

[RJM19] O. Richardson, A. Jalba, and A. Muntean. The effect of environment knowledge in evacuation scenarios involving fire and smoke – a multiscale modelling and simulation approach. *Fire Technology*, 55:415–436, 2019.

[RMK12] N. Ray, A. Muntean, and P. Knabner. Rigorous homogenization of a Stokes-Nernst-Planck-Poisson system. *Journal of Mathematical Analysis and Applications*, 390(1):374–393, 2012.

[RN19] E. Ronchi and D. Nilsson. *Pedestrian movement in smoke: theory, data and modelling approaches*, volume 1: Theory, Models and Safety Problems. in G. Libelli, N. Bellomo (Eds), Crowd Dynamics, Modeling and Simulation in Science, Engineering and Technology, Boston, Birkhauser, Springer, 2019.

[RvNFK12] N. Ray, T. van Noorden, F. Frank, and P. Knabner. Multiscale modeling of colloid and fluid dynamics in porous media including an evolving microstructure. *Transport in Porous Media*, 95(3):669–696, 2012.

[Sai87] Y. Saisho. Stochastic differential equations for multi-dimensional domain with reflecting boundary. *Probability Theory and Related Fields*, 74:455–477, 1987.

[Sch06] D. Schieborn. *Viscosity Solutions of Hamilton-Jacobi Equations of Eikonal Type on Ramified Spaces*. PhD thesis, University Tübingen, Germany, 2006.

[Sch12] M. Schmuck. First error bounds for the porous media approximation of the Poisson-Nernst-Planck equations. *ZAMM - Journal of Applied Mathematics and Mechanics / Zeitschrift für Angewandte Mathematik und Mechanik*, 92(4):304–319, 2012.

[Sch13] M. Schmuck. New porous medium Poisson-Nernst-Planck equations for strongly oscillating electric potentials. *Journal of Mathematical Physics*, 54(2):021504, 2013.

[SK17] M. Schmuck and S. Kalliadasis. Rate of convergence of general phase field equations in strongly heterogeneous media toward their homogenized limit. *SIAM Journal on Applied Mathematics*, 77(4):1471–1492, 2017.

[Sko61] A. V. Skorohod. Stochastic equations for diffusion process in a bounded domain. *Theory of Probability and Its Applications*, VI:264–274, 1961.

[SLH09] M. J. Simpson, K. A. Landman, and B. D. Hughes. Pathlines in exclusion processes. *Physical Review E*, 79:031920, 2009.

[Slo01] M. Slodivcka. Error estimates of an efficient linearization scheme for a nonlinear elliptic problem with a nonlocal boundary condition. *ESAIM: Mathematical Modelling and Numerical Analysis*, 35(4):691–711, 2001.

[Spo91] H. Spohn. *Large Scale Dynamics of Interacting Particles*. Springer-Verlag Berlin Heidelberg, 1991.

[SPPK12] M. Schmuck, M. Pradas, G. A. Pavliotis, and S. Kalliadasis. Upscaled phase-field model for interfacial dynamics in strongly heterogeneous domains. *Proceedings of the Royal Society A*, 468:3705–3724, 2012.

[SSV17] C. Schumacher, F. Schwarzenberger, and I. Veselic. A Glivenko–Cantelli theorem for almost additive functions on lattices. *Stochastic Processes and their Applications*, 127(1):179–208, 2017.

[Str14] B. Straughan. *The Energy Method, Stability, and Nonlinear Convection*. New York: Springer-Verlag, 2014.

[STU13] K. Suzuno, A. Tomoeda, and D. Ueyama. Analytical investigation of the faster-is-slower effect with a simplified phenomenological model. *Physical Review E*, 88:052813, 2013.

[Sus13] T. A. Suslina. Homogenization of the Dirichlet problem for elliptic systems: L_2-operator error estimates. *Mathematika*, 59(2):463–476, 2013.

[TB96] N. Triantafyllidis and S. Bardenhagen. The influence of scale size on the stability of periodic solids and the role of associated higher order gradient continuum models. *Journal of the Mechanics and Physics of Solids*, 44(11):1891–1928, 1996.

[TCM19] T. K. T. Thieu, M. Colangeli, and A. Muntean. Weak solvability of a fluid-like driven system for active-passive pedestrian dynamics. *Nonlinear Studies*, 26:991–1006, 2019.

[TCM20] T. K. T. Thieu, M. Colangeli, and A. Muntean. Uniqueness and stability with respect to parameters of solutions to a fluid-like driven system for active–passive pedestrian dynamics. *Accepted for publication in Journal of Mathematical Analysis and Applications*, 2020.

[TM20] T. K. T. Thieu and A. Muntean. Solvability of a coupled nonlinear system of Skorohod-like stochastic differential equations modeling active–passive pedestrians dynamics through a heterogeneous domain and fire. Submitted (arXiv:2006.00232), 2020.

[vKS17] C. von Krüchten and A. Schadschneider. Empirical study on social groups in pedestrian evacuation dynamics. *Physica A*, 457:129–141, 2017.

[VS06] H. M. Versieux and M. Sarkis. Numerical boundary corrector for elliptic equations with rapidly oscillating periodic coefficients. *International Journal for Numerical Methods in Biomedical Engineering*, 22:577–589, 2006.

[VVM19] A. Vromans, F. V. D. Ven, and A. Muntean. Parameter delimitation of the weak solvability for a pseudo-parabolic system coupling chemical reactions, diffusion and momentum equations. *Advances in Mathematical Sciences and Applications*, 28:273–311, 2019.

[WN19] I. Wijaya and H. Notsu. Stability estimates and a Lagrange-Galerkin scheme for a Navier-Stokes type model of flow in non-homogeneous porous media. *Discrete and Continuous Dynamical Systems - Series S (Doi: 10.3934/dcdss.2020234)*, 2019.

[WS14] J. H. Wang and J. H. Sun. Principal aspects regarding to the emergency evacuation of large–scale crowds: A brief review of literatures until 2010. *Procedia Engineering*, 71:1–6, 2014.

[WWLS19] D. Wang, H. Wu, L. Liu, and D. K. Schwartz. Macroscopic transport equations in many-body systems from microscopic exclusion processes in disordered media: a review. *Physical Review Letters*, 123:118002, 2019.

[XJJS16] S. Xue, B. Jia, R. Jiang, and J. Shan. Pedestrian evacuation in view and hearing limited condition: The impact of communication and memory. *Physics Letters A*, 380:3029–3035, 2016.

[YDW+14] X. Yang, H. Dong, Q. Wang, Y. Chen, and X. Hu. Guided crowd dynamics via modified social force model. *Physica A : Statistical Mechanics and its Applications*, 411:63–73, 2014.

[YJQH16] L. I. Yang, C. Jianzhong, Z. Qian, and Y. Huizhen. Study of pedestrians evacuation model considering familiarity with environment. *China Safety Science Journal*, 26:168–174, 2016.

[Zei86] E. Zeidler. *Nonlinear Functional Analysis and Its Applications*, volume 1. 9th ed. Springer-Verlag, 1986.

[ZLX11] J. B. Zeng, B. Leng, and Z. Xiong. Pedestrian dynamics in a two-dimensional complex scenario using a local view floor field model. *International Journal of Modern Physics C*, 8:775–803, 2011.

[ZP16] V. V. Zhikov and S. E. Pastukhova. Operator estimates in homogenization theory. *Russian Mathematical Surveys*, 71(3):417–511, 2016.